

**REPUBLIC OF TURKEY
YILDIZ TECHNICAL UNIVERSITY
GRADUATE SCHOOL OF NATURAL AND APPLIED SCIENCES**

**INVESTIGATION OF DYNAMIC SOIL – PILE – STRUCTURE
INTERACTION IN CLAYEY SOILS BY NUMERICAL ANALYSIS**

MUSTAFA KIRKİT

**PhD. THESIS
DEPARTMENT OF CIVIL ENGINEERING
PROGRAM OF GEOTECHNICAL ENGINEERING**

**ADVISER
PROF. DR. MEHMET BERİLGEN**

İSTANBUL, 2015

REPUBLIC OF TURKEY
YILDIZ TECHNICAL UNIVERSITY
GRADUATE SCHOOL OF NATURAL AND APPLIED SCIENCES

**INVESTIGATION OF DYNAMIC SOIL – PILE – STRUCTURE
INTERACTION IN CLAYEY SOILS BY NUMERICAL ANALYSIS**

A thesis submitted by Mustafa KIRKIT in partial fulfillment of the requirements for the degree of **DOCTOR OF PHILOSOPHY** is approved by the committee on 28.05.2015 in Department of Civil Engineering, Geotechnical Engineering Program.

Thesis Adviser

Prof. Mehmet BERİLGEN
Yıldız Technical University

Co- Adviser

Assoc. Prof. Cem AKGÜNER
TED University

Approved By the Examining Committee

Prof. Mehmet BERİLGEN
Yıldız Technical University

Prof. Kutay ÖZAYDIN, Member
Yıldız Technical University

Prof. Bilge SİYAHİ, Member
Gebze Technical University

Assoc. Prof. Cem AKGÜNER
TED University

Assoc. Prof. Havvanur KILIÇ, Member
Yıldız Technical University

Assoc. Prof. Pelin ÖZENER, Member
Yıldız Technical University

Assoc. Prof. Mesut ŞİMŞEK, Member
Yıldız Technical University

This study was supported by the Scientific and Technological Research Council of Turkey (TUBITAK) Grant No: 2210 and 2214.

ACKNOWLEDGEMENTS

First, I would like to express my sincere gratitude to my advisers Prof. Mehmet Berilgen and Assoc. Prof. Cem Akgüner for their guidance, caring, and patience. I am grateful to Prof. Ertuğrul Tacirođlu, who gave me opportunity to work with him and his team at University of California – Los Angeles, which was an excellent experience for me. I would also like to thank Assoc. Prof. Mesut ŐimŐek, Assoc. Prof. Yasin Fahjan, and Elnaz Esmaeilzadeh for their contribution to my dissertation. Besides, I would like to thank my thesis committee, Prof. Kutay Özaydın and Prof. Bilge Siyahi, for their encouragement and insightful comments.

I would like to thank Geotechnics Division staff at Yıldız Technical University Civil Engineering Department: Prof. Mustafa Yıldırım, Prof. Őükrü Ersoy, Prof. Suat Akbulut, Assoc. Prof. Havvanur Kılıç, Assoc. Prof. Pelin Özener, Assoc. Prof. Őükrü Özçoban, Asst. Prof. Saadet Berilgen, Asst. Prof. Nejat Çetinkaya, Asst. Prof. Murat Tonarođlu, Asst. Prof. Dođan Çetin, Dr. Murat E. Selçuk, Res. Asst. Selçuk Demir, and Res. Asst. Ali Coşandal.

The financial support provided by TUBITAK (The Scientific and Technological Research Council of Turkey) is gratefully acknowledged.

I would also like to thank all of my friends who supported me in writing, and encouraged me to strive towards my goal.

I would like to thank my beloved wife Fatma for her tremendous support during my graduate studies. A special thanks to our family as well. Words cannot express how grateful I am to my mother, late father, mother-in law, father-in law, sisters, and brothers for all of the sacrifices that you've made on my behalf.

May, 2015

Mustafa KİR KİT

TABLE OF CONTENTS

	Page
LIST OF SYMBOLS	vii
LIST OF ABBREVIATIONS	x
LIST OF FIGURES	xi
LIST OF TABLES	xvi
ABSTRACT	xvii
ÖZET	xix
CHAPTER 1	
INTRODUCTION	1
1.1 Literature Review	1
1.1.1 Analysis Methods of <i>SSI</i>	3
1.2 Objectives of the Thesis	6
1.3 Hypothesis	7
1.4 Organizations	7
CHAPTER 2	
LITERATURE REVIEW	9
2.1 Early History of Kinematic Interaction	9
2.1.1 Kinematic Interaction Studies Associated with Pile Foundations	10
2.2 Forces on Pile under Seismic Loading	11
2.3 Pile Performance during Earthquakes	13
2.4 Analysis Methods	15
2.4.1 General Overview of Multi-Step (Substructure) Method	16
2.4.2 General Overview of Analysis Methods	18
2.5 Previous Studies with respect to Kinematic Interaction	20
CHAPTER 3	
METHODOLOGY	41
3.1 The Established Model in <i>OpenSees</i>	41
3.2 The Established Model with <i>Plaxis</i>	44
3.3 Verification of the Established <i>FE</i> models	46

3.3.1	Site Response Analysis	46
3.3.2	Closed-form Solution for Kinematic Interaction.....	47
CHAPTER 4		
SOIL – PILE (KINEMATIC) INTERACTION		51
4.1	General Response of Single Pile	52
4.1.1	Harmonic Loading	54
4.1.2	Earthquake Loading	58
4.1.3	Discussion of Harmonic vs. Earthquake Input Motion	61
4.2	Effect of Phase Angle on Kinematic Interaction.....	65
4.2.1	Problem Definition.....	65
4.2.2	Parametric Studies.....	67
4.3	Concluding Remarks	83
CHAPTER 5		
SOIL – PILE – STRUCTURE INTERACTION		85
5.1	Complete Soil – Pile – Structure Model.....	86
5.1.1	Hypoplastic Soil Model.....	87
5.1.2	User Defined Hypoplastic Model for Clay in Plaxis.....	88
5.1.3	Embedded Pile Element	92
5.1.4	Single-Degree-of-Freedom (SDOF) System.....	95
5.2	Investigation of Pile and Superstructure Responses by Parametric Studies	98
5.2.1	Pile Response	101
5.2.2	Superstructure Response	114
5.3	Concluding Remarks	126
CHAPTER 6		
RESULTS AND DISCUSSION		127
6.1	Conclusions	128
6.2	Recommendations	130
REFERENCES.....		131
APPENDIX-A		
OPENSEES SCRIPT FOR SOIL – PILE INTERACTION.....		140
APPENDIX-B		
PILE BENDING AND DISPLACEMENT FOR DIFFERENT PILE GROUP CASES		146
CURRICULUM VITAE		158

LIST OF SYMBOLS

A_b	Base area of the finite element model
A_f	Amplitude of motion at free-field
a_{ff}	Free-field acceleration
a_o	Dimensionless frequency
a_p	Pile acceleration
A_p	Amplitude of motion at pile head
a_r	Rock acceleration
a_s	Horizontal ground acceleration
a_{st}	Structure acceleration
A_f	Amplitude of motion at free-field
a_1 and a_2	Constants for Rayleigh damping
c	Damping coefficient
c_u	Undrained cohesion
d	Distance between two Gauss stress points
D	Pile diameter
D_{eq}	Embedded pile diameter
E_p	Young's modulus of pile
E_s	Young's modulus of soil
f	Frequency
$f(t)$	Force time history
f_{avg}	Average frequency of layered soil
f_b and f_c	Frequencies at b -th and c -th modes
f_{inp}	Input motion frequency
F_{max}	Base resistance
f_n	Natural frequency
G	Shear modulus
G_{ur}	Unloading reloading shear modulus
H	Soil thickness
ISF_{KF}	Interface stiffness factor for embedded pile at base
ISF_{RN}	Interface stiffness factor for embedded pile in lateral direction
ISF_{RS}	Interface stiffness factor for embedded pile in axial direction
j	A positive constant defining variations of G and B
I_a	Kinematic interaction factor in terms of acceleration
I_p	Pile inertial moment
I_u	Kinematic interaction factor in terms of displacement
k	Stiffness
K	Bulk modulus

K_F	Embedded pile stiffness parameters for base
K_w	Bulk modulus of water
L	Pile length
$L_{spacing}$	Pile spacing in out-of-plane direction
L_1 and L_2	SDOF system lengths of column and mass, respectively
m	Mass
$M_{inertial}$	Inertial moment
$M_{kinematic}$	Kinematic moment
m_p	Pile mass
m_R and m_T	Parameters of hypoplastic soil constitutive model for clay
N	Parameter of hypoplastic soil constitutive model for clay
N_{pile}	Total pile bearing capacity
NYS	Number of yield surfaces
p_t	Parameter of hypoplastic soil constitutive model for clay
P_{ref}	Reference mean effective confining pressure
PI	Plasticity index
q	Wavenumber
R	Parameter of hypoplastic soil constitutive model for clay
R_N and R_S	Embedded pile stiffness parameters in lateral and axial directions
s	Spacing between adjacent piles
t	Time
T_{max}	Skin resistance
t_s	Shear force at a particular point
u	Displacement
$u_{bending}$	Deflection due to bending
u_{shear}	Deflection due to shear
u_b	Base input motion
u_{ff}	Free-field ground displacement
\dot{u}	Velocity
\ddot{u}	Acceleration
V_{avg}	Average shear wave velocity of soil deposit
V_s	Soil shear wave velocity
$V_{s,r}$	Rock shear wave velocity
$V_{s,30}$	Average shear wave velocity of soil to a depth of 30 m
W_D	Dissipated energy in a load cycle
W_S	Energy stored at maximum strain
z	Depth
α	Skin resistance factor
α_1 and α_2	Rayleigh coefficients
γ and β	Newmark integrator parameters
$\gamma_{cut-off}$	Certain lower limit of shear strain
γ_{peak}	Peak shear strain
γ_s	Shear strain
$\gamma_{0.7}$	Shear strain at which G/G_{max} is equal to 0.7
Γ	Dimensionless response coefficient
γ_{eff}	Effective shear strain
Δt	Time increment
θ	Friction angle
κ	Curvature

λ	Characteristic wavenumber
λ^* and κ^*	Parameters of hypoplastic soil constitutive model for clay
λ_{wave}	Wavelength
ν	Poisson's ratio
ξ	Damping ratio
ρ_p	Pile density
ρ_s	Soil density
ρ_r	Rock density
σ	Normal stress
τ	Shear stress
ϕ_c	Critical state friction angle
ϕ_p	Pile phase angle
ϕ_f	Free-field phase angle
χ	Parameter of hypoplastic soil constitutive model for clay
ω	Circular frequency
$(1/R)$	Curvature
$[C]$	Damping matrix
$\{I\}$	Unit vector
$[K]$	Stiffness matrix
$[M]$	Mass matrix
$[M_{soil}]$	Soil mass matrix
$[M_{structure}]$	Structure mass matrix
$\{u\}$	Displacement vector
$\{u_{iner}\}$	Inertial relative displacement vector
$\{u_{kin}\}$	Kinematic relative displacement vector
$\{\ddot{u}_{ff}(t)\}$	Free-field acceleration vector

LIST OF ABBREVIATIONS

BDWF	Beam on Dynamic Winkler Foundation
BEM	Boundary Element Method
FEM	Finite Element Method
FIM	Foundation Input Motion
NEES	Network for Earthquake Engineering Simulation
PEER	Pacific Earthquake Engineering Research Center
PGA	Peak Ground Acceleration
PGD	Peak Ground Displacement
SDOF	Single Degree of Freedom
SFSI	Soil – Foundation – Structure Interaction
SPSI	Soil – Pile – Structure Interaction
SSI	Soil - Structure Interaction
SSP	Stabilized Single Point Integration

LIST OF FIGURES

		Page
Figure 1.1	SDOF system on an elastic soil deposit [2].....	3
Figure 1.2	Entire soil-foundation-structure model in the direct method [2].....	4
Figure 1.3	Kinematic interaction with free-field motions indicated by dashed lines: (a) flexural mat foundation on surface; (b) rigid embedded foundation; (c) stiff slab on surface [2]	5
Figure 1.4	Analysis of (a) kinematic interaction and (b) inertial interaction [2].....	5
Figure 2.1	Forces acting on pile along its length during seismic excitation.....	13
Figure 2.2	Possible failure modes for pile foundations under seismic shaking [62]	14
Figure 2.3	Sketch of the soil-pile-structure interaction problem	16
Figure 2.4	Decomposition of the soil-pile-structure problem into kinematic and inertial interaction.....	17
Figure 2.5	Analysis of inertial interaction in two steps	18
Figure 2.6	Comparison of the pile displacement and free surface displacement for different values of H/R [27].....	20
Figure 2.7	Transfer function and rotation of the pile cap for 3x3 pile groups in soft soil medium [72].....	21
Figure 2.8	Transfer function and rotation of the pile cap for pile groups in stiff soil medium [72]	22
Figure 2.9	Studied soil-pile-structure problem [53]	23
Figure 2.10	Soil profiles [53].....	24
Figure 2.11	Influence of stiffness ratio (E_p/E_s) on kinematic interaction factors; L/D = 40, Soil Model A, $\beta_s = 0.05$, $\nu_s=0.4$, $\rho_p/\rho_s=1.6$ [53]	24
Figure 2.12	Influence of soil type on kinematic interaction factors; $L/D = 40$, $\beta_s =$ 0.05 , $\nu_s=0.4$, $\rho_p/\rho_s=1.6$ [53].....	25
Figure 2.13	Complete soil-pile-structure analysis [53]	25
Figure 2.14	Studied problem and soil profiles [36].....	26
Figure 2.15	General form of the displacement kinematic interaction factor [36]	27
Figure 2.16	Kinematic seismic response of pile groups [36]	28
Figure 2.17	Three-step procedure for estimating the influence of Pile 1 upon the next Pile 2 under kinematic loading [64]	29
Figure 2.18	Pile deflection due to kinematic loading at dimensionless frequency $a =$ 0.3 : amplitude and phase angle corresponding to the homogeneous, the particular, and the total solution to the governing equation (24) in [64].....	30
Figure 2.19	Kinematic seismic response of 1 x 2 fixed-head pile group: comparison of proposed method with rigorous results by Fan et al. [36] ($\rho_p/\rho_s=1.42$, $L/D=20$, $\nu = 0.4$, $\beta=0.05$) [64].....	31
Figure 2.20	The bridge – pier systems and soil profile [76].....	32

Figure 2.21	Soil – structure interaction model: (1) model parameters and (2) sketch of response in terms of displacement and rotation [76]	32
Figure 2.22	Results of the complete analysis in terms of time histories for bridge – pier system carried by single-column pile under Pacoima (1994) motion [76]	33
Figure 2.23	Kinematic bending of a free-head pile subjected to vertical seismic S-waves in a two-layer soil profile [66].....	34
Figure 2.24	(a) The pile-soil model studied. (b) The representation of BDWF formulation for soil-pile interaction [66].....	35
Figure 2.25	Strain transmissibility for a solid pile embedded in a homogeneous soil layer subjected to harmonic vertical S-waves ($\rho_p / \rho_s = 1.4$, $\nu = 0.4$, $\beta = 0$) [66]	35
Figure 2.26	Strain transmissibility at interface of two soil layers of different stiffness for low frequencies. (Curves were obtained for $h_1 / d = 7, 10, 20$, and ∞ ; L_a : active pile length) [66].....	36
Figure 2.27	Simple superposition approach to solve embedded footing supported by vertical piles [79].....	37
Figure 2.28	Comparison of horizontal impedances of embedded footing on piles obtained rigorously K^W and by superposition K^P [79].....	37
Figure 2.29	Translational and rotational kinematic interaction factor for embedded footing on piles under SH waves [79]	38
Figure 2.30	Problem associated boundary conditions at the pile head and tip [47] .	39
Figure 2.31	Kinematic response factor for free-head free-tip piles: (a) $E_p / E_s = 1000$; (b) $E_p / E_s = 10000$ [47]	39
Figure 3.1	Representative delineation of established finite element model with boundary conditions in OpenSees	42
Figure 3.2	Mesh of entire soil – pile system.....	45
Figure 3.3	Mesh generated near the pile.....	46
Figure 3.4	Comparison for a linear soil with 5% damping: results from two-dimensional OpenSees and Plaxis models versus calculations in Shake2000 and DeepSoil.....	47
Figure 3.5	The schematic representation of the embedded pile in homogeneous soil on rigid base (Anoyatis et al. [47]).....	50
Figure 3.6	Comparison of FEM results with the analytical solution by Anoyatis et al. [47].....	50
Figure 4.1	Pressure independent soil material constitutive model: (a) shape of yield surface in principal effective stress space, and (b) response of constitutive model (figure adapted from [81])	53
Figure 4.2	Kinematic interaction factors in terms of displacement and acceleration considering linear and nonlinear soil behavior for C1 (soft) soil ($H=30$ m, $L=20$ m, $D=1$ m).....	55
Figure 4.3	Effect of soil stiffness on kinematic interaction ($H=30$ m, $L=20$ m, $D=1$ m).....	55
Figure 4.4	Pile slenderness effect on response of the soil-pile system (C1: soft soil, $H=30$ m, $L=20$ m)	56
Figure 4.5	Over-estimating shear stress by the equivalent linear method [110]	57
Figure 4.6	Time histories and Fourier spectra of earthquakes recorded at very stiff soil or outcropping rock ($V_s > 500$ m/s) used in analyses	59
Figure 4.7	Calculated accelerations and displacements with depth at free-field and at a distance of 2 m from the pile).....	61

Figure 4.8	Effect of the presence of the pile on frequency content	62
Figure 4.9	Shear time histories of earthquake and harmonic motions with peak identical shear strains [2]	63
Figure 4.10	The amplitude of accelerations and displacements with dimensionless frequency for C3 soil and pile diameter of 1 m	64
Figure 4.11	Geometry of a single pile embedded in a layered soil rest on elastic bedrock	66
Figure 4.12	Pile and free field soil curvature amplitude for homogeneous soil condition	69
Figure 4.13	Pile and free field phase angle for homogeneous soil condition	70
Figure 4.14	Pile and free field soil curvature for layered soil condition with intermediate soft layer	72
Figure 4.15	Pile and free field phase angle for layered soil condition with intermediate soft layer	73
Figure 4.16	Spatial variation of real and imaginary components of the steady state pile curvature with depth for $f_{inp}/f_{avg} = 1$	74
Figure 4.17	Spatial variation of real and imaginary components of the steady state pile curvature with depth for $f_{inp}/f_{avg} = 4$	75
Figure 4.18	Free field response of a homogeneous soil on bedrock	77
Figure 4.19	Effects of kinematic phase difference on real components of pile displacement in homogeneous soil	78
Figure 4.20	Effects of kinematic phase difference on imaginary components of pile displacement in homogeneous soil	79
Figure 4.21	Spatial variation of the amplitude and phase angle of the pile and free field soil steady-state response in polar coordinate for the homogeneous soil	80
Figure 4.22	Effects of kinematic phase difference on real components of pile displacement in three-layered soil with an intermediate soft layer	81
Figure 4.23	Effects of kinematic phase difference on imaginary components of pile displacement in three-layered soil with an intermediate soft layer	82
Figure 4.24	Spatial variations of the amplitude and the phase angle of the steady-state responses of the pile and the free field soil in polar coordinates for the three-layered soil with an intermediate soft layer	83
Figure 5.1	The complete soil – pile – structure model	86
Figure 5.2	Isotropic compression and unloading lines defining parameters N , λ^* , and κ^* (adapted from [124])	88
Figure 5.3	Shear stiffness degradation curve of London clay with comparison by curves of fine-grained material for different PI recommended by Vucetic & Dobry [109]	90
Figure 5.4	Damping ratio calculated by equation (5.2) and comparison with curves of fine-grained material for different PI recommended by Vucetic & Dobry [109]	91
Figure 5.5	Mohr circle of London clay under undrained condition calculated through the “Soil Test” simulation feature in <i>Plaxis</i>	91
Figure 5.6	Schematic representation of embedded pile in the plane strain model [133]	92
Figure 5.7	Soil-pile interaction model in <i>Plaxis</i> [102]	93
Figure 5.8	Elastic zone in the surrounding soil [102]	94
Figure 5.9	Mass-spring system with a cantilever beam and a mass on top	95

Figure 5.10	Fixed-base <i>SDOF</i> system created by <i>Plaxis</i> to verify superstructure model	97
Figure 5.11	Periods of <i>SDOF</i> system obtained by FEM for different weight in Table 5.5	98
Figure 5.12	Investigated cases for single pile.....	100
Figure 5.13	Pile group cases considered in analyses	101
Figure 5.14	Minimum and maximum bending moments (M_{min} & M_{max}) and minimum and max pile displacements (u_{min} & u_{max}) calculated by applying Düzce earthquake motion	103
Figure 5.15	M_{min} & M_{max} and u_{min} & u_{max} calculated by applying Kocaeli earthquake motion.....	104
Figure 5.16	M_{min} & M_{max} and u_{min} & u_{max} calculated by applying Loma Prieta earthquake motion	105
Figure 5.17	M_{max} for different cases with inertial interaction calculated by applying Düzce earthquake	106
Figure 5.18	M_{max} for different cases with inertial interaction calculated by applying Kocaeli earthquake	106
Figure 5.19	M_{max} for different cases with inertial interaction calculated by applying Loma Prieta earthquake	107
Figure 5.20	M_{min} & M_{max} calculated by applying Düzce earthquake motion for Case V.....	108
Figure 5.21	M_{min} & M_{max} calculated by applying Düzce earthquake motion for Case VI.....	109
Figure 5.22	M_{min} & M_{max} calculated by applying Düzce earthquake motion for Case VII.....	110
Figure 5.23	u_{min} & u_{max} calculated by applying Düzce earthquake motion for Case V	111
Figure 5.24	u_{min} & u_{max} calculated by applying Düzce earthquake motion for Case VI.....	112
Figure 5.25	u_{min} & u_{max} calculated by applying Düzce earthquake motion for Case VII.....	113
Figure 5.26	Time histories calculated at base level of <i>SDOF</i> system for different cases applying Düzce Earthquake Mudurnu station record ($D = 1$ m; $T = 0.5$ sec).....	116
Figure 5.27	Time histories calculated at base level of <i>SDOF</i> system for different cases applying Kocaeli Earthquake Ereğli station record ($D = 1$ m; $T = 0.5$ sec).....	117
Figure 5.28	Time histories calculated at base level of <i>SDOF</i> system for different cases applying Loma Prieta Earthquake Gilroy #1 station record ($D = 1$ m; $T = 0.5$ sec).....	118
Figure 5.29	Acceleration time histories calculated at mass of <i>SDOF</i> system with and without pile ($D = 1.0$ m; $T = 0.5$ sec)	119
Figure 5.30	Displacement Time histories calculated at mass of <i>SDOF</i> system with and without pile ($D = 1.0$ m; $T = 0.5$ sec)	120
Figure 5.31	Response spectra for damping of 5 % for different cases applying Düzce motion ($D = 1$ m and $T = 0.5$ sec).....	121
Figure 5.32	Response spectra for damping of 5 % for different cases applying Kocaeli motion ($D = 1$ m and $T = 0.5$ sec)	122
Figure 5.33	Response spectra for damping of 5 % for different cases applying Loma motion ($D = 1$ m and $T = 0.5$ sec).....	123

Figure 5.34	Average acceleration response spectra for different site conditions [137]	124
Figure A.1	Small model to demonstrate analysis performed by OpenSees.....	140
Figure B.1	M_{min} & M_{max} calculated by applying Kocaeli earthquake motion for <i>Case V</i>	146
Figure B.2	M_{min} & M_{max} calculated by applying Kocaeli earthquake motion for <i>Case VI</i>	147
Figure B.3	M_{min} & M_{max} calculated by applying Kocaeli earthquake motion for <i>Case VII</i>	148
Figure B.4	u_{min} & u_{max} calculated by applying Kocaeli earthquake motion for <i>Case V</i>	149
Figure B.5	u_{min} & u_{max} calculated by applying Kocaeli earthquake motion for <i>Case VI</i>	150
Figure B.6	u_{min} & u_{max} calculated by applying Kocaeli earthquake motion for <i>Case VII</i>	151
Figure B.7	M_{min} & M_{max} calculated by applying Loma Prieta earthquake motion for <i>Case V</i>	152
Figure B.8	M_{min} & M_{max} calculated by applying Loma Prieta earthquake motion for <i>Case VI</i>	153
Figure B.9	M_{min} & M_{max} calculated by applying Loma Prieta earthquake motion for <i>Case VII</i>	154
Figure B.10	u_{min} & u_{max} calculated by applying Loma Prieta earthquake motion for <i>Case V</i>	155
Figure B.11	u_{min} & u_{max} calculated by applying Loma Prieta earthquake motion for <i>Case VI</i>	156
Figure B.12	u_{min} & u_{max} calculated by applying Loma Prieta earthquake motion for <i>Case VII</i>	157

LIST OF TABLES

	Page
Table 3.1	Soil and pile material properties used in comparison of FEM and Analytical method 49
Table 4.1	Pile and soil properties used in parametric analyses 54
Table 4.2	Other parameters used in analysis proposed by Opensees 54
Table 4.3	Results of earthquake analyses 60
Table 4.4	Soil profiles considered in parametric phase angle studies 67
Table 5.1	Used parameters for the London clay in the hypoplastic model 90
Table 5.2	Geometric and stiffness features of <i>SDOF</i> system 97
Table 5.3	Weight of mass based on the natural frequency of fixed-base beam 97
Table 5.4	Comparison of bending deflection calculated by FEM and analytical method 98
Table 5.5	Earthquake records used in analyses 99
Table 5.6	Parameters used for embedded pile 99
Table 5.7	<i>SDOF</i> system parameters considering system period T and width (which is equal to pile diameter D) 100
Table 5.8	Summarization of results including the effects of pile diameter (slenderness) and structure period 125

**INVESTIGATION OF DYNAMIC SOIL – PILE – STRUCTURE
INTERACTION IN CLAYEY SOILS BY NUMERICAL ANALYSIS**

Mustafa KIRKİT

Department of Civil Engineering

Ph.D. Thesis

Adviser: Prof. Dr. Mehmet BERİLGİN

Co-adviser: Assoc. Prof. Dr. Cem AKGÜNER

The response of a pile-supported structures under seismic loads is generally influenced by the interaction between the surrounding soil, the supporting piles, and the structure itself (soil-foundation-structure interaction, “*SFSP*”). These interaction effects are typically classified into two distinct categories: inertial and kinematic. During an earthquake, the soil medium vibrates the piles and the superstructure, and when inertial interaction is significant, the accelerated/mobilized masses of the piles and superstructure shake the soil back. Kinematic interaction, on the other hand, is the collective term given to the effects of the rigidity of piles, which usually is significantly larger than that of the soil, leading to alterations in the incoming seismic waves.

In this study, soil-pile-structure interaction is investigated through simulations utilizing the two-dimensional (plane-strain) finite element method (FEM). Initially, the established models are verified by a site response analysis involving elastic behavior, which is then compared to the analytical closed-form solution suggested for kinematic interaction in literature. Subsequently, parametric studies are performed. The scope of study are: (i) the kinematic interaction between soil and pile is investigated through numerical methods considering effective parameters such as the material model for soil (linear and nonlinear), the stiffness ratio between pile and soil (E_p/E_s), and the slenderness ratio (L/D : pile length over its diameter); (ii) the effect of variation in phase angle of the soil’s movement, which is omitted in prior studies focusing only on amplitudes, is scrutinized and a new kinematic interaction factor that considers the phase angle variations is proposed; (iii) the complete soil-pile-structure model is

investigated considering elasto-plastic soil behavior in time domain. Additionally, foundation input motion at base level of the superstructure and the pile response under seismic event are examined.

The important findings of this research are: (i) Nonlinear soil behavior substantially influences the kinematic interaction. The elasto-plastic properties of soil reduce the seismic motion effect, especially in terms of acceleration. On the other hand, piles have a linear behavior increasing the outcomes. Consequently, kinematic interaction factor in terms of acceleration (I_a) is larger than unity. (ii) The inertial interaction due to superstructure vibration is more dominant on the pile response; however, the kinematic interaction should not be neglected since it increases the bending moment acting on pile. (iii) The presence of piles in the ground creates a relatively stiffer area below the superstructure. This condition may increase the forces acting on the superstructure.

Key words: Inertial Interaction, Kinematic Interaction, Pile Foundations, Numerical Modelling, Seismic Analysis

KİLLİ ZEMİNLERDE DİNAMİK KAZIK – ZEMİN – YAPI ETKİLEŞİMİNİN SAYISAL ANALİZLERLE İNCELENMESİ

Mustafa KİRKİT

İnşaat Mühendisliği Anabilim Dalı

Doktora Tezi

Tez Danışmanı: Prof. Dr. Mehmet BERİLGEN

Eş Danışman: Doç. Dr. Cem AKGÜNER

Kazıklı yapı sistemlerinin deprem yükleri altındaki tepkisi sistemin içerisinde bulunduğu zeminin, yapı yüklerini zemine ileten kazıklı temellerin ve yapının kendisi arasında bulunan etkileşimden etkilenmektedir (zemin-temel-yapı etkileşimi). Bu etkileşimler tipik olarak iki kategoride ele alınmaktadır: *atalet etkileşimi* ve *kinematik etkileşim*. Deprem esnasında zemin ortamı kazık ve yapı sisteminde titreşime neden olmakta ve *atalet etkileşimi* etkili olduğu zaman ivmelenmiş/hareket ettirilmiş yapı ve kazık kütlesi zemini geri sarsmaktadır. Diğer taraftan *kinematik etkileşim* kazıklı temelin zemine göre daha rijit olmasından kaynaklanmakta ve kazıklı yapı sistemine gelen sismik dalgalarda değişime neden olmaktadır.

Bu çalışmada, zemin-kazık-yapı etkileşimi iki boyutlu sonlu eleman modelleri yardımıyla araştırılmıştır. Öncelikle, oluşturulan sonlu eleman modelleri, elastik davranışı dikkate alan zemin davranış analizi ve literatürde kinematik etkileşim için önerilmiş analitik kapalı çözüm yöntemi ile doğrulanmıştır. Devamında parametrik çalışmalar gerçekleştirilmiştir. Çalışma kapsamında: (i) zemin ve kazık arasındaki kinematik etkileşim kurulan nümerik model yardımıyla etkili parametreleri– malzeme modeli (doğrusal ve doğrusal olmayan), kazık ile zemin arasındaki rijitlik oranı (E_p/E_s) ve kazık narinliği (L/D)– dikkate alınarak araştırılmıştır; (ii) zeminin faz açısının değişiminin etkileri, önceki çalışmalar bunu ihmal ederek genliğe yoğunlaşmışlardır, incelenmiş ve bunu dikkate alan yeni bir kinematik etkileşim faktörü önerilmiştir; (iii) zemin-kazık-yapı arasındaki etkileşim, elasto-plastik zemin davranışı dikkate alınarak

zaman tanım alanında incelenmiştir. Ayrıca üstyapı taban seviyesindeki girdi hareketi ve kazığın sismik etkiler altındaki tepkisi değerlendirilmiştir.

Yapılan araştırmanın sonucunda elde edilen önemli bulgular: (i) Zeminin doğrusal olmayan davranışı kinematik etkileşimi önemli derecede etkilemektedir. Zeminin elasto-plastik özellikleri sismik hareket etkisini, özellikle de ivmeler cinsinden azaltmaktadır. Buna karşılık, kazık temel davranışı lineer sınırlar içinde kalmakta ve zeminin lineer olmayan davranışı ile karşılaştırıldığında daha yüksek ivme değerleri vermektedir. Sonuç olarak ivmeler cinsinden kinematik etkileşim faktörü I_a birim değerinden büyük çıkmaktadır. (ii) Üst yapı titreşiminden kaynaklı atalet etkileşimi kazık temellerin dinamik tepkisi üzerinde daha baskındır; ancak, kinematik etkileşim kazık temele gelen eğilme momentlerini artırdığından dolayı hesaplarda ihmal edilmemelidir. (iii) Zemin içerisinde kazık temellerin varlığı üst yapı altında daha sert bir bölge meydana getirmektedir. Bu durum üst yapıya etkiyen yükleri artırabilmektedir.

Anahtar Kelimeler: Atalet Etkileşimi, Kinematik Etkileşim, Kazık Temeller, Sayısal Modelleme, Sismik Analiz

CHAPTER 1

INTRODUCTION

The demands of growing populations from today's civil engineering profession for safe/affordable living spaces and an improved infrastructure are ever increasing. Thus, civil engineers are challenged to build structures that are larger, higher, and heavier; such as massive skyscrapers, multi-storied highways, grand concrete dams, off-shore platforms at large water depths, and large underground and underwater structures. Engineers are forced to find solutions for additional risks involved with new/little-experienced problems in construction and design, especially in less-desirable areas/conditions. Most of the vital structures are supported by pile foundations in order to transmit heavy structural (static) and dynamic (earthquake, winds) loads to competent soil layers. Recent destructive earthquakes in Northridge, (USA, 1994), Kobe (Japan, 1995), Izmit (Turkey, 1999), Tohoku (Japan, 2011) have proven the necessity of considering the interaction between structure, foundation, and soil.

Pile foundations have been used for hundreds of years, especially when the properties of the underlying soils do not provide the necessary support through a shallow foundation. Dynamic behavior and analysis of single piles and pile groups under dynamic loadings, such as in earthquakes, have become an area of interest for researchers and practitioners in civil engineering for over forty years because of serious damages observed in structures.

1.1 Literature Review

Soil-structure interaction (*SSI*) is a very complex phenomenon. *SSI* studies require an interdisciplinary approach with contributions from soil and structural mechanics, soil and structural dynamics, earthquake engineering, geophysics, material science,

computational and numerical methodologies, applied mathematics among others. Some of the principal problems related to *SSI* are summarized below (Kausel [1]):

- Response of a soil domain to external static or dynamic loads that acts on (or near) the surface. The loads originated from superstructures could be concentrated (column footing) or distributed (mat foundations), and they may be harmonic (machine foundations) in time or arbitrary (wind or wave).
- Response of the soil to seismic vibrations (called ground-borne) arising from earthquakes or some other sources such as fast moving trains in an underground tunnel.
- Response of rigid structures to ground-borne waves propagating in soil domain.
- Response of footings, foundations, piles, caissons, or tunnels embedded in soils to static, harmonic, or transient loads applied directly onto these structural elements.

Structures founded in rock are considered to be fixed-base structures because the extremely high stiffness (rigidity) of solid rock constrains the rock motion. However, structures in a soft soil deposit have a different response [2]. Ground motions that are not influenced by the existence of structures are referred to as the free-field motions; however, the inability of the foundation to conform to the deformations of the free-field motion would cause the motion of the base of the structure to deviate from the free-field motion. Secondly, the dynamic response of the structure itself would induce the deformation of the supporting soil. Thus, the response of the soil influences the motion of the structure and the response of the structure influences the motion of the soil, which is commonly referred to as the soil-structure interaction.

The most important effects of *SSI* is illustrated by Wolf [3] considering the case of the single degree of freedom (*SDOF*) system mounted on a rigid, massless, L-shaped foundation supported on an elastic soil deposit with a shear modulus, G , and a Poisson's ratio, ν , impacted with a harmonic base input motion, $u_b(t)$ (Figure 1.1). The *SDOF* structure is characterized by its mass, m , stiffness, k , and damping (dissipation of energy stored in the oscillation) coefficient, c .

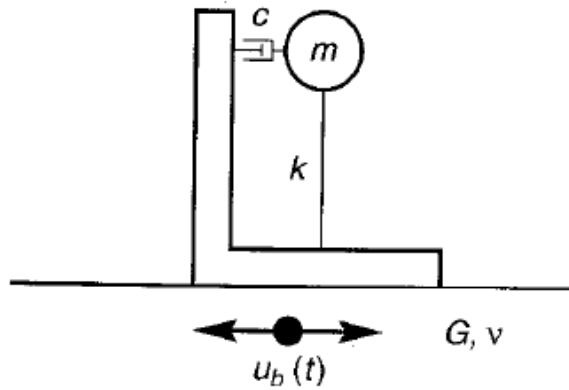


Figure 1.1 SDOF system on an elastic soil deposit [2]

Two significant effects of *SSI* on soil-foundation-structure system are as following:

- *SSI* reduces the natural frequency of the soil-structure system to a value lower than that of the structure under fixed-base condition. In other words, the period of the system increases.
- *SSI* increases the effective damping ratio to a value greater than that of the structure itself.

1.1.1 Analysis Methods of *SSI*

Analysis methods of *SSI* can be divided into two main categories: the *direct method* and the *multi-step method*.

1.1.1.1 Direct Method

In the direct method the entire soil-foundation-structure system (Figure 1.2) is modeled and analyzed in a single step. Its use requires a computer program that can consider models behavior of both the soil and the structure with equal rigor. The dynamic response of the interacting system is computed (for a finite element model) from the equations of motion

$$[M]\{\ddot{u}\} + [K]\{u\} = -[M]\{\ddot{u}_{ff}(t)\} \quad (1.1)$$

where $[M]$ mass matrix, $[K]$ stiffness matrix, $\{u\}$ displacement vector, and $\{\ddot{u}_{ff}(t)\}$ the specified free-field accelerations.

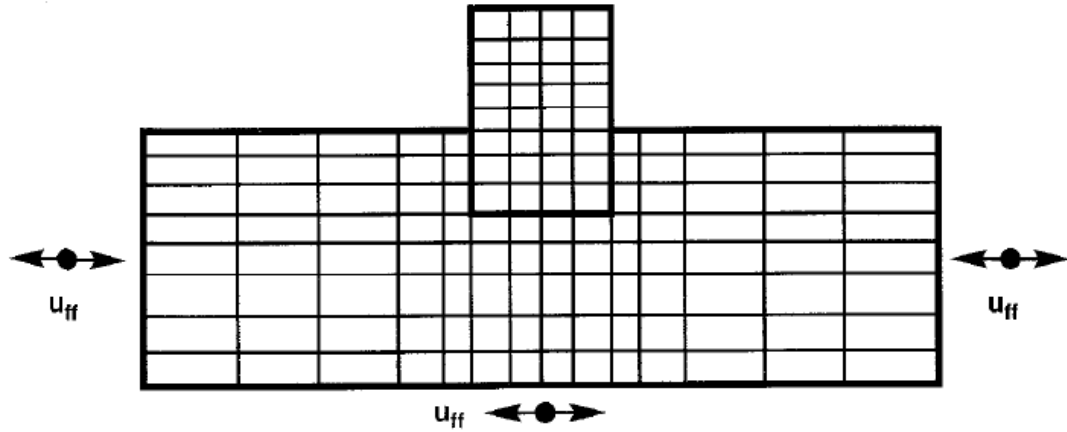


Figure 1.2 Entire soil-foundation-structure model in the direct method [2]

1.1.1.2 Multi-step (Substructure) Method

The multi-step method utilizes the principle of superposition to analyze the response of an entire system. In this method, the soil-foundation and superstructure are evaluated separately. This method is limited to the analysis of linear (or equivalent linear) systems because of its dependence on superposition.

The multi-step procedure consists of two steps:

- 1) Kinematic interaction analysis: foundation input motion is determined.
- 2) Inertial interaction analysis: the foundation input motion is applied to the superstructure and then the response of entire model is examined.

Kinematic Interaction

Earthquakes cause soil displacements in both horizontal and vertical directions due to seismic shaking. A structural foundation on the ground surface, or embedded in a soil layer, resists soil deformations since it is much stiffer than the soil; therefore, the deformations are different from that observed in the free-field. Thus, the presence of foundation influences the free-field soil motion. The relationship between soil and foundation is termed *kinematic interaction*.

The flexural mat foundation shown in Figure 1.3(a), for example, cannot follow the horizontally varying vertical component of the free-field motion. The rigidity of the embedded foundation in Figure 1.3(b) prevents it from following the vertically varying horizontal free-field motion. Likewise, the axial stiffness of the slab (Figure 1.3(c)) prevents developments of the incoherent deformation in immediately underlying soil. In

each of these cases, the motion of the foundation is affected by the kinematic interaction.

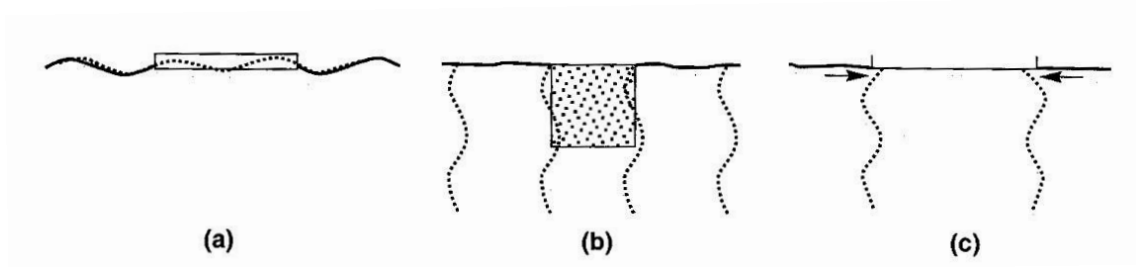


Figure 1.3 Kinematic interaction with free-field motions indicated by dashed lines: (a) flexural mat foundation on surface; (b) rigid embedded foundation; (c) stiff slab on surface [2]

The deformations due to kinematic interaction can be computed by assuming that the foundation has a stiffness but no mass. The equation of motion for this case is then:

$$[M_{soil}]\{\ddot{u}_{kin}\} + [K]\{u_{kin}\} = -[M_{soil}]\ddot{u}_b(t) \quad (1.2)$$

where $[M_{soil}]$ is the mass matrix assuming that the structure and the foundation have no mass (Figure 1.4(a)). Equation (1.2) is solved for $\{u_{kin}\}$, which is referred to as the foundation input motion (*FIM*).

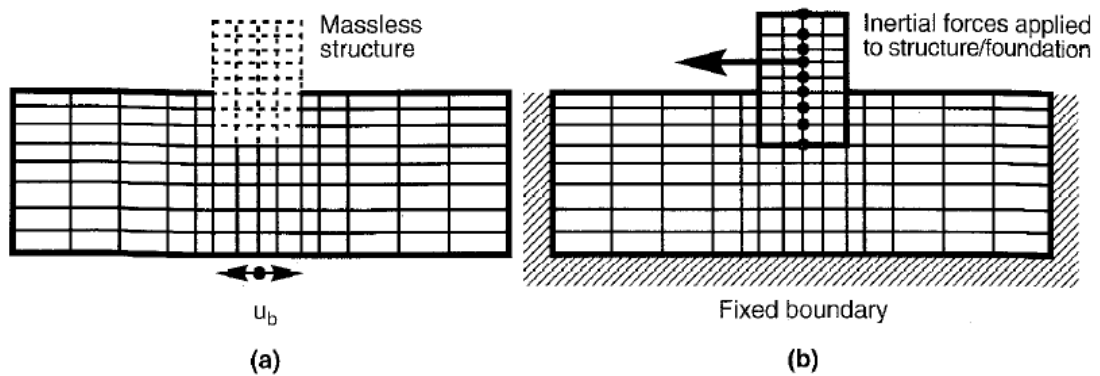


Figure 1.4 Analysis of (a) kinematic interaction and (b) inertial interaction [2]

Inertial Interaction

Structures and their foundation have a dynamic response to earthquake loads due to their mass. If the supporting soil is compliant, the dynamic forces of superstructure

transmitted through its foundation will produce foundation movements. The soil compliance effects on the resulting response are due to *inertial interaction*. The deformations related to inertial interaction can be computed from the equation of motion:

$$[M]\{\ddot{u}_{II}\} + [K]\{u_{iner}\} = -[M_{structure}]\{\ddot{u}_{kin}(t) - \ddot{u}_b(t)\} \quad (1.3)$$

where $[M_{structure}]$ is the mass matrix assuming that the soil has no mass (Figure 1.4(b)).

Note: A comprehensive literature review regarding subject of this thesis is presented in Chapter 2

1.2 Objectives of the Thesis

Pile foundations, as structural elements, are used to transfer structural loads through soft compressible soils, onto stiffer or less compressible soils (or rock) at depth, if and when the support provided by shallow foundations is inadequate. Weak soils, which may amplify ground motions, create a serious risk in earthquake-prone areas. Liquefaction and/or strain softening may impose additional demands on pile foundations.

Soil-pile-structure interaction (*SPSI*) problem may be investigated through numerous methods, such as through using an analytical solution, the multi-step (substructure) method, the p-y method, the finite element method, etc., recommended in literature. Analytical solutions are attractive for researchers investigating the basis of a problem although typically many simplifying assumptions are required. On the other hand, practicing/design engineers are typically interested in the stress and strain relationship of the piled-structure system under static and dynamic loads, thus only need tools to solve the problem. Advanced computer software that are able to consider soil and structure response using sophisticated constitutive material models have been developed in the last decade. Practical engineers use these programs creating numerical model of the problem during design and analysis process.

The objectives of the present study are listed in the following:

- To establish a numerical model for the *SPSI* problem that considers boundary conditions that are as realistic and as accurate as possible.
- To analyze soil – pile – structure interaction.
- To show the importance of kinematic interaction in piled-structure response.

- To investigate parameters (soil material behavior, phase angle, input motion characteristics, pile slenderness, period of superstructure) affecting the *SPSI*.
- To examine seismic motion acting on foundation in which site response, kinematic interaction, and inertial interaction are taken into account.
- To analyze pile response under dynamic earthquake loading.

1.3 Hypothesis

The analysis of piled-structures under earthquake loading is a formidable task for design engineers due to interaction within soil, foundation system embedded in ground, and superstructure (“*SFSI*” soil-foundation-structure interaction). The piles, which transfer superstructure loads to the ground as structural elements, and the superstructure are main components of the design problem.

With respect to pile foundations, only the inertial loads due to vibration of the superstructure are considered or soil displacements due to seismic waves propagating in soil domain (kinematic loading) are applied along the pile directly. However, both loading conditions should be taken into account in evaluation of pile response under seismic loading.

On the other hand, it is a common design practice regarding superstructure to neglect or simplify the effect of pile foundations on ground motions applied to the structure assuming a flexible pile results in period lengthening and increased damping that corresponds decreased structural forces relative to a fixed-base condition. However, the presence of piles influences system response significantly by refracting and reflecting incoming waves. Additionally, the superstructure and piles radiate vibration waves into the ground because of their mass.

1.4 Organizations

In Chapter 2: A literature review is presented including early history of soil-pile interaction, forces on pile during earthquakes, analysis methods, and pile performance under dynamic loads. Pioneering studies and important findings in them are explained briefly as well.

In Chapter 3: Established numerical models created by *OpenSees v.2.4.4* and *Plaxis 2D AE.02* are elucidated in detail. Model geometry, boundary conditions (significant for

dynamic loading), material models, damping properties, and solution method are provided in a comprehensive manner. Model is verified by analytical method (regarding soil-pile interaction) and different numerical tools (with respect to site response analysis).

In Chapter 4: Kinematic interaction between soil and pile is investigated using numerical tool created by *OpenSees v.2.4.4* under harmonic load and transient earthquake loads. The presence of solid piles in ground alters the wave propagation by refracting and reflecting incoming waves and, therefore, free-field motion and near pile motion indicate differences. Parametric analysis are performed to research effective parameters such as material model (linear or nonlinear), stiffness ratio between soil and pile, pile slenderness ratio, and input motion in terms of displacement and acceleration. Additionally, a kinematic interaction factor is proposed that considers phase angle variation in spatial direction.

In Chapter 5: Complete soil-pile-structure interaction problem has been addressed by numerical tool *Plaxis 2D AE.02* to make evaluation regarding soil-structure interaction phenomenon in which soil influences piled-superstructure response and vice versa. Sophisticated hypoplastic soil material model and embedded pile element features are used in the numerical model. The superstructure is modeled as single-degree-of-freedom system. Pile and superstructure responses are investigated by different parametric cases. Discussion is also made on the input motion.

In Chapter 6: The results of the parametric studies are summarized and recommendations for future research are made.

CHAPTER 2

LITERATURE REVIEW

A detailed review of the literature regarding the pile response to dynamic effects, specifically to earthquake loading, is presented in this chapter. A brief summary of the history of kinematic interaction is followed by a discussion of the forces acting on piles during earthquakes and performance of piles to this type of loading. Then, analyses used to solve such problems are given. Finally, important findings from previous works regarding soil-pile-structure interaction are presented.

2.1 Early History of Kinematic Interaction

French mathematicians Gabriel Lamé and Benoit Paul Emily Clapeyron have studied the problem of loads on or within an infinite (or semi-infinite) elastic body in the early part of the 19th century [1]. Thomson [4] gave expressions related to the problem of static forces acting on an elastic, infinite solid. This was followed by the solution of time varying problem about point forces in an infinite medium provided by Sir Gabriel Stokes [5]. The Stokes solution was adopted as a cornerstone in the boundary element method (*BEM*) and also that exerted influence in geophysics, acoustics, and other branches of science.

Joseph Boussinesq [6]–[8], another French mathematician, presented a solution for static, point vertical loads on the surface of elastic half-space, and also gave a closed-form solution for a rigid disk with flexible contact on the surface of a half-space in the last quarter of the 19th century. Sir Horace Lamb [9], a mathematician from South Australia, developed a fundamental solution for a homogeneous half-space subjected to a dynamic load on its surface. Raymond David Mindlin [10], who worked with Timoshenko at University of Michigan on applied mechanics, gave closed-form equations for the displacement relating to vertical and horizontal point loads buried at

an arbitrary depth below the surface of an elastic half-space. Erich Reissner [11] investigated the behavior of circular disks on elastic half-spaces subjected to harmonic vertical loads. He made notable contributions especially in analyzing *radiation damping* and *equivalent mass-spring-damper* analog system.

A great number of previous studies were focused on the behavior of a foundation system. The alteration of seismic waves because of the interaction between soil and the overlying structure is another substantial problem. Sezawa and Kanai [12]–[14], who published remarkable and pioneering papers with respect to scattered waves, claimed the severity of the motion in the superstructure was limited by the loss of energy in the form of waves that feedback into the soil and thus *SSI* is beneficial. This topic was taken up again by R. G. Merrit and G. Housner in 1954 [15]. They stated that lateral compliance of foundation has little effect or no effect on motions based on observed data. However, Housner [16] continued his observations and realized that motions were altered by actual strong motion. He noted that the waves in the ground were subjected to significant filtering. Nathan Newmark [17] discovered the *Tau Effect*, which provided the time delay in excitation to parts of the foundation.

The beginning of the modern era on this subject began four decades ago with profoundly influential papers by Veletsos and Wei [18] and Luco and Westmann [19], in which complete rigorous solutions related to circular plates on elastic half-spaces under dynamic excitations over a broad range of frequencies could be found.

“*Kinematic and Inertial Interaction*” terms were coined by Prof. Robert V. Whitman at MIT and first appeared in Kausel’s lecture notes in 1976 [20] and publication written by Seed, Whitman, and Lysmer [21].

2.1.1 Kinematic Interaction Studies Associated with Pile Foundations

The earliest theoretical studies related to pile foundations and kinematic interactions were made by Parmelee et al., Tajimi, Penzien, and Novak [22]–[25]. The first researchers focused on the complex dynamic stiffness of pile, which is called the “*impedance function*” [26].

The soil – pile interaction was studied using the finite element method (*FEM*) by Blaney et al. [27], Wolf and von Arx [28], Kuhlemeyer [29], and also using boundary element method (*BEM*) by Banerjee [30] and Banerjee & Sen [31].

Matlock et al. [32], [33] developed a lumped-mass model called the *p-y method* because large displacements and nonlinear behavior are extremely difficult to consider with the continuum theory. In addition to this, gapping between pile and soil was found to have an influence on the kinematic interaction by Trochanis et al. [34].

Piles are typically used in groups and their interaction with each other is referred to as the pile-soil-pile interaction or group effects. The first analyses involving pile-soil-pile interaction was conducted by Wolf and von Arx [28] using a model based on the *FEM*. Dynamic interaction factors considering the pile-to-pile effect due to pile grouping were proposed by Dobry and Gazetas [35] and Fan et al. [36].

Mostly shaking table tests and centrifuge tests were conducted to study the behavior of kinematic interaction between the soil and pile. Scott et al. [37] were the first to test model piles in a centrifuge; then Finn and Gohl [38] implemented a base shaker device to apply earthquake and harmonic motion to their centrifuge models. The first shaking table test was conducted by Kubo [39]. Moreover, Kagawa and Kraft [40] developed a nonlinear p-y method using shaking table results.

In 1990 - 2010, Gazetas and Mylonakis [41], [42] have contributed to kinematic interaction studies. Additionally, nonlinear behavior of soils was considered in kinematic interaction analyses by El-Naggar and Novak [43], [44]. Moreover, experimental tests were performed by Boulanger et al. [45] and Tokimatsu et al. [46].

Recently, Anoyatis et al. [47] have suggested an analytical formulation including pile boundary conditions to calculate the kinematic interaction. Shaking table tests were conducted to examine the effect of soil heterogeneity and nonlinearity on site response and kinematic pile bending by Chidichimo et al. [48]. Additionally, pile response under seismic excitation has been researched using numerical tools (*FEM*) by several researchers [49]–[51].

2.2 Forces on Pile under Seismic Loading

Forces acting on embedded pile foundations during a seismic event result from two phenomena: the first one is the resistance of the piles to the ground movements during the passages of seismic waves, called *kinematic forces*; the latter is the response of piles to the *inertial forces* generated by vibration of the superstructure [52].

In most of the actual cases, the deformation of piles due to vibration of a superstructure (inertial effect) attenuate very rapidly with depth and it typically vanishes within 10 – 15 pile diameters from the ground surface. Therefore, inertial forces acting on pile may be significant only near the ground surface. Conversely, displacements of soil due to wave propagation in the soil (kinematic forces) act only at relatively deep elevations [53]. Kaynia and Mahzooni [52] investigated forces on pile under dynamic loads by numerical method using a soil – pile – structure model. The numerical results showed that the kinematic interaction can be the main factor for the developed seismic shear force and bending moment in the piles except when the impacting frequencies are close to the natural frequency of the soil – structure system. At or around a system's natural frequency, the effects of inertial interaction may significantly be larger than that from kinematic interaction.

Tokimatsu et al. [46] performed tests to investigate the soil – pile – structure interaction with the help of a large shaking table test facility at Japan National Research Institute for Earth Science and Disaster Prevention (NIED). They found that inertial forces due to superstructure vibration are dominant in stiff and/or non-liquefied ground. On the other hand, in soft and/or liquefied grounds as well as laterally spreading ground, both kinematic and inertial forces play an important role.

The response of pile foundations under seismic loading can be considered in three zones (Figure 2.1) [54]:

- i. *Near surface zone*: This zone, which extends to approximately eight pile diameters beneath the soil surface, is dominated by the effects of inertial loads.
- ii. *Intermediate zone*: This zone, which exists between the near surface and deep zone, is influenced by both inertial and kinematic effects.
- iii. *Deep Zone*: This zone, which is below 12 to 15 pile diameters from the ground surface, is dominated by kinematic effects.

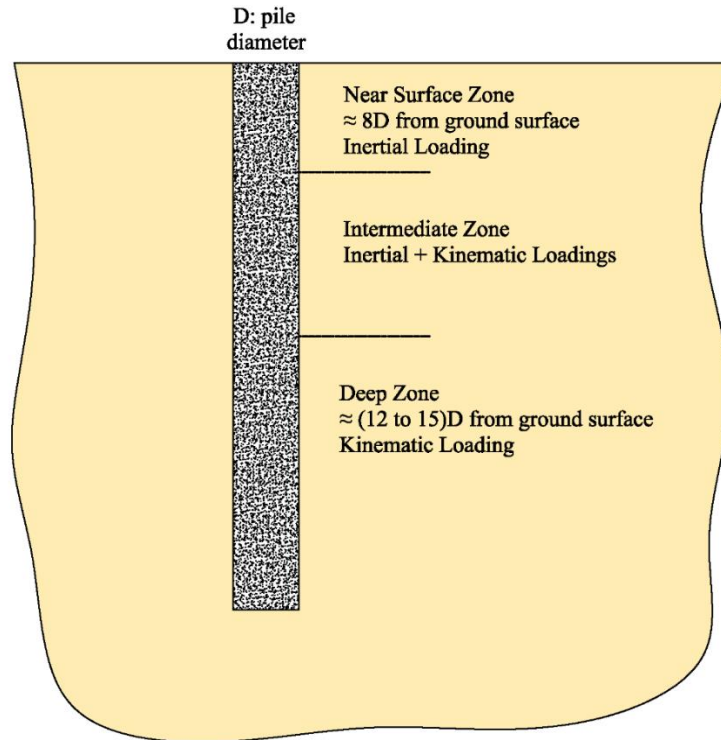


Figure 2.1 Forces acting on pile along its length during seismic excitation

2.3 Pile Performance during Earthquakes

Many cases of damage to piles and pile-supported structures have been observed in major earthquakes that have occurred in the last century, such as Alaska (1964), Niigata (1964), Mexico City (1985), Loma Prieta (1989), Kobe (1995), and Kocaeli (1999). Mizuno [55] investigated pile damages during earthquakes in Japan from 1923 to 1983. Ross, Seed, and Migliacio [56] made a comprehensive survey related to pile supported structures, especially bridges, after Alaska (1964) earthquake. Matsui and Oda [57] observed damages on foundations supporting the six major elevated highways in the Kobe area. Tokimatsu et al. [58] made observations related to liquefaction effects in Fukaehama. In addition to qualitative observations after seismic shaking, data from instrumented pile-supported structures has been obtained [59]–[61].

Meymand [62] made a comprehensive compilation of the literature related to pile performance during earthquakes. From instrumented cases, it can be seen that soil-pile-structure interaction often results in spectral de-amplification of pile cap motions relative to free-field motions. It was generally seen to happen at periods less than the period of the entire soil-pile-structure system. This condition was observed for a number

case histories of building structures subjected to low intensity shaking in Japan and bridge structures subjected to moderate to high levels of ground shaking. Kinematic interaction is generally the dominant effect at low intensity; inertial forces from the superstructure dominate the system response at high levels of shaking. The following failure modes can be recognized from observed damage after seismic shaking:

- Loss of soil bearing capacity may occur because of strain softening of cohesive soils or liquefaction of granular soil. Pile head (or pile – cap connection) is subjected to excessive displacements from structural inertial loads and bending strain due to kinematic interaction. Additionally, the piles frequently undergo settlement, punching failure, and/or tensile pull-out failure.
- Lateral spreading, large lateral loads and lateral displacements due to liquefaction often cause damages in pile.
- Piles may be subjected to large bending moment at interfaces between soil layers due to difference of stiffness between soft and stiff soil layers.

Potential failure modes of pile foundations under seismic shaking are given in Figure 2.2.

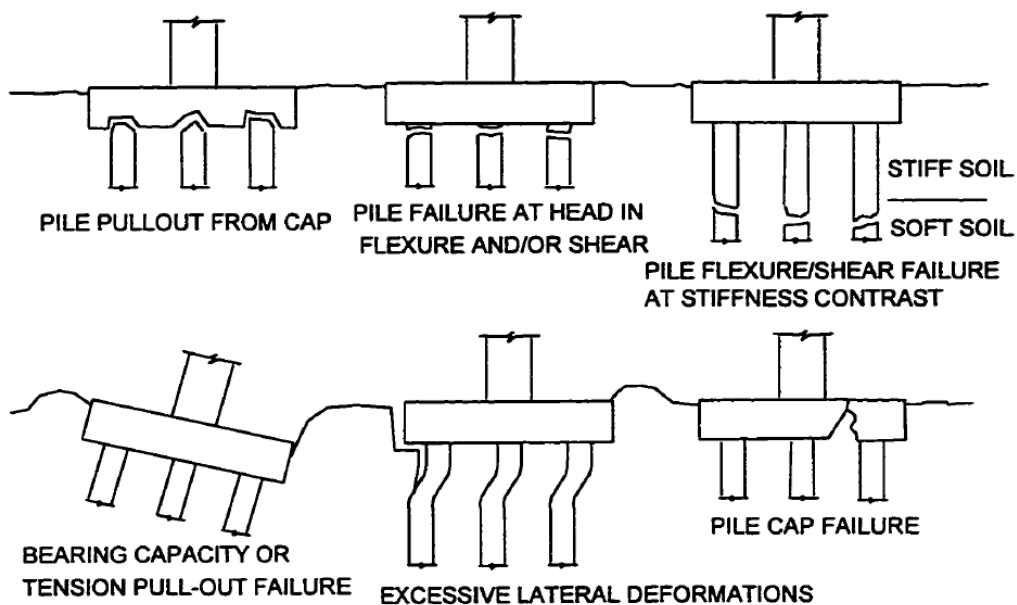


Figure 2.2 Possible failure modes for pile foundations under seismic shaking [62]

2.4 Analysis Methods

As previously explained, the soil-pile-structure interaction problem can be analyzed with the direct (one-step) method or the multi-step (substructure) method. Both methods have their advantages and disadvantages. The sketch of the problem is shown in Figure 2.3, where M represents the mass of superstructure, a_{st} , a_p , and a_r correspond to the acceleration of structure, pile foundation, and rock input motion, respectively.

The decomposition of the problem into subtasks enables the designer to consider particular aspects of the problem. Empirical knowledge accumulated over years, can be readily utilized as well. For instance, well-established methods of determining lateral pile deflection can be used in determining pile-head stiffness and damping. However, in the superposition theorem the values of the kinematic interaction and inertial interaction are valid only if linearity for the soil, pile, and structure behavior is assumed. Nevertheless, the superposition can be applied to moderately nonlinear systems as an engineering approximation [42]. This is because pile deformations due to superstructure load attenuate very rapidly with depth. They practically disappear below a pile length on the order of 10 pile diameters below the ground surface. Hence, shear strains induced in the soil due to superstructure loads can be significant only near the ground surface. By contrast, soil displacements due to vertical S-waves can be important at relatively deep elevations.

On the other hand, complete interaction analysis of a soil-pile-structure system is only possible through utilizing computer codes that employ the finite element or the finite difference method. However, few computer codes are readily available to analyze a complete system response with foundations consisting of a group of piles. Additionally, analysis outcomes are questionable especially when the nonlinear range for the soil behavior is reached under strong seismic excitation.

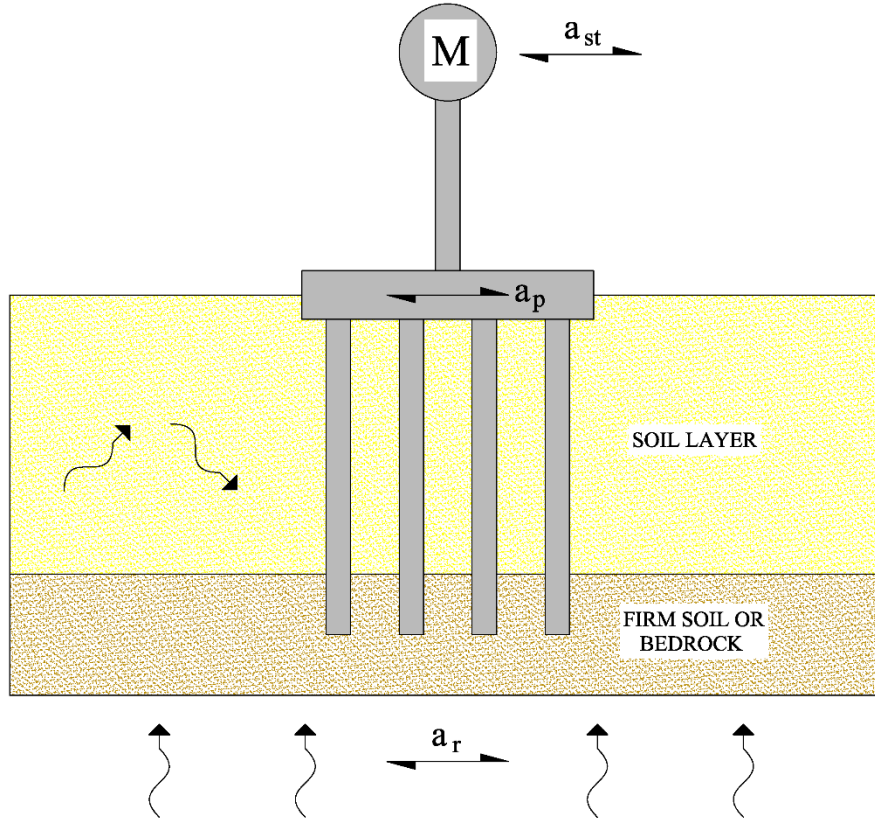


Figure 2.3 Sketch of the soil-pile-structure interaction problem

2.4.1 General Overview of Multi-Step (Substructure) Method

The seismic response of the system (such as in Figure 2.3) to a basal rock acceleration, a_r , can be computed either in a single step, by solving the following equation:

$$[M]\{\ddot{u}\} + [K]\{u\} = -[M]\{I\}a_r \quad (2.1)$$

where:

$\{u\}$ = relative displacement vector of points in the soil, piles, or the structure

$\{I\}$ = unit directional vector

$\{M\}$ = mass matrix of the system

$\{K\}$ = stiffness matrix of the system

Alternatively, the relative displacement vector $\{u\}$ can be expressed as the sum of inertial and kinematic displacements:

$$\{u\} = \{u_{iner}\} + \{u_{kin}\} \quad (2.2)$$

where: $\{u_{iner}\}$ = inertial relative displacement vector and $\{u_{kin}\}$ = kinematic relative displacement. Then the following two coupled equations can be solved:

$$[M_{soil}]\{\ddot{u}_{kin}\} + [K]\{u_{kin}\} = -[M_{soil}]\{I\}a_r \quad (2.3)$$

$$[M_{structure}]\{\ddot{u}_{iner}\} + [K]\{u_{iner}\} = -[M_{structure}](\{\ddot{u}_{kin}\} + \{I\}a_r) \quad (2.4)$$

where:

$[M_{soil}]$ = mass matrix assuming that only the soil and pile have a mass

$[M_{structure}]$ = mass matrix assuming that only the structure has a mass

The superposition of Equations (2.3) and (2.4) results in Equation (2.1). Equations (2.3) and (2.4) are the mathematical explanation of kinematic and inertial interaction, respectively. The problem can be subdivided into two analyses: *kinematic interaction* effect and *inertial interaction* effect, shown schematically in Figure 2.4.

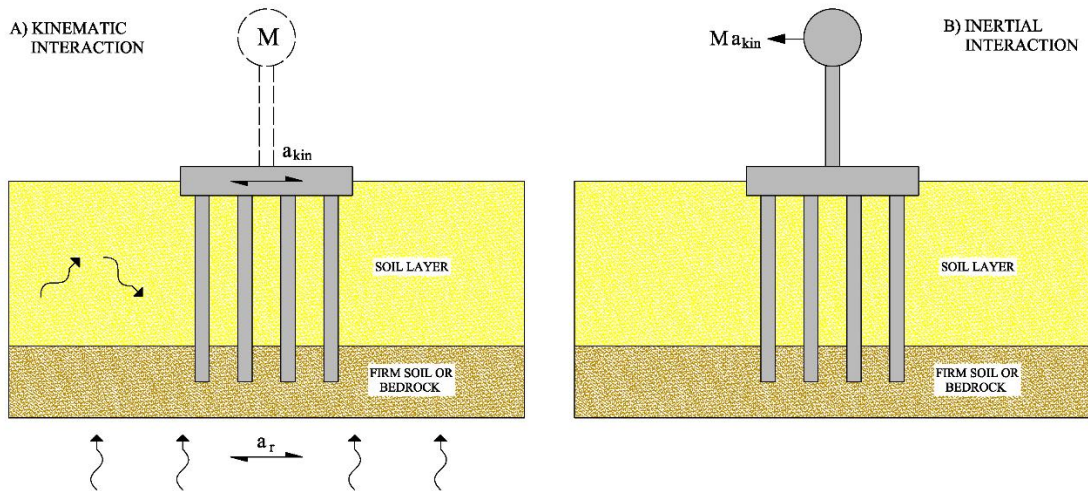


Figure 2.4 Decomposition of the soil-pile-structure problem into kinematic and inertial interaction

For convenience, the inertial response is further subdivided into two consecutive independent analysis steps, as follows:

- i. Estimation of the dynamic impedances, springs and dashpots, at pile head or the pile group cap, associated with the swaying, rocking, and cross-swaying-rocking motion of the foundation, Figure 2.5(a).
- ii. Analysis of the dynamic response of the superstructure supported on the springs and dashpots, Figure 2.5(b).

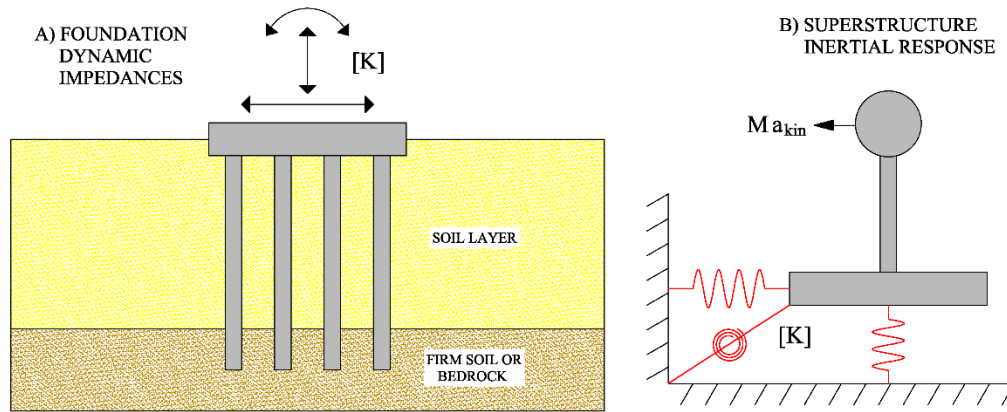


Figure 2.5 Analysis of inertial interaction in two steps

2.4.2 General Overview of Analysis Methods

The soil-pile-structure system under seismic excitation can be analyzed using one of the analysis methods that have been developed and suggested in the literature. Most prominent analysis procedures are the *Winkler model*, the *boundary element method*, and the *finite element method*.

2.4.2.1 Winkler Model

Pile deflection and settlement under static top loading (at pile-head) can be estimated by a “*Winkler foundation*” considering the pile as a beam or column supported by a series of independent horizontal (lateral) and/or vertical (axial) springs distributed along its length. Based on field experiments and measurements, the soil response at a particular point at depth is represented by a given p - y curve for lateral loading or a t - z curve for axial loading.

The Winkler model has been applied to dynamic soil-structure interaction problem with success [24]. With respect to soil-pile interaction, the soil reaction is represented by a set of continuously-distributed *springs*, k , and *dashpots*, c , which are functions of the loading frequency. An elasto-dynamic solution was developed by Novak et al. [63] to estimate k and c , in which a rigid cylindrical rod of unit thickness (pile slice) is surrounded by soil (extending radially to infinity) and is subjected to horizontal or vertical oscillations. The spring parameter may be obtained with the finite element

method to overcome some of the limitations of Novak's solution [64], [65]. The Winkler Model has been successfully extended to analyze soil-pile-structure interaction for different boundary conditions of pile or layered soil profile [47], [66].

2.4.2.2 Finite Element Method (*FEM*)

The *FEM* is one type of numerical procedure from a class of finite methods and it is most frequently used in practice. In analyses of dynamic problems by the *FEM*, important points regarding boundary condition and element size must be considered.

The infinite soil geometry in the horizontal and vertical directions must be represented by a model of finite size. Such a finite model can create a fictitious box effect that alters wave propagation and, therefore, distorts its dynamic characteristics. Therefore, wave absorbing boundaries are placed to consider the radiation of wave-carried energy into the outer region, which is not included in the model.

Various boundary types are presented in literature. A *viscous boundary* absorbs most (not all) of the incident outward going waves and it is placed at a definite distance from the area of interest (foundation – structure system) [67]. A *consistent boundary* was developed by Kausel et al. [68] and was utilized in dynamic analysis of pile by Blaney et al. [27]. Additionally, the *Domain Reduction Method* [69] and the *Periodic Boundary Condition* can also be used [70].

With respect to the element size, the general recommendation is to remain below one-fifth to one-eighth of the shortest wavelength [2].

2.4.2.3 Boundary Element Method (*BEM*)

This semi-analytical method (*BEM*) utilizes closed-form solutions for the related wave equations for the soil domain and discretizes only the boundaries and interfaces of the system. This closed-form solution, known as “*fundamental*” solution or “*Green's function*”, is able to exactly reproduce radiation of wave energy to infinity, without lateral boundaries. It also involves discretization of the pile-soil interface into a number of cylindrical segments with the base of the pile as a circular disk.

Formulations of *BEM* have been developed for a single pile and a pile group subjected to dynamic loading [71]–[74]. A method combining *BEM* and *FEM* has been developed by Padrón et al. [75].

2.5 Previous Studies with respect to Kinematic Interaction

Great number of studies exist in the literature researching soil-pile interaction and kinematic interaction. Several pioneering studies are summarized below.

Note: Symbols in this section are given as they were used in their respective references and were also not included in the symbol list. However, relevant explanations are given as necessary.

Blaney et al. [27] studied pile behavior under dynamic loads using a discrete model and finite elements method. The effect of the pile on the motion at the free surface was investigated by comparing displacements atop the pile (u_p) and displacements at the free surface of the soil (u_s) without pile with increasing frequency ($b_0 = \omega H/V_s - \omega$: circular frequency, H : soil thickness, and V_s : soil shear wave velocity). The change in the ratio of u_p/u_s is shown Figure 2.6. In the small frequency range, the pile displacement can be larger than the free surface soil displacement. Small H/R values represent caisson type of a foundation ($H/R \leq 20$) while large values represent pile foundations (R : width of the pile). The caisson foundations restrict dynamic motion in low frequency values (u_p/u_s drops quickly); pile foundation follow the soil displacement in those frequency range.

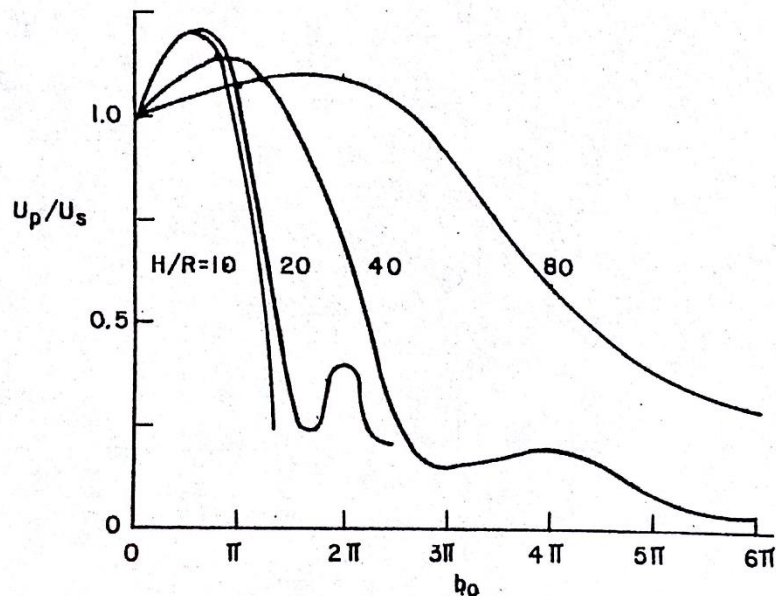


Figure 2.6 Comparison of the pile displacement and free surface displacement for different values of H/R [27]

The seismic response of pile groups was studied by Kaynia [72]. He proposed an analytical formulation to estimate dynamic response of single pile and pile groups. He performed parametric studies considering the boundary condition at the pile head (fixed and hinged), different spacing “ s ” between adjacent piles, and soil strength (soft and stiff) to gain insight into the response of piles under dynamic loading. The lateral displacement at the pile head u was compared with the free-field displacement u_g and a transfer function was defined by increasing dimensionless frequency a_o (2.5) in which ω is angular frequency, D is pile diameter, and V_s^* is a characteristic value of the soil S-wave velocity:

$$a_o = \omega D / V_s^* \quad (2.5)$$

Absolute value of transfer functions (u/u_g) and rotation of the pile cap, $\phi d/u_g$ in which ϕ is rotation, for the horizontal displacement and 3x3 fixed head pile groups in soft soils is given in Figure 2.7. The effect of pile number in group is presented in Figure 2.8 for stiff soil with $s/d = 5$.

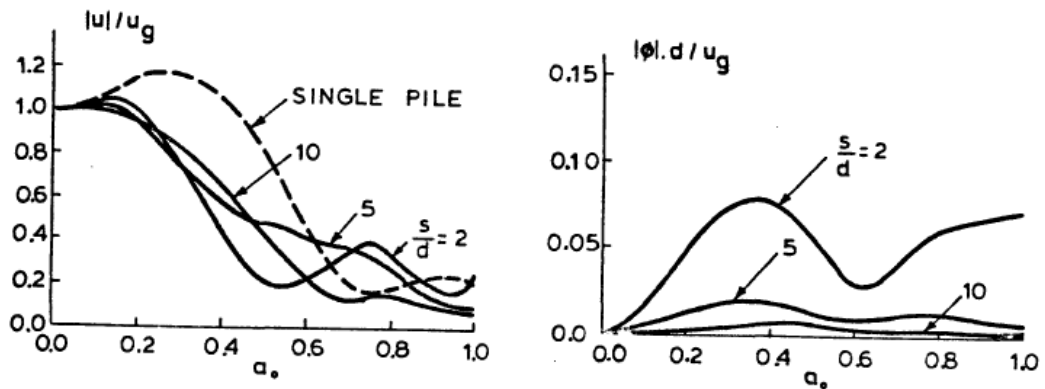


Figure 2.7 Transfer function and rotation of the pile cap for 3x3 pile groups in soft soil medium [72]

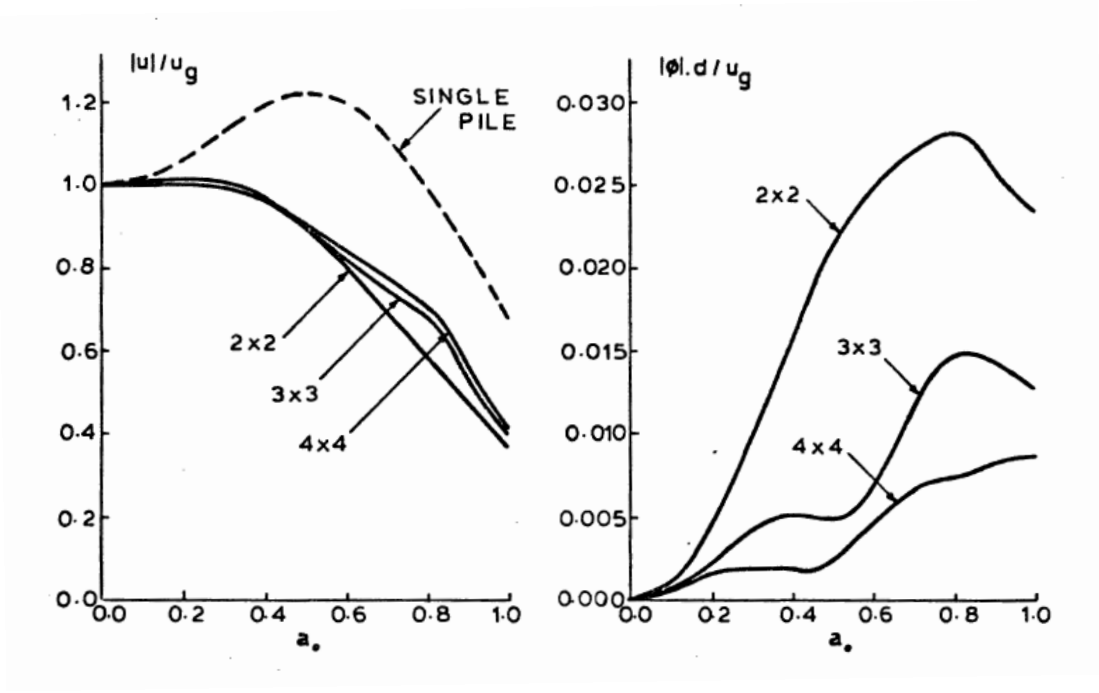


Figure 2.8 Transfer function and rotation of the pile cap for pile groups in stiff soil medium [72]

The results of Kaynia's study indicate that: 1) behavior of pile group is strongly frequency-dependent; 2) spacing and number of piles have minor effect on the lateral seismic response; 3) interaction effects are more significant for flexible soil media; and 4) the rotation of the foundation can be neglected for foundations having a large width.

Gazetas [53] investigated the seismic response of end-bearing single piles embedded in a number of idealized soil deposits and subjected to vertically propagating S-waves using the finite element formulation suggested by Blaney et al. [27]. The studied problem and soil profiles are shown in Figure 2.9 and Figure 2.10, respectively. The pile was modeled as a linearly elastic flexural beam with a circular cross-section of diameter D , stiffness E_p , and mass density of pile ρ_p . The soil is linearly hysteretic continuum with a constant Poisson's ratio ν_s , mass density of soil ρ_s , and hysteretic damping ratio β_s , and Young modulus $E(z)$ varying with depth. Vertically harmonic S waves were applied at the base as a displacement: $u_g(t) = u_g \cdot \exp(i2\pi ft)$.

The displacement of the pile due to lateral excitation transmitted from the superstructure (inertial interaction) may attenuate rapidly with depth which is typically within 10 – 15 diameters from the ground surface. Hence, shear strains induced in the soil due to inertial effects may be significant only near the ground surface. Conversely, shear

strains induced by vertical S-waves in the soil (kinematic interaction) may be important at only relatively deep levels.

If there was no pile, vertically S-waves would cause only horizontal displacements in the free-field soil. However, a pile is relatively much stiffer and may change the wave motion by diffracting and reflecting the vertical S-waves. Thus, the displacement atop pile u_p differs from the free field displacement u_o . Furthermore, the same conclusion is also valid for rotational ϕ behavior. Therefore, displacement and rotation kinematic interaction factors (these are equal to transfer functions defined by Kaynia [72]) were defined as given by Equations (2.6) and (2.7), respectively. In these equations, I_u : displacement kinematic interaction factor; I_ϕ : rotation kinematic interaction factor; ϕ_p : rotation atop pile; r_o : radius of pile (D/2).

$$I_u = \frac{u_p}{u_o} \quad (2.6)$$

$$I_\phi = \frac{\phi_p \cdot r_o}{u_o} \quad (2.7)$$

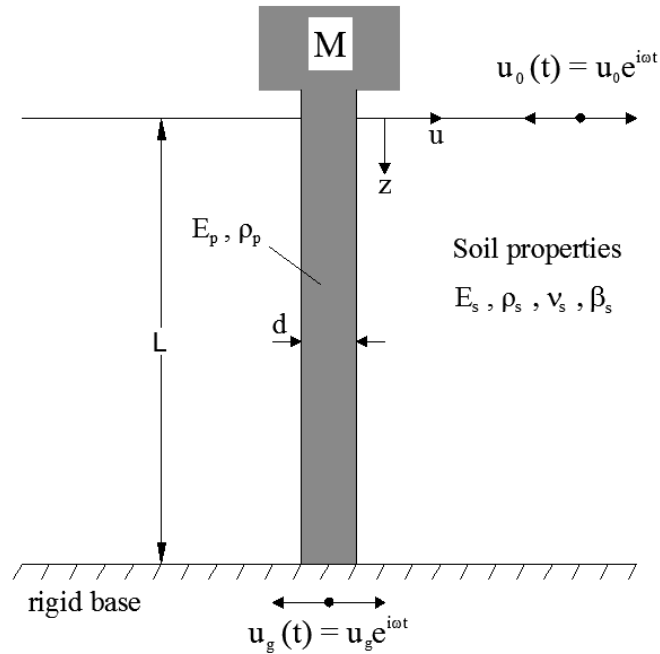


Figure 2.9 Studied soil-pile-structure problem [53]

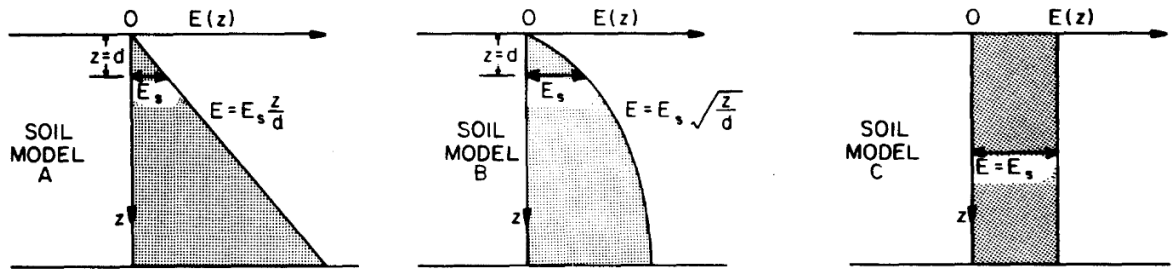


Figure 2.10 Soil profiles [53]

An extensive parametric study was presented by Gazetas [53] and the following parameters were found to be the most influential factors for the response of a soil-pile system:

- The stiffness ratio E_p/E_s of the pile Young's modulus over a characteristic Young's modulus of the soil.
- The slenderness ratio L/D (length over diameter) of the pile.
- The frequency ratio f/f_1 (excitation frequency over the fundamental frequency) of undisturbed soil deposit.
- The relative frequency factor f_{st}/f_1 (fundamental frequency of the pile-supported superstructure over the fundamental frequency of the soil deposit).

Results from parametric studies for the variation of kinematic interaction factors considering the stiffness ratio and the soil type are shown in Figure 2.11 and Figure 2.12, where interaction factors vary with increasing frequency ratio f/f_1 .

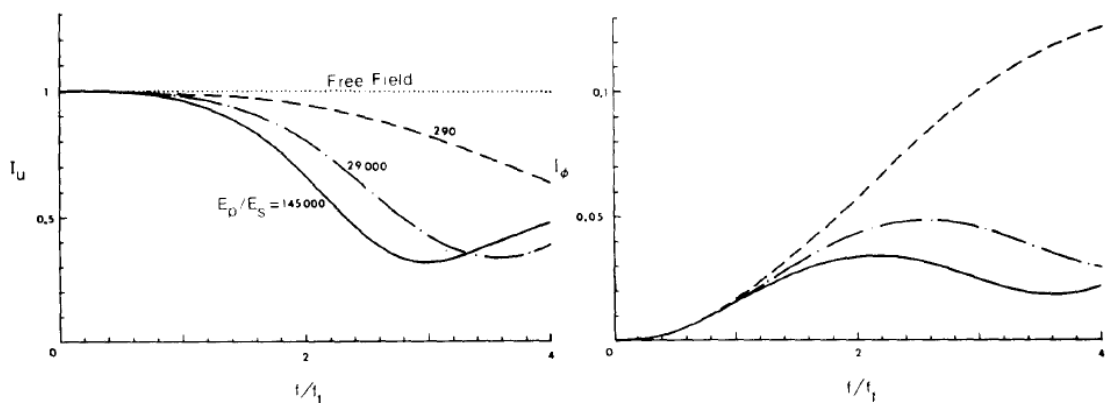


Figure 2.11 Influence of stiffness ratio (E_p/E_s) on kinematic interaction factors; $L/D = 40$, Soil Model A, $\beta_s = 0.05$, $\nu_s = 0.4$, $\rho_p/\rho_s = 1.6$ [53]

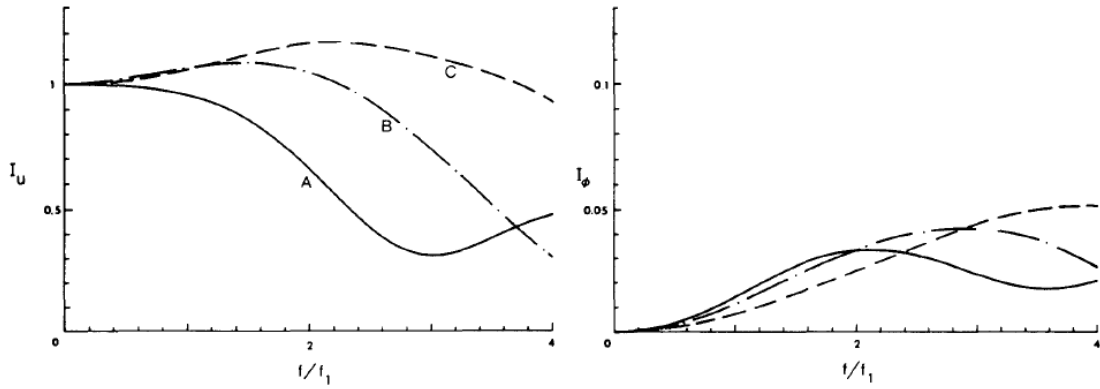


Figure 2.12 Influence of soil type on kinematic interaction factors; $L/D = 40$, $\beta_s = 0.05$, $\nu_s = 0.4$, $\rho_p/\rho_s = 1.6$ [53]

An example of a complete analysis of soil-pile-structure interaction is depicted in Figure 2.13, in which the effects of both kinematic and inertial interaction are combined. First resonant peak occurs at natural frequencies of the superstructure. Furthermore, the highest peaks of the displacement interaction curves occur at approximately the same frequency, $f \approx f_{st}$. Therefore, as the mass m of the superstructure increases, the peak tends to occur at lower frequencies of excitation. On the contrary, small mass means very flat resonant peaks.

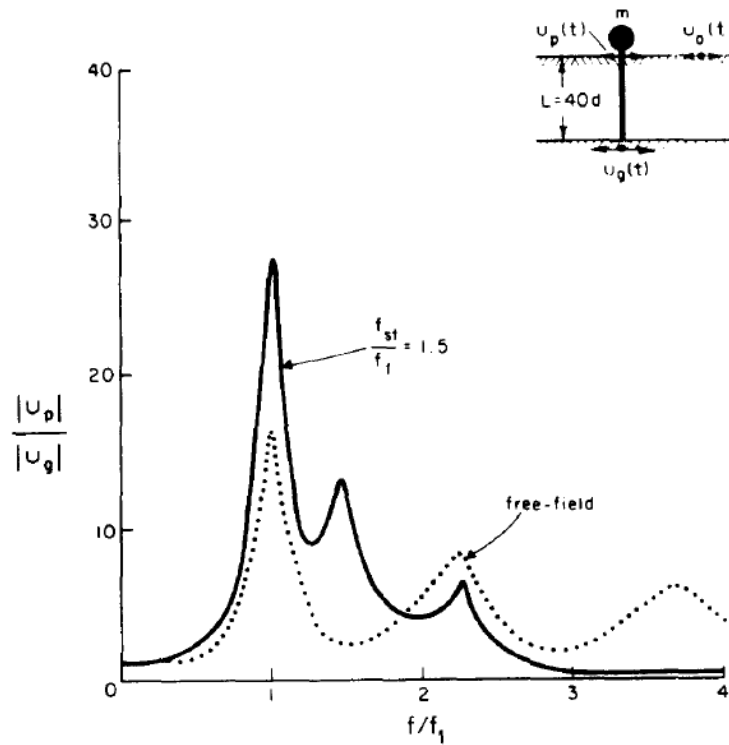


Figure 2.13 Complete soil-pile-structure analysis [53]

Fan et al. [36] studied kinematic response of floating single piles and pile groups connected through rigid massless caps and subjected to vertically propagating S waves. Three categories of floating vertical piles were investigated in this paper with given soil profiles (Figure 2.14):

- A single free-head and fixed-head pile.
- A rigidly capped (fixed) pile group, which are two, three, four, six, and nine in a row.
- A rigidly capped square group with configurations of 2x2, 4x4, and 6x6.

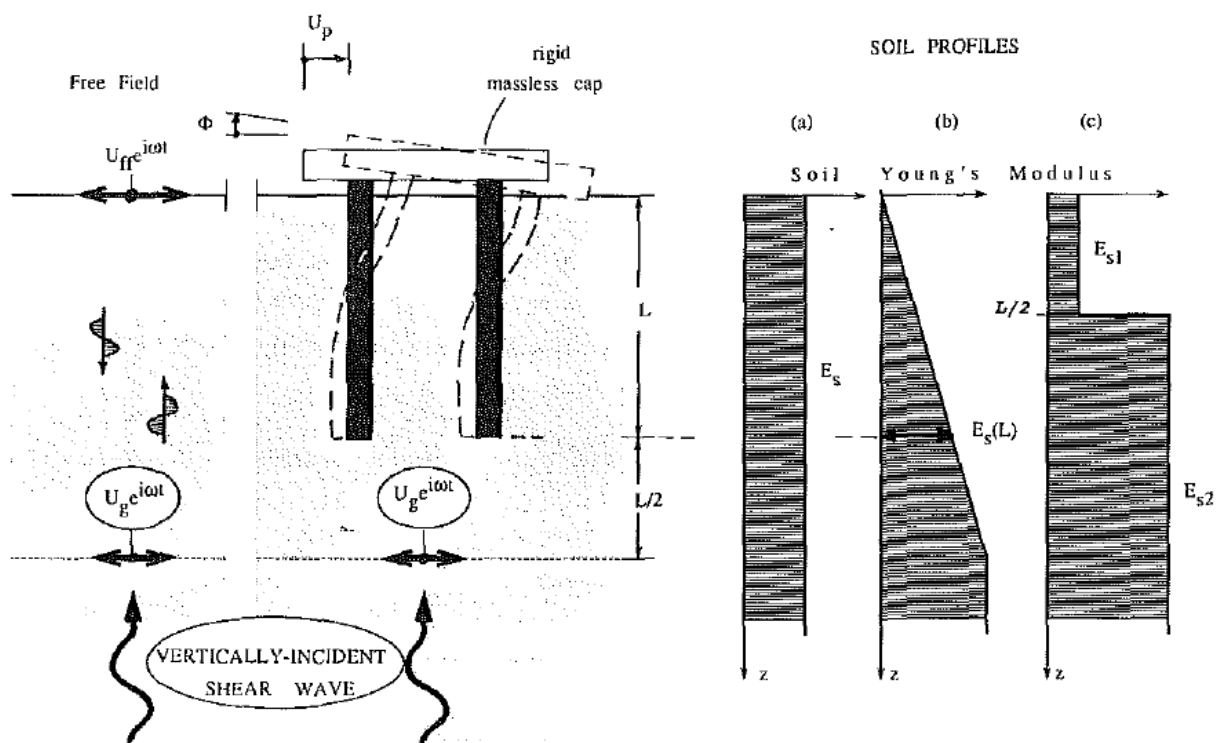


Figure 2.14 Studied problem and soil profiles [36]

All piles were considered as linear-elastic beam with constant stiffness and embedded in three different soil deposits (Figure 2.14). The soil was assumed to be linear hysteretic continuum with constant Poisson's ratio ν_s , mass density of soil $\rho_s = 0.7\rho_p$, and hysteretic damping ratio β_s . Each soil – pile – foundation system was excited by vertically propagating harmonic S-waves. Analyses were performed using the formulation by Kaynia and Kausel [72], Blaney et al. finite element formulation [27], and Ahmad boundary element formulation [74].

Pile foundations resist soil motion when they are subjected to propagating seismic waves. Therefore, seismic waves are scattered near piles and need to be modified. As a result, the seismic excitation at the structure base differs from the free-field motion. The kinematic interaction effect on soil-pile-foundation system were portrayed in the form of two kinematic response factors I_u (2.6) and I_ϕ (2.7) as function of dimensionless frequency (see (2.5)). The horizontal displacement u_p and angle rotation ϕ_p are complex numbers due to generation of both radiation damping (diffracted waves spreading away from each pile) and material damping (hysteretic action in the soil).

The general shape of kinematic interaction factor consists of three fairly distinct regions in the frequency range (Figure 2.15). At low frequency region ($0 < a_0 < a_{01}$), pile follows the seismic ground motion. At intermediate frequency region ($a_{01} < a_0 < a_{02}$), I_u declines rapidly with increasing frequency. At high frequency region ($a_{02} < a_0$), fluctuates around a constant value.

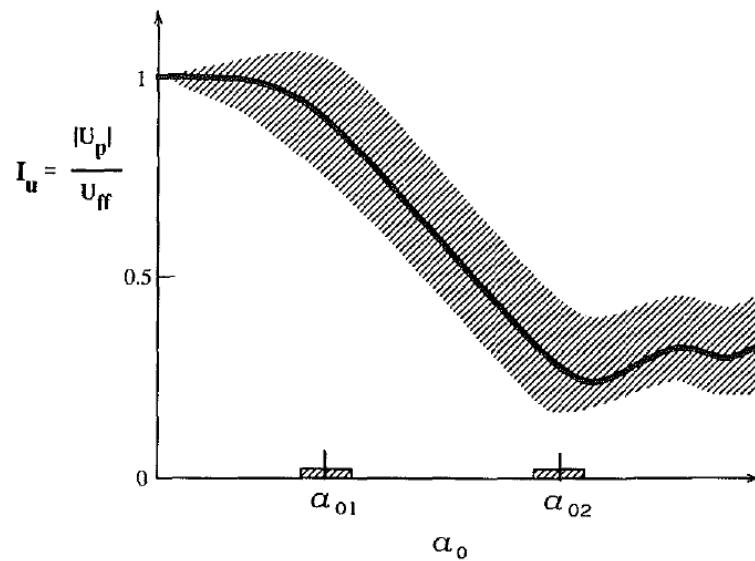


Figure 2.15 General form of the displacement kinematic interaction factor [36]

A few results with respect to pile groups are also shown in Figure 2.16 and kinematic interaction effects can easily be seen.

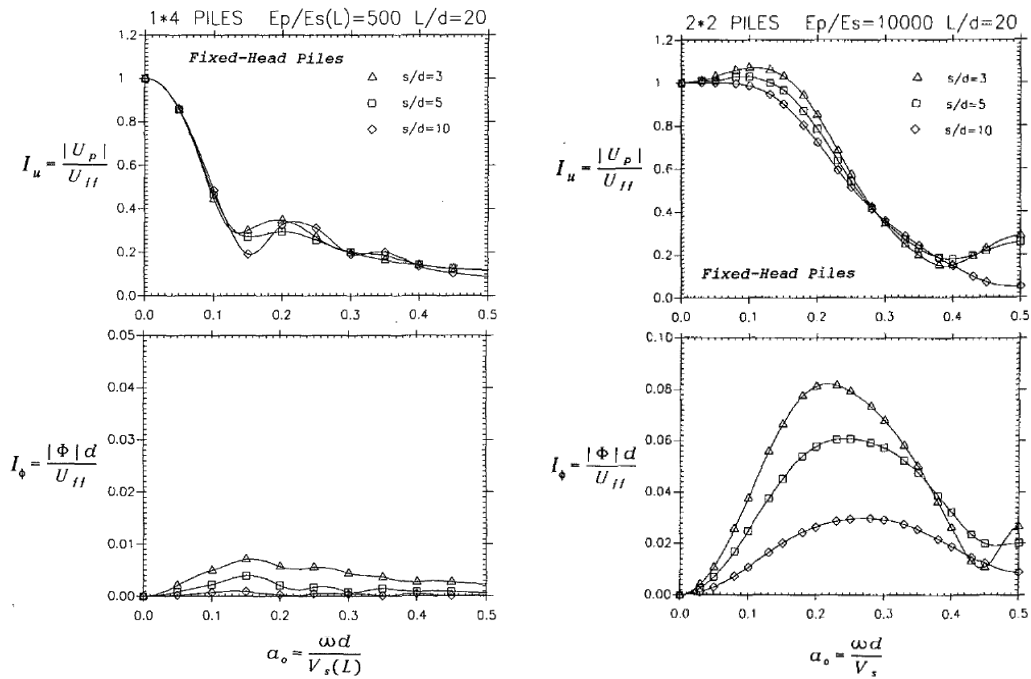


Figure 2.16 Kinematic seismic response of pile groups [36]

Makris and Gazetas [64] researched dynamic pile-soil-pile interaction and lateral seismic response of a pile group embedded in a homogeneous soil layer. The seismic response of a pile group may differ from the response of each single pile in a group because each pile is affected not only by its own load but also by the load and deflection of neighboring piles. A simplified three-step procedure was proposed to estimate dynamic interaction of two vertical piles in this study. Two loading types were considered: lateral pile-head loading (inertial interaction) and vertically propagating seismic S waves (kinematic interaction) (Figure 2.17).

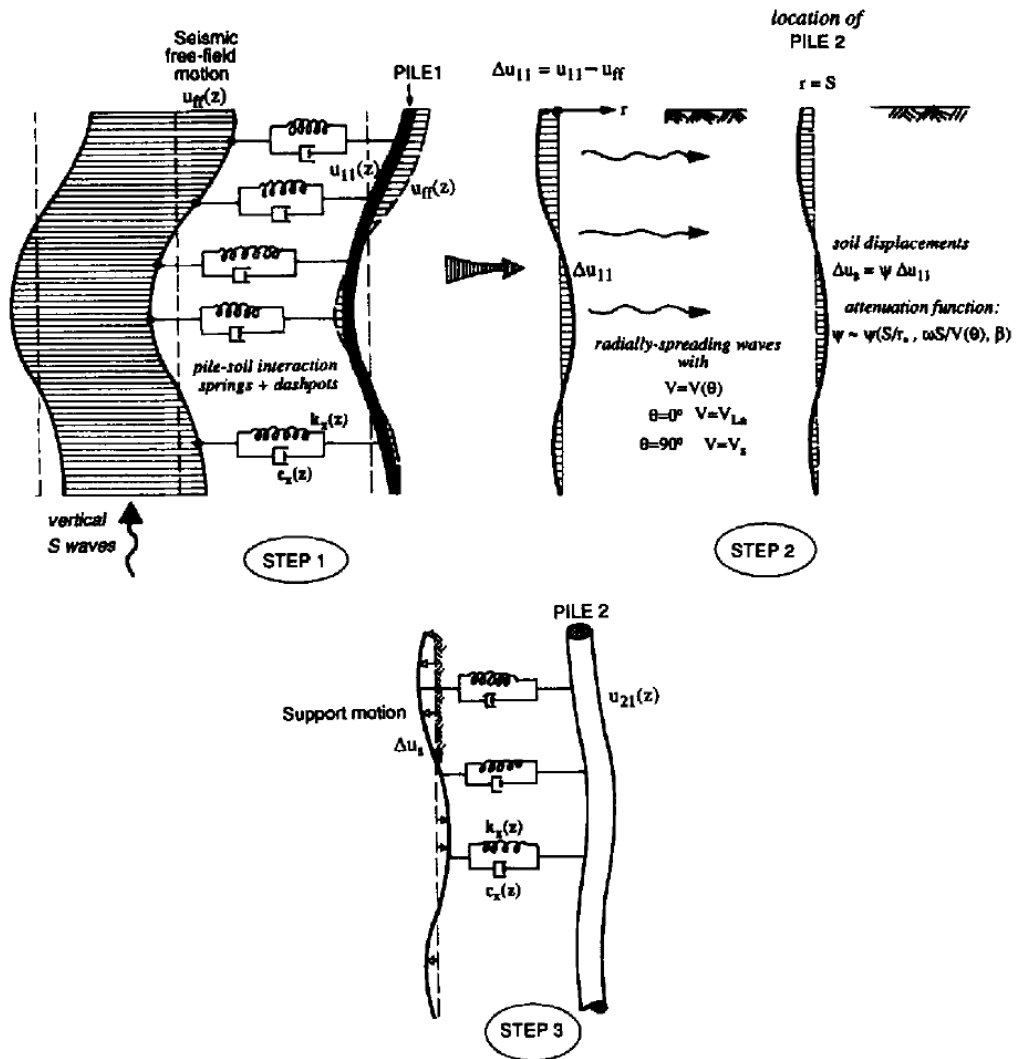


Figure 2.17 Three-step procedure for estimating the influence of Pile 1 upon the next Pile 2 under kinematic loading [64]

In the first step, the lateral deflection, $u_{11}(z)$, of a single pile (pile 1) is determined using procedures available such as FEM, BEM, or semi-analytical formulation. After that the difference between single pile deflection and free-field soil is calculated in second step ($\Delta u_{11} = u_{11} - u_{ff}$). Finally, soil displacements are applied on next pile (pile 2) considering the effect of pile 1 and pile 2 resists incoming waves and will modify the motion. An analysis result is shown in Figure 2.18 related to kinematic loading.

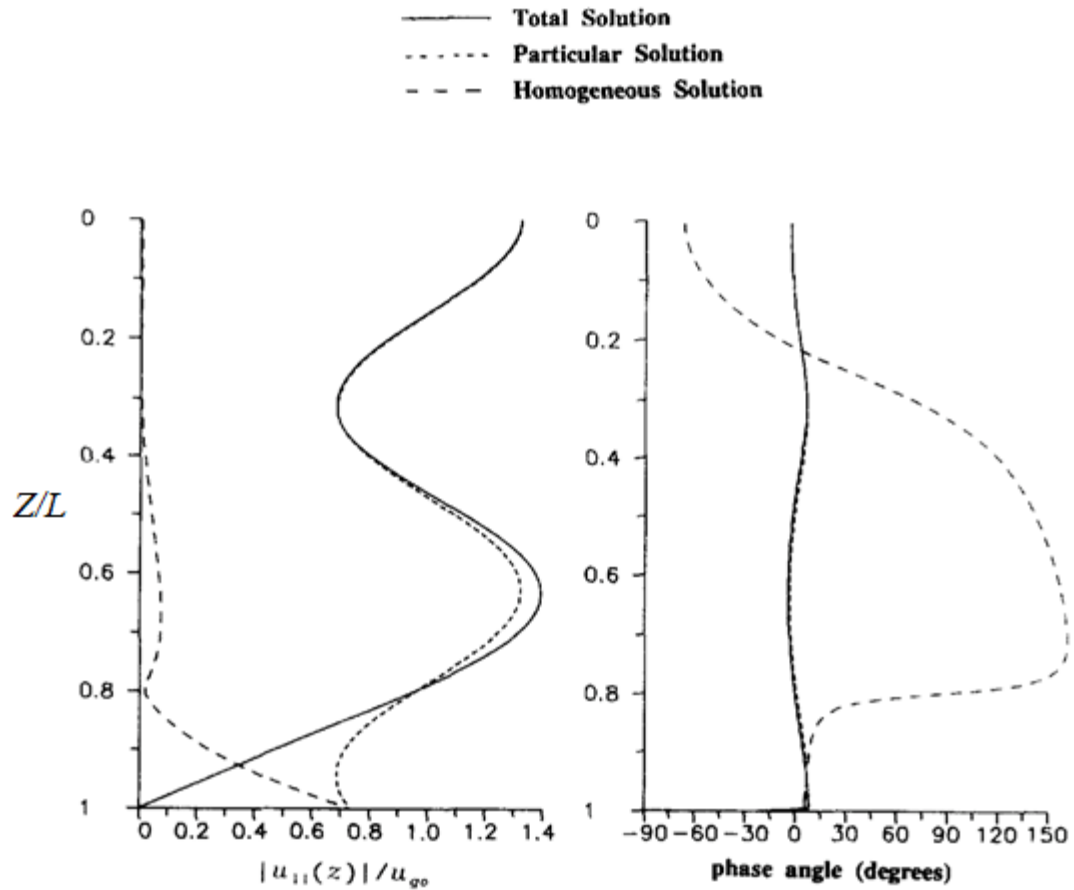


Figure 2.18 Pile deflection due to kinematic loading at dimensionless frequency $a = 0.3$: amplitude and phase angle corresponding to the homogeneous, the particular, and the total solution to the governing equation (24) in [64]

Additionally, the proposed model was compared with rigorous solution from literature [36] (Figure 2.19). According to analyses performed in this study regarding inertial and kinematic loading, pile-to-pile interaction is significant mainly in the inertial condition and group effects may be negligible for kinematic loading.

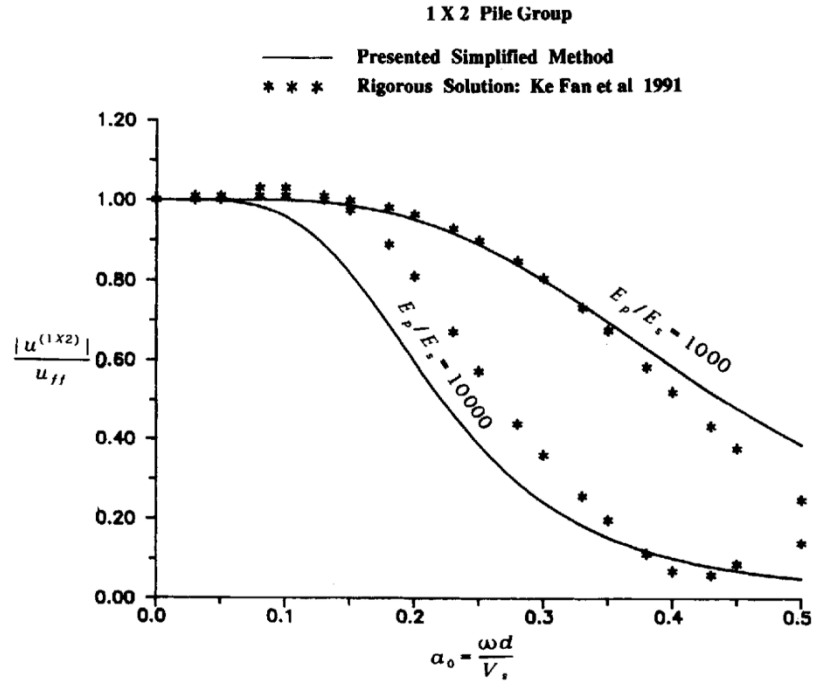


Figure 2.19 Kinematic seismic response of 1 x 2 fixed-head pile group: comparison of proposed method with rigorous results by Fan et al. [36] ($\rho_p/\rho_s=1.42$, $L/D=20$, $\nu=0.4$, $\beta=0.05$) [64]

A soil-pile-structure interaction study was performed by Mylonakis et al. [76] regarding pile embedded in two-layered soil and two types of bridge as shown in Figure 2.20. To analyze the problem, the multi-step (substructure) method was used and kinematic and inertial interaction were estimated separately. Dynamic impedances were calculated from kinematic loading by *BWDF* method under harmonic excitation or real earthquake time history and then applied to superstructure as *FIM* (foundation input motion) (Figure 2.21). A complete system analysis result as time histories calculated at pile cap and bridge deck is shown in Figure 2.22 for single-column pile under Pacoima (1994) downstream motion.

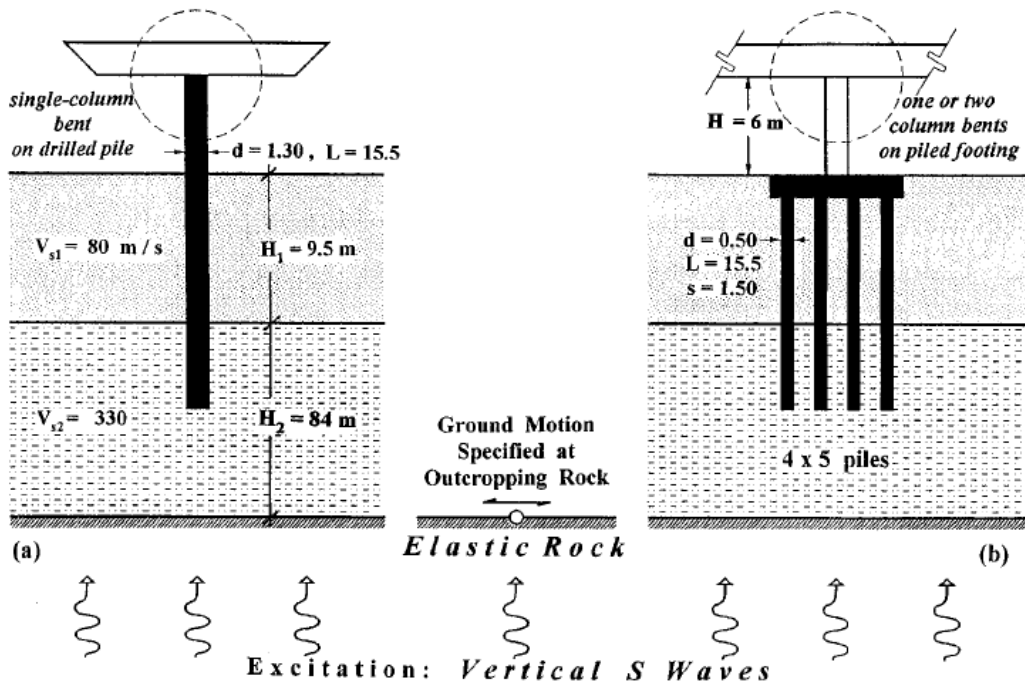


Figure 2.20 The bridge – pier systems and soil profile [76]

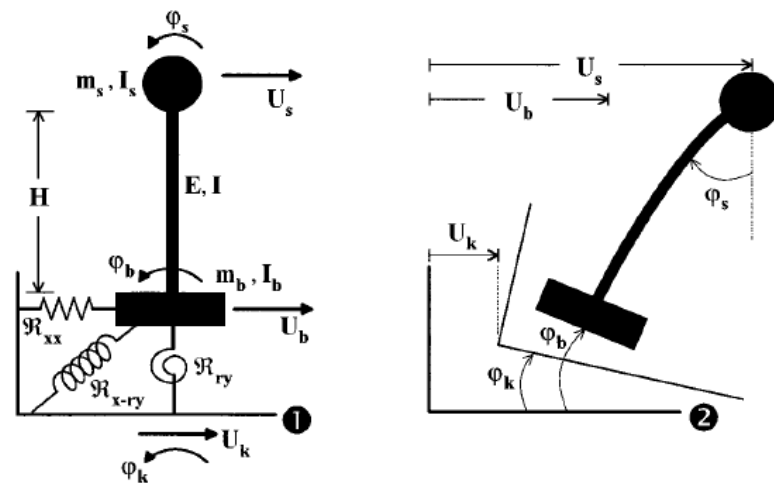


Figure 2.21 Soil – structure interaction model: (1) model parameters and (2) sketch of response in terms of displacement and rotation [76]

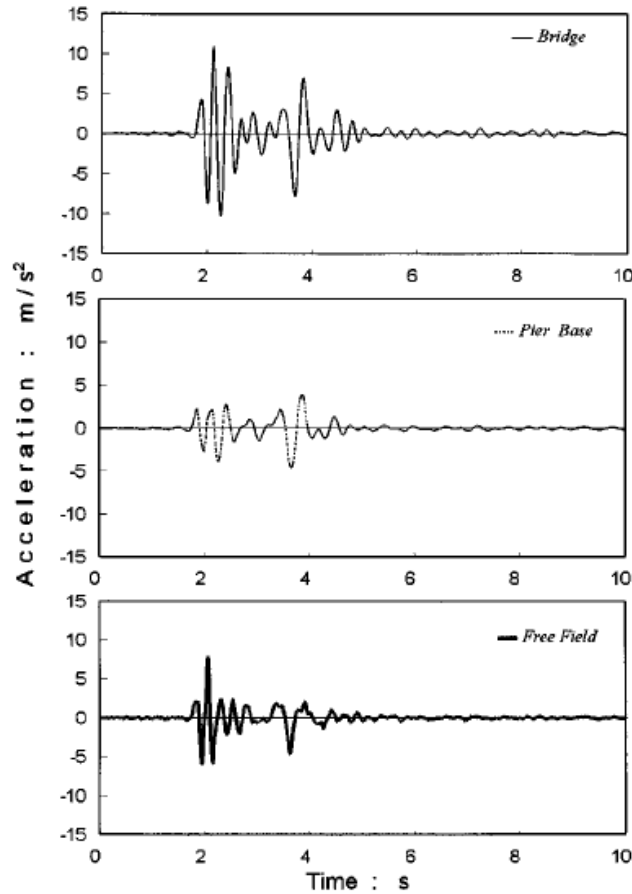


Figure 2.22 Results of the complete analysis in terms of time histories for bridge – pier system carried by single-column pile under Pacoima (1994) motion [76]

Mylonakis [66] has developed a simplified analytical model for kinematic bending moment due to the passage of the waves at soil layer interfaces. Kinematic bending may be severe in the presence of sharp stiffness discontinuities in the soil profile and may cause damage on pile or superstructure. Previous studies focused on seismic motion at pile head [65], [77], [78]. However, kinematic bending occurs along pile length with depth, even in the absence of the superstructure, due to soil deformation.

Kinematic bending moments tends to be amplified near at interfaces between stiff and soft soil layer (Figure 2.23). Maximum kinematic bending may be shown at interface level or at pile head (for fixed-head condition). Several pile damages were observed deep below the soil surface during post-earthquake investigations because of kinematic loading [55].

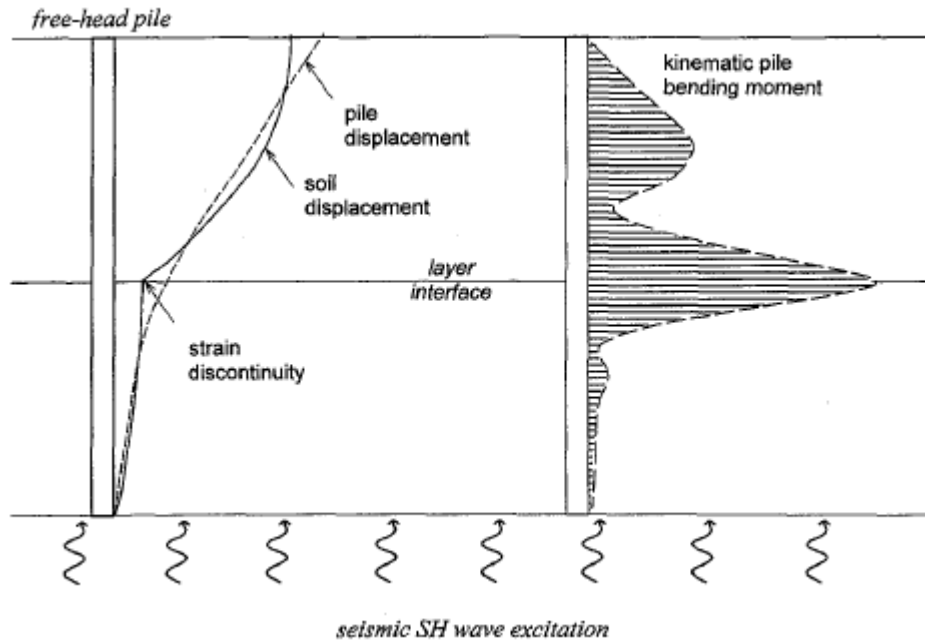


Figure 2.23 Kinematic bending of a free-head pile subjected to vertical seismic S-waves in a two-layer soil profile [66]

The proposed analytical model by Mylonakis [66] is based on Beam-on-Dynamic-Winkler-Foundation (*BDWF*) formulation. Bending strain (2.8) was used to quantify kinematic bending that has several advantages such as it is dimensionless, experimentally measurable, and it can be used to quantify pile damage. Also, results were presented in terms of strain transmissibility (ε_p / γ_1), γ_1 is peak soil shear strain. The studied problem which is single pile embedded in two layered soil subjected to vertically-propagating seismic S-waves is shown in Figure 2.24. Soil material in each layer was assumed as homogeneous and linear, and the pile was estimated long and linearly elastic. Applied load at base was in the form of harmonic displacement: $u_g(t) = \exp(i\omega t)$. Both radiation and material damping in the soil were accounted.

$$\varepsilon = \frac{M}{E_p I_p} r \quad (2.8)$$

Kinematic bending strain transmissibility are shown in Figure 2.25 for homogeneous soil layer and in Figure 2.26 for two-layered soil layer. At the low frequency region, both pile and soil move together. On the other hand, the pile resists the input motion at high frequency without bending. In the intermediate frequency region, kinematic bending strain could be seen.

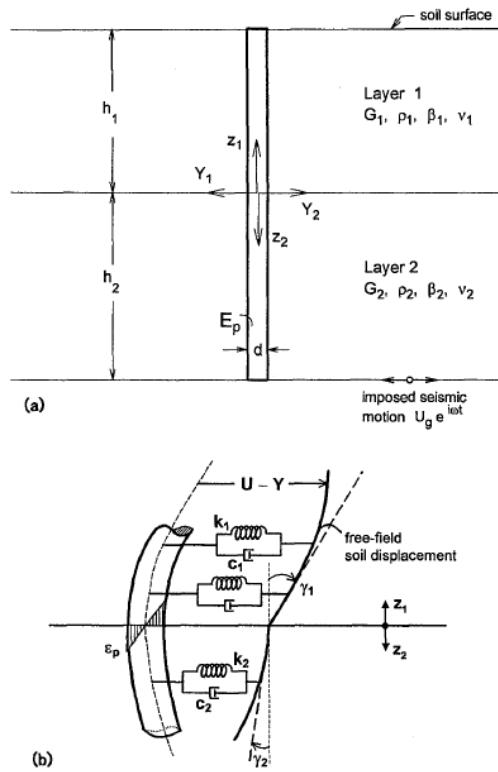


Figure 2.24 (a) The pile-soil model studied. (b) The representation of BDWF formulation for soil-pile interaction [66]

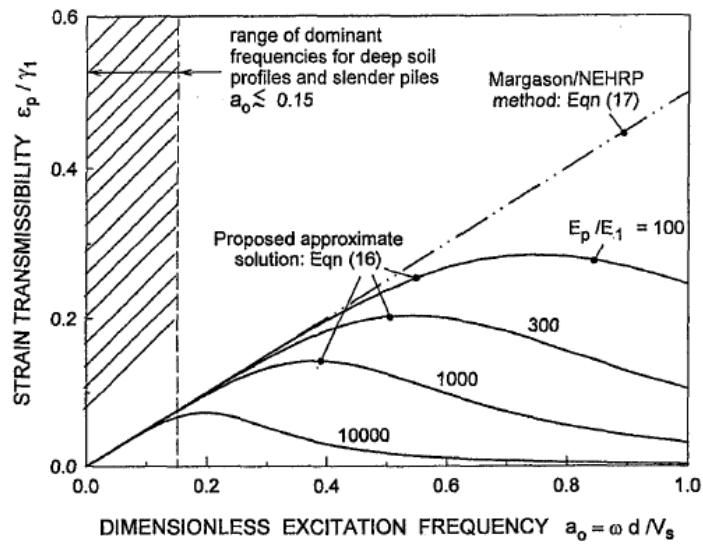


Figure 2.25 Strain transmissibility for a solid pile embedded in a homogeneous soil layer subjected to harmonic vertical S-waves ($\rho_p / \rho_s = 1.4$, $\nu = 0.4$, $\beta = 0$) [66]

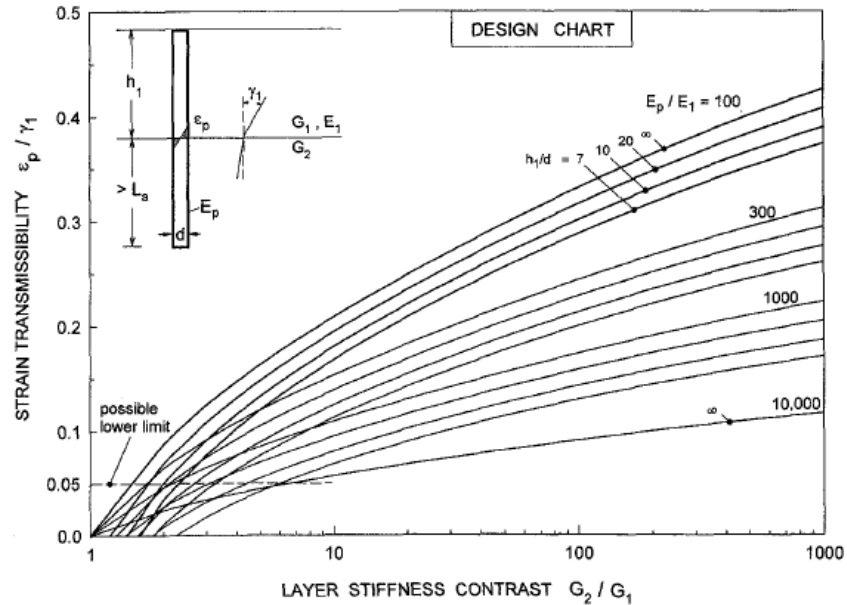


Figure 2.26 Strain transmissibility at interface of two soil layers of different stiffness for low frequencies. (Curves were obtained for $h_1/d = 7, 10, 20$, and ∞ ; L_a : active pile length) [66]

Padrón et al. [79] studied impedance function of embedded footings supported by vertical piles in homogeneous viscoelastic soil (Figure 2.27). Parametric analyses were carried out using coupled *BEM-FEM* method, in which *BEM* was used to model the soil and footing and *FEM* was used to model piles. The impedance functions are complex functions as given of the form $K = k + ia_0c$, where k and c are the frequency dependent dynamic stiffness and damping coefficient. Impedance functions of system obtained by superposition method (K^P) were compared with whole system impedance function (K^W) and comparisons are shown in Figure 2.28 in terms of dimensionless real-valued relative difference of moduli (χ) and phase in degrees ($\Delta\theta$). According to results, s/d and n affect significantly the difference of impedances and also pile-soil stiffness ratio and embedment ratio are relevant. Kinematic interaction factor for embedded footing supported by piles is shown in Figure 2.29.

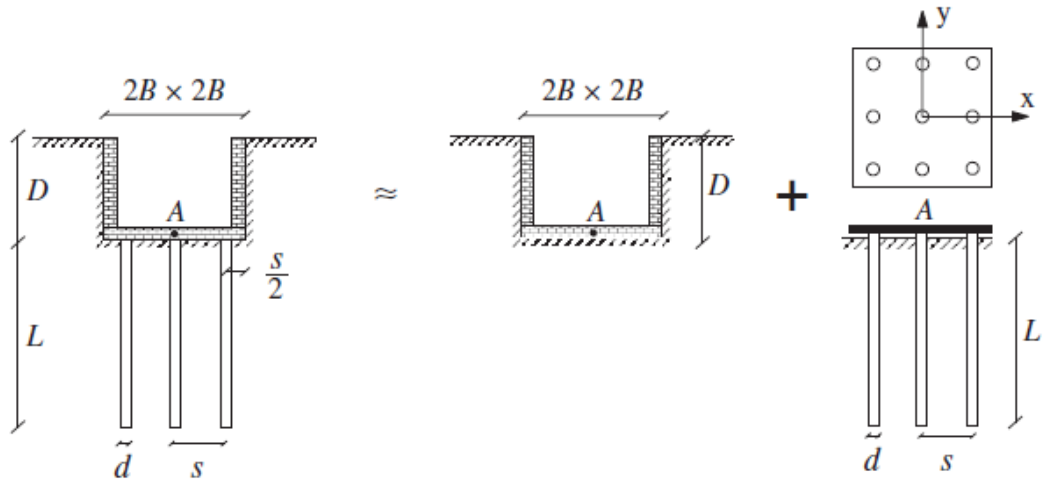


Figure 2.27 Simple superposition approach to solve embedded footing supported by vertical piles [79]

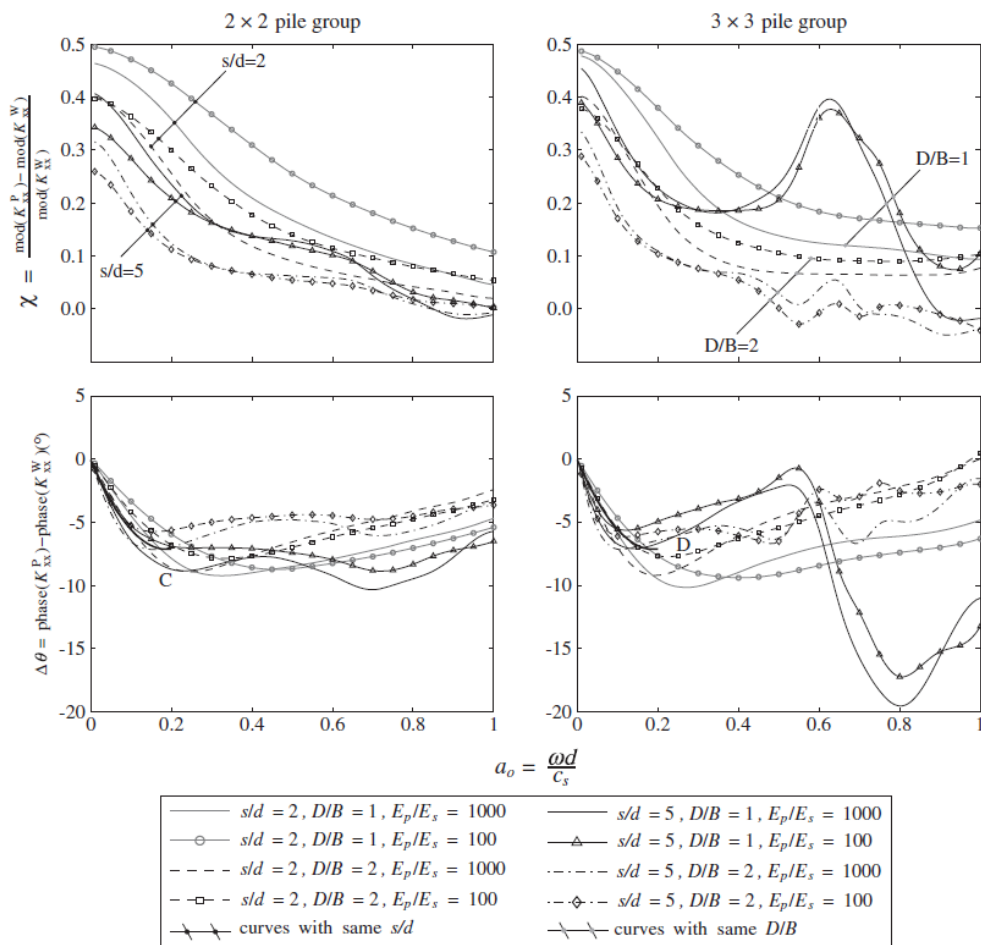


Figure 2.28 Comparison of horizontal impedances of embedded footing on piles obtained rigorously K^W and by superposition K^P [79]

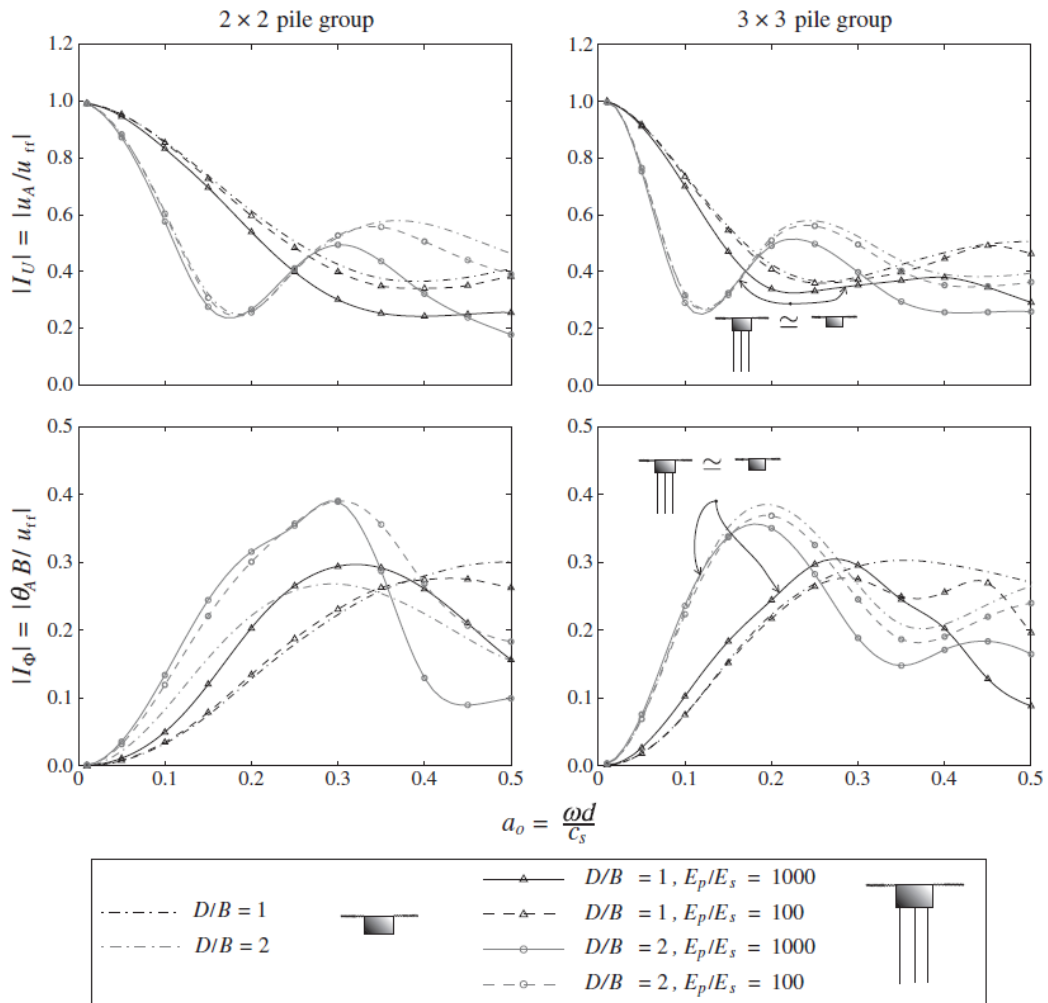


Figure 2.29 Translational and rotational kinematic interaction factor for embedded footing on piles under SH waves [79]

A recent study on the kinematic response of piles has been conducted by Anoyatis et al. [47]. Kinematic soil-pile interaction was studied analytically utilizing a *BDWF* (Beam-on-dynamic Winkler foundation) model. A cylindrical vertical pile embedded in a homogeneous soil layer resting on a rigid base and subjected to vertically propagating harmonic S-waves for different boundary conditions at the head (fixed, free) and tip (fixed, hinged, free) was examined utilizing the linear viscoelastic material model (Figure 2.30). Solutions from such analyses were expressed by kinematic response factors I_u and I_ϕ . New closed-form solutions were derived considering different boundary conditions for the head and the tip.

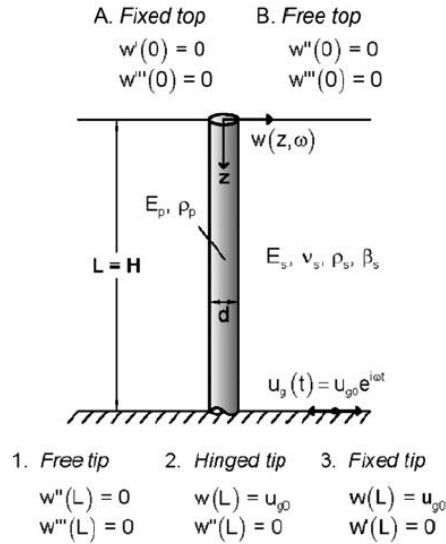


Figure 2.30 Problem associated boundary conditions at the pile head and tip [47]

Additionally, *FEM* analyses in two-dimension were performed to validate proposed equations using ANSYS commercial software. A comparison also was made with solution proposed by Fan et al. [36] (Figure 2.31).

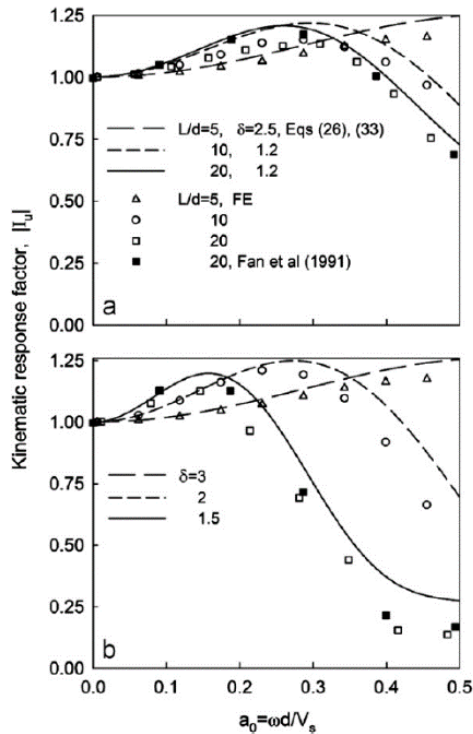


Figure 2.31 Kinematic response factor for free-head free-tip piles: (a) $E_p / E_s = 1000$; (b) $E_p / E_s = 10000$ [47]

The following summary can be made of the previous work related to pile-structure interaction:

- The kinematic interaction factor (in terms of displacement or acceleration) is utilized to compare the free-field and the pile motions.
- The response of soil – pile system is frequency dependent. Additionally, effective parameters are: stiffness ratio between pile and soil (E_p/E_s), slenderness ratio (L/D), pile boundary conditions, and soil thickness (H).
- Group effect (number of piles and pile spacing) has a minor effect on the kinematic interaction factor; however, its effect is significant on impedance functions of pile.
- Inertial interaction is dominant near the soil surface while kinematic interaction is significant at higher depths.
- Maximum bending appears at (or near) pile head or at the interface between two different layers.

METHODOLOGY

The soil – pile – structure interaction under the effect of earthquake loading is investigated with the help of plane-strain finite element (*FE*) models created in *OpenSees v2.4.4* and *Plaxis 2D AE.02* computer software. Software details, geometry of model, boundary conditions, element size, material models and damping properties, and solution of equation of motion are explained in this section.

3.1 The Established Model in *OpenSees*

OpenSees is an open-source development supported by NEES (Network for Earthquake Engineering Simulation) and PEER (Pacific Earthquake Engineering Research Center) used in to simulate the performance of structural and geotechnical systems subjected to earthquake loads [80]. This program is typically preferred by researchers as it is free to use and offers the possibility to write your own code to any material model.

Model set up is similar to earlier numerical studies on *SPSI* problems [81]–[84]. A schematic configuration of the established plane-strain *FE* model of a single pile embedded in a soil domain stratified on a bedrock is shown in Figure 3.1. A Lysmer-Kuhlemeyer [67] dashpot was used at the truncated boundary within the elastic bedrock – with shear wave velocity of $(V_s)_r = 760$ m/s – to take the effects of radiation damping into account. The damping coefficient is calculated by Equation (3.1) where ρ_r represents the density of the elastic bedrock (which is taken as 2.4 t/m³ here) and A_b is the base area of the FEM. The nodes at the base of the mesh are fixed in vertical direction while these nodes are left free to move in horizontal direction.

$$c = \rho_r (V_s)_r A_b \quad (3.1)$$

In order to replicate the far field wave propagation effects within the soil region, free field soil columns are attached to the vertical/side boundaries of the model [85]. The

elements of soil columns are given increased thickness to ensure that they are considerably more massive than the soil elements in the interior mesh. The increased thicknesses of free field soil columns are determined through comparisons with separate site response analyses, and are set at 100 m on both sides of the mesh. The displacement degrees of freedom for the nodes on either side of these columns are tied together to create periodic boundary conditions, following the example presented by McGann [86]. The free field columns must be located sufficiently far away from the critical region (i.e., the location of the pile). Padrón et al. [87] recommend a horizontal distance of $70D$ from the pile as being a sufficient distance to mark the free field in their FEM-BEM analyses. Here, the free field soil columns are placed at 200 m (i.e., $200D$) on both sides of the pile to ensure minimal interaction between the free-field and the pile.

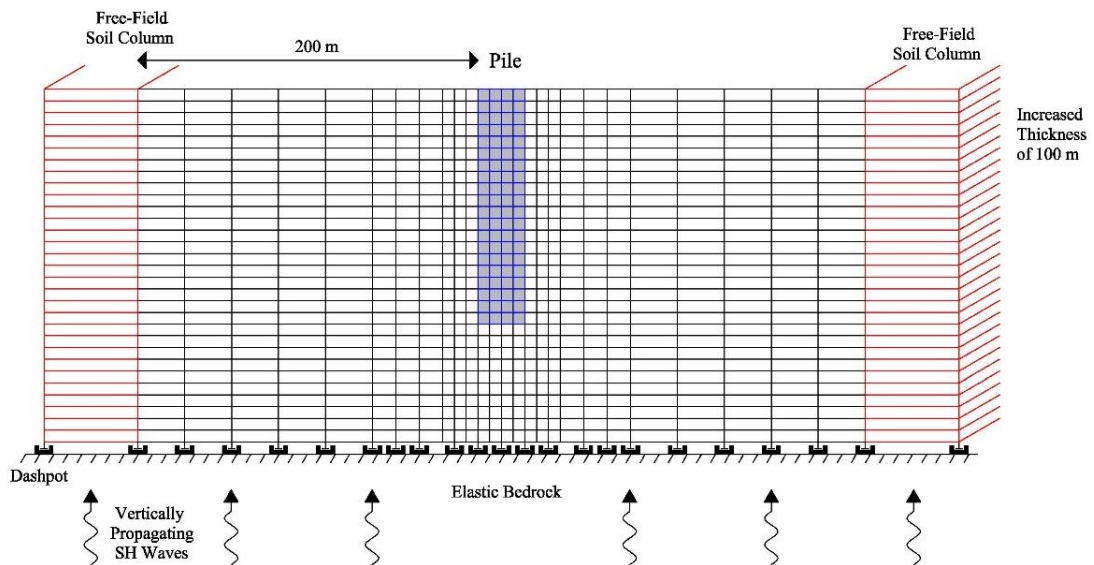


Figure 3.1 Representative delineation of established finite element model with boundary conditions in OpenSees

The pile is modeled as a linearly elastic solid with diameter of D , Young's modulus of E_p , and mass density of ρ_p . The soil can be modeled both as a linear solid continuum (with Young's modulus of E_s , mass density of ρ_s , shear wave velocity of V_s , and damping ratio of ξ) or elasto-plastic solid continuum. To consider elasto-plastic material behavior of soil, pressure independent multi yield soil model developed by Yang et al. [88] was used.

Four-noded quadrilateral *SSP* (Stabilized Single Point integration) elements are used for discretizing both the pile and the soil domain, which circumvent volumetric and shear locking effects [89]. The element sizes in the vertical direction are set to 0.5 m or less to remain below the one-fifth to one-eighth of the shortest wavelength [2]. The finite element mesh is graded along the horizontal direction with the finest mesh located at and around the pile region. The width of the elements are gradually reduced from 2 m at the interface of the interior mesh and the free-field soil column to 0.5 m toward the pile, and it is set to 0.25 m in and around the pile region (see Figure 3.1).

In reality, the interface elements between soil and structure are weaker and more flexible than the surrounding soil, which means that a reduction coefficient should be applied to the soil strength. The strength reduction coefficient for soil-structure interface was studied by experimental methods [90], [91] or by pile settlement analysis [92] and it can be considered to be in the range of 0.7–1.0. It may be assumed that the reduction coefficient is in the order of $2/3$ in the absence of detailed information as an engineering approximation. Based on previous experiences of modelling piles under similar conditions, zero length elements [93]–[95] are employed with a reduction coefficient of 0.8 applied to the soil strength.

The loads are applied in two stages: first, gravity loading is applied to determine the initial stress state within the domain; then, dynamic loading is applied as a force time history given by:

$$f(t) = \rho_r (V_s)_r A_b v_0(t) \quad (3.2)$$

along the base of the model, using the method proposed by Joyner and Chen [96]. This force history is obtained by multiplying the velocity time history of the input motion $v_0(t)$ by the mass density ρ_r and shear wave velocity of the underlying bedrock $(V_s)_r$, and the area of the base of the model A_b . The general semi-discrete form of the equations of motion is:

$$[M]\{\ddot{u}(t)\} + [C]\{\dot{u}(t)\} + [K]\{u(t)\} = f(t) \quad (3.3)$$

where $[M]$ denotes the mass matrix; $[C]$, the viscous damping matrix; $[K]$, the stiffness matrix; $\{\ddot{u}\}, \{\dot{u}\}, \{u\}$ the acceleration, velocity and displacement vectors; and $f(t)$, the force vector with non-zero entries at degrees of freedom where the input motion is described. The unconditionally stable implicit Newmark integrator with parameters $\gamma = 0.5$ and $\beta = 0.25$ is used to solve the Equation (3.3).

Theoretically, it is possible to construct a frequency-independent damping matrix using extended rational Rayleigh damping [97]. However, based on available damping models in *OpenSees*, a two-parameter Rayleigh damping formulation, given in equation (3.4), is used to consider dissipation of energy within the small-strain range [98]:

$$[C] = a_1[M] + a_2[K] \quad (3.4)$$

The values of a_1 and a_2 can be computed through the following equation, which sets the damping ratio (ξ) to be constant throughout the soil profile at b -th and c -th modes:

$$\begin{bmatrix} \xi_b \\ \xi_c \end{bmatrix} = \frac{1}{4\pi} \begin{bmatrix} \frac{1}{f_b} & 4\pi^2 f_b \\ \frac{1}{f_c} & 4\pi^2 f_c \end{bmatrix} \begin{Bmatrix} a_1 \\ a_2 \end{Bmatrix} \quad (3.5)$$

The n -th natural frequency of the homogeneous soil layer on a bedrock with thickness H and shear wave velocity V_s can be calculated using:

$$f_n = \frac{V_s}{4H} (2n - 1) \quad (3.6)$$

where n is the mode number. In (3.5), indices b and c are, respectively, considered as those the first mode of the soil column, obtained from (3.6) and a higher mode that corresponds to the predominant frequency of the input motion [99]. Kwok et al. [100] proposed a value equal to five times the natural frequency for the higher mode. Accordingly, the values of b and c are assumed as 1 and 3, respectively. The average shear wave velocity is computed based on the Eurocode EN 1998-1 standard [101] to be used in (3.6) to evaluate the equivalent natural frequency of multi-layered soil profiles.

3.2 The Established Model with *Plaxis*

Soil – pile – structure interaction problem is investigated by *Plaxis*, which is a finite element software to analyze geotechnical problems in civil engineering projects. It is able to consider the different aspects of geotechnical problems such as elasto-plastic behavior of soils, dynamic loading, time dependent behaviors, drainage conditions, anisotropic behavior of soils and rocks etc. Easy-to-use user interface helps to designer (or researcher) in modelling, calculation, and evaluation of results. Quadratic 6-node and 4th order 15-node triangular elements are available to model the stress and strain in the soil. Joint elements, as an interface, are usable for soil-structure interaction.

Dynamic boundary conditions, existing in *Plaxis*, are used for truncated boundaries. *Free-field boundary conditions* are defined to horizontal borders, simulating the

continuation of waves into the far field with minimum reflection. *Compliant base boundary condition* is applied to base border. The compliant base consists of a combination of a line prescribed displacement, transferred into load history, and viscous boundary. This combination allows for input of an earthquake motion while still absorbing incoming waves [102]. *Free-field boundaries* are placed at distance of 200 m from the pile as in *OpenSees*.

The pile can be modeled as elastic solid or embedded-pile element defined in *Plaxis*. The mechanical behavior of soil can be modeled by various material models, such as Mohr-Coulomb, Hardening Soil, Soft Soil (Cam-Clay), Hypoplastic, etc., defined in material library of *Plaxis* [103], [104]. The pile element (embedded-pile) and the soil model (hypoplastic model) used in this study are explained in detail in Chapter 5.

15-node triangular elements with a relative element size of 0.5 m are used for discretizing both the pile and the soil domain. The generated mesh for the entire soil – pile system is shown in Figure 3.2 and the near pile mesh is shown in Figure 3.3.

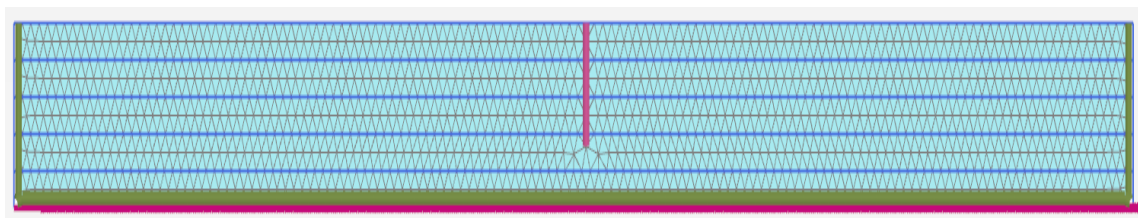


Figure 3.2 Mesh of entire soil – pile system

Loading steps, material damping (Rayleigh), and solution of motion Equation (3.3) in time domain with Newmark integrator are identical to those considered in *OpenSees*.

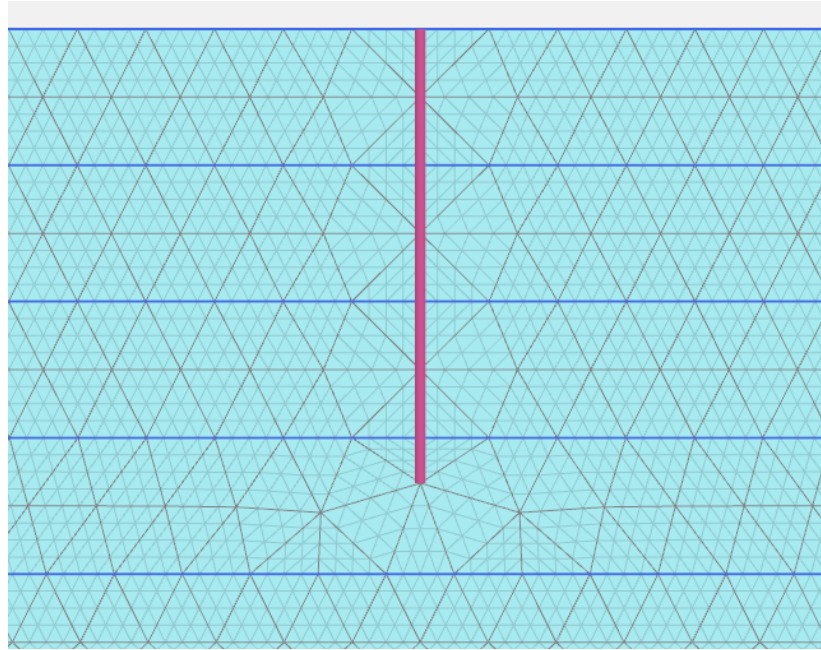


Figure 3.3 Mesh generated near the pile

3.3 Verification of the Established *FE* models

An established numerical model must be validated by experimental methods or verified by analytical closed-form solutions [105]. Therefore, site response analysis is performed without a pile and the results are compared with those from two well-established software packages, namely *Shake2000* [106] and *DeepSoil* [107]. Moreover, the kinematic interaction factor calculated by the *FE* model in *OpenSees* and in *Plaxis* are compared with the analytical solution suggested by Anoyatis et al. [47].

3.3.1 Site Response Analysis

Shake and its algorithm, originally developed by Schnabel et al. [106], has for many years been utilized as reference for site response analyses in geotechnical earthquake engineering. It has linear and equivalent-linear soil models and performs analysis in the frequency domain. On the other hand, *DeepSoil* is more extensive since it includes a large library of material models for various soils (linear, equivalent linear, and nonlinear) and can conduct analyses in the frequency domain and the time domain.

An actual earthquake time-history from the 1999 Kocaeli earthquake recorded at the Duzce Station is used for validation purposes. The soil is modeled as linear-elastic material with elastic shear modulus of 200 m/s and damping of 5% to consider comparable conditions. The results of the site response analyses in terms of acceleration

and displacement are shown in Figure 3.4 where z denotes the depth, $a_{\max}(z)$ and $u_{\max}(z)$ are the maximum acceleration and displacement at depth z , respectively. a_{rock} is the acceleration of the bedrock input motion and u_{rock} is the displacement of the bedrock input motion. The results obtained from the established models (OpenSees and Plaxis) agree well with those from *Shake2000* and *DeepSoil*.

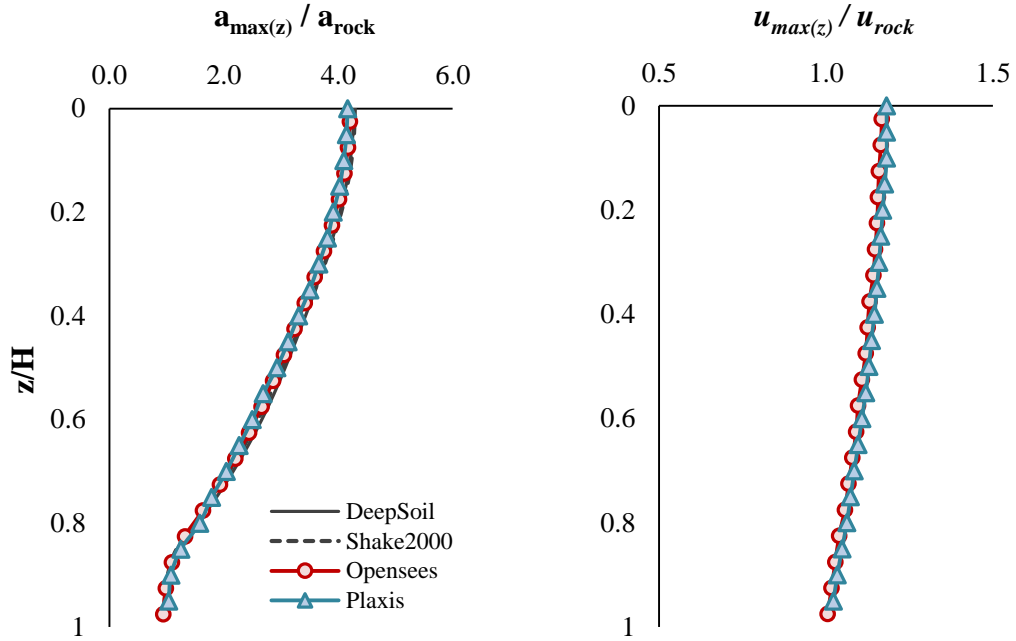


Figure 3.4 Comparison for a linear soil with 5% damping: results from two-dimensional OpenSees and Plaxis models versus calculations in Shake2000 and DeepSoil.

3.3.2 Closed-form Solution for Kinematic Interaction

The analytical formulation by Anoyatis et al. [47], which is based on the Beam-on-Dynamic-Winkler-Foundation model (BDWF), presents closed-form solutions for bending, displacements, and rotations on top of a pile for different boundary conditions at its head (fixed and free) and tip (fixed, hinged, and free). A single cylindrical vertical pile embedded in a homogeneous soil layer resting on rigid base is considered Figure 3.5. The material behavior of the pile and soil are assumed as linear elastic with Young's modulus E , Poisson's ratio ν , mass density ρ , and frequency-independent material damping β , where s and p are subscripts for soil and pile, respectively. A harmonic horizontal displacement $u_o(t) = U_o \sin(\omega t)$ is applied at rock level. Soil-pile interaction is expressed by the kinematic interaction factor I_u as given in (2.6).

The free-field displacement at ground surface level ($z = 0$) u_{ff} is determined by amplification function Equation (3.7) using the known motion at base level ($z = H$) u_g :

$$\frac{u_{ff}}{u_g} = \frac{1}{\cos(\omega H/V_s^*)} \quad (3.7)$$

where $V_s^* = V_s\sqrt{1 + 2i\beta_s}$ is the complex shear wave velocity of soil.

The equation governing pile motion that is caused by free-field displacement in the Navier form:

$$\frac{d^4 u_p}{dz^4} + 4\lambda^4 u = \frac{k^*}{E_p I_p} u_{ff} \quad (3.8)$$

where k^* corresponds to complex-valued Winkler modulus ($k^* = k + i\omega c$) and λ represents the characteristic wavenumber:

$$\lambda = \frac{k^* - \omega^2 m_p}{4E_p I_p} \quad (3.9)$$

where m_p is the mass per unit length of the pile ($= \rho_p A_p$).

The coefficient for the dashpot is as follows:

$$c = 6a_0^{-1/4} \rho_s V_s D + 2\beta_s \delta E_s / \omega \quad (3.10)$$

The general solution of the pile motion is given below:

$$u_p(z, \omega) = (P \cos \lambda z + R \sin \lambda z) e^{-\lambda z} + (S \cos \lambda z + T \sin \lambda z) e^{\lambda z} + \Gamma u_{ff}(z, \omega) \quad (3.11)$$

where P , R , S , and T are integration constants determined based on the boundary conditions. Γ is a dimensionless response coefficient:

$$\Gamma = \frac{k^*}{E_p I_p (q^4 + 4\lambda^4)} \quad (3.12)$$

where q is wavenumber ($= \omega / V_s^*$).

The kinematic interaction factor I_u for fixed-head and free-tip pile:

$$I_u = \Gamma \left[1 - \left(\frac{q}{\lambda} \right)^2 \frac{\cos(qL) [\cosh(\lambda L) \sin(\lambda L) - \cos(\lambda L) \sinh(\lambda L)] - \left(\frac{q}{\lambda} \right) \cos(\lambda L) \cosh(\lambda L) \sin(qL)}{\sin(2\lambda L) + \sinh(2\lambda L)} \right] \quad (3.13)$$

The kinematic interaction factor calculated by the established finite element model is compared with those obtained from the closed-form solution (3.13). A pile length (L) of 20 m, which is equal to soil thickness on the rigid base (H), and a pile diameter (D) of 1 m are assumed for this purpose. With respect to the soil, shear wave velocity of 120

m/s, which represents a soft clay is considered and a soil damping of 5% is estimated. A stiffness ratio of 500 between soil and pile (E_p/E_s) is taken into account. Parameters used in analyses are summarized in Table 3.1.

Table 3.1 Soil and pile material properties used in comparison of FEM and Analytical method

Material	ρ (t/m ³)	V_s (m/s)	ν	G (MPa)	E (MPa)
Soil	1.5	120	0.4	21.6	60.5
Pile	2.5	2300	0.15	13150	30250

As seen in Figure 3.6, the results from *FE* models and analytical solution are in good agreement, although slight differences are observed at higher frequencies (i.e., for $a_o > 0.2$). These differences can be attributed to the fact that different methods are used for (i) modelling the pile (continuum elements for *FE* models and beam elements for the semi-analytical model) and (ii) for representing damping (Rayleigh for *FE* models and linearly hysteretic model for the semi-analytical model). Frequency independency of the springs used in the semi-analytical solution may yet be another factor causing the discrepancies. However, the most pertinent a_o values usually range between 0 and 0.25 for pile-soil interaction problems. This is because the fundamental natural frequencies of soil deposits are quite small and the pile diameter ranges from 0.5 m to 1.5 m in most practical applications.

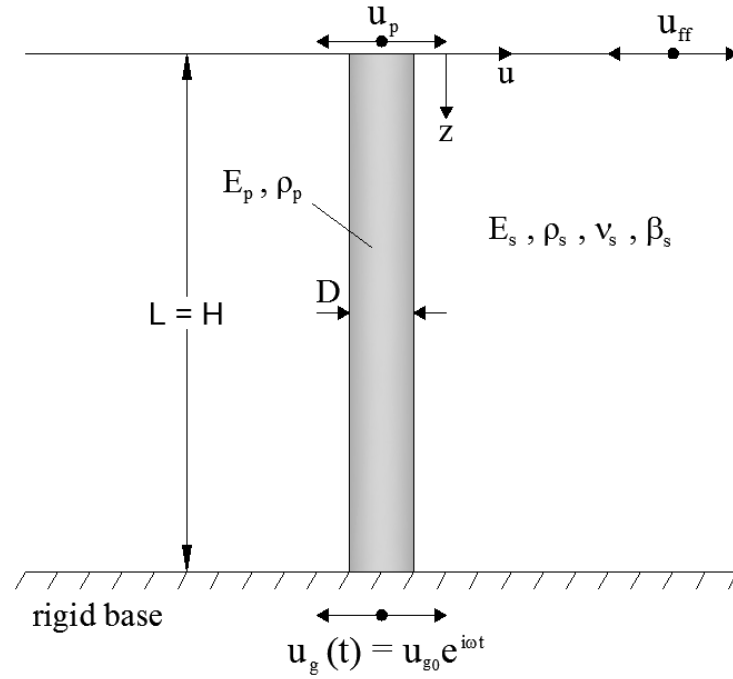


Figure 3.5 The schematic representation of the embedded pile in homogeneous soil on rigid base (Anoyatis et al. [47])

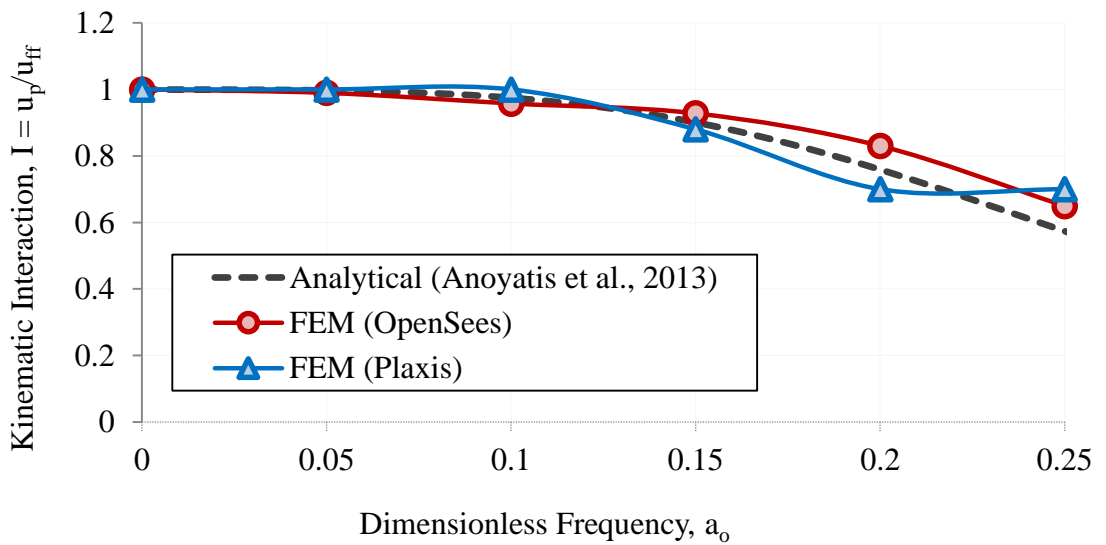


Figure 3.6 Comparison of FEM results with the analytical solution by Anoyatis et al. [47].

In summary, two working numerical models have been created by *OpenSees* and *Plaxis* and have been verified by site response analysis and analytical method suggested for soil – pile interaction.

SOIL – PILE (KINEMATIC) INTERACTION

A pile foundation displays complex behavior during earthquakes because of its interaction with the surrounding soil and the superstructure. Seismic waves propagate within the soil domain, arrive to, and excite the embedded piles and their superstructure. In turn, the vibrating superstructure reacts back with dynamic loads to the pile foundation, which causes deformations within the surrounding soil. This is the so-called *inertial interaction*. Additionally, even for a case where there is no superstructure — i.e. when there is no inertial feedback from the superstructure to the foundation or the soil — the motion in the vicinity of the pile will still be different from the free field motion (the latter may be obtained through conventional site response analyses). This is due to the difference between the rigidities of a pile foundation and its surrounding soil, which prevents the pile to conform to soil's deformations. This may alter not only the amplitude of the motion within the pile but also its phase angle relative to the free field. These effects are known as *kinematic interaction*, which generate moments and shear forces in the pile even in the absence of a superstructure. It should be noted that the pile foundation itself might induce inertial effects due to its mass. However, this is not usually considered separately in studying kinematic interaction effects.

With respect to the design of pile foundations in practice, only the loads transmitted from the superstructure (inertial effects) are considered, or free-field soil displacements are applied along the pile directly without modifications [61], [66]. That is while the free field and near pile motions are different because of the presence of the pile as mentioned above. Then, the simplest approach to compute the bending moment along the pile is to assume that the soil and pile movements coincide at all times. Margason [77] suggested the following predictive equation for the pile bending moment:

$$M = E_p I_p (1/R)_p = E_p I_p (1/R)_s = E_p I_p \frac{a_s}{V_s^2} \quad (4.1)$$

where E_p is Young's modulus of the pile, I_p is cross-sectional moment of inertia of the pile, $(1/R)_p$ and $(1/R)_s$ are the pile and soil curvatures, respectively, a_s is the horizontal ground acceleration, and V_s is the shear wave velocity of the soil. This simplified method is incapable of considering boundary conditions (of the pile-head and pile-tip) and layered soils [47].

In this section kinematic soil – pile interaction is investigated. Parametric studies are performed by applying harmonic input motions and real earthquake records to examine the behavior of the soil-pile system. Parameters considered in these analyses are soil behavior model (linear and elasto-plastic), pile-soil stiffness ratio (E_p/E_s), and slenderness ratio defined as the pile length over pile diameter (L/d). Additionally, the effect of phase angle (time lag between the free-field motion and the pile motion), which little attention has been directed to by researchers and practical engineers, on kinematic interaction is examined. *OpenSees* is preferred in analyses because it provides the acceleration, displacement, stress, and strain data for all points and elements (different from *Plaxis*).

The results are evaluated in terms of both displacement kinematic interaction factor (I_u) and acceleration kinematic interaction factor (I_a) defined in (4.2), in which a_{ff} is the free-field acceleration at surface and a_p is acceleration at pile head.

$$I_a = a_p/a_{ff} \quad (4.2)$$

4.1 General Response of Single Pile

Soil layer properties have a substantial effect on the site response and the kinematic interaction; the soil domain directly affects the response characteristics with the layers either amplifying or de-amplifying the motions depending on the frequency content of the input excitation. Natural soils may be gravels, sands, clays, silts, or mixtures such as sandy clay; and the constitutive behavior of these different soil types can remarkably be different from each other. In the present study, piles only in homogeneous clayey soils are considered, where the effects of kinematic interaction may be significant.

Parametric studies are conducted using three cohesive soils with differing shear strengths (C1: soft, C2: firm and C3: stiff) to consider the effects of quick loading (undrained) as in earthquakes. A pressure-independent elasto-plastic model is used that can simulate responses under monotonic as well as cyclic loading. Plastic behavior

occurs only in the deviatoric stress-strain response in this model and volumetric stress-strain response is linear-elastic and it is independent of the deviatoric response as well. This material was developed to simulate monotonic or cyclic response of materials such as clay under fast loading conditions, in which shear behavior of soil is insensitive to the change of confinement. Von-Mises type yield surfaces delineate the hardening zone as shown in Figure 4.1. The outmost surface determines the shear strength of the material. Masing-type hysteretic behavior is reproduced by employing a nonlinear kinematic hardening and associative flow rules as described in [81]. The shear stress τ –shear strain γ nonlinearity at a constant confinement P' is defined by a backbone curve:

$$\tau = \frac{G\gamma}{1 + \frac{\gamma}{\gamma_r} \left(\frac{P'_r}{P'} \right)^j} \quad (4.3)$$

where P'_r and γ_r are reference effective confining pressure and strain, respectively.

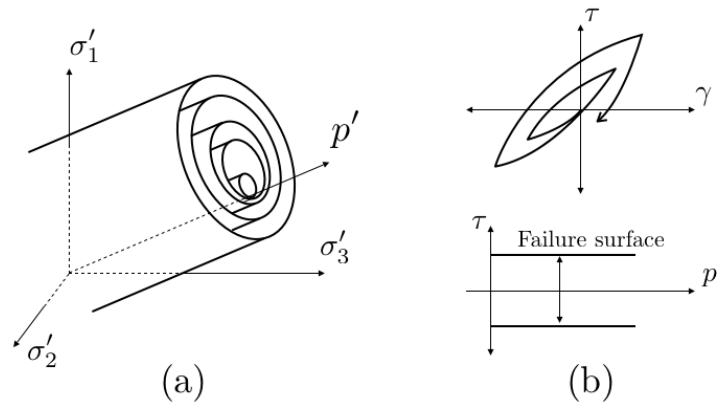


Figure 4.1 Pressure independent soil material constitutive model: (a) shape of yield surface in principal effective stress space, and (b) response of constitutive model (figure adapted from [81])

Shear wave velocity (V_s) and undrained cohesion (c_u) values are taken from Mayne et al. [108]. Shear modulus (G), Young's modulus (E_s), and bulk modulus (K) of soil are calculated by Equations (4.3), (4.4), and (4.5), respectively. Soil and pile properties are presented in Table 4.1.

$$G = \rho \cdot V_s^2 \quad (4.3)$$

$$E = 2 \cdot G \cdot (1 + \nu) \quad (4.4)$$

$$K = \frac{E}{3 \cdot (1 - 2\nu)} \quad (4.5)$$

For convenience, the pile is assumed as a reinforced concrete cast-in-place pile (most common type of piles in Turkey) and E_p/E_s (stiffness ratio) is adjusted to ratios of 100, 200, and 400 by varying the Young's modulus of pile (E_p), which had a range that varied is approximately between 28-33 GPa.

The elasto-plastic material parameters suggested by the developers of the *OpenSees* software are utilized for the reference pressure and pressure dependency coefficient (Table 4.2).

Table 4.1 Pile and soil properties used in parametric analyses

Material	ρ (Mg/m ³)	V_s (m/s)	ν	G_{max} (MPa)	E (MPa)	c_u (kPa)	E_p/E_s
Pile (Elastic)	2.5	--	0.15		$\approx (28-33) \cdot 10^3$		
C1 (Soft)	1.7	120	0.4	≈ 24	≈ 70	40	400
C2 (Medium)	1.8	180	0.4	≈ 58	≈ 160	80	200
C3 (Stiff)	1.9	240	0.4	≈ 100	≈ 290	150	100
Elastic Bedrock	2.4	760	--	--	--	--	--

Table 4.2 Other parameters used in analysis proposed by *OpenSees*

Symbol	Definition	Value
γ_{peak}	Peak shear strain	0.05
θ	Friction angle (degree)	0
P_r	Reference mean effective confining pressure (kPa)	100
j	A positive constant defining variations of G and K (If $\phi = 0$, $j = 0$)	0
NYS	Number of yield surfaces	25

The pile is considered fixed-head (no rotation) and free-tip to better represent actual pile boundary conditions. In general, a superstructure constructed on pile foundations limits the pile head movement but frees the pile tip, with the exception of rock-socketed piles.

4.1.1 Harmonic Loading

In order to gain insight about kinematic interaction between pile and soil regarding elasto-plastic soil behavior, further parametric studies are performed using harmonic input motions with increasing dimensionless frequency " $a\omega$ ". The soil-pile system is loaded at the base level by vertically propagating shear waves expressed as harmonic horizontal displacement $u_g(t) = u_{go} \cdot \sin(\omega t)$ for a duration of 10 seconds. The input

motion amplitude in terms of acceleration of 0.3g is used in the analyses to consider strong ground motion. The time increment Δt of 0.005 sec is considered. In these analyses, the effects of the soil material model (linear and elasto-plastic nonlinear), the stiffness ratio between pile and soil (E_p/E_s), and the pile slenderness ratio (L/D) on kinematic interaction are examined. Analysis results in terms of displacement and acceleration are shown in Figures 4.2 – 4.4. In general, kinematic interaction factor with respect to displacement (I_u) decreases with increasing frequency as suggested by Fan et al. [36] (Figure 2.15). However, similar behavior cannot be attributed to the changes in the estimated values of acceleration.

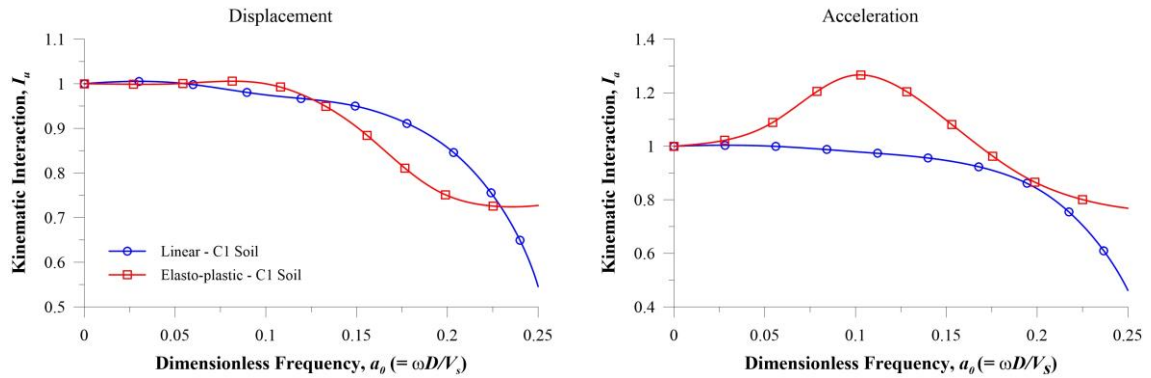


Figure 4.2 Kinematic interaction factors in terms of displacement and acceleration considering linear and nonlinear soil behavior for C1 (soft) soil ($H=30$ m, $L=20$ m, $D=1$ m)

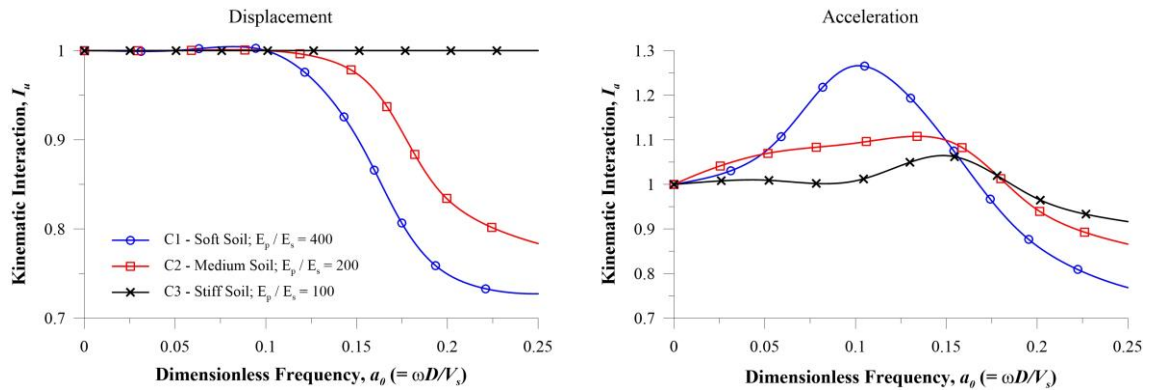


Figure 4.3 Effect of soil stiffness on kinematic interaction ($H=30$ m, $L=20$ m, $D=1$ m)

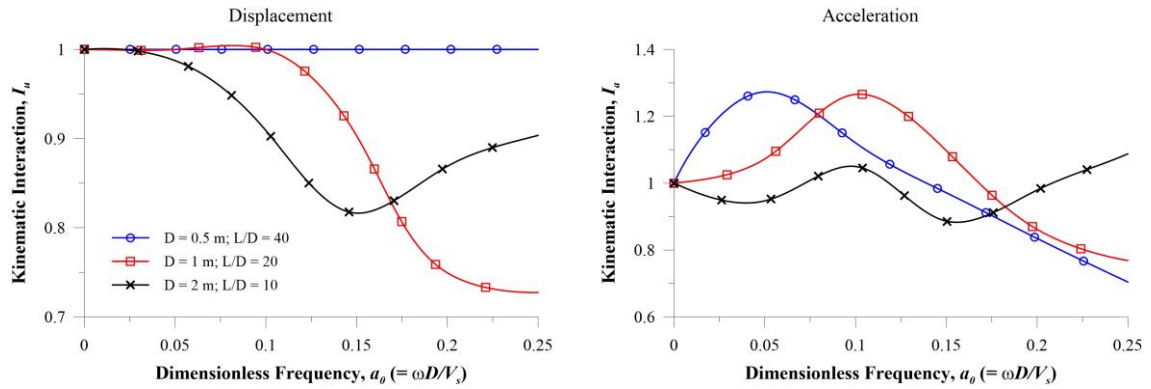


Figure 4.4 Pile slenderness effect on response of the soil-pile system (C1: soft soil, $H=30$ m, $L=20$ m)

Soil nonlinearity effects can be seen in Figure 4.2 considering displacements and acceleration. In the analyses, the effects of the soil material model are investigated with the following parameters: a soft soil (C1) thickness (H) of 30 m on the elastic base, a floating pile diameter (d) and length (L) of 1 m and of 20 m, respectively. The same geometry ($H = 30$ m and $L = 20$ m) is used in other parametric analyses within this study. Both kinematic interaction factors related to displacement (I_u) and acceleration (I_a) decrease with frequency for linear soil. On the other hand, for a nonlinear response, I_u decreases with increasing frequency while I_a increases up to a dimensionless frequency of 0.15 ($I_a > 1$). The difference between linear and elasto-plastic kinematic interaction factor with respect to acceleration ($I_a < 1$ for linear; $I_a > 1$ for elasto-plastic) can be explained by nonlinear soil response. Plastic behavior of soil is related to cyclic shear strain level of the soil (Vucetic & Dobry [109]). Subjected to small strains ($\gamma_c \approx 0.001$), soils commonly demonstrate linear-elastic material properties. G/G_{max} decreases and damping ratio increases with increasing strain level so that plastic soil behavior occurs. Additionally, overestimation of shear stress τ by linear method affects the response. The mechanism of overestimation of the shear stress employed in equivalent-linear method, where the shear stress increase with shear strain is linear, is plotted schematically by Yoshida et al. [110] (Figure 4.5). The shear stress – strain relationship is given by the solid line. When a maximum shear strain is reached, the shear stress obtained by the equivalent-linear method (O – A – C line) τ_1 is larger than τ_2 that corresponds to point B on the actual stress-strain curve. In small strain range, this overestimation may be ignored without much error, however, this mechanism becomes influential when soils are subjected to strong ground excitations. Shear strength of the soil governing the response is affected from this overestimation, therefore, the peak

acceleration is also overestimated. Regarding kinematic interaction problem, the free-field acceleration at the surface (a_{ff}) for plastic behavior might be lower than that for linear behavior since damping increases with shear strain. On the other hand, acceleration calculated at pile head (a_p) indicates a linear response. Hence, the kinematic interaction factor related to acceleration could be greater than unity.

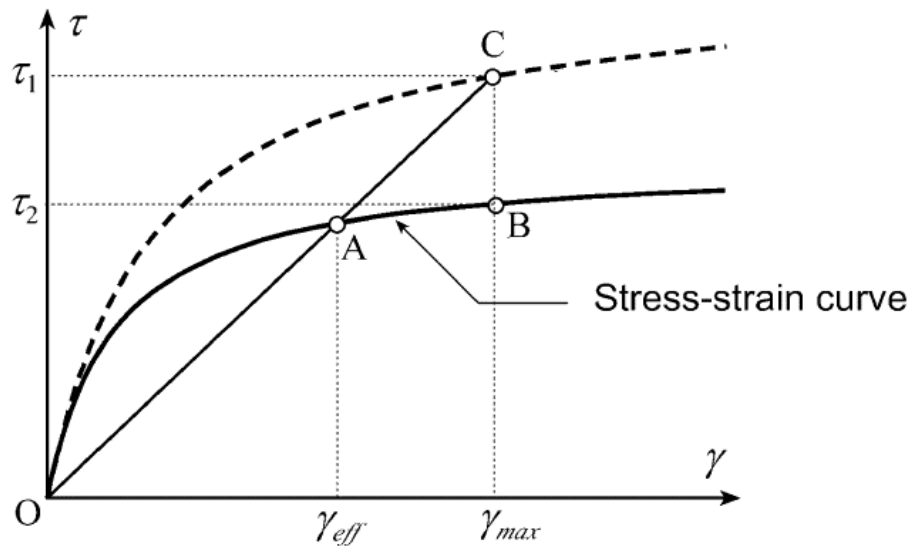


Figure 4.5 Over-estimating shear stress by the equivalent linear method [110]

The stiffness ratio between soil and pile is crucial for kinematic interaction (see Figure 4.3). Pile embedded in stiff soil ($E_p/E_s = 100$) follows the soil movement while it resists soil displacements for $E_p/E_s = 200 - 400$. Moreover, the pile amplifies accelerations for all types of soil as shown in Figure 4.3. The slenderness ratio (L/D) of pile is another significant parameter for soil-pile interaction. The effects of the slenderness ratio are investigated by changing the pile diameter and keeping its length constant ($L=20$ m). Results are presented in Figure 4.4. For a rather flexible pile, where L/D is high, the displacements are similar to those obtained for the soil; conversely, kinematic interaction declines with decreasing slenderness/increasing diameter. Pile slenderness magnifies the kinematic interaction factor for acceleration except for a diameter of 2 m, in which I_a fluctuates around unity. This behavior can also be evaluated as the effect of increasing pile diameter.

4.1.2 Earthquake Loading

The changes in kinematic interaction is investigated for six real earthquake acceleration-time histories. The records are selected based on an average shear wave velocity to a depth of 30 m ($V_{s,30}$) that is commonly considered an indicator of the site condition (EN 1998-1 2013 [101]; TDY 2007 [111]). Motions recorded at sites with $V_{s,30} > 500$ m/s are selected so that very stiff soil or bedrock outcropping motion are used as the input motion. The chosen time histories with respective earthquakes, station names, and the Fourier spectra of the signals are shown in Figure 4.6. Seismic intensity and frequency content of the input motion are important properties for the response of soils and structures to earthquakes. The record of 1989 Loma Prieta earthquake Gilroy # 1 station have high amplitude (peak ground acceleration $> 0.4g$). The predominant frequency for all input motions range between 0 Hz and 5 Hz. Peak ground displacement measured during 1999 Kocaeli earthquake Gebze station ($=0.427$ m) is larger than others. In these analyses, only floating piles are investigated, where a soil thickness of 30 m, a pile length of 20 m, and a pile diameter of 1 m are used. Peak ground acceleration (PGA) and displacement (PGD) of the records, soil types and models used in the analyses, and the results of analyses in terms of acceleration and displacement are given in Table 4.3.

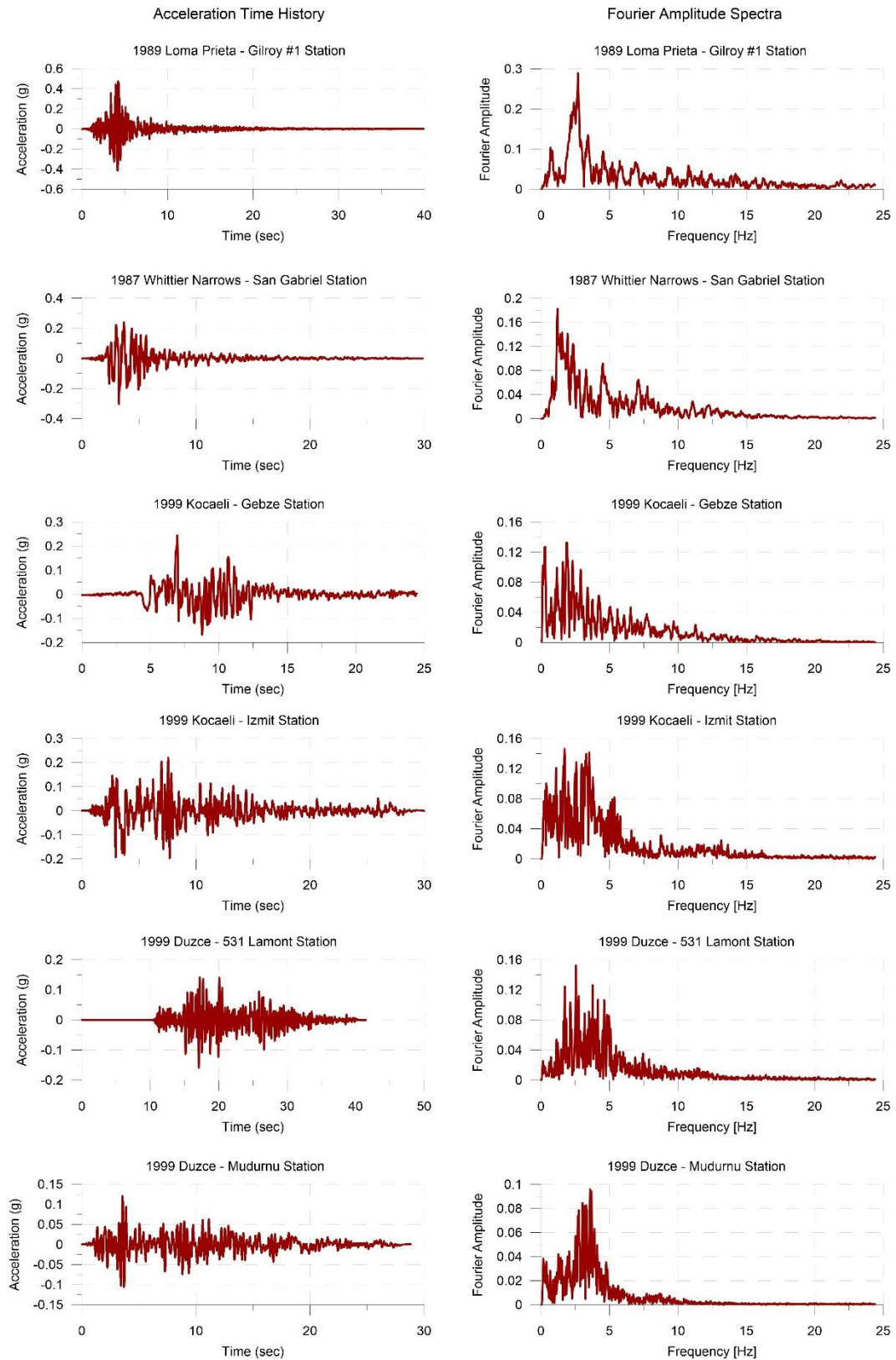


Figure 4.6 Time histories and Fourier spectra of earthquakes recorded at very stiff soil or outcropping rock ($V_s > 500$ m/s) used in analyses

Table 4.3 Results of earthquake analyses

Earthquake and Station	PGA (g)	PGD (m)	Soil Type and Material Model	a_p (g)	a_{ff} (g)	$I_a = a_p / a_{ff}$	u_p (m)	u_{ff} (m)	$I_u = u_p / u_{ff}$
1989 Loma Prieta Gilroy #1 Station	0.473	0.08	C1 - NL	0.238	0.200	1.19	0.11	0.11	1.0
			C1 - L	0.692	0.689	1.00	0.12	0.12	1.0
			C2 - NL	0.323	0.303	1.07	0.10	0.10	1.0
			C3 - NL	0.435	0.399	1.09	0.08	0.08	1.0
1987 Whittier Narrows San Gabriel Station	0.304	0.03	C1 - NL	0.163	0.193	0.84	0.04	0.04	1.0
			C1 - L	0.366	0.399	0.92	0.08	0.08	1.0
			C2 - NL	0.235	0.250	0.94	0.04	0.04	1.0
			C3 - NL	0.32	0.335	0.96	0.05	0.05	1.0
1999 Kocaeli Gebze Station	0.244	0.427	C1 - NL	0.14	0.145	0.97	0.43	0.43	1.0
			C2 - NL	0.181	0.163	1.11	0.42	0.42	1.0
			C2 - L	0.387	0.390	0.99	0.43	0.43	1.0
			C3 - NL	0.279	0.241	1.16	0.42	0.42	1.0
1999 Kocaeli Izmit Station	0.22	0.171	C1 - NL	0.145	0.150	0.97	0.23	0.23	1.0
			C2 - NL	0.241	0.220	1.10	0.19	0.19	1.0
			C2 - L	0.391	0.393	0.99	0.19	0.19	1.0
			C3 - NL	0.271	0.258	1.05	0.18	0.18	1.0
1999 Duzce Lamont 531 Station	0.159	0.078	C1 - NL	0.128	0.124	1.03	0.08	0.08	1.0
			C2 - NL	0.196	0.187	1.05	0.07	0.07	1.0
			C2 - L	0.269	0.272	0.99	0.08	0.08	1.0
			C3 - NL	0.182	0.182	1.00	0.08	0.08	1.0
1999 Duzce Mudurnu Station	0.12	0.076	C1 - NL	0.124	0.120	1.03	0.08	0.08	1.0
			C2 - NL	0.138	0.133	1.04	0.08	0.08	1.0
			C2 - L	0.139	0.139	1.00	0.08	0.08	1.0
			C3 - NL	0.131	0.132	0.99	0.08	0.08	1.0

*C1: Soft, C2: Medium, C3: Stiff, L: Linear, NL: Nonlinear

Kinematic interaction factors related to displacement are equal to one for all motions and soil types. With respect to acceleration, some of the kinematic interaction factors (I_a) are greater than one, some are lower, and while others are almost equal to one. The values depend mainly on the stiffnesses of the soil layer and the pile foundation, along with the frequency content of the input signal. Moreover, the free-field accelerations calculated by the linear material model are greater than those from the nonlinear model in which the plastic properties of soils come into play. Consequently, kinematic interaction substantially influences the design of superstructures because input motion for the foundations of pile-supported structures is different from that calculated in the free-field.

The variation of accelerations and displacements with depth for both near pile and free-field are presented in Figure 4.7. Additionally, frequency contents of calculated time histories at pile head and at free-field are compared for a several earthquakes and conditions (Figure 4.8). It can clearly be seen that relatively high frequency content (> 5 Hz) are filtered by the presence of piles.

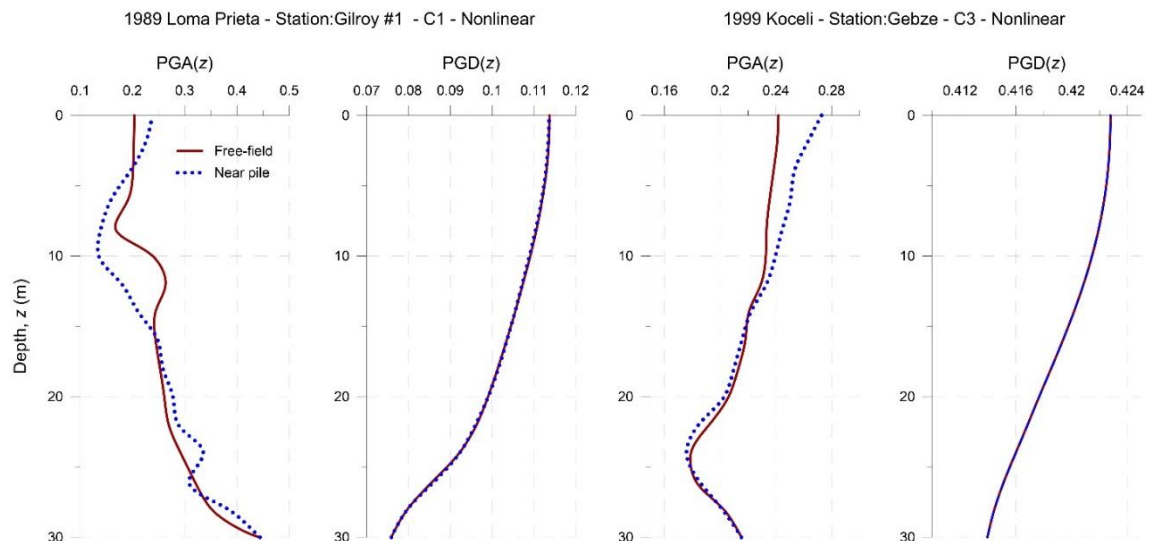


Figure 4.7 Calculated accelerations and displacements with depth at free-field and at a distance of 2 m from the pile)

4.1.3 Discussion of Harmonic vs. Earthquake Input Motion

There are significant differences between the findings when harmonic motion rather than actual earthquake loading is applied as input motion to simplify analyses. Kinematic interaction factor changes according to both acceleration and displacement under harmonic loading ($I_u, I_a < 1$ or $I_a > 1$), whereas, I_a varies under earthquake loading while I_u remains equal to one. A similar result regarding pile deflection under dynamic earthquake loading was also obtained by de Sanctis et al. [112].

Harmonic loading is widely used in soil dynamics problems including soil-structure interaction to study the response of a system to seismic loading. However, one should be careful in using it since this type of loading *does* have some disadvantages. As for the kinematic soil-pile interaction in this study, the following reasons may explain the differences in outcomes when harmonic vs. earthquake records are used as input motions and why the latter should be preferred.

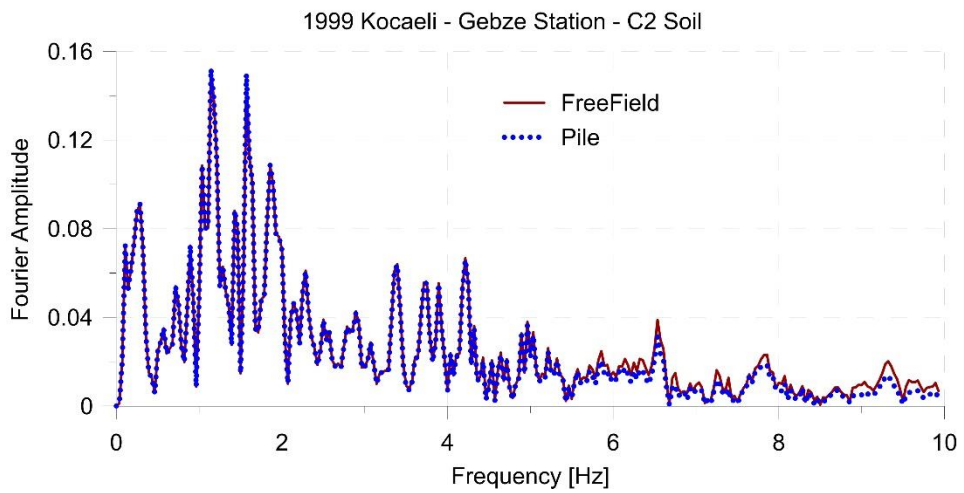
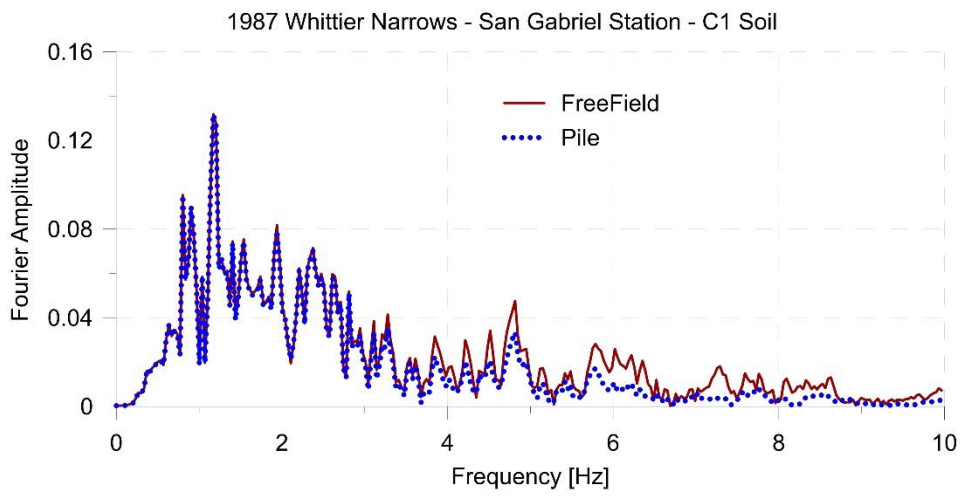
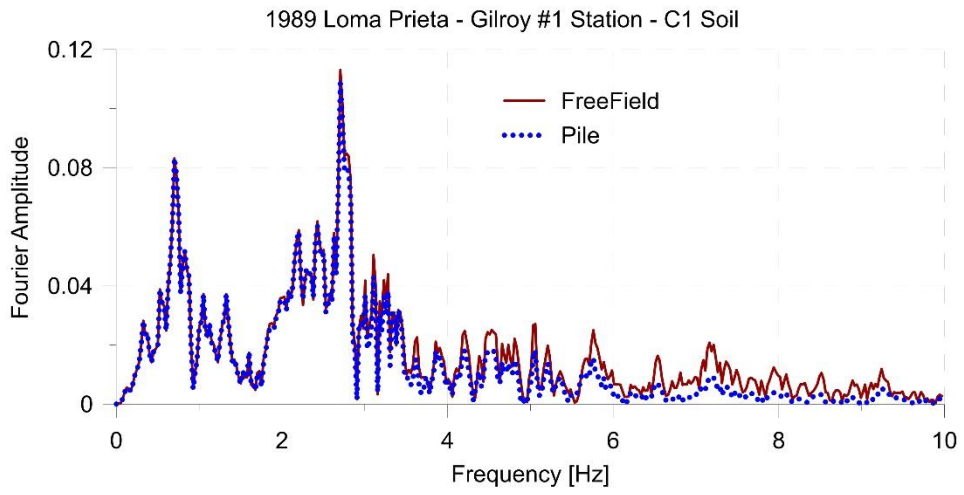


Figure 4.8 Effect of the presence of the pile on frequency content

- Harmonic loading represents a more severe loading than any actually recorded earthquake loading, even when their peak values may be identical. Both harmonic and transient (as in a typical earthquake) shear strain-time histories having the same peak cyclic shear strain are shown in Figure 4.9. The overall time history of shear strain for a typical earthquake motion is considerably lower than that for a harmonic load. Therefore, the strain level of a transient motion is characterized in terms of effective shear strain, which varies between about 50 % or 70 % of the maximum shear strain (Kramer [2]).

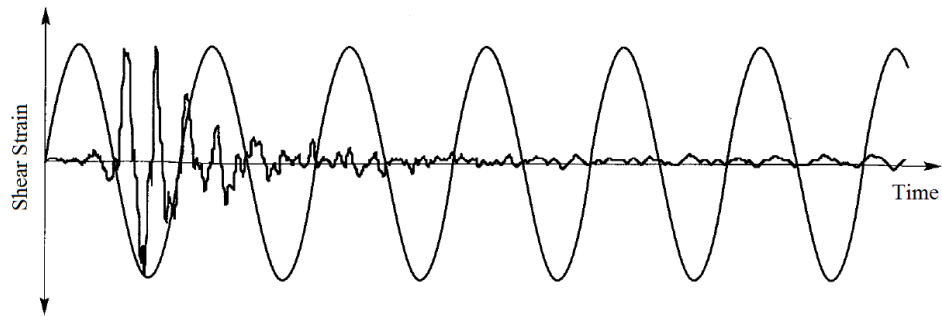


Figure 4.9 Shear time histories of earthquake and harmonic motions with peak identical shear strains [2]

- The wavelength becomes smaller with increasing frequency (wavelength $\lambda_{wave} = V_s / f$) and stiffer piles deflect differently (both in terms of amount and frequency) as compared to the soil surrounding them. As a result, the displacement interaction factor might be lower than one in the high frequency range.
- The magnitude of harmonic input motion in terms of acceleration depends on the amplitude of displacement U and time increment Δt . In Figure 4.10, steady-state harmonic motions in terms of acceleration and displacement for a C3 soil based on dimensionless frequency is depicted. In the low frequency ($a_o = 0.05$) range, the amplitude of input motion for displacement is equal to 0.02 m, which is a reasonable value for soil dynamics problems, corresponding to an acceleration of 0.3g; however, the amplitude of the acceleration is very large (approximately 8g!), which is not possible for an input displacement of 0.02 m in the high frequency range ($a_o = 0.25$). When the acceleration is scaled down to 0.3g, the displacement amplitude decreases to 0.00085 m, which can safely be ignored for most practical purposes.

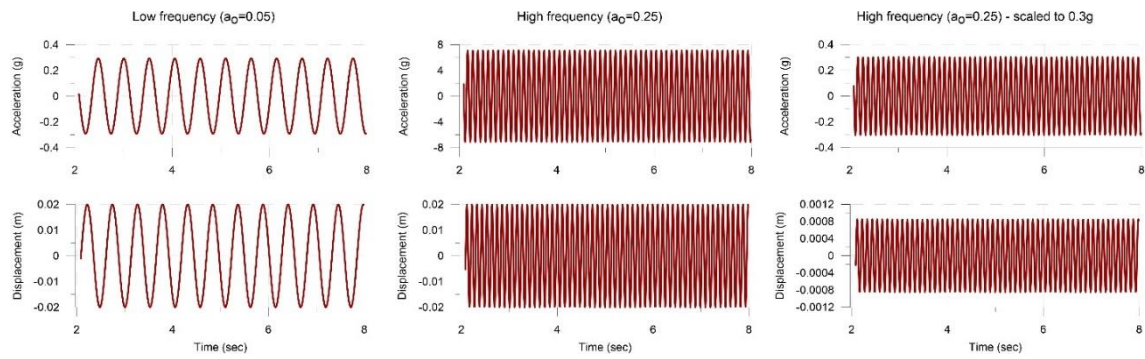


Figure 4.10 The amplitude of accelerations and displacements with dimensionless frequency for C3 soil and pile diameter of 1 m

- With respect to the dimensionless frequency, it depends on the frequency of input motion, the pile diameter, shear wave velocity of the soil, and the thickness of soil deposit. As can be seen in Figure 4.6, the frequency content of outcropping bedrock motions vary between 0 Hz and 5 Hz. The fundamental natural frequencies of soil deposits, however, are usually significantly smaller. Moreover, generally pile diameters vary from 0.5 m to 1.5 m in practical applications¹. Furthermore, loose-to-medium cohesionless soil or predominantly soft-to-firm cohesive soil deposits are high risk areas prone to earthquake damages. The shear wave velocity of such soils are defined smaller than 180 m/s (ground type D) in Eurocode 8 [101]. Reasonable and relevant parameters (ω , D , and V_s) should be selected within the framework of analyzing dynamic geotechnical problems.

Consequently, the reasonable parameters of soil and structure are taken into account when selecting harmonic motion. It is preferable to consider data recorded in actual earthquakes for kinematic soil response analyses where more rigorous solutions may be obtained by incorporating computers and numerical approaches.

¹ In geotechnical literature, piles having a diameter less than 0.5 m are commonly referred to as micropiles, whereas piles larger than 1.5 m diameter may not be very practical. Thus, these are not considered in this study.

4.2 Effect of Phase Angle on Kinematic Interaction

Even when SPSI is considered, kinematic interaction effects are either completely neglected, or partially taken into account by modifying only the amplitude (but not the phase angle!) of the earthquake input motion along the embedded portion of the pile [52]. In the present study, a more realistic representation of kinematic interaction is researched by considering changes in both amplitude and phase angle, and show that phase angle variations relative to the free field can become significant for pile/deep foundations. These phase angle variations can induce (or more precisely, they are signs of) additional bending moments/curvatures within the pile, and may even affect the response of superstructures.

All of the aforementioned studies [27], [36], [47], [53], [72], [78] have solely focused on amplitude variations due to kinematic interaction effects, and only a few studies explored the evaluation of changes in the phase angle of the response. Makris and Gazetas [113] studied the phase difference of displacement response for a top loaded single pile using dynamic Winkler model to investigate pile-to-pile interaction under dynamic loads and this influence was found to have a negligible contribution. Recently, Kirkit et al. [114] studied phase variations for a pile in homogeneous soil that is subjected to base excitations. They concluded that the presence of the pile disturbs the spatial variation of the phase angle of the ground motions (to be used as the input) relative to the free field, in addition to their amplitudes. This meant that the free field soil displacements are not necessarily in phase with those adjacent to the pile and that these differences may also have variations with respect to depth — a recipe for inducing additional curvatures within the pile. Therefore, some sections of pile might be subjected to higher or lower forces, and neglecting the phase effects could be detrimental.

In the present study, the previous work in this area [114] is extended and an extensive parametric study is performed to examine the effects of kinematic interaction on the steady-state behavior of free and fixed head piles embedded in multi-layered soil deposits.

4.2.1 Problem Definition

The geometry of a single pile embedded in a multi-layered soil medium that rests on top of an elastic bedrock is depicted in Figure 4.11. It is assumed that the input seismic

waves are vertically propagating horizontally polarized shear (SH) waves, which are applied at the soil's bedrock boundary. Wave reflections and refractions in multi-layered media —along with the nominally higher stiffness of the pile relative to its surrounding soil— may significantly alter the input waveforms from their initial states, which, in turn, influence the effective loading acting on the pile.

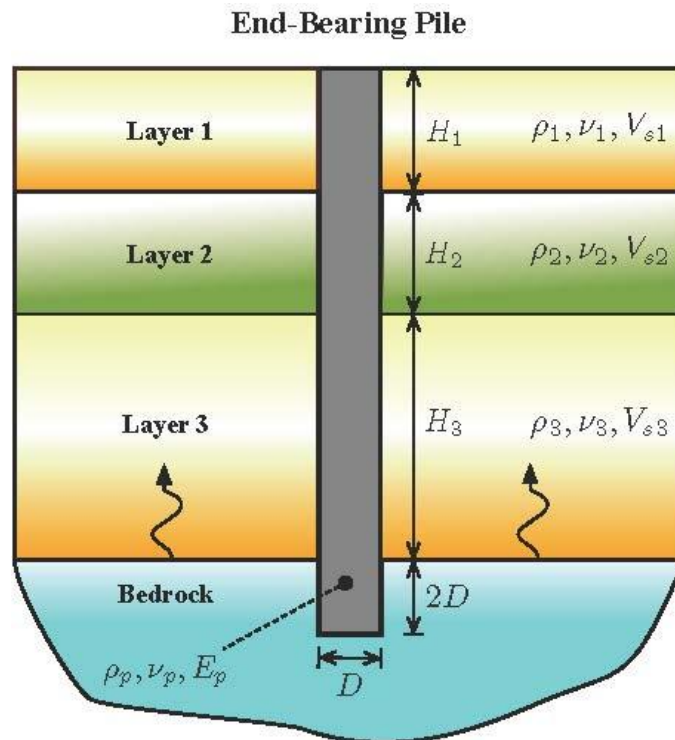


Figure 4.11 Geometry of a single pile embedded in a layered soil rest on elastic bedrock

In this study, the effects of soil layering, pile boundary condition, and frequency content of the input excitations on pile-soil kinematic interaction is examined. The model matrix comprised of a homogeneous and a three-layered soil domain (with a soft intermediate layer), and free- and fixed-head piles.

Based on literature research for this study it can be deemed that past studies on soil layering effects on kinematic interaction have been limited to two-layered soils, and these studies concluded that the pile is subject to force constraints at the interface of those two layers [11, 24, 28-30]. It should also be noted that in geotechnical engineering practice, soil profiles are usually idealized to simplify and accelerate the analyses, and adverse conditions are taken into account only indirectly by applying safety factors. The

simplest idealization is to assume that the soil layer is completely homogeneous. The consequences of using this simplifying assumption will also be examined.

4.2.2 Parametric Studies

Two types of soil configurations are considered to investigate the effects of soil heterogeneity on the spatial variation of the phase angle: (i) homogeneous (single-layer) soil on elastic bedrock and (ii) three-layered soil with an intermediate soft layer on elastic bedrock. Analyses are carried out for both free and fixed pile-head conditions.

The total soil layer thickness on elastic bedrock is taken as $H = 20$ m. Linear elastic material model is considered for pile and soil in phase angle study. The pile diameter is $D = 1$ m, and it is socketed into the stiff rock layer by $2D = 2$ m (i.e., the pile length is $L = 22$ m)². The pile's (i.e., cast-in-place concrete's) mass density, Poisson's ratio, and Young's modulus are taken as $\rho_p = 2.5$ t/m³, $\nu_p = 0.15$, $E_p = 30$ GPa, respectively. The layered soil profile consists of three layers —with mass densities of $\rho_1 = 1.6$ t/m³, $\rho_2 = 1.5$ t/m³, and $\rho_3 = 1.7$ t/m³, thicknesses of H_1 , H_2 , and H_3 , and shear wave velocities of V_{S1} , V_{S2} , and V_{S3} —resting on elastic bedrock. The shear wave velocities of the layers are determined according to EC8 (Eurocode 8) [101], considering “Ground type D”. Details of soil layering and parameters used in subsequent parametric studies are provided in Table 4.4, where f_{avg} (calculated by equation (3.6) using V_{avg}) represents the average natural frequency of the multi-layered soil, which is also used to evaluate the coefficients of the Rayleigh damping. Four different input frequencies f_{inp} ranging from low to high values are considered in all cases —i.e. $f_{inp}/f_{avg} = 1, 2, 4,$ and 8 .

Table 4.4 Soil profiles considered in parametric phase angle studies

Case	H_1 (m)	H_2/H_1	V_{S1} (m/s)	V_{S1}/V_{S2}	V_{S1}/V_{S3}	V_{avg} (m/s)	f_{avg} (Hz)
Single-layered	20	—	180	—	—	180	2.25
Three-layered	5	0.6	150	2.0	0.5	175	2.20

² It is useful to note here that in previous studies concerning kinematic interaction, the end-bearing piles were placed directly on the bedrock — a configuration that is actually rare in engineering practice — but were not socketed as they are in the present study.

4.2.2.1 Kinematic Steady-State Curvature Response

The curvature time history at each depth z can be computed as follows:

$$\kappa(z, t) = \frac{\sigma_{zz}^R(z, t) - \sigma_{zz}^L(z, t)}{E(z)d} \quad (4.6)$$

where $\sigma_{zz}^R(z, t)$ and $\sigma_{zz}^L(z, t)$ are stresses recorded at depth z at two Gauss points (right and left) within the width of the pile or free-field soil column and d is the distance between these two points (it is useful to mention that the SSP quadrilateral element has only one Gauss point); $E(z)$ is the Young's modulus, which can be a function of z . Then, the steady-state part of the curvature response is used to fit a two-parameter sinusoidal function oscillating with frequency $\omega = 2\pi f_{inp}$. To wit,

$$\kappa(z, t) \approx (1/R)(\omega, z) \cos[-\omega t + \phi(\omega, z)] \quad (4.7)$$

where $(1/R)(\omega, z)$ and $\phi(\omega, z)$ are the curvature amplitude and its phase angle at frequency ω and at depth z , respectively. This procedure is used to compute pile and free field soil curvatures in all cases studied.

The variation of the curvature amplitude and phase angle with depth for free and fixed head piles embedded in homogeneous and layered soil, respectively, are presented in Figures 4.12 – 4.15. Free field soil curvature is also shown. The green dashed line at $z = -20$ m shows the interface of the soil and elastic bedrock, at which a sudden change occurs in the soil curvature due to the change in Young's modulus.

As seen in Figure 4.12 and Figure 4.13:

- In all cases, the amplitude of soil curvature is negligible in comparison to the pile curvature. This is mainly because the dominant mode of vibration of vertically propagating horizontally polarized waves within the soil is shear when there is no pile.
- The pile curvature becomes large when the input frequency is equal to natural frequency of the soil layer. As ω increases, the pile curvature decreases while its fluctuations along the pile-length increases. It is also interesting to note that the soil curvature is higher when the input frequency is two times the natural frequency of the soil layer — i.e., $f_{inp}/f_{avg} = 2$. This is probably so, because the bending behavior is more active in the second mode than the first, which is more dominated by shear-type deformations.

- At low and moderate frequencies, the maximum curvatures occur at the pile-head and somewhere at mid-length for fixed and free head piles, respectively. However, this trend is not true for high frequencies —viz. $f_{inp}/f_{avg} = 8$. Moreover, as we move away from the pile-head, the effect of the pile boundary condition on both the amplitude and the phase angle of the curvature diminishes, and fixed- and free-head pile behaviors converge to each other.

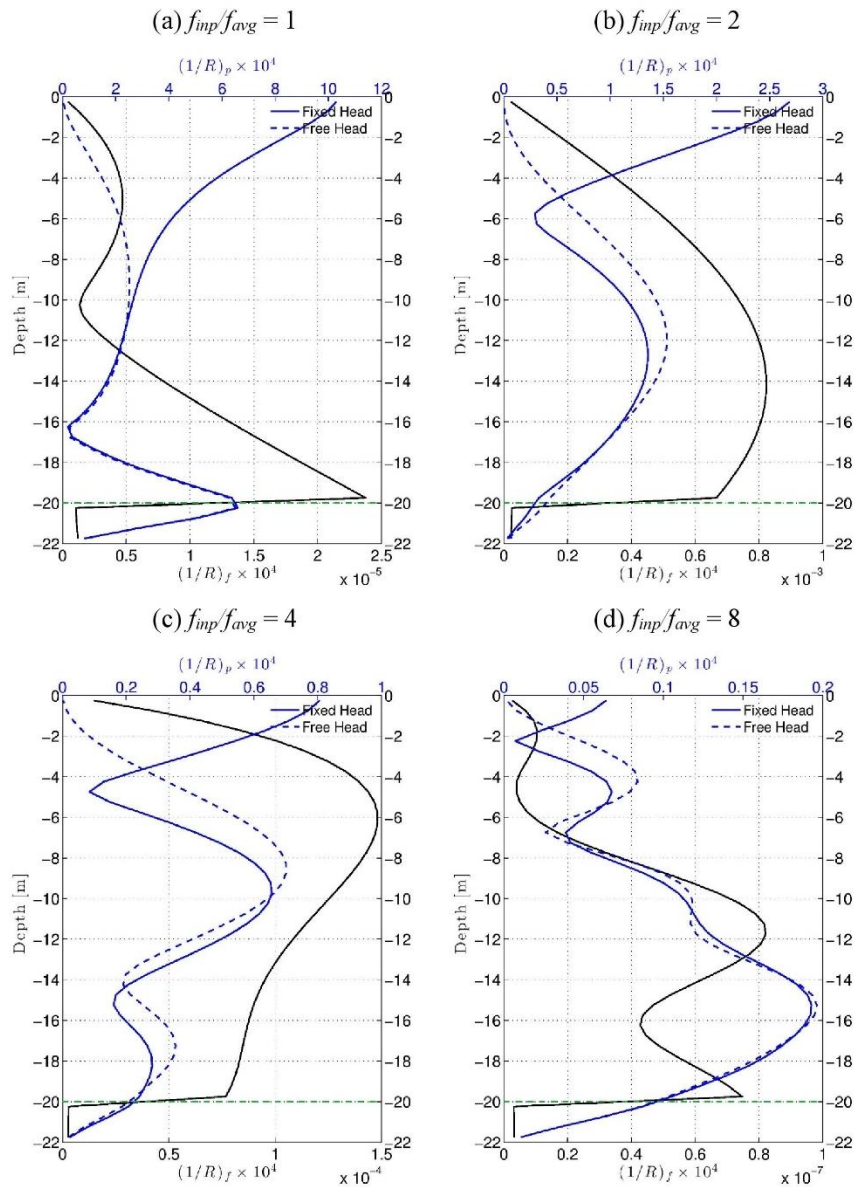


Figure 4.12 Pile and free field soil curvature amplitude for homogeneous soil condition

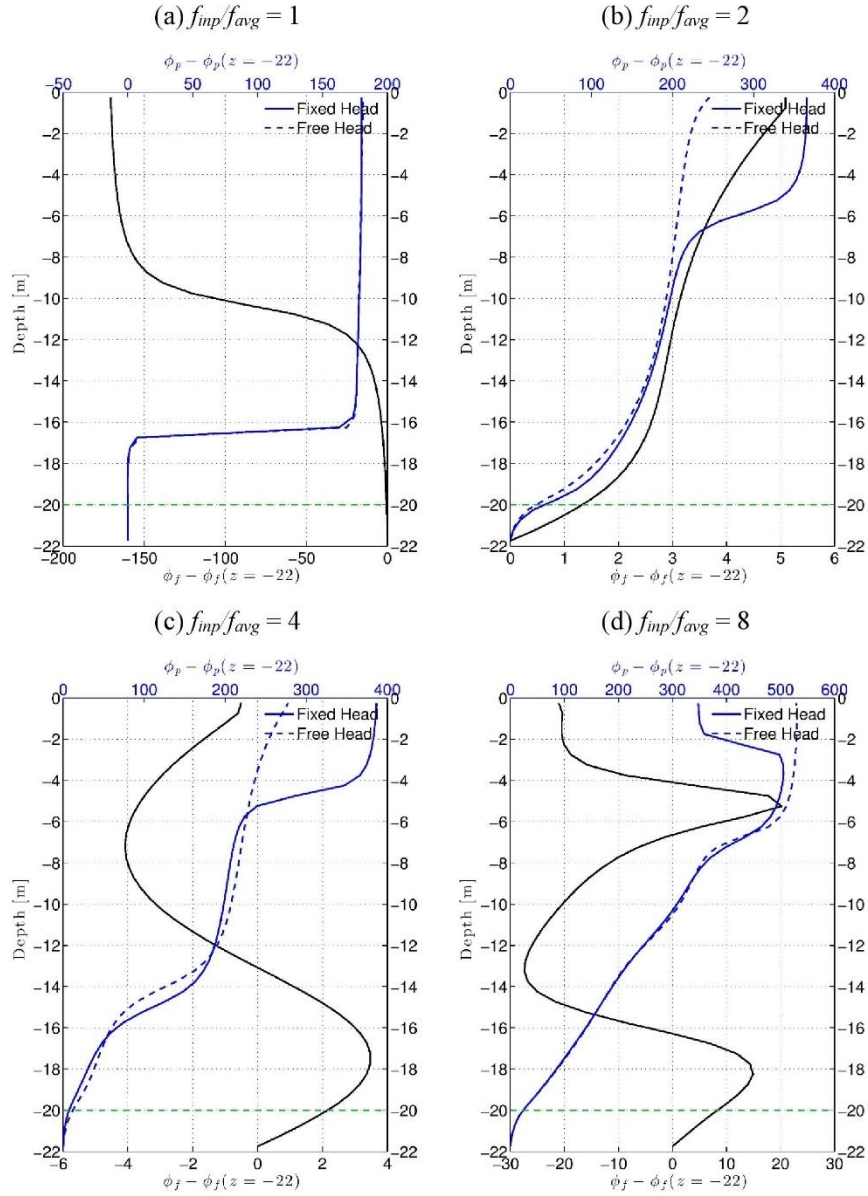


Figure 4.13 Pile and free field phase angle for homogeneous soil condition

- In order to visualize the phase variation along the pile length, the curvature phase angle at depth $z = -22$ m, which is equal to the pile length, is subtracted from the phase angles ϕ_p and ϕ_f . As seen, for $f_{imp}/f_{avg} = 2$ and 4, the soil phase shift is negligible (less than 5 degrees). However, for $f_{imp}/f_{avg} = 1$, the free-field soil and pile phase angles change approximately 180 degrees at $z \approx -10$ m and $z \approx -16$ m, respectively, where the curvatures become minimum. This, in fact, depicts a change in the sign of curvature. In order to show this clearly, we rewrite the steady state curvature in the following form, considering the Hilbert transform of the real curvature data:

$$\kappa(z, t) = \left(\frac{1}{R}\right) (\omega, z) \{ \cos[-\omega t + \phi(\omega, z)] + i \sin[-\omega t + \phi(\omega, z)] \} \quad (4.8)$$

or

$$\kappa(z, t) = K(\omega, z) e^{(-i\omega t)} \quad (4.9)$$

where $K(\omega, z) = \left(\frac{1}{R}\right) (\omega, z) [\cos\phi(\omega, z) + i\sin\phi(\omega, z)]$. The spatial variation of the real and imaginary components of $K(\omega, z)$ for fixed- and free-head piles in homogeneous soil layer are given in Figure 4.16 – Figure 4.17 for $f_{inp}/f_{avg} = 1$ and $f_{inp}/f_{avg} = 4$, respectively. As seen, for $f_{inp}/f_{avg} = 1$, ϕ_p is constant along the pile except at $z \approx -16$ m where the curvature changes sign. For $f_{inp}/f_{avg} = 4$, again, we can see the change in sign at $z = -5$ and -15 m for the fixed-head pile, and at $z \approx -15$ m for the free-head pile. However, in each segment, there are slight changes in the phase angle as well, which in turn result in open- and closed-loop behavior as shown in the top-view plots in Figure 4.17, respectively.

As seen in Figure 4.14 and Figure 4.15 in most cases, the introduced heterogeneity increases the curvature amplitudes in comparison to the homogeneous cases. For $f_{inp}/f_{avg} = 1$, the pile curvature behavior for both fixed- and free-head conditions is changed significantly. Moreover, in all cases, the intermediate soft layer causes building up of curvatures and thus the maximum curvatures occur in its vicinity. This, in turn, will cause the intensification of pile moments in this area. Also, the phase patterns are changed significantly in comparison with their homogeneous counterparts, which again will result in completely different curvature behavior. These results highlight the detrimental effects that a simplifying approach may have in pile design.

4.2.2.2 Kinematic Steady-State Displacement Response

As mentioned earlier, the kinematic pile interaction alters the space and frequency dependency of the amplitude and the phase angle of the free field soil response. An accurate knowledge of these effects can be used to properly transform the free field motions into kinematic pile input motions to be used in inertial SPSI analysis.

In this section, the effects of using the free field phase angle ϕ_f –instead of the kinematic phase angle of the pile ϕ_p – to compute the kinematic response of the pile (the input motion) is investigated. Considering a harmonic loading with frequency ω , the

steady-state response $u(z,t)$ can be written in the same way introduced in §4.2.2.1. To wit:

$$u(z,t) = U(\omega,z)e^{-i\omega t} \quad (4.10)$$

$$\text{where } U(\omega,z) = A(\omega,z)[\cos\phi(\omega,z) + i\sin\phi(\omega,z)] \quad (4.11)$$

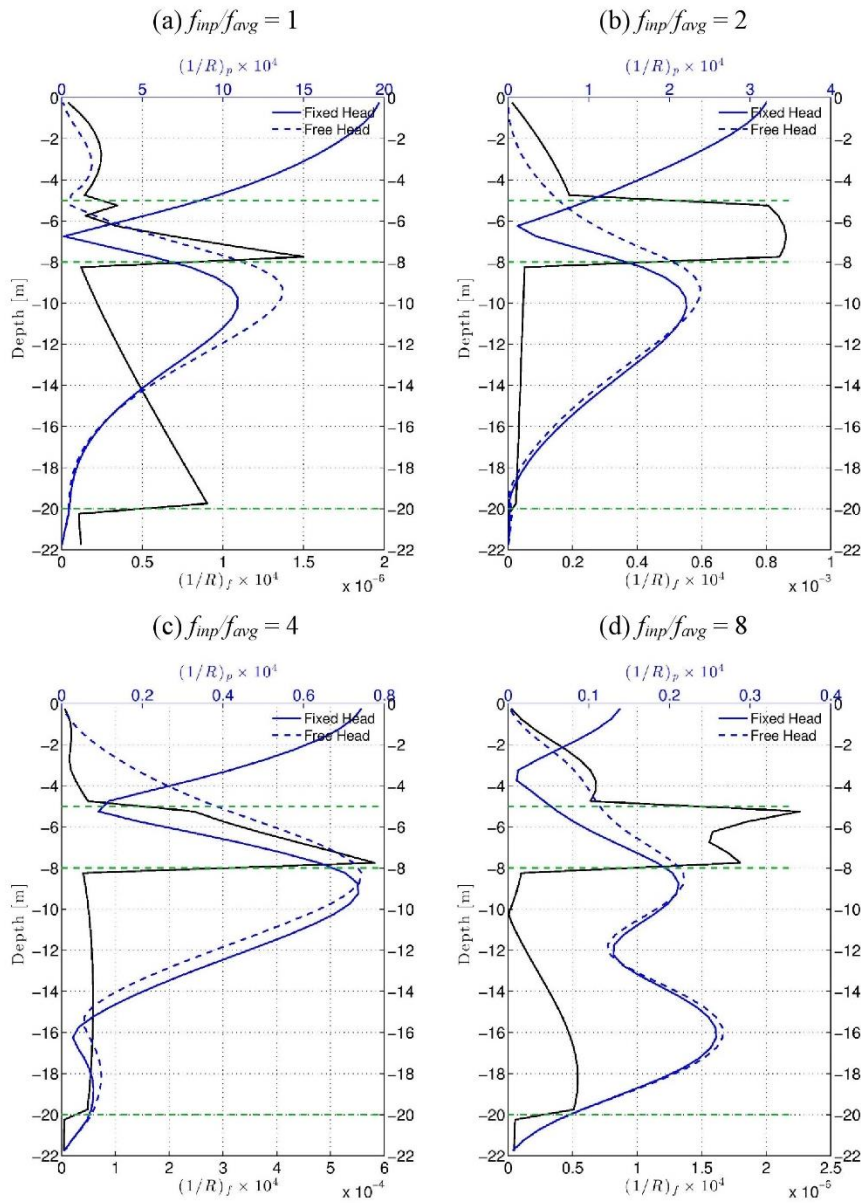


Figure 4.14 Pile and free field soil curvature for layered soil condition with intermediate soft layer

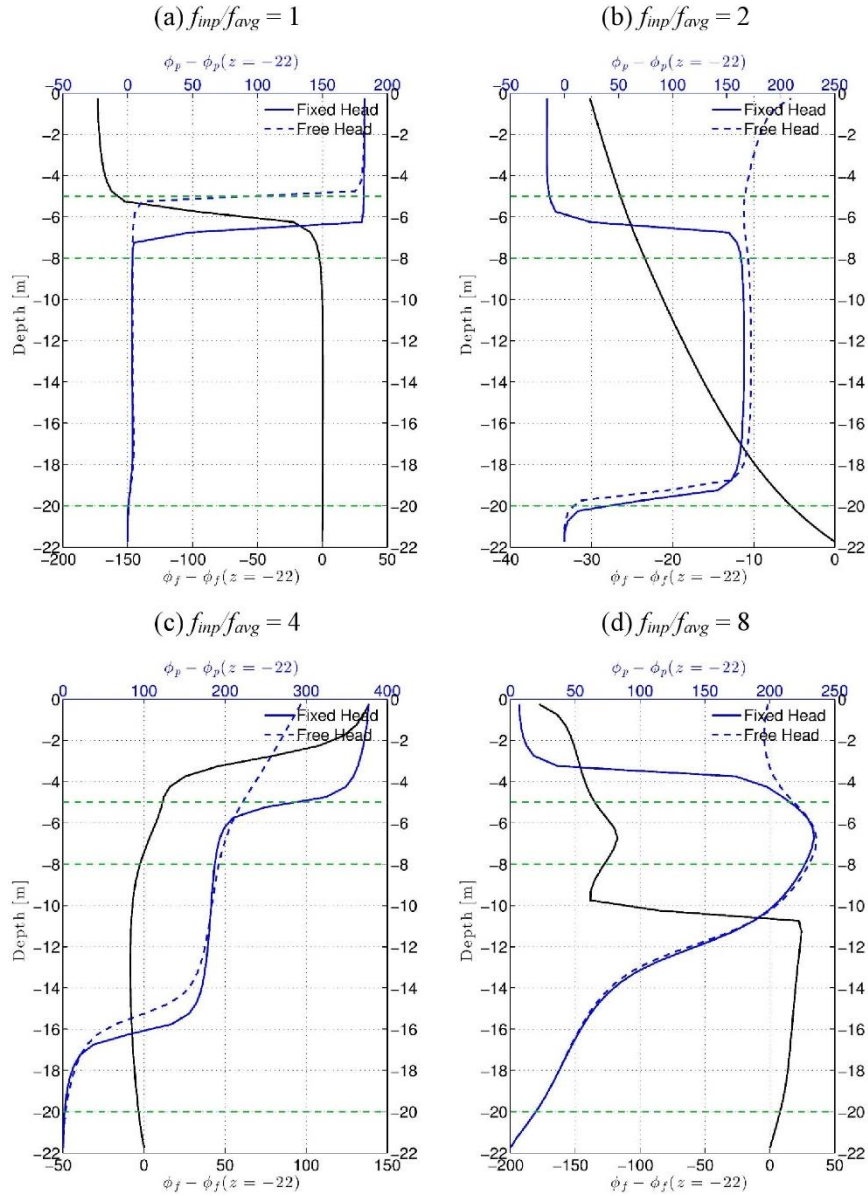


Figure 4.15 Pile and free field phase angle for layered soil condition with intermediate soft layer

Again, in all numerically studied cases, the steady state part of the calculated simulation data is used to fit a two-parameter sinusoidal function in order to obtain the amplitude $A(\omega, z)$ and the phase angle $\phi(\omega, z)$ of the pile, and the free field soil response. Then, the kinematic interaction factor $I(\omega, z)$ —taking the spatial variations of both amplitude and phase into account—can be defined as follows:

$$I(\omega, z) = \frac{A_p(\omega, z)}{A_f(\omega, z)} [\cos\Delta\phi(\omega, z) + i\sin\Delta\phi(\omega, z)] \quad (4.12)$$

where $\Delta\phi(\omega, z) = \phi_p(\omega, z) - \phi_f(\omega, z)$. It is useful to note here that previously defined kinematic interaction factor I_u –is a point-wise factor that only takes the amplitude changes into account–is equal to $I_u(\omega, 0)$ if $\Delta\phi(\omega, 0)$ is set zero in Equation (4.12).

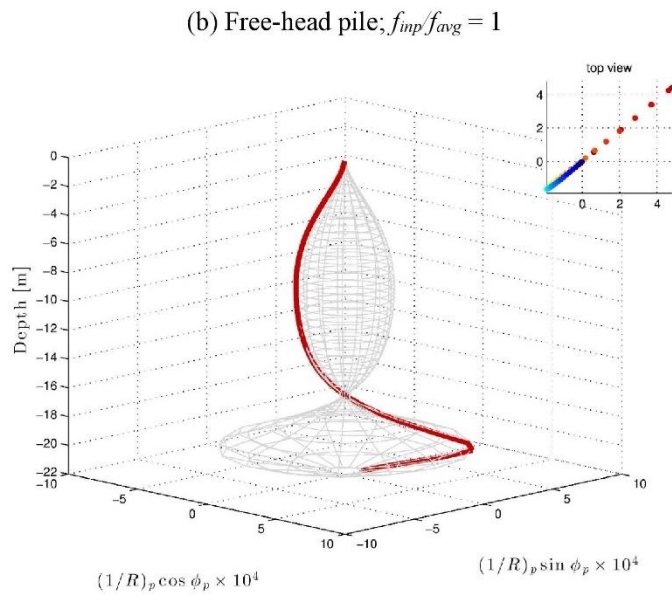
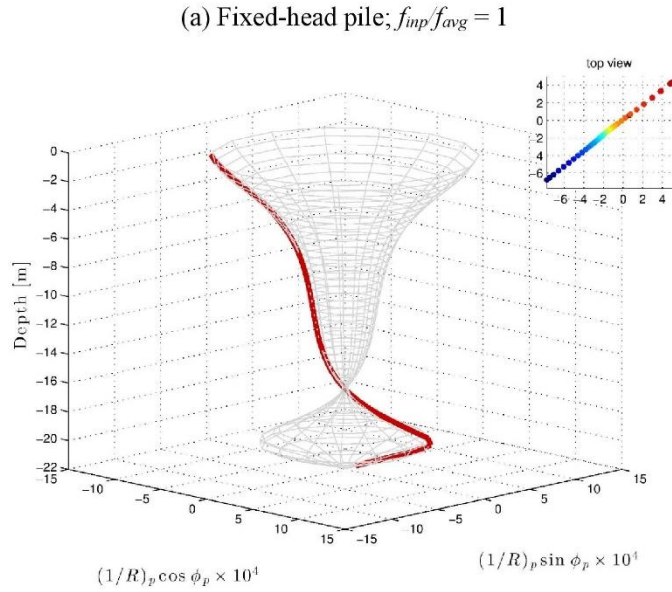


Figure 4.16 Spatial variation of real and imaginary components of the steady state pile curvature with depth for $f_{inp}/f_{avg} = 1$

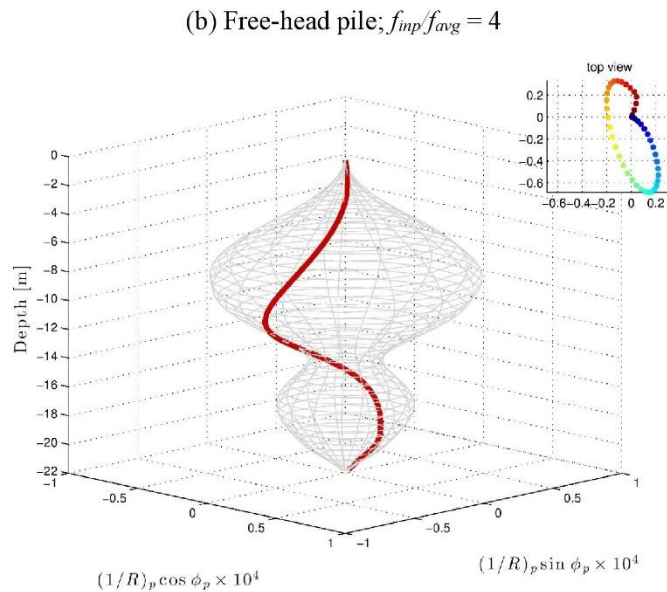
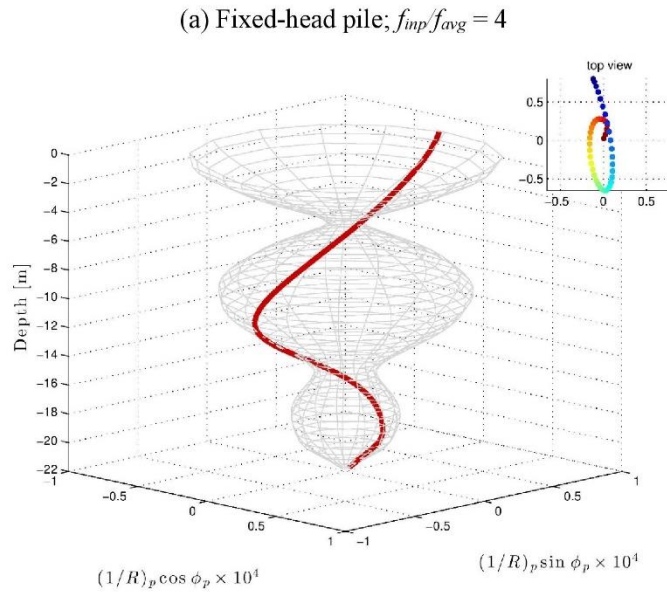


Figure 4.17 Spatial variation of real and imaginary components of the steady state pile curvature with depth for $f_{inp}/f_{avg} = 4$

Free field response of a homogeneous soil layer on elastic rock

The spatial variation of the free field response with depth is shown in Figure 4.18. The response is normalized using the reference point—filled dot in Figure 4.18—at depth $z_r = -20$ m. As seen, the maximum displacement occurs when the bedrock is excited at the natural frequency of the soil layer. By increasing ω , the amplitude decreases while its

fluctuations increase with depth, which can be approximately related to the number of wavelengths encompassed in the soil layer at each frequency. In other words:

$$\lambda \approx \frac{4H}{f_{inp}/f_{avg}} \quad (4.13)$$

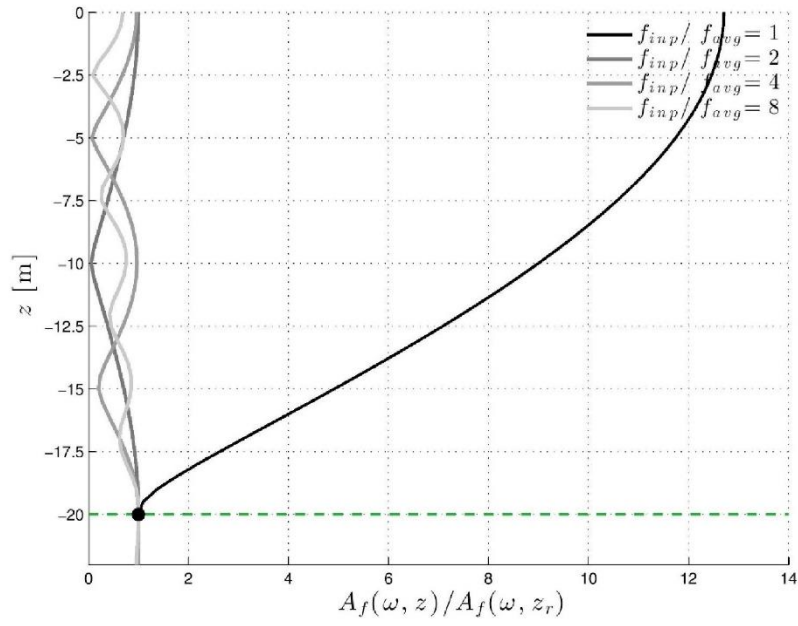
where λ is the wavelength, H is the layer thickness, and f_{avg} is the natural frequency of the homogenous soil layer. Using Equation (4.13), H becomes equal to $\lambda/4$, $\lambda/2$, λ , and 2λ for $f_{inp}/f_{avg} = 1, 2, 4$, and 8 , respectively. The existing phase shifts are also related to the minimums that are visible in the amplitude plots (see Figure 4.18(a)), which again are indications of sign changes in the soil response at those locations. As ω increases, the number of these shifts increases commensurately. It is useful to note here that the entire phase shifts from the bottom to the top of the soil layer ($\Delta\phi^H$) are approximately $\pi/2$, π , 2π and 4π for $f_{inp}/f_{avg} = 1, 2, 4$, and 8 , respectively. This can be justified by the following equation.

$$\Delta\phi^H \approx 2\pi H/\lambda \quad (4.14)$$

Effects of phase angle on steady state response of the pile

The changes of the real and imaginary parts of the pile response with depth for the homogeneous soil case is given in Figure 4.19 and Figure 4.20, respectively. In order to explore the effects of neglecting the kinematically induced phase differences with respect to free field condition, the pile responses—when they are in-phase with the free-field condition—are also plotted. Again, the free field response at the interface of the soil layer and the bedrock is used to normalize the pile amplitude and phase angle. The spatial variation of the amplitude and phase angle of the pile and the free field soil responses in polar coordinates is shown in Figure 4.21, wherein the horizontal and vertical axes measure the real and imaginary parts of the response, respectively. As seen in these figures, fixed- and free-head piles respond in almost identical fashion, except near the pile head. At $f_{inp}/f_{avg} = 1$, the actual pile response becomes significantly different along the entire length of the pile from the case where phase changes are neglected. This is mainly because an almost constant phase shift of about 45 degrees exists between free field and kinematic pile responses in this case (see Figure 4.21(a)). As ω increases, these differences become more localized. Moreover, the increase in loop behavior for higher frequencies (see Figure 4.21) depict the increase in changes of phase angle with depth and with a pattern that is different from the free field condition.

(a) Amplitude



(b) Phase angle

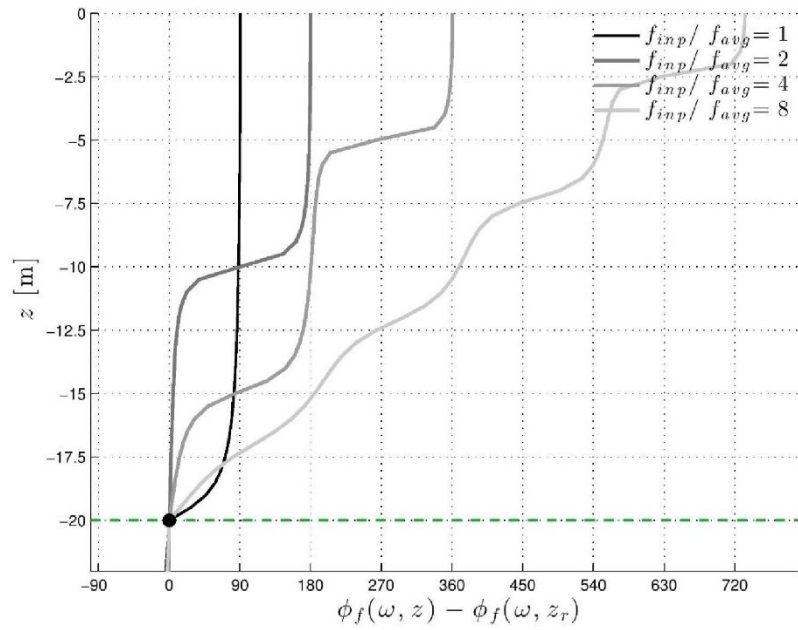


Figure 4.18 Free field response of a homogeneous soil on bedrock

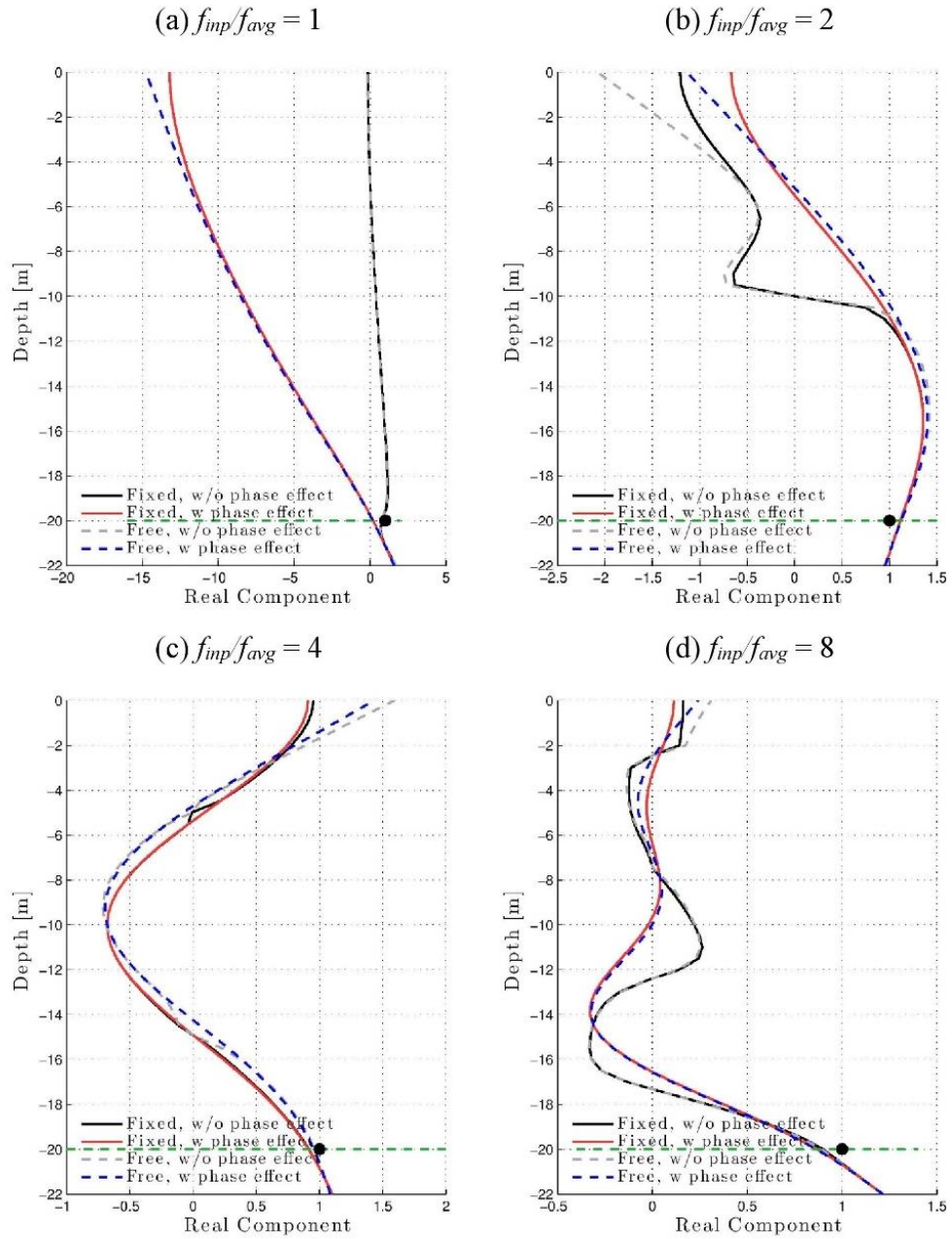


Figure 4.19 Effects of kinematic phase difference on real components of pile displacement in homogeneous soil

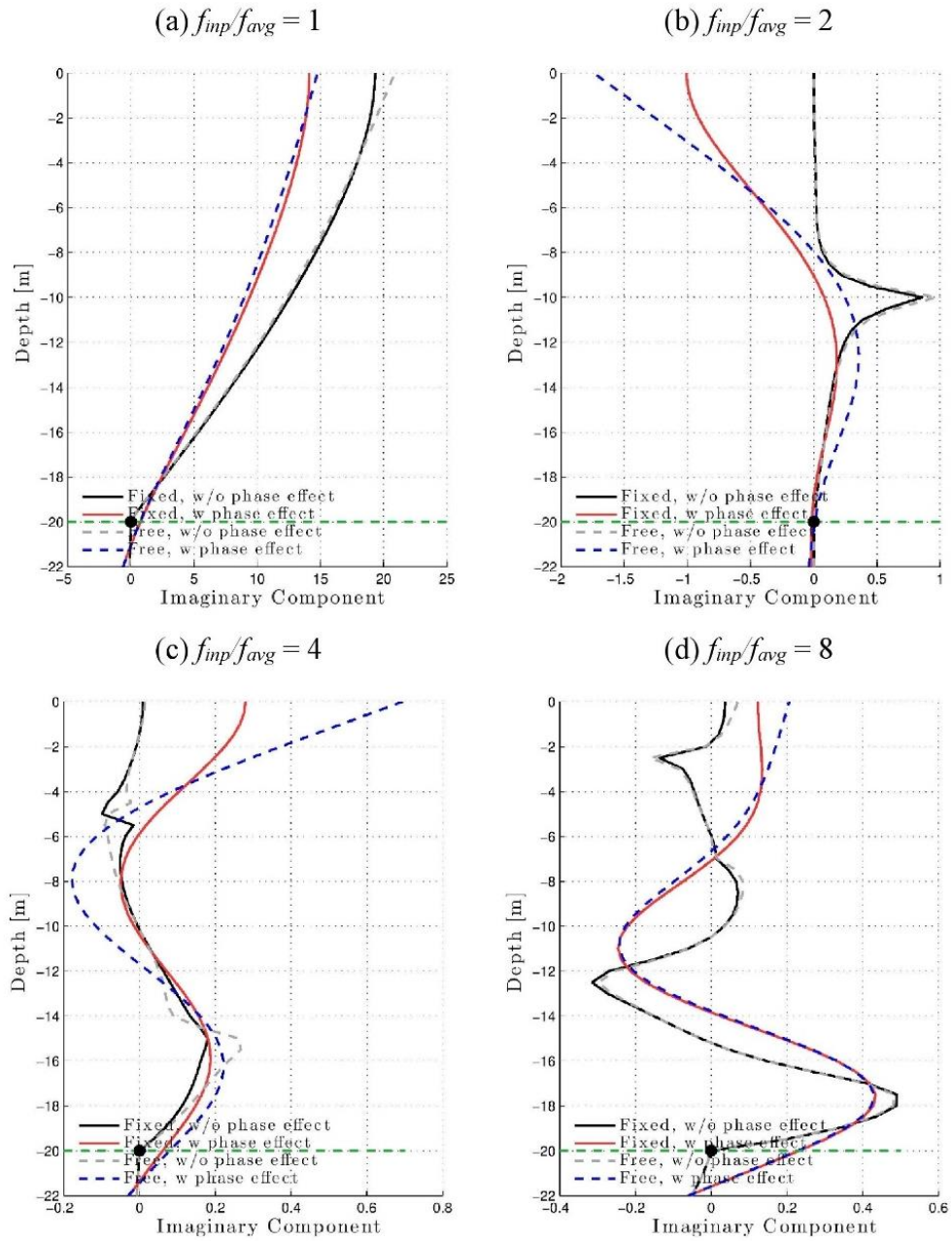


Figure 4.20 Effects of kinematic phase difference on imaginary components of pile displacement in homogeneous soil

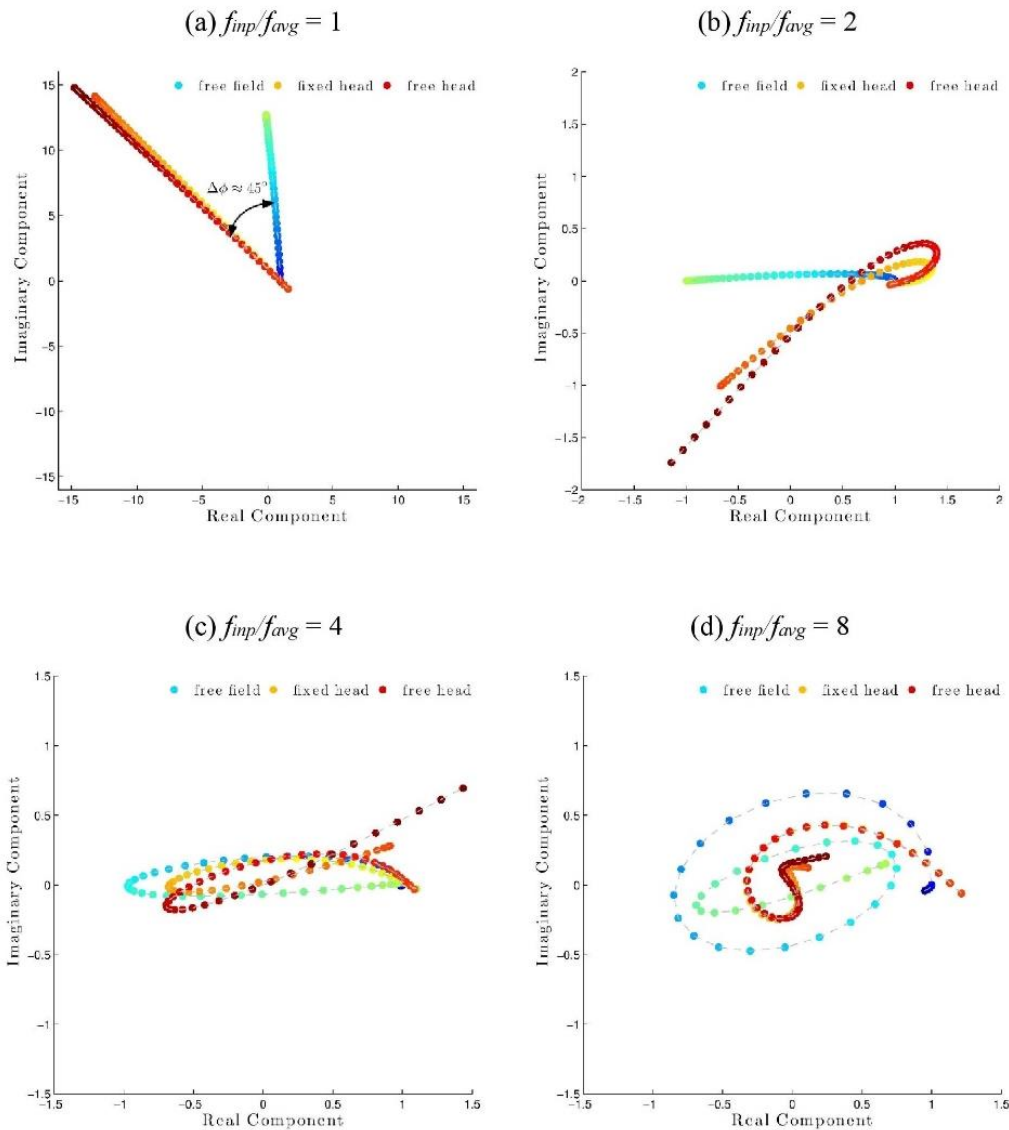


Figure 4.21 Spatial variation of the amplitude and phase angle of the pile and free field soil steady-state response in polar coordinate for the homogeneous soil

The same variations for the three-layered soil case are plotted in Figures 4.22 – 4.24. Again, we see that by taking the kinematic phase angle to be the same as its free field counterpart, errors are created in computing the actual kinematic responses of the pile. Moreover, phase differences between the fixed- and free-head pile become more pronounced at $f_{inp}/f_{avg} = 1$ (although this difference is almost constant along the pile length).

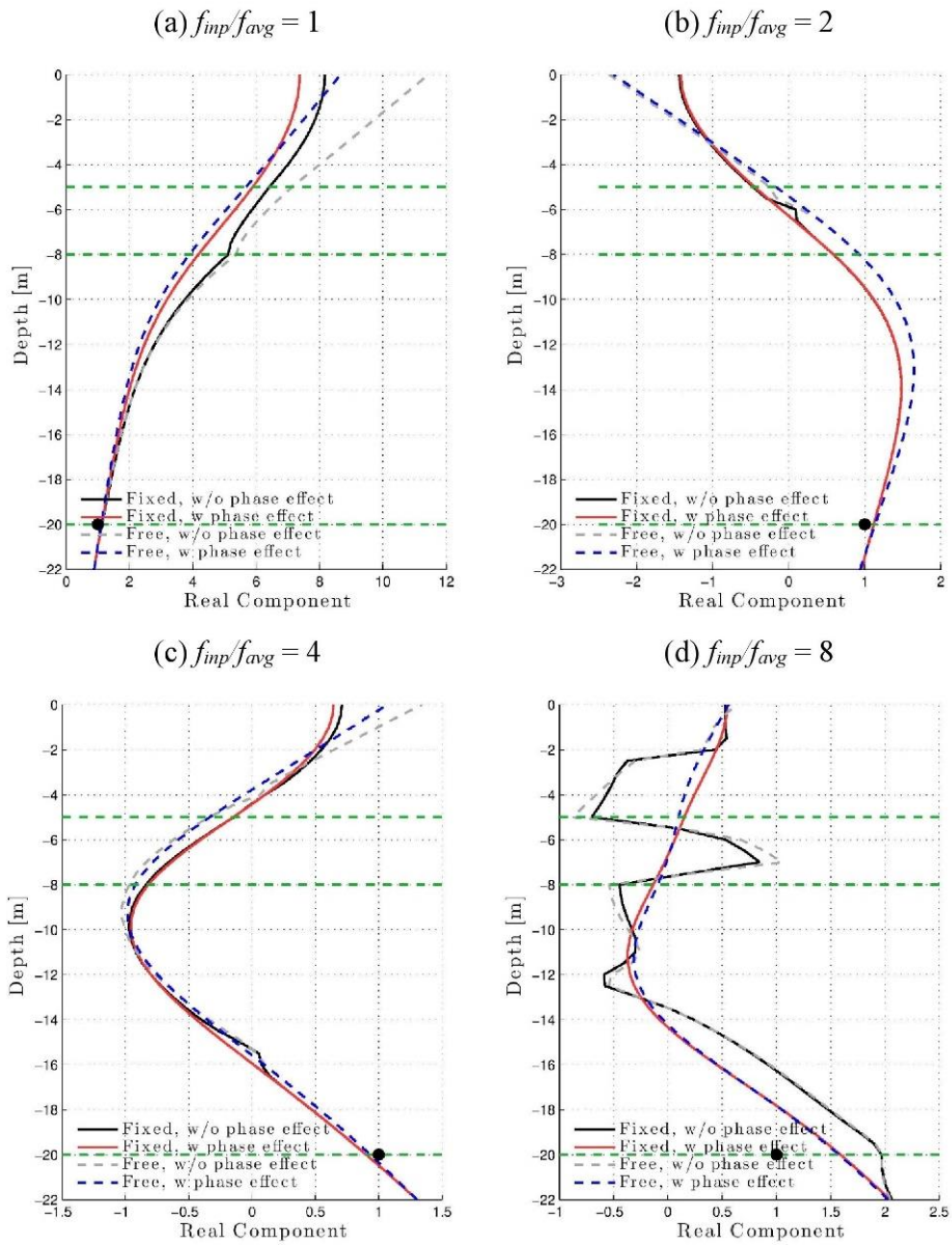


Figure 4.22 Effects of kinematic phase difference on real components of pile displacement in three-layered soil with an intermediate soft layer

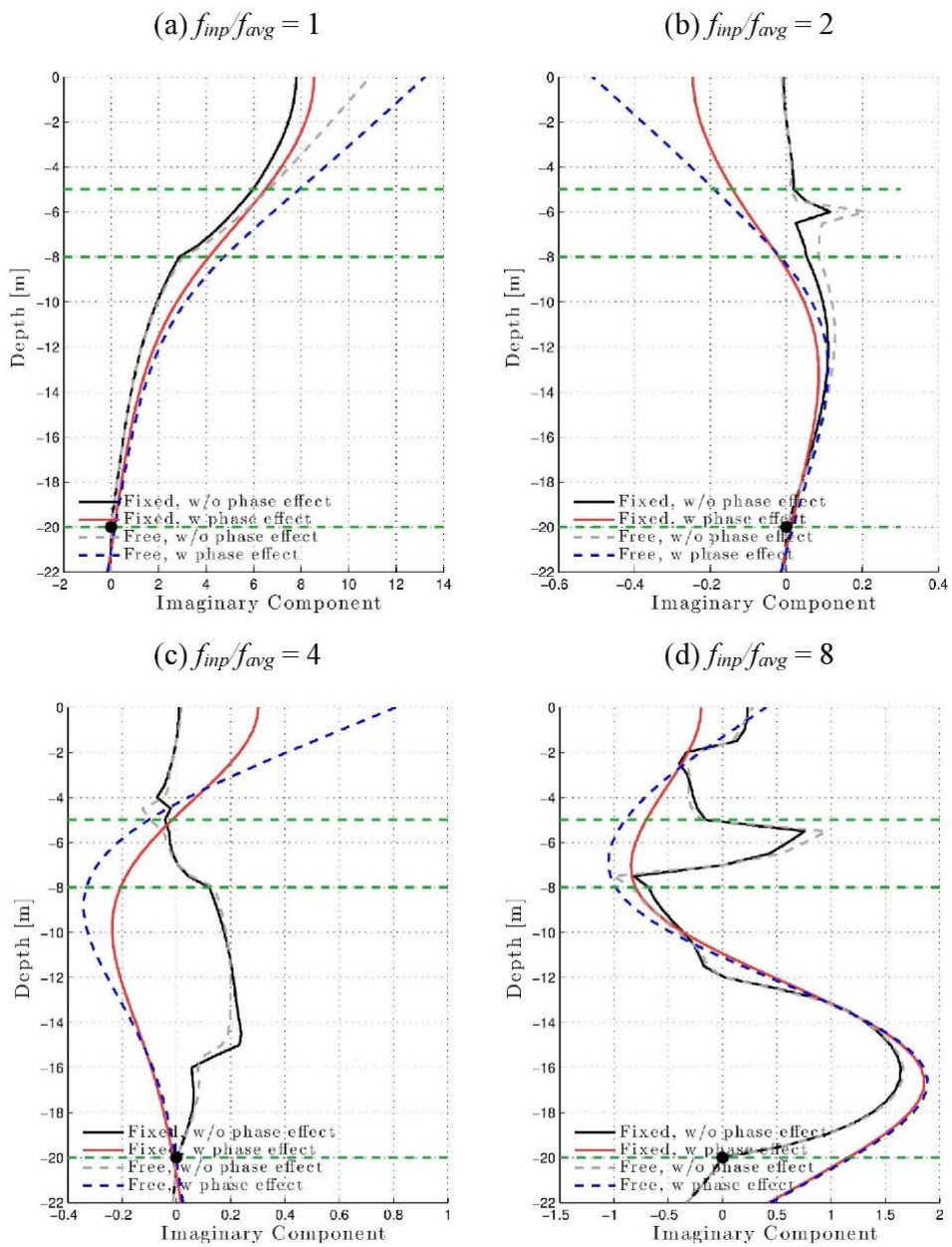


Figure 4.23 Effects of kinematic phase difference on imaginary components of pile displacement in three-layered soil with an intermediate soft layer

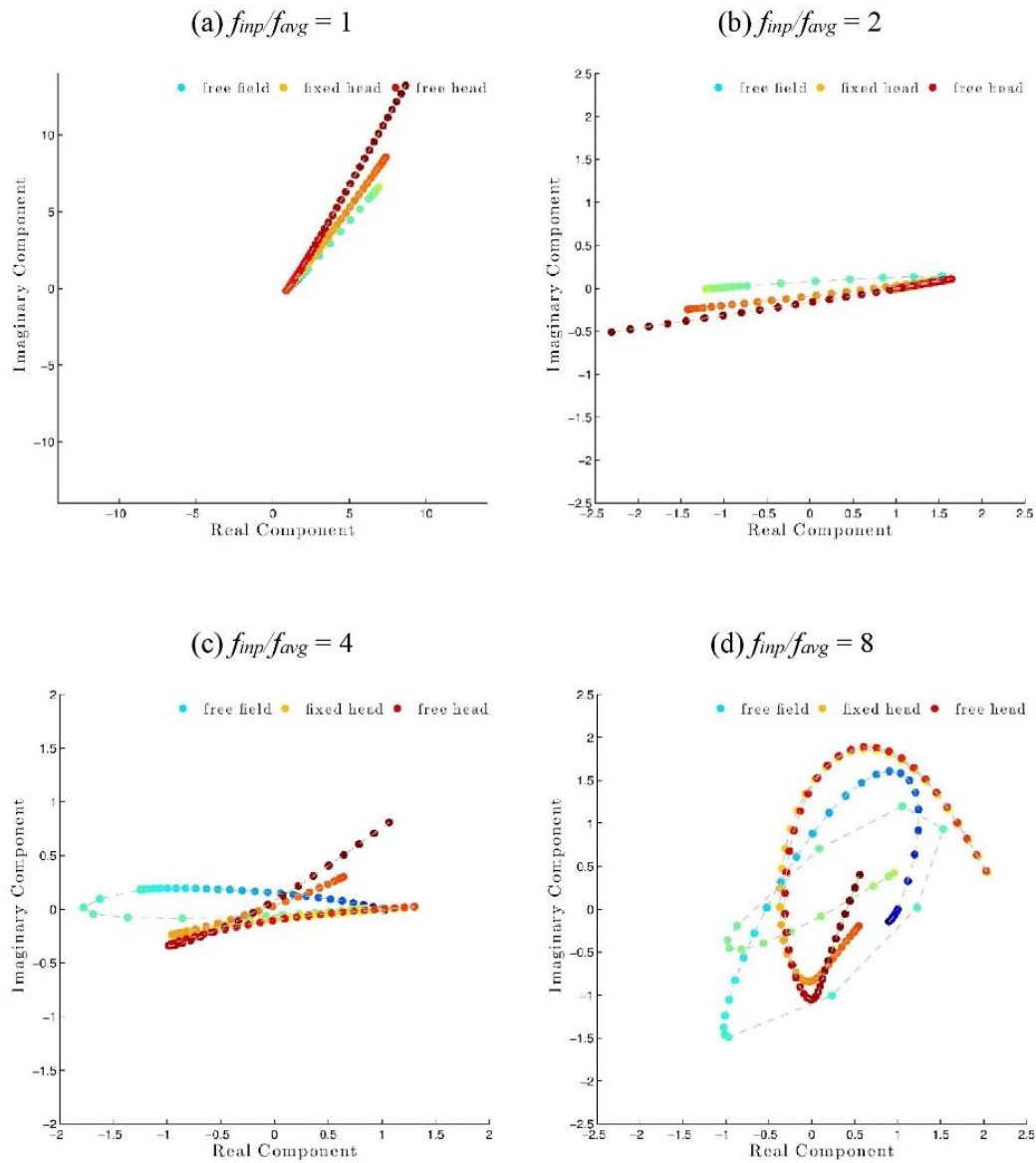


Figure 4.24 Spatial variations of the amplitude and the phase angle of the steady-state responses of the pile and the free field soil in polar coordinates for the three-layered soil with an intermediate soft layer

4.3 Concluding Remarks

In this chapter, the kinematic interaction between pile and soil is examined by an established numerical model with *OpenSees*. The significant findings are summarized below:

- Nonlinear soil behavior substantially influences the kinematic interaction. The elasto-plastic properties of soil reduce the seismic motion effect (especially in terms of acceleration). On the other hand, piles have a linear behavior

increasing the outcomes. Consequently, kinematic interaction factor in terms of acceleration (I_a) is larger than unity.

- Based on results obtained from earthquake loading, the kinematic interaction factor in terms of displacement is one, while in terms of acceleration it is variable depending on soil properties, pile properties, and motion features.
- A new kinematic interaction factor including phase angle have been suggested.

SOIL – PILE – STRUCTURE INTERACTION

The analysis of piled-structures under earthquake loading is a formidable task for design engineers due to interaction within soil, foundation system embedded in ground, and superstructure (“*SFSI*” soil-foundation-structure interaction). The piles, which transfer superstructure loads to the ground as structural elements, and the superstructure are main components of the design problem.

SFSI can be taken into consideration by *direct method* or *substructure method* [2]. In the *direct method*, complete soil – foundation – structure system is modeled as a continuum (e.g., with finite elements) and analyzed in single step. This method is rarely used in practice because a direct solution of *SFSI* problems is difficult, especially when the system is geometrically complex or the soil/structure behaves nonlinearly once loaded. Furthermore, conducting analyses through this method requires a computer program with which soil and structural elements can appropriately be modeled. On the other hand, in the *substructure method*, the foundation-superstructure system is analyzed separately and the response of the entire system is obtained by superposition, which actually is only valid for linear soil, pile, and structure. Nevertheless, the superposition can be applied to moderately-nonlinear systems as an engineering approximation [42], [115]. The *substructure method* includes the following steps [116]: (i) an evaluation of free-field soil motions; (ii) an estimation of transfer functions to convert free-field motions to foundation input motions (*FIM*); (iii) incorporation of springs and dashpots to represent stiffness and damping at the soil-foundation interface; and (iv) a response analysis of the combined structure-foundation system.

In this section, the responses of pile and structure under earthquake loading are investigated with a separate soil-pile-structure model established in *Plaxis 2D*. Various cases are modeled considering the complete soil-pile-superstructure system (i.e.,

kinematic and inertial effects) and the soil-pile system (only the kinematic effect) for a single pile and pile groups. The inertial effect, by an engineering approximation, is calculated by taking difference between complete model and soil-pile model.

5.1 Complete Soil – Pile – Structure Model

The geometry, boundary conditions, and solution of equation of motion are explained in Chapter 3 for the established model in *Plaxis*. Advanced features is used, such as hypoplastic soil material model to consider plastic behavior of soil and embedded-pile element. The superstructure is modelled as a single-degree-of-freedom system (*SDOF*). The piles and superstructure are linked by a massless pile cap resting directly on the soil. The complete model in *Plaxis* is shown schematically in Figure 5.1.

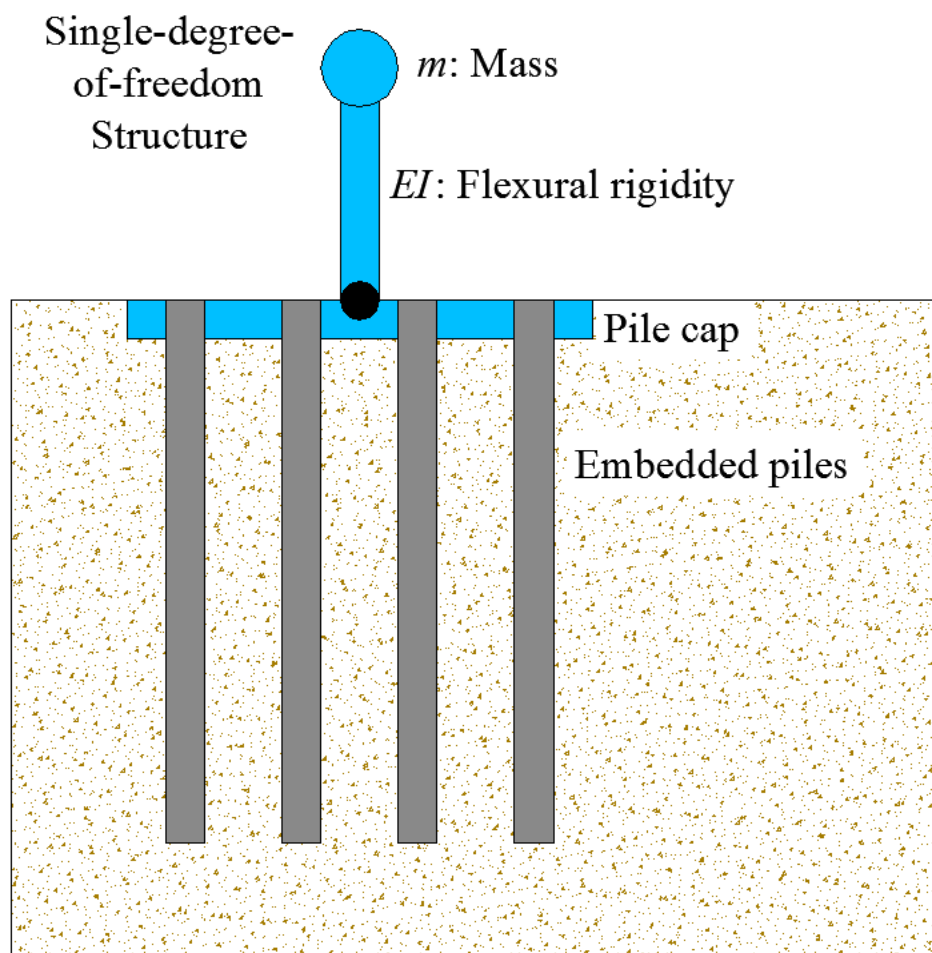


Figure 5.1 The complete soil – pile – structure model

5.1.1 Hypoplastic Soil Model

Many constitutive soil models, from simple to sophisticated, have been proposed for various geotechnical engineering problems. Design engineers need to select an applicable model in accordance with their project requirements. They want to be familiar with the *scopes* and *limitations* of the soil model; on the other hand, they do not interest and do not need to have a detailed background on the formulation of yield surfaces and complicated hardening rules. Constitutive model of soils are developed through laboratory experiments on specimens considering some fundamental properties of soils, such as [117]:

- Soil nonlinearity
- Soil irreversibility (loading – unloading - reloading)
- Asymptotic behavior in proportional stress and strain paths
- Failure criteria
- Stress-volumetric coupling
- Deformation history
- Anisotropy
- Time-dependence (rate-effects).

Goldscheider [118] initially developed hypoplasticity through an investigation of the sand behavior under cuboidal deformations, which has the following properties: (1) limited elastic behavior with a flow rule, (2) with a constant mean pressure the amount of contraction (negative dilatancy) after a reversal is larger than the one of dilatancy before a reversal, and (3) the proportional compressive deformation paths asymptotically lead to proportional stress paths. Kolymbas [119] proposed constitutive equations considering the aforementioned properties, however, the determination and physical meaning of the parameters were unsatisfactory. The hypoplastic model was improved by Kolymbas [120] by combining the effects of pressure and density. The hypoplastic model, contrary to the elasto-plastic model, does not separate deformations into elastic and plastic components, and hence, explicit definitions of yield function, flow rule, hardening, softening, etc. are not required [121]. Nevertheless, it is capable of predicting significant features of soil behavior, such as the critical state, dependency of the peak strength on density of soil, non-linear behavior for a wide range of strains (small to large), dependency of the soil stiffness on the loading direction.

The early hypoplastic models focused on the development of constitutive models for granular materials, i.e., sands and gravels. Niemunis & Krieg [122], Herle & Kolymbas [123], and Mašin [124] have applied hypoplastic principles to fine grained soils.

The general form of hypoplastic equation is:

$$\dot{\mathbf{T}} = \mathcal{L} : \mathbf{D} + \mathbf{N} \|\mathbf{D}\| \quad (5.1)$$

where $\dot{\mathbf{T}}$ represents the objective (Jaumann) stress rate, which is a function of Cauchy stress; \mathbf{D} is the Euler's stretching tensor; \mathcal{L} and \mathbf{N} are fourth- and second- order constitutive tensors, respectively. The model features and parameters considering soil type (clay and sand) are given in detail by Lanier et al. [125]; Weifner & Kolymbas [126]; Fuentes et al. [127]; and Mašin [128].

5.1.2 User Defined Hypoplastic Model for Clay in Plaxis

The hypoplastic model for clay implemented in *Plaxis 2D AE.02* [104] requires five constitutive parameters (N , λ^* , κ^* , ϕ_c , and r), which correspond to the parameters of the modified Cam-clay model and can be obtained by standard laboratory experiments. The model parameters N , λ^* , and κ^* are determined from isotropic compression line (Figure 5.2). The parameter ϕ_c is critical state friction angle; the parameter r controls the shear stiffness and needs to be calibrated by laboratory experiments.

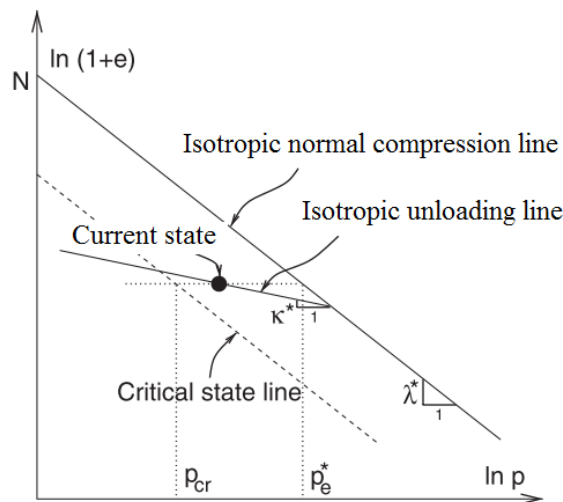


Figure 5.2 Isotropic compression and unloading lines defining parameters N , λ^* , and κ^* (adapted from [124])

The small strain behavior of clay is taken into consideration by the intergranular strain concept requiring five additional parameters [104]: R for the size of the elastic range; β_r and χ for the rate of stiffness degradation; m_R controls the initial shear stiffness for the initial and reverse loading conditions; and m_T for the stiffness on neutral loading conditions. The parameters must be calibrated by laboratory experiments utilizing dynamic methods capable of measuring very-small strains (less than 10^{-6} %), such as in bender elements and resonant column testing.

The parameter p_t represents the shift of the mean stress due to cohesion and non-zero value of p_t is required to overcome problems related to the stress-free state. Default value in *Plaxis* for p_t is 10 kPa and it may be set to a very low number, e.g. $p_t = 10^{-6}$, for basic hypoplasticity applications. The bulk modulus of water K_w for undrained analysis should be set to 0.

London clay properties determined by Gasparre [129] are used in the present study. Typical parameters are given in Table 5.1. Additionally, the shear strength degradation curve (G/G_{max}) (Figure 5.3) and damping ratio (ξ) (Figure 5.4) with increasing stiffness of London clay by hypoplastic model is compared with proposed curves for clay considering plasticity index (PI) by Vucetic & Dobry [109]. G/G_{max} curve is calculated by the ‘‘Soil Test’’ feature of *Plaxis* and ξ is computed by:

$$\xi = \frac{W_D}{4\pi W_S} \quad (5.2)$$

where, W_D (dissipated energy in a load cycle) and W_S (energy stored at maximum strain γ_s) are calculated by Equations (5.3) and (5.4), respectively, though they are derived for a small strain model by Brinkgreve et al. [130]:

$$W_D = \frac{4G_{max}\gamma_{0.7}}{a} \left[2\gamma_s - \frac{\gamma_s}{1+\gamma_{0.7}/\gamma_s a} - \frac{2\gamma_{0.7}}{a} \ln \left(1 + \frac{\gamma_s a}{\gamma_{0.7}} \right) \right] \quad (5.3)$$

$$W_S = \frac{G_{max}\gamma_s^2}{2+2\gamma_s a/\gamma_{0.7}} \quad (5.4)$$

$\gamma_{0.7}$ corresponds to shear strain at which G/G_{max} is equal to 0.7 and a is a constant value of 0.385. Damping ratio bounded by a certain lower limit of shear strain $\gamma_{cut-off}$:

$$\gamma_{cut-off} = \frac{\gamma_{0.7}}{a} \left(\sqrt{\frac{G_{max}}{G_{ur}}} - 1 \right) \quad (5.5)$$

in which G_{ur} denotes unloading reloading shear modulus ($G_{ur} \approx G_{max}/10$ for soft soils).

A damping of 5 % is considered in *Plaxis* using the Rayleigh method [98], in which a_1 and a_2 are calculated for a shear wave velocity of $V_s = 180$ m/s and a soil thickness of the top $H = 30$ m from the surface, which are determined considering a soil type of Z4 in the Turkish Earthquake Code [111] for $V_s < 200$ m/s and $H > 10$ m.

Table 5.1 Used parameters for the London clay in the hypoplastic model

Hypoplastic model parameters		Intergranular strain concept parameters	
ϕ_c	21.9°	R	5.00E-05
λ^*	0.1	m_R	9.0
κ^*	0.02	m_T	9.0
N	1.26	βr	0.1
r	0.5	χ	1.0

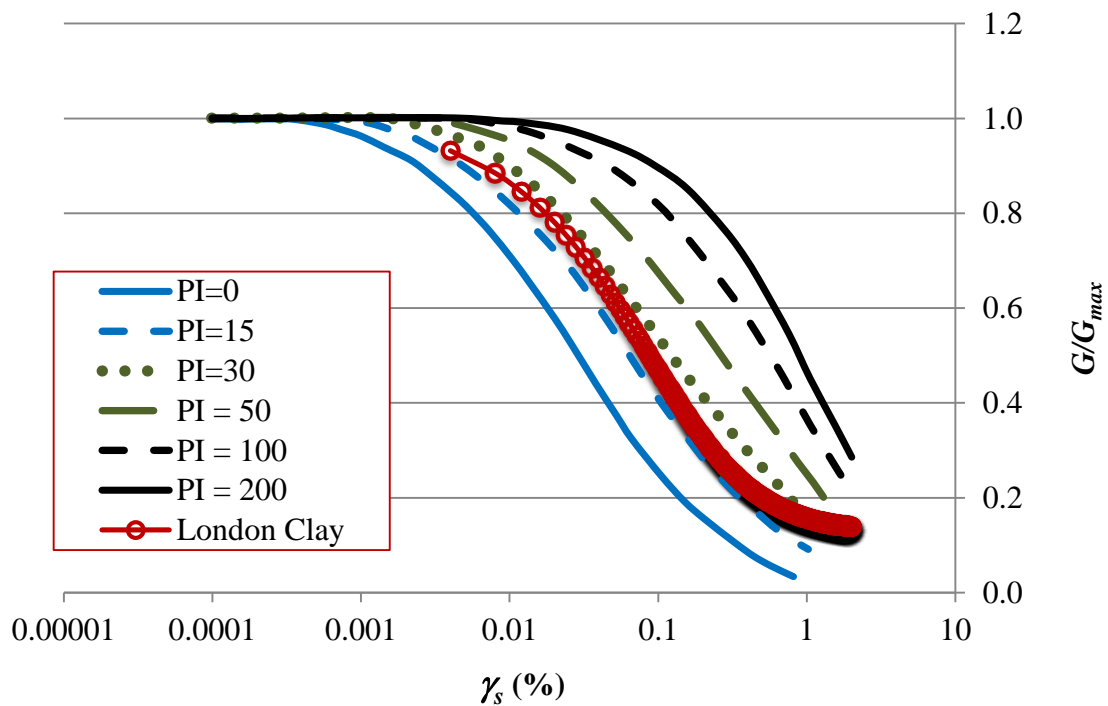


Figure 5.3 Shear stiffness degradation curve of London clay with comparison by curves of fine-grained material for different PI recommended by Vucetic & Dobry [109]

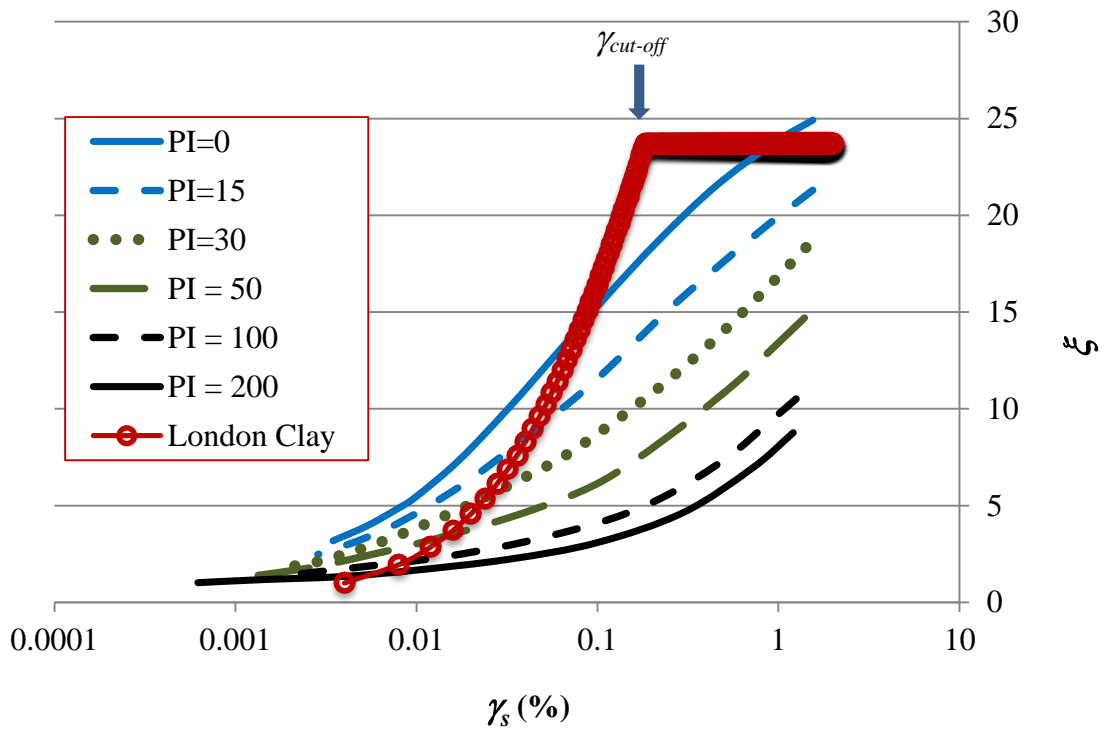


Figure 5.4 Damping ratio calculated by equation (5.2) and comparison with curves of fine-grained material for different PI recommended by Vucetic & Dobry [109]

The undrained cohesion c_u of clay layer is determined by simulation in “Soil Test” in Plaxis, similar to G/G_{max} curve. The relationship between shear and normal stresses are shown in Figure 5.5. Accordingly, the value of c_u is calculated as 60 kPa.

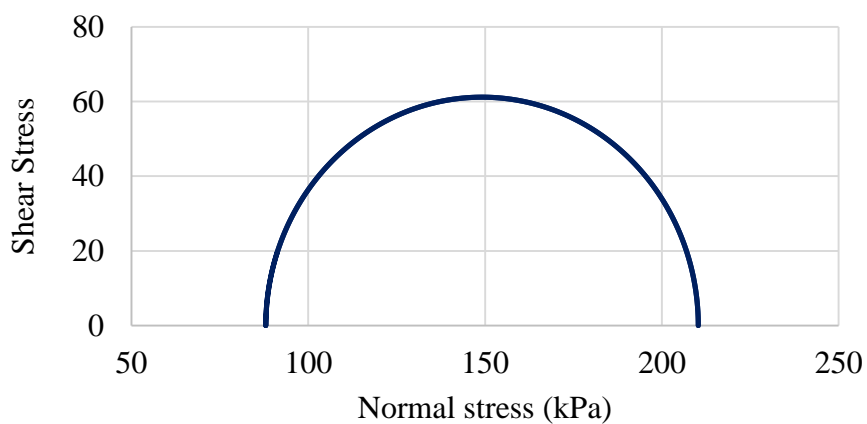


Figure 5.5 Mohr circle of London clay under undrained condition calculated through the “Soil Test” simulation feature in *Plaxis*

5.1.3 Embedded Pile Element

A special modeling element called the “*embedded pile*” is defined in *Plaxis* to model the pile based on the embedded beam approach [131], [132]. Embedded piles comprise of beam elements (represented by Mindlin beam element allowing deflections due to shearing as well as bending) to model pile itself and interface elements to model the interaction between the pile and the surrounding soil at the pile skin and tip. Moreover, the embedded pile element, unlike the solid or plate elements, deals with a row of piles in the out-of-plane direction in a two-dimensional plane strain model. As seen in Figure 5.6 the pile is not in a two-dimensional mesh, where the soil element is continuous, and the pile is superimposed on the mesh by special out-of-plane interface elements. The stiffness of the interface element should be determined considering loads transferred from the pile onto the soil and vice versa.

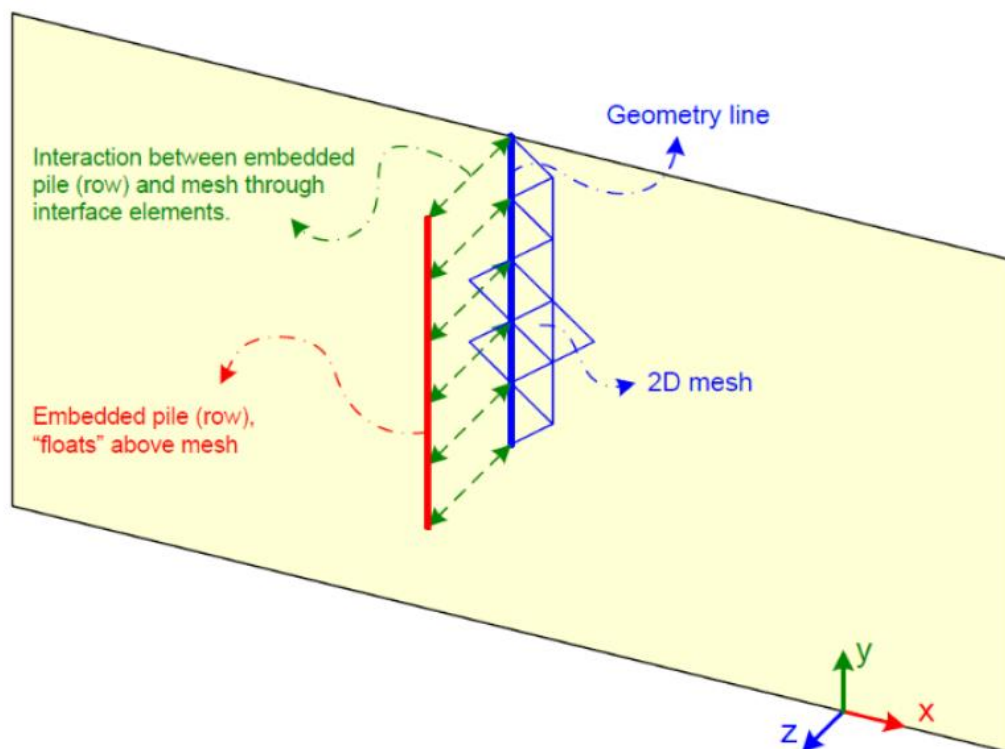


Figure 5.6 Schematic representation of embedded pile in the plane strain model [133]

5.1.3.1 Material Properties of Embedded Pile

The embedded pile is defined by a certain type of material data set: the properties of pile material and its geometric features, the interaction properties with the surrounding soil, and the out-of-plane pile spacing $L_{spacing}$ in a row. The pile is considered as an

elastic beam with a Young's modulus E_p and unit weight γ_p . Geometric features of the pile are defined by a predefined pile shape given by a *massive circular pile* and *pile diameter* D which determines the elastic zone around the actual pile.

5.1.3.2 Soil – Pile Interaction

The behavior of interface between the pile and the surrounding soil is described by an elastic-plastic model. The elastic behavior considers the differences between the pile displacements and the average soil displacements in out-of-plane direction. A skin resistance T_{max} (in unit of force per length) and a base resistance F_{max} (in unit of force) are defined with a failure criteria to distinguish the elastic and plastic behavior.

In the elastic region, the shear force t_s at a particular point:

$$|t_s| < T_{max} \quad (5.6)$$

For the plastic behavior:

$$|t_s| = T_{max} \quad (5.7)$$

The shaft resistance is defined by means of skin resistance at the pile top and bottom: $T_{top,max}$ and $T_{bot,max}$. The total pile bearing capacity N_{pile} is calculated by:

$$N_{pile} = F_{max} + 1/2 L_{pile}(T_{top,max} + T_{top,min}) \quad (5.8)$$

The equivalent bearing capacity per unit of width in the out-of-plane direction is calculated by dividing the bearing capacity by the pile spacing $L_{spacing}$.

Modelling of soil-pile interaction is portrayed in Figure 5.7.

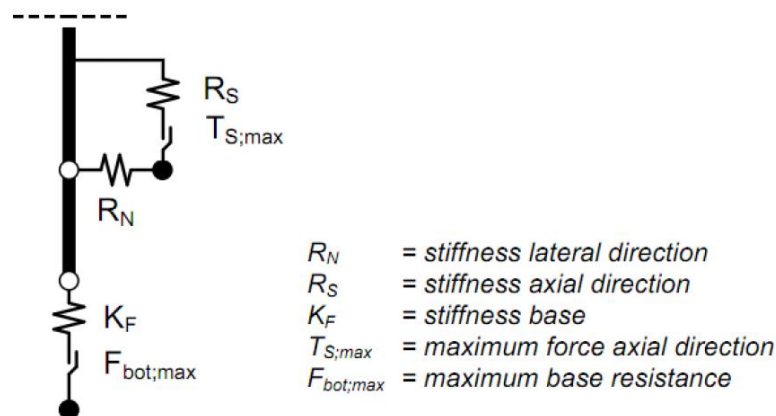


Figure 5.7 Soil-pile interaction model in *Plaxis* [102]

The interface stiffnesses:

$$R_S = ISF_{RS} \frac{G_s}{L_{spacing}} \quad (5.9)$$

$$R_N = ISF_{RN} \frac{G_s}{L_{spacing}} \quad (5.10)$$

$$K_F = ISF_{KF} \frac{G_s}{L_{spacing}} \quad (5.11)$$

The interface stiffness factors for axial ISF_{RS} , lateral ISF_{RN} , and base ISF_{KF} :

$$ISF_{RS} = ISF_{RN} = 2.5 \left(\frac{L_{spacing}}{D_{eq}} \right)^{-0.75} \quad (5.12)$$

$$ISF_{KF} = 25 \left(\frac{L_{spacing}}{D_{eq}} \right)^{-0.75} \quad (5.13)$$

where D_{eq} is the embedded pile diameter (5.14).

$$D_{eq} = \sqrt{\frac{12EI}{EA}} \quad (5.14)$$

An elastic zone around the embedded pile row in the surrounding soil is automatically defined by the *Plaxis* software. The size of this zone is equal to the equivalent diameter of embedded pile along the pile and is equal to the equivalent radius R_{eq} ($=D_{eq}/2$) at the base of the pile (Figure 5.8).

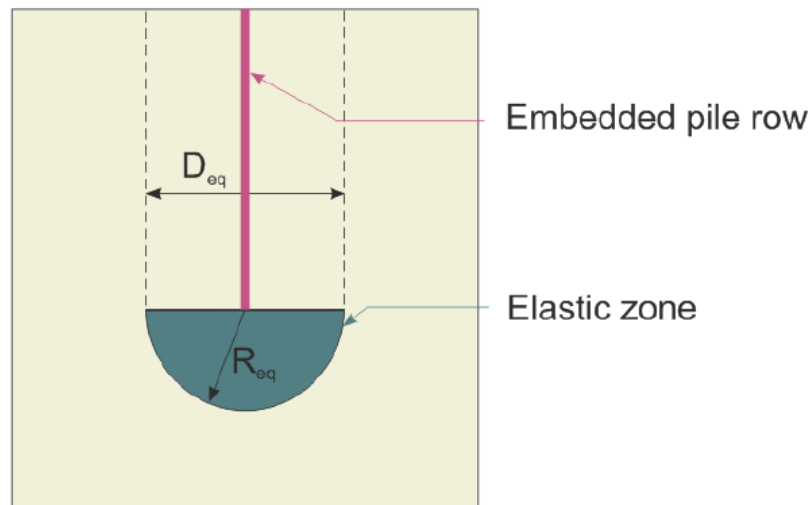


Figure 5.8 Elastic zone in the surrounding soil [102]

Parameters used in analysis for the pile geometry and bearing capacity vary according to pile diameter D and material (concrete or steel). The skin resistance is calculated by the α method (5.15) assuming an α value of 0.6 based on c_u and the base resistance is determined by (5.16) [134].

$$T = \alpha c_u \pi D \quad (5.15)$$

$$F = 9c_u \pi D^2 / 4 \quad (5.16)$$

5.1.4 Single-Degree-of-Freedom (SDOF) System

The superstructure is modelled as a linear mass-spring system represented by a mass on top of a beam (Figure 5.9) and verified by a free-vibration analysis.

The natural frequency f_n of the beam is:

$$f_n = \omega_n / 2\pi = \frac{1}{2\pi} \sqrt{\frac{k}{m}} = \frac{1}{2\pi} \sqrt{\frac{F/u}{m}} \quad (5.17)$$

where ω_n natural frequency, k spring constant, F force, u deflection, m mass.

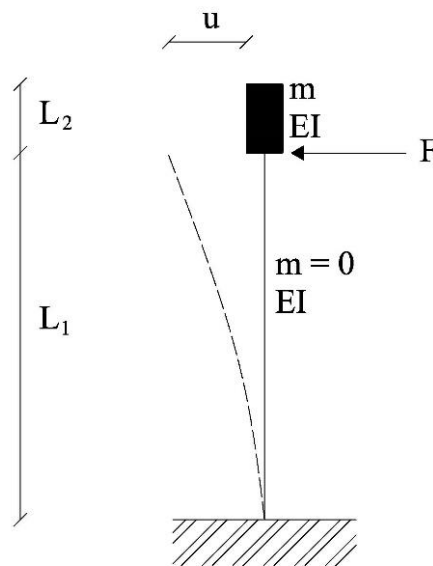


Figure 5.9 Mass-spring system with a cantilever beam and a mass on top

The deflection of the beam (u) consists of two components: deflection due to the load applied at the top of the beam $u_{bending}$ (5.18) and deflection due to in the cross-section of the beam u_{shear} (5.19) [102].

$$u_{bending} = \frac{FL^3}{3EI} \quad (5.18)$$

$$u_{shear} = \frac{12FL(1+\nu)}{5EA} \quad (5.19)$$

The natural frequency f_n of a beam with mass on top can be calculated by:

$$f_n = \frac{1}{2\pi} \sqrt{\frac{F}{\left(\frac{mFL^3}{3EI} + \frac{12mFL}{5EA}\right)}} \quad (5.20)$$

In the two dimensional model, a rectangular cross-section is considered with a width b of 1 m. Then, cross-sectional area is $A = b \cdot h = h$ m² and moment of inertia is $I = b \cdot h^3/12 = h^3/12$. A slender beam ($h/L < 0.1$) is chosen to minimize (or ignore) the effect of the shear part (< 1 %).

The mass-spring system is modelled by two plate elements in the *FE* model. The first element representing the spring has a length L_1 equal to the height of the center of the mass; the latter is mass, which has a very small length ($L_2 = 0.02 \times L_1$).

The geometry (Figure 5.10) and stiffness parameters of plates are given in Table 5.2. The structural elements are assumed as reinforced concrete. The weight of mass varies according to the natural frequency (or period) of *SDOF* system (Table 5.3), which is calculated using equation (5.20). The soil geometry and properties are insignificant (for *SDOF* system) without affecting the results and this is necessary for mesh and calculation because *Plaxis* cannot run without soil with error: “stiffness matrix is nearly singular and cannot be solved”. The column plate element is extended due to similar reason as well.

Free-vibration analysis, for verifying of the *SDOF* system, is performed in four phases.

1. Initial phase
2. Construction of *SDOF* structure
3. Loading: the beam is loaded at the top with a horizontal force of -10 kN/m.
4. Free-vibration: the applied force is released and then the system is allowed to vibrate.

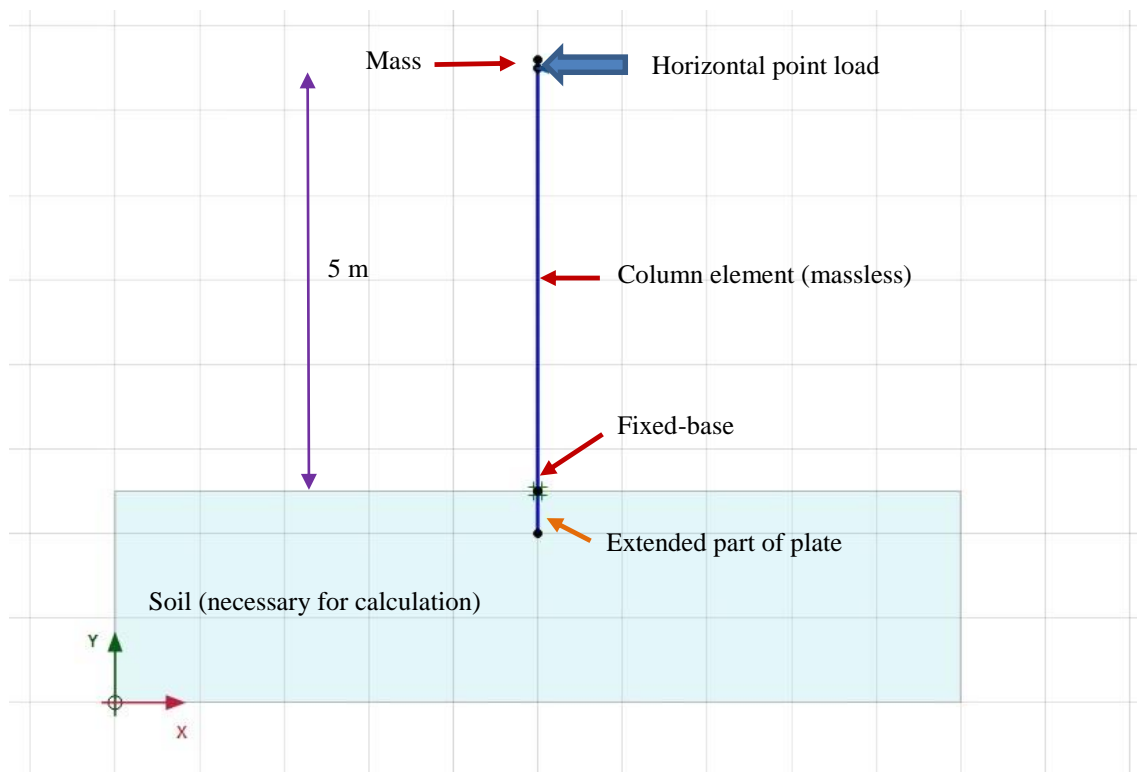


Figure 5.10 Fixed-base *SDOF* system created by *Plaxis* to verify superstructure model

Table 5.2 Geometric and stiffness features of *SDOF* system

Parameter	Plate 1 (Spring)	Plate 2 (Mass)
Material Type	Isotropic Linear Elastic	Isotropic Linear Elastic
Length, L	5 m	0.1 m
Young's modulus, E	30 GPa	30 GPa
Cross-sectional area, A	0.1 m ²	0.1 m ²
Moment of inertia, I	8.33E-5 m ⁴	8.33E-5 m ⁴
Weight, w	0 kN/m/m	variable

Table 5.3 Weight of mass based on the natural frequency of fixed-base beam

Frequency, f (Hz)	Period, T (sec)	Weight, w (kN/m/m)
2.0	0.5	38
0.5	2.0	607

Results calculated by the finite element method (*Plaxis*) are compared with the analytical solutions in terms of bending deflection $u_{bending}$ (5.18) and presented in Table 5.4. Moreover, the periods of *SDOF* system calculated by *FEM* using definite weights computed by equation (5.20) to reach the desired period (Table 5.5) are shown in Figure

5.11. It could be seen that the obtained values by established FEM are in accord with the calculated values by analytical methods.

Table 5.4 Comparison of bending deflection calculated by FEM and analytical method

$u_{bending}$ (FEM)	$u_{bending}$ Eq.(5.15)	Difference
0.174 m	0.167 m	4.19 %

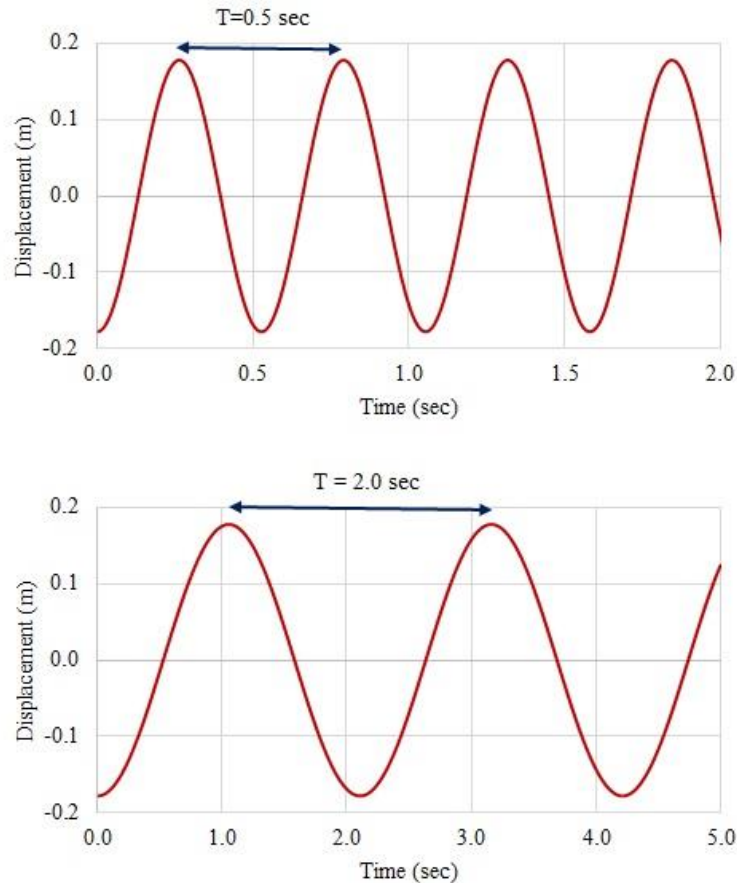


Figure 5.11 Periods of *SDOF* system obtained by FEM for different weight in Table 5.5

5.2 Investigation of Pile and Superstructure Responses by Parametric studies

The response of pile have been investigated in this study by complete model created by *FEM (Plaxis)* applying three real earthquake records at the base of the model (Table 5.5). Besides, the response of superstructure and foundation input motion have been addressed. Analyses were performed considering situations presented in Figure 5.12 for single pile and Figure 5.13 for pile group. The cases are as the following:

- *Case I* represents free-field condition.

- *Case II* corresponds to kinematic loading; *Case III* reflects complete situation (soil-pile-structure) for a single pile.
- *Case IV* is modeled to compare mass response with pile (*Case III*: point E) and without pile (point F).
- *Case V* and *Case VI* is modeled to simulate pile response against kinematic loading considering free-head and restrained-head (with cap).
- *Case VII* demonstrates complete model which is similar in practical problem.

Table 5.5 Earthquake records used in the analyses

Motion ID	Earthquake	Station (Direction)	$V_{s,30}$ (m/s) *	PGA (g)
Düzce	1999 Düzce	Mudurnu (000)	535	0.120
Kocaeli	1999 Kocaeli	Ereğli (090)	585	0.101
Loma Prieta	1989 Loma Prieta	Gilroy #1 (090)	1428	0.473

* $V_{s,30}$ represents site condition where the station is located.

Parameters used in analyses for embedded-pile and *SDOF* system are presented in Table 5.6 and Table 5.7, respectively. The diameter of 1 m and the *SDOF* system period of 0.5 sec is preferred in analyses, except pile diameter and *SDOF* system period effects on complete (soil-pile-structure) system response. The pile cap is considered as a massless plate element with a Young's modulus of 30 GPa and thickness of 1 m. Pile, *SDOF* system, and cap are considered as undamped. With respect to soil, London clay properties are used considering hypoplastic material model (Table 5.1).

Table 5.6 Parameters used for embedded pile

Parameter	Values		
	1	0.5	2
Diameter, D (m)	1	0.5	2
Length, L_{pile} (m)	20	20	20
Slenderness ratio, L/D	20	40	10
Spacing in out-of-plane, $L_{spacing}$ (m) $\approx 3D$	3	1.5	6
Young's modulus, E_{pile} (GPa)	30	30	30
Unit weight, γ_p (kN/m ³)	25	25	25
Skin resistance at pile top, $T_{top,max}$ (kN/m)	120	60	240
Skin resistance at pile top, $T_{bot,max}$ (kN/m)	120	60	240
Base resistance, F_{max} (kN)	425	105	1700

Table 5.7 SDOF system parameters considering system period T and width (which is equal to pile diameter D)

Parameter	$T = 0.5$ sec $D = 1.0$ m	$T = 2.0$ sec $D = 1.0$ m	$T = 1.0$ sec $D = 1.0$ m	$T = 0.5$ sec $D = 0.5$ m	$T = 0.5$ sec $D = 2.0$ m
Spring length, L_{spring} (m)	5	10	10	5	10
Mass length, L_{mass} (m)	0.1	0.2	0.2	0.1	0.2
Young's modulus, E (Gpa)	30	30	30	30	30
Cross-sectional area, A (m ²)	1	1	1	0.5	2
Moment of inertia, I (m ⁴)	8.33E-02	8.33E-02	8.33E-02	1.04E-02	6.66E-01
Weight of mass, w (kN/m/m)	3800	3800	950	950	950

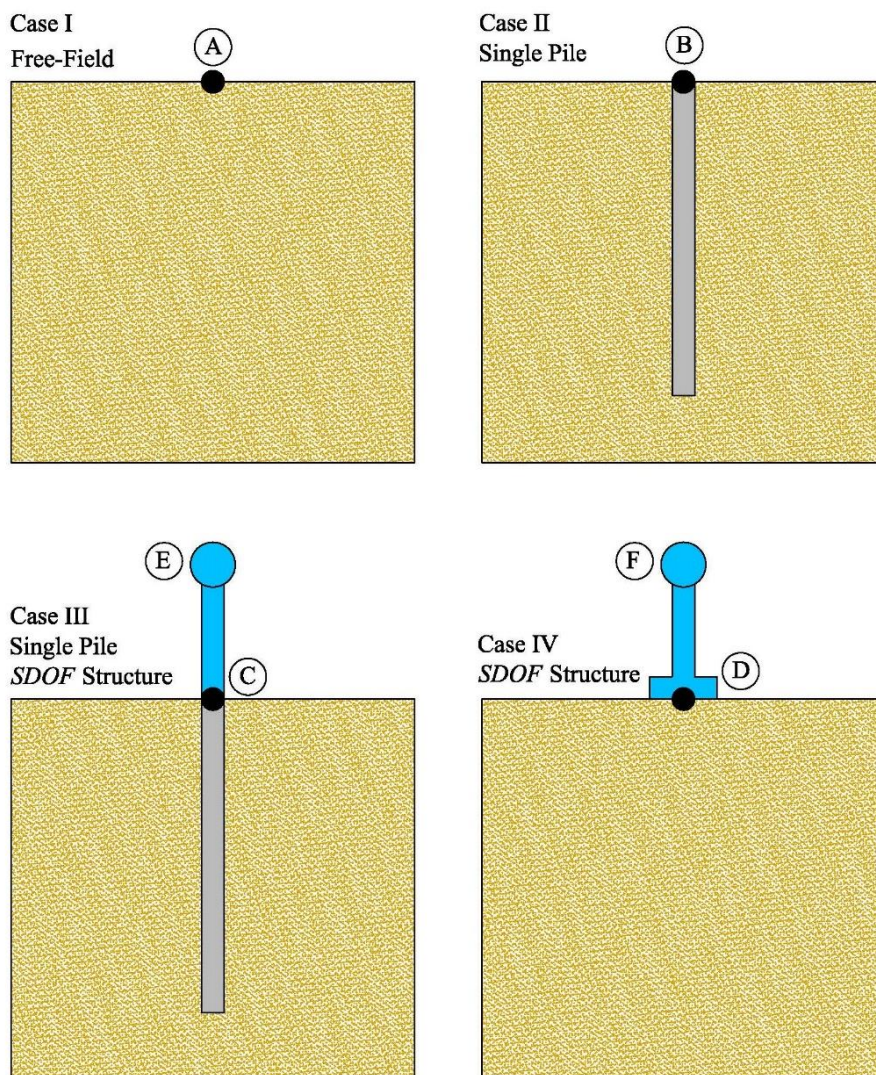


Figure 5.12 Investigated cases for single pile

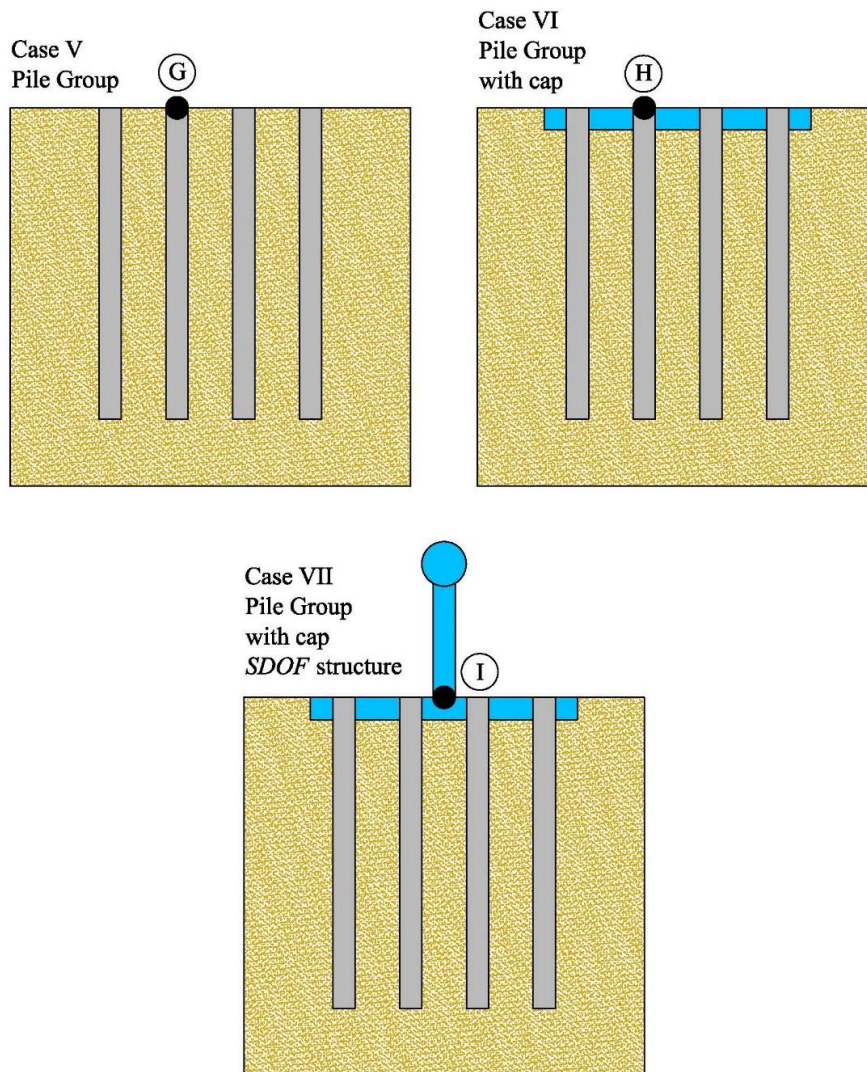


Figure 5.13 Pile group cases considered in analyses

5.2.1 Pile Response

In design of the pile foundations, only the inertial loads due to vibration of the superstructure are considered or soil displacements due to seismic waves propagating in soil domain are applied along the pile directly [61], [66].

Turkish Earthquake Code [111] and Eurocode 8 [101] suggest that the piles should be designed to resist the inertial loading due to superstructure with axial loads and kinematic loading because of the soil deformation during earthquake.

Pile bending moments occurred along the pile and pile displacement are presented in Figures 5.14 – 5.16 for single pile cases (*Case II* and *Case III* in Figure 5.12). Firstly,

the absolute maximum bending moment in *Case II* (kinematic) occurs at deep level that is approximately in the middle level of pile length; on the other hand, the maximum moment appears near surface in *Case III* (kinematic + inertial). Secondly, the moment increases significantly by superstructure effect. Furthermore, the displacement of pile near surface for *Case III* is larger than *Case II*. Here, it is clear that the inertial interaction is more dominant in homogeneous soil condition under earthquake loading. Additionally, the large earthquake record (Loma Prieta) causes greater bending moment on pile as expected.

The maximum moment $M_{max,inertial}$ (5.21) due to superstructure vibration (inertial interaction) is calculated by taking the difference between complete soil-pile-structure $M_{max,total}$ (*Case III*: inertial + kinematic) and soil-pile $M_{max,kinematic}$ (*Case II*: kinematic) moments considering absolute values of maximum moments.

$$M_{max,inertial} = |M_{max,total}| - |M_{max,kinematic}| \quad (5.21)$$

The maximum inertial, kinematic, and total moments for different earthquake motion are presented in Figures 5.17 – 5.19. Accordingly, the vibration of superstructure (inertial interaction) has the greatest impact on pile response. However, the kinematic interaction should not be neglected as it increases the bending moment.

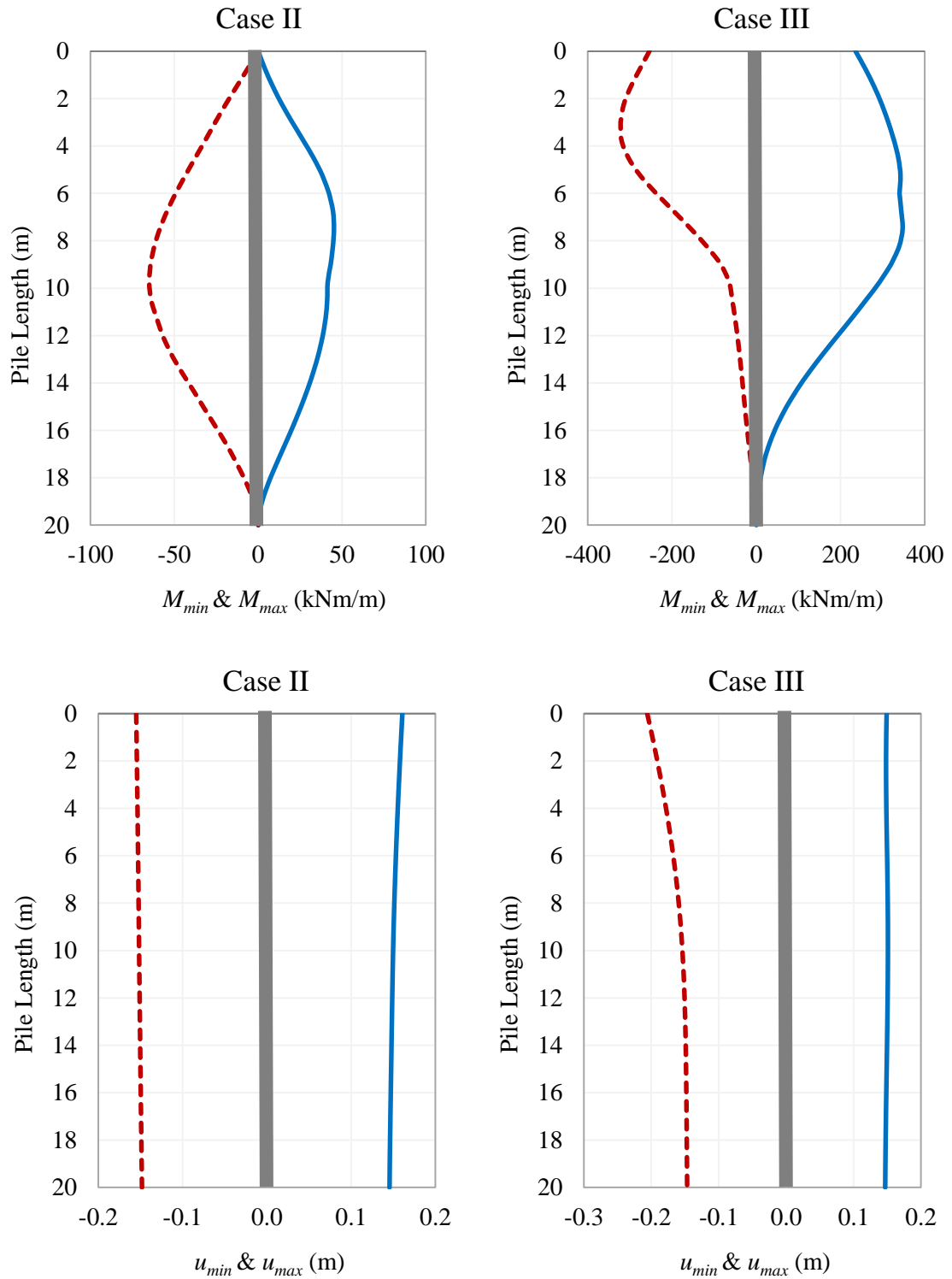


Figure 5.14 Minimum and maximum bending moments (M_{min} & M_{max}) and minimum and max pile displacements (u_{min} & u_{max}) calculated by applying Düzce earthquake motion

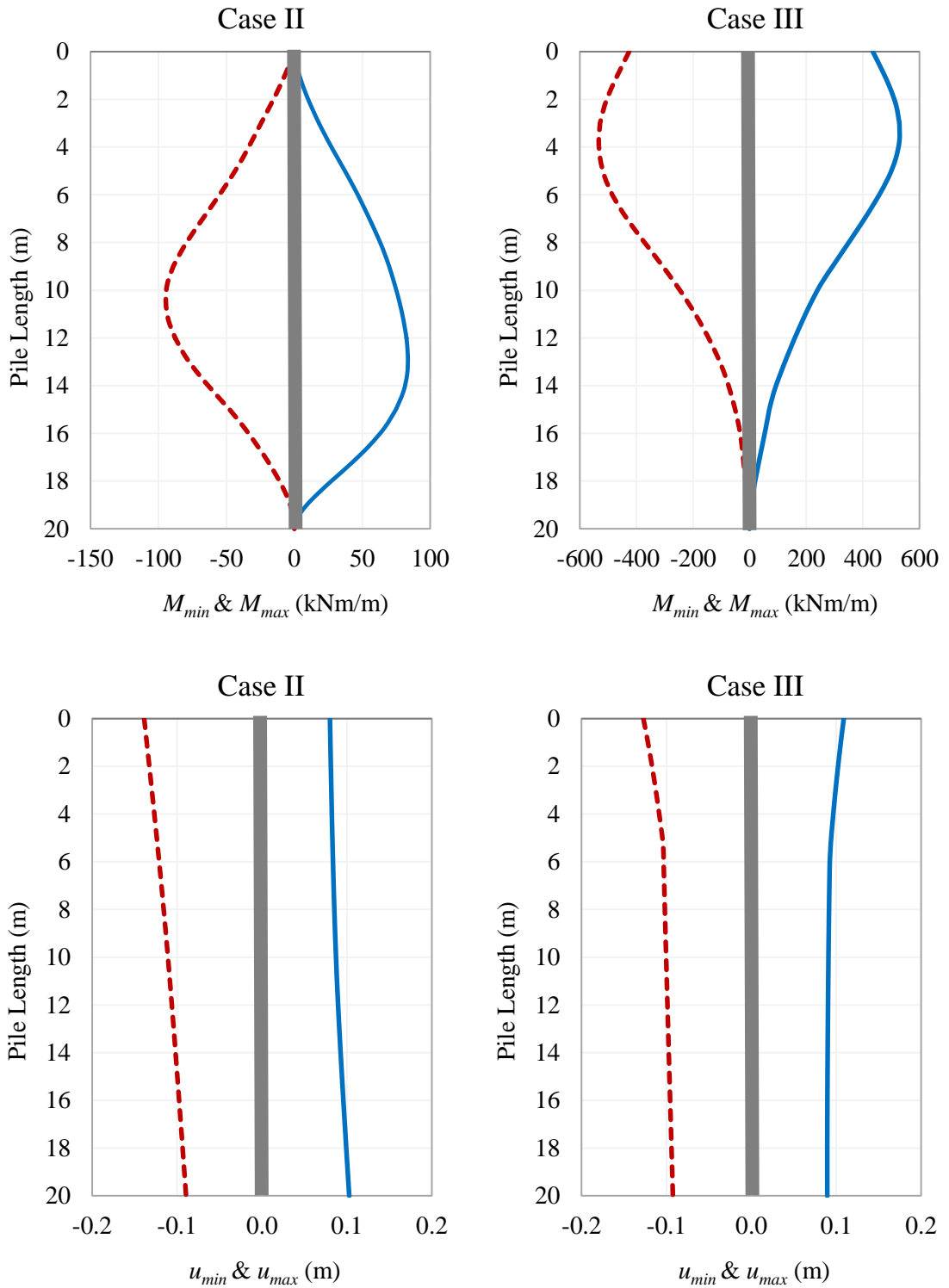


Figure 5.15 M_{min} & M_{max} and u_{min} & u_{max} calculated by applying Kocaeli earthquake motion

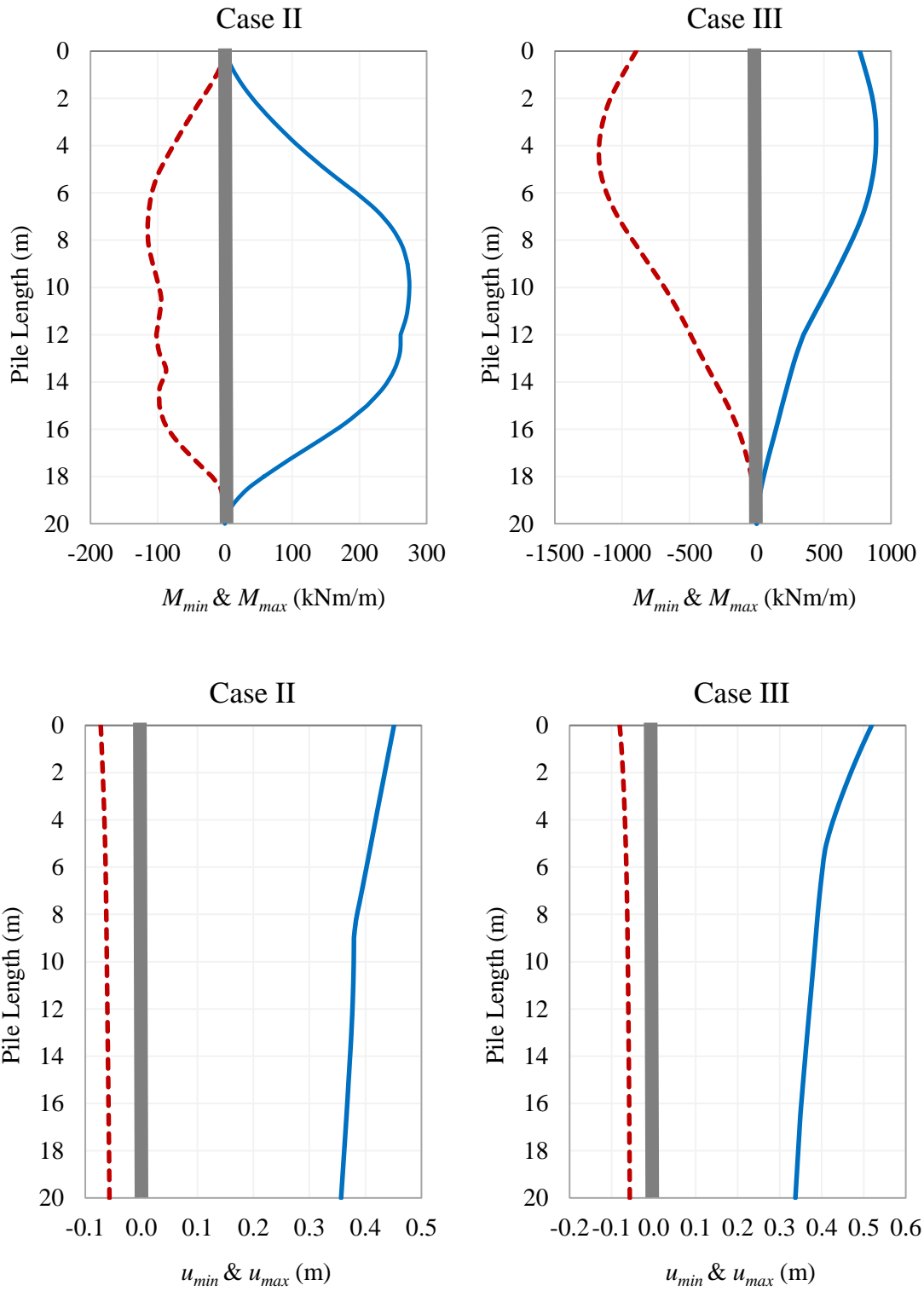


Figure 5.16 M_{min} & M_{max} and u_{min} & u_{max} calculated by applying Loma Prieta earthquake motion

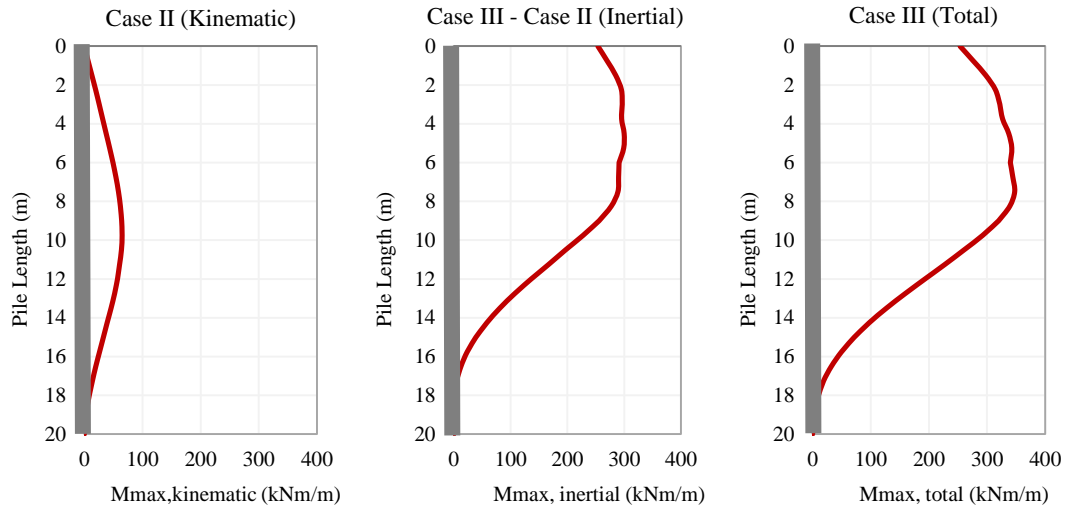


Figure 5.17 M_{max} for different cases with inertial interaction calculated by applying Düzce earthquake

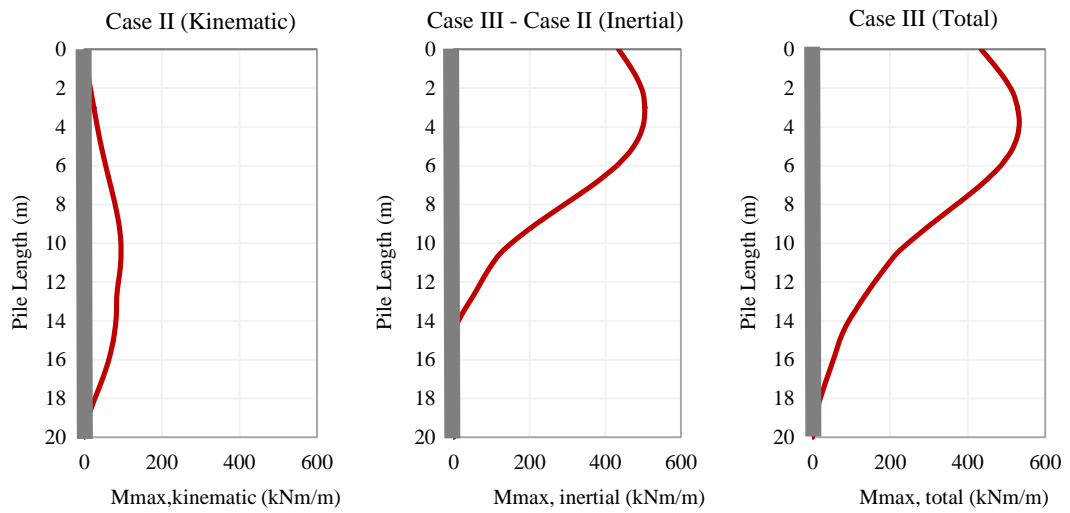


Figure 5.18 M_{max} for different cases with inertial interaction calculated by applying Kocaeli earthquake

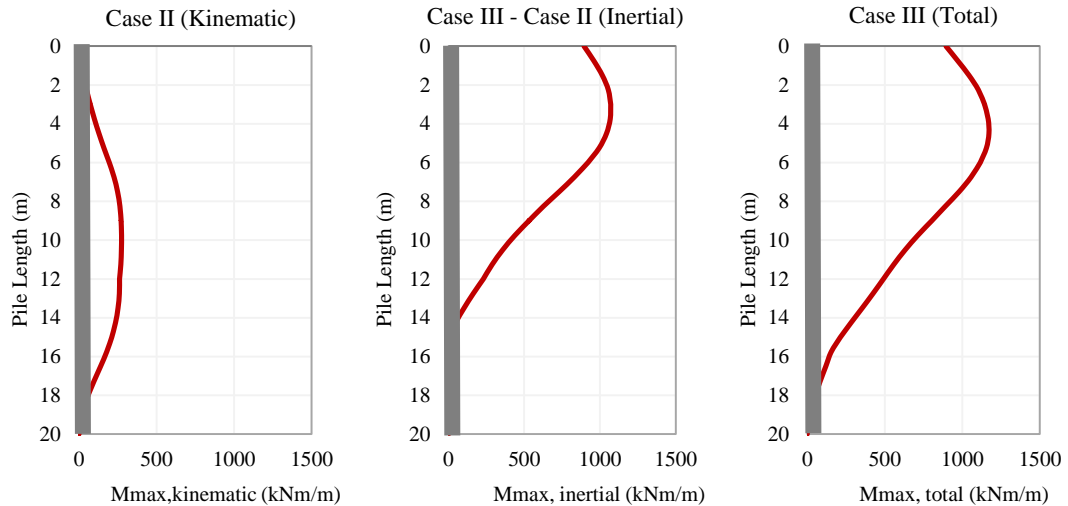


Figure 5.19 M_{max} for different cases with inertial interaction calculated by applying Loma Prieta earthquake

Even though in some cases (such as monopile with wind turbine or under a bridge pier) the singular pile is used, piles, in general, are designed as a group to support a given structure. A basic 1x4 (Figure 5.13) pile group model with and without structure including cap (boundary condition of pile at head level) is developed to investigate the group effects on general response of pile and superstructure. The distance between two piles is selected as 3D center-to-center to minimize pile-to-pile interaction (pile-to-pile interaction is outside of the context of this study). The pile maximum bending moments and displacements with depth are presented for Düzce earthquake without cap (*Case V*), with cap (*Case VI*), and with cap and superstructure (*Case VII*) in Figures 5.20 – 5.25. Piles are identified as #1 to #4 representing left-to-side in a group. The pile group response under other earthquake motions (Kocaeli and Loma Prieta) show similar behavior. Moments and displacements of them are presented in Appendix-B. The following results are observed regarding pile group behavior.

- In *Case V* (free-head piles), the maximum moment occurs at deep level, approximately near $L_{pile}/2$, as single pile condition in *Case II*. The magnitude of moment is almost identical for all piles in group (*Case V*) and there is no significant difference in magnitude when compared by single pile (*Case II*).
- With respect to *Case VI* (fixed-head piles), the maximum moment appears at surface level (pile-head) and its magnitude (≈ 80 kNm/m) is a bit larger than free-head condition *Case V* (≈ 60 kNm/m).

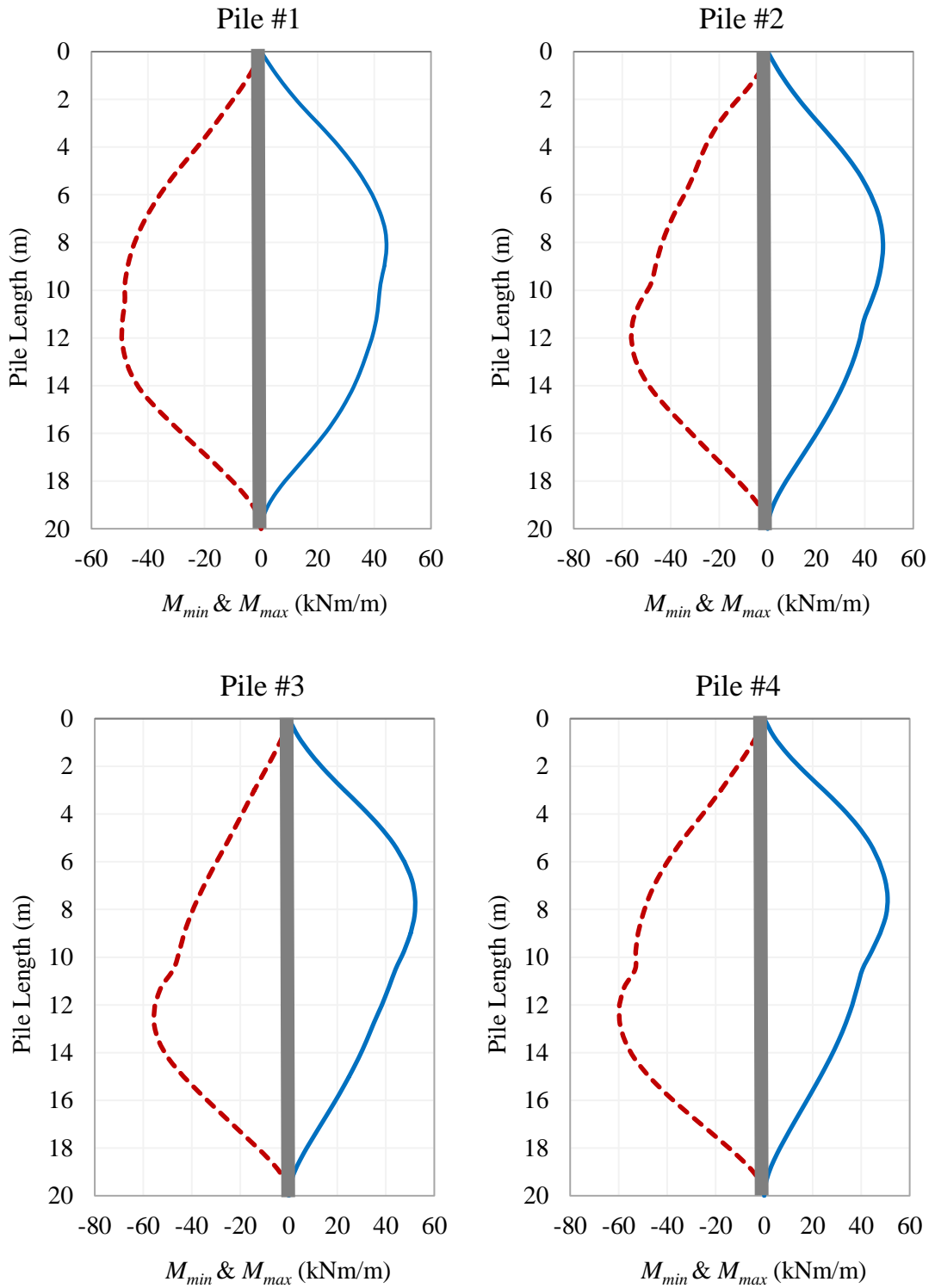


Figure 5.20 M_{min} & M_{max} calculated by applying Düzce earthquake motion for Case V

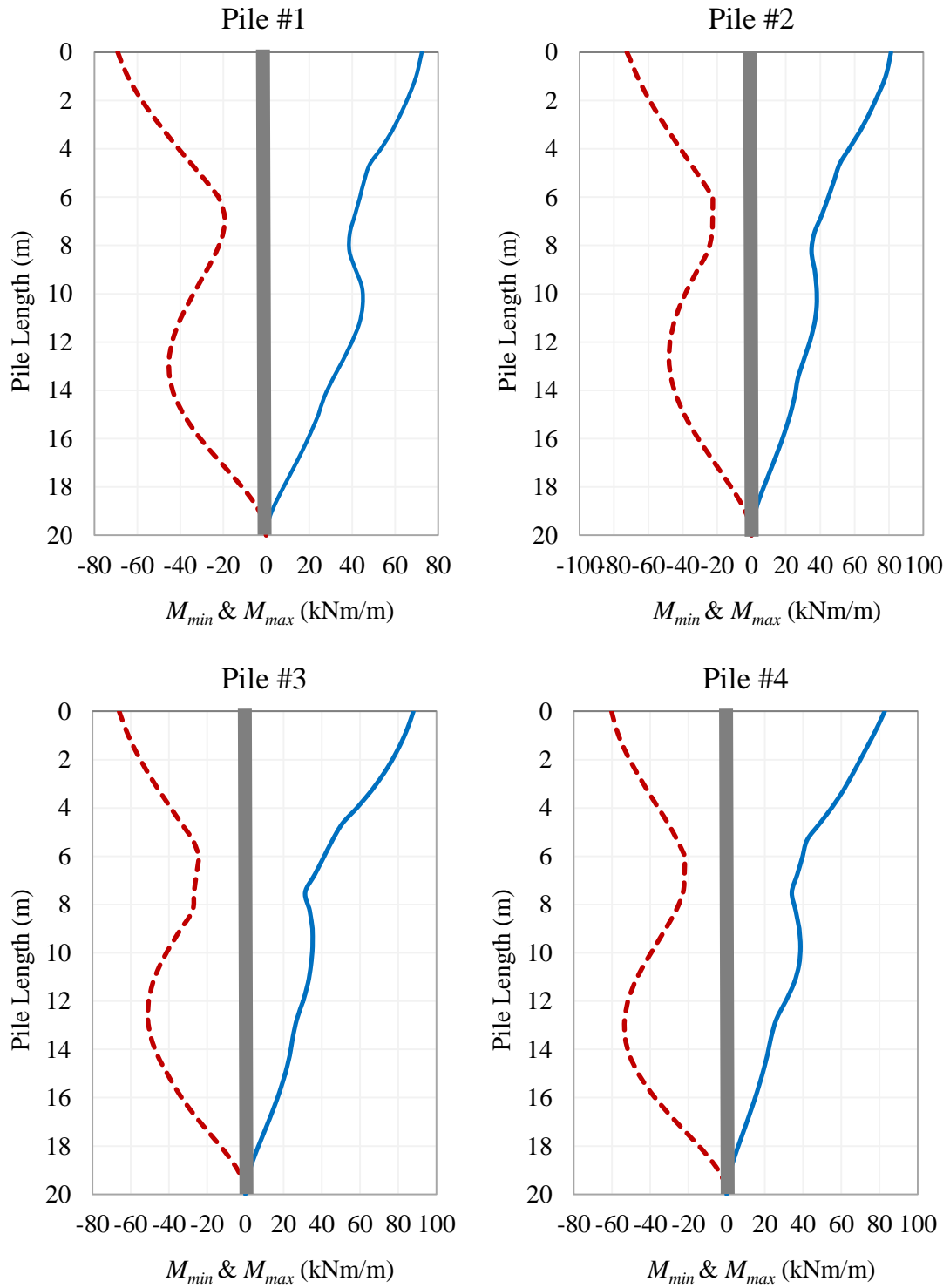


Figure 5.21 M_{min} & M_{max} calculated by applying Düzce earthquake motion for Case VI

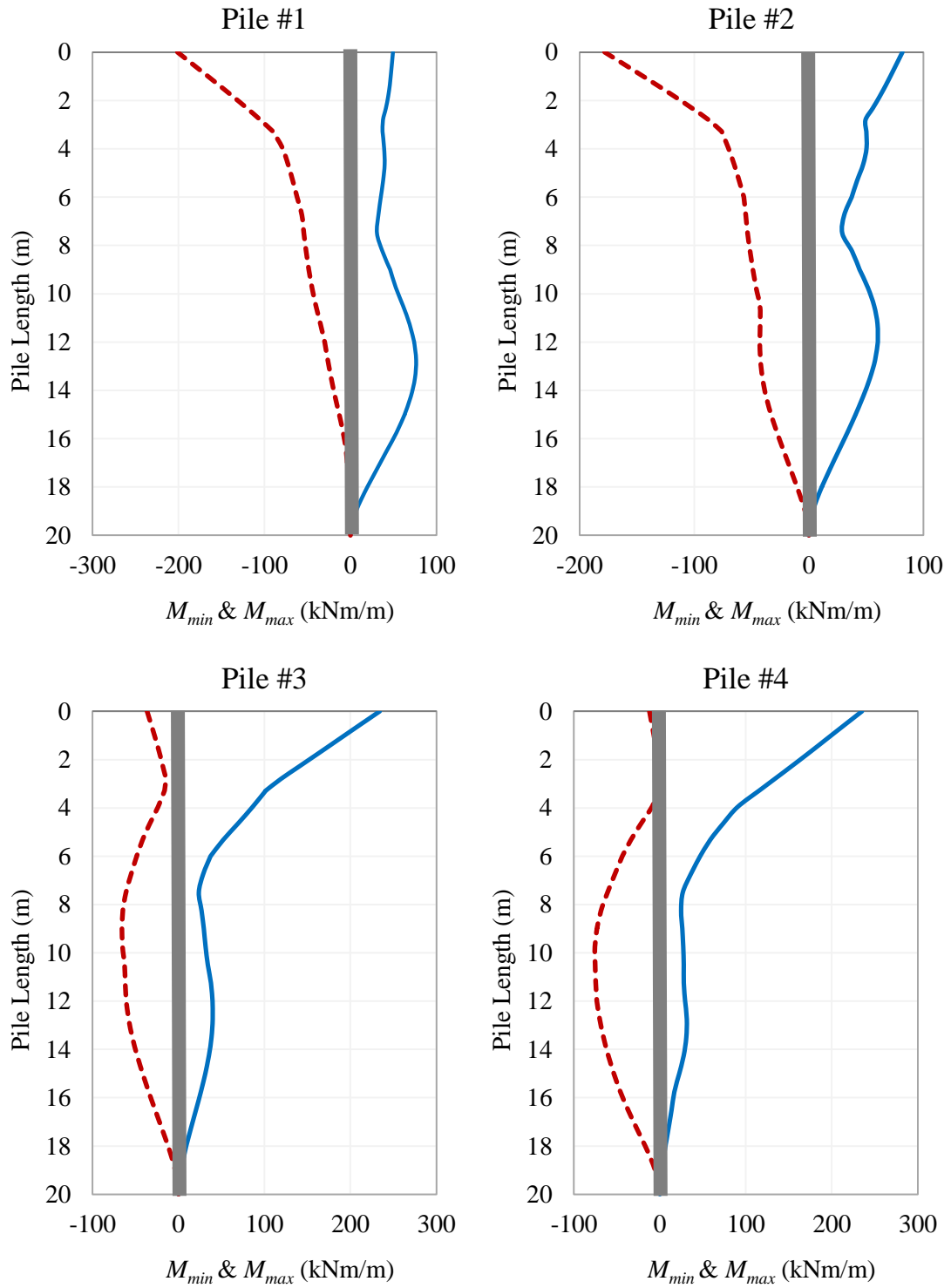


Figure 5.22 M_{min} & M_{max} calculated by applying Düzce earthquake motion for Case VII

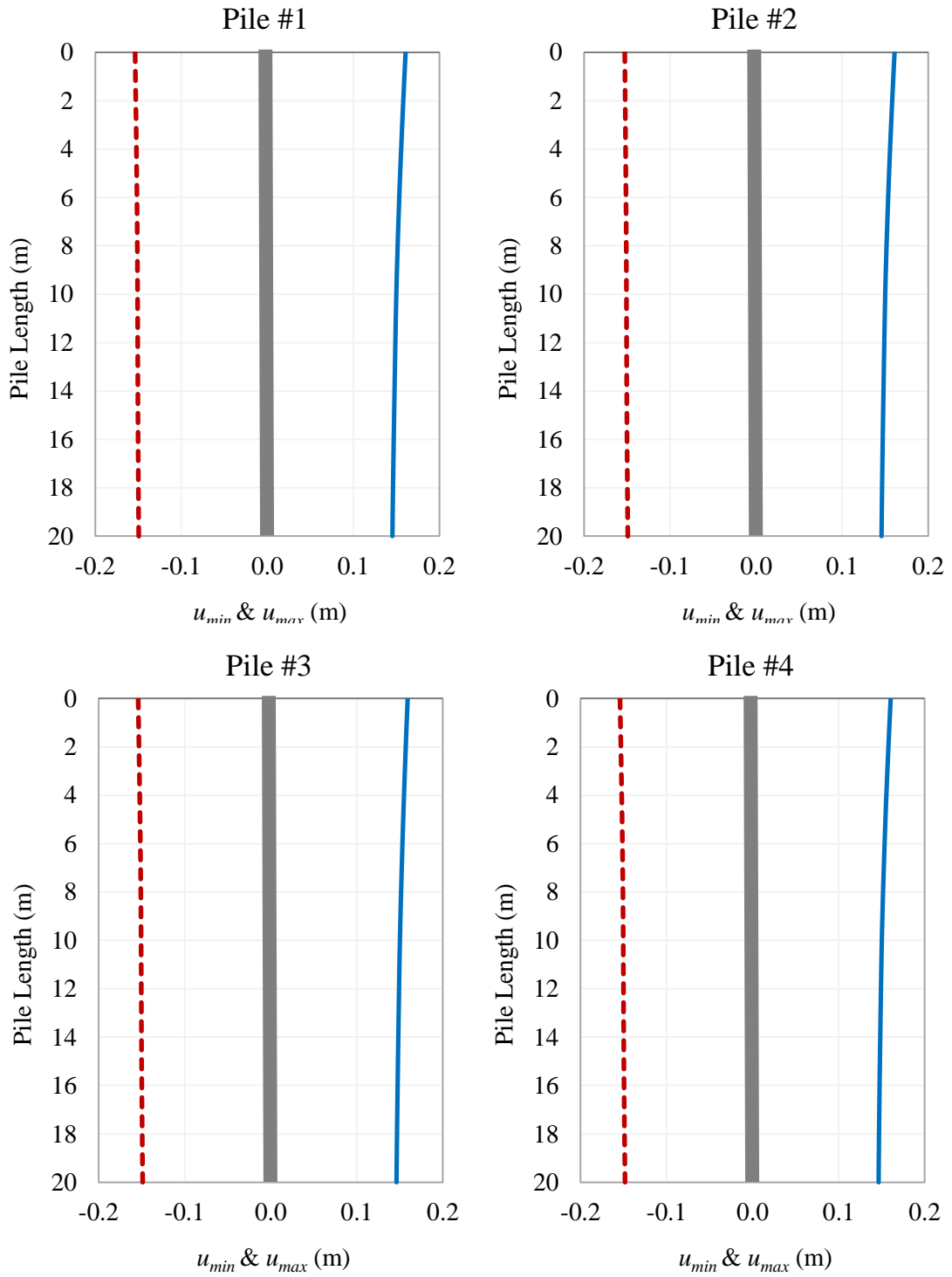


Figure 5.23 u_{min} & u_{max} calculated by applying Düzce earthquake motion for Case V

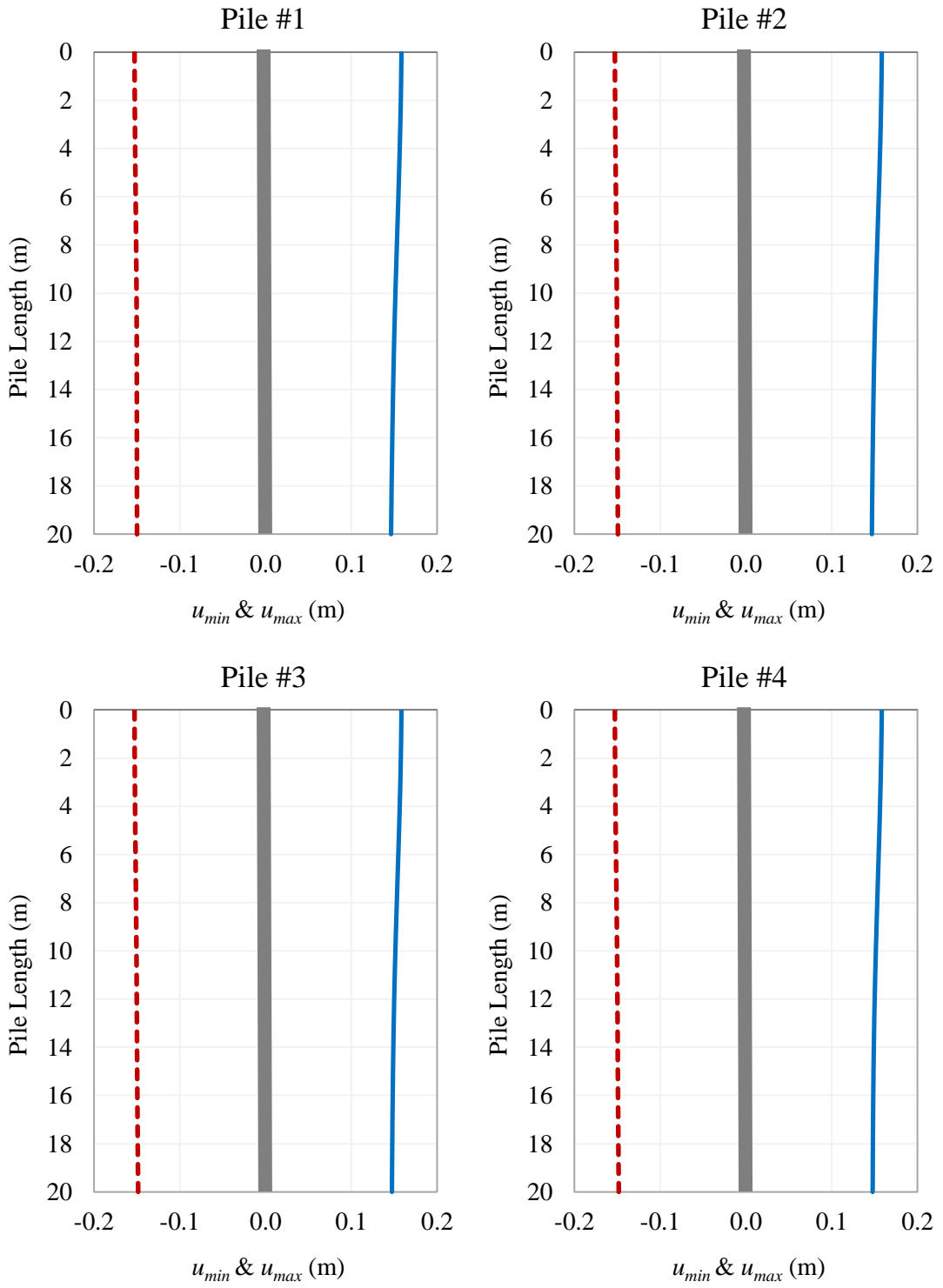


Figure 5.24 u_{min} & u_{max} calculated by applying Düzce earthquake motion for Case VI

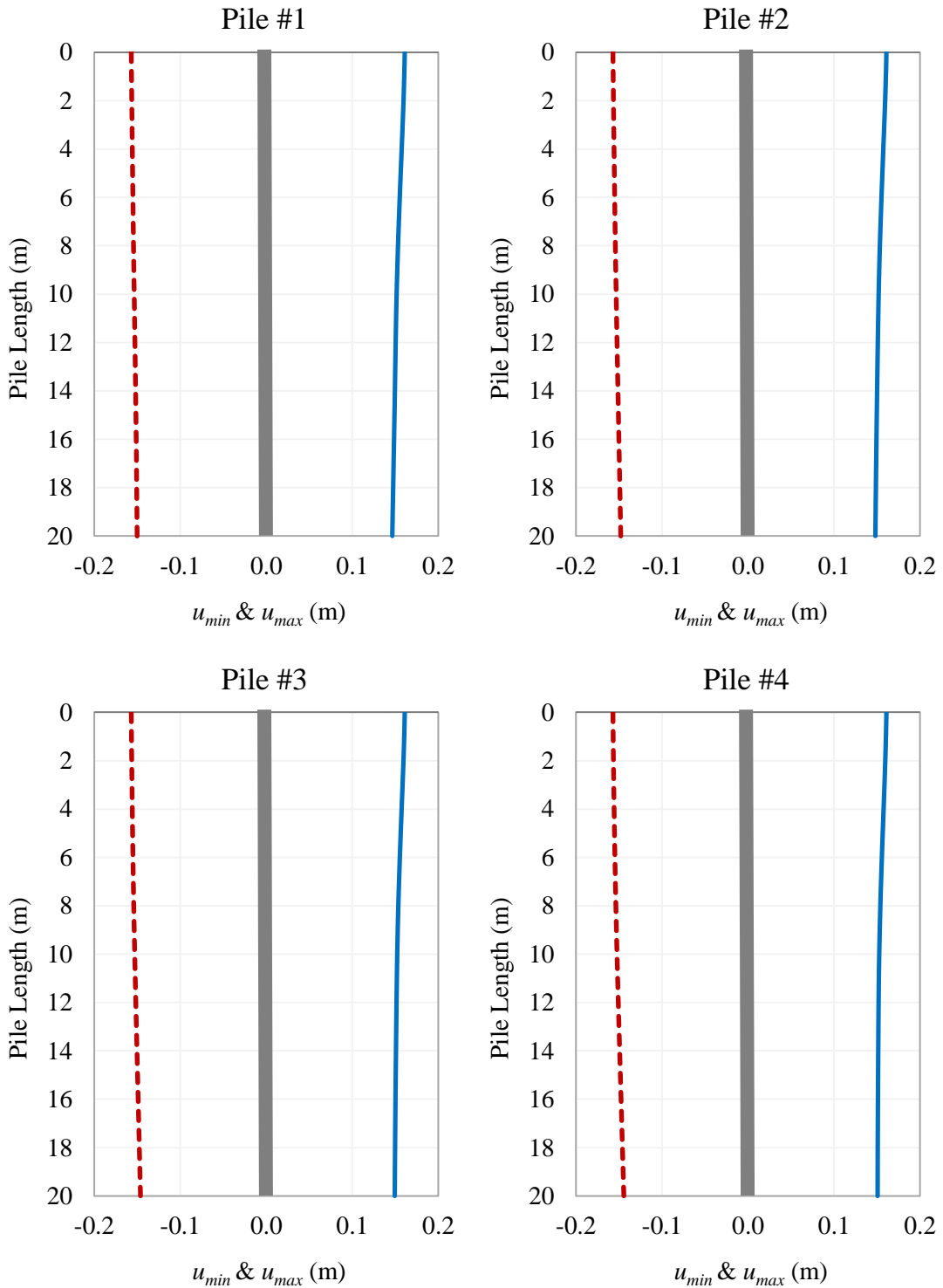


Figure 5.25 u_{min} & u_{max} calculated by applying Düzce earthquake motion for Case VII

- With regard to complete model *Case VII* (soil-pile-structure interaction), the maximum moment takes place at pile-head; however, the increase of magnitude is significant (≈ 80 kNm/m for *Case VI* and ≈ 235 kNm/m for *Case VII*). If *Case*

VII (group pile) is compared with *Case III* (single pile), each pile in the group takes less bending moment than single pile condition (≈ 350 kNm/m). The dominance of inertial interaction can be seen here again. Additionally, all pile in a group do not take the same bending moment.

- The pile #1 and pile #2 takes the moment in (-) direction while pile #3 and pile #4 returns to (+) direction. Here, placing the superstructure at center of pile cap and the symmetry of the system are effective, otherwise, some piles in a group might take larger moments (or load).
- For all cases, any significant change is not observed in terms of displacement (Figures 5.23 – 5.25)

5.2.2 Superstructure Response

With respect to superstructure design, it is widely believed that the presence of piles is beneficial to the response of structure system under earthquake loading. Pile foundations are generally assumed to be rigid enough and fixed-base model is deemed suitable for structures [115]. This perception stems from analytical studies performed for fixed- and flexible- base showing that *SFSI* increases elastic structural period which means smaller acceleration and stresses in the structure according to design spectrum recommended in seismic provisions [135], [136].

The structures (except tall buildings, bridges, etc.) are generally analyzed against seismic loading using elastic response spectra. This spectra can be plotted basically considering soil type as proposed in regulations or it can be represented by more than one shape of spectra generated by different earthquake sources. Time history analysis may be performed as well. Here, the following questions regarding piled-structures must be answered:

- How should the response spectra be plotted?
- Which motion should be used in analysis of time history?

The free-field motion is altered due to the presence of piles, which is explained in Chapter 4 and will further be discussed here. Hence, the motion below (or near) the structure may be different from the free-field motion.

Turkish Earthquake Code [111] suggests the soil layer at the lower tip of the shortest pile may be taken into consideration as soil class used in design response spectra.

However, in such a case, it is essential to take piles into account as structural elements of support system together with the superstructure in the seismic analysis or to idealize horizontal and vertical rigidities of piles with equivalent springs under the pile caps.

Time histories calculated for different cases pointed in Figure 5.12 under different earthquake loadings, including input motion at base, are presented in Figures 5.26 – 5.28. The pile diameter of 1 m and the period of *SDOF* system of 0.5 sec were considered. For all cases, maximum acceleration a_{max} is the largest in *Case II* (single pile). In complete model *Case III*, though a_{max} value is slightly smaller than calculated in *Case II*, nevertheless, it is larger than input motion. Accordingly, the use of input motion in calculations directly does not make sense.

The effect of pile on mass responses are presented in terms of acceleration in Figure 5.29 and in terms of displacement in Figure 5.30 considering *Case III* and *Case IV* in Figure 5.12. It can be seen that the existence of pile affects mass acceleration severely in an unfavorable side increasing the mass acceleration. This is expected situation because the presence of pile raises the a_{max} . On the other hand, *Case III* and *Case IV* show similar manner in terms of displacement, except results calculated by Loma earthquake.

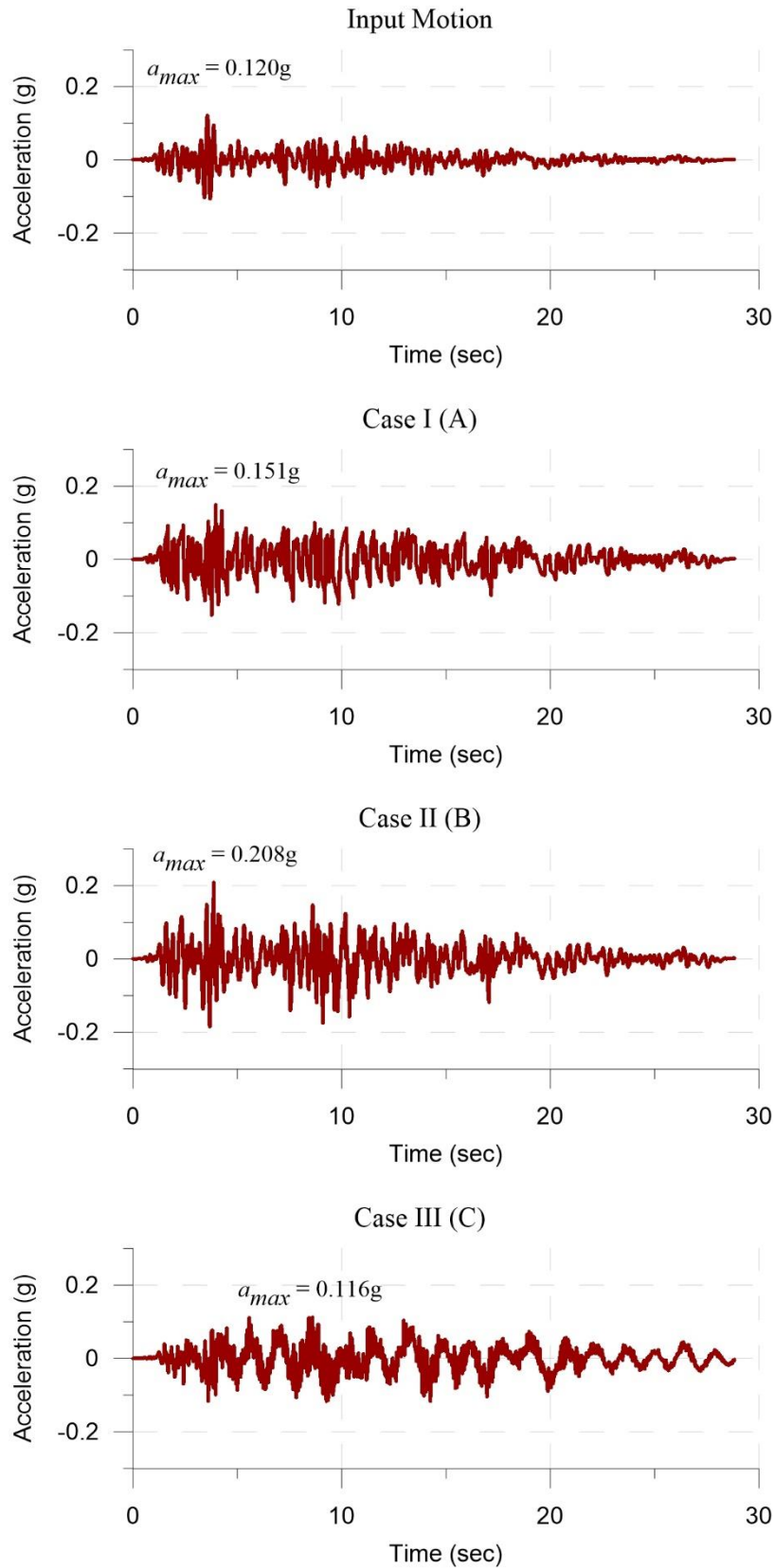


Figure 5.26 Time histories calculated at base level of SDOF system for different cases applying Düzce Earthquake Mudurnu station record ($D = 1$ m; $T = 0.5$ sec)

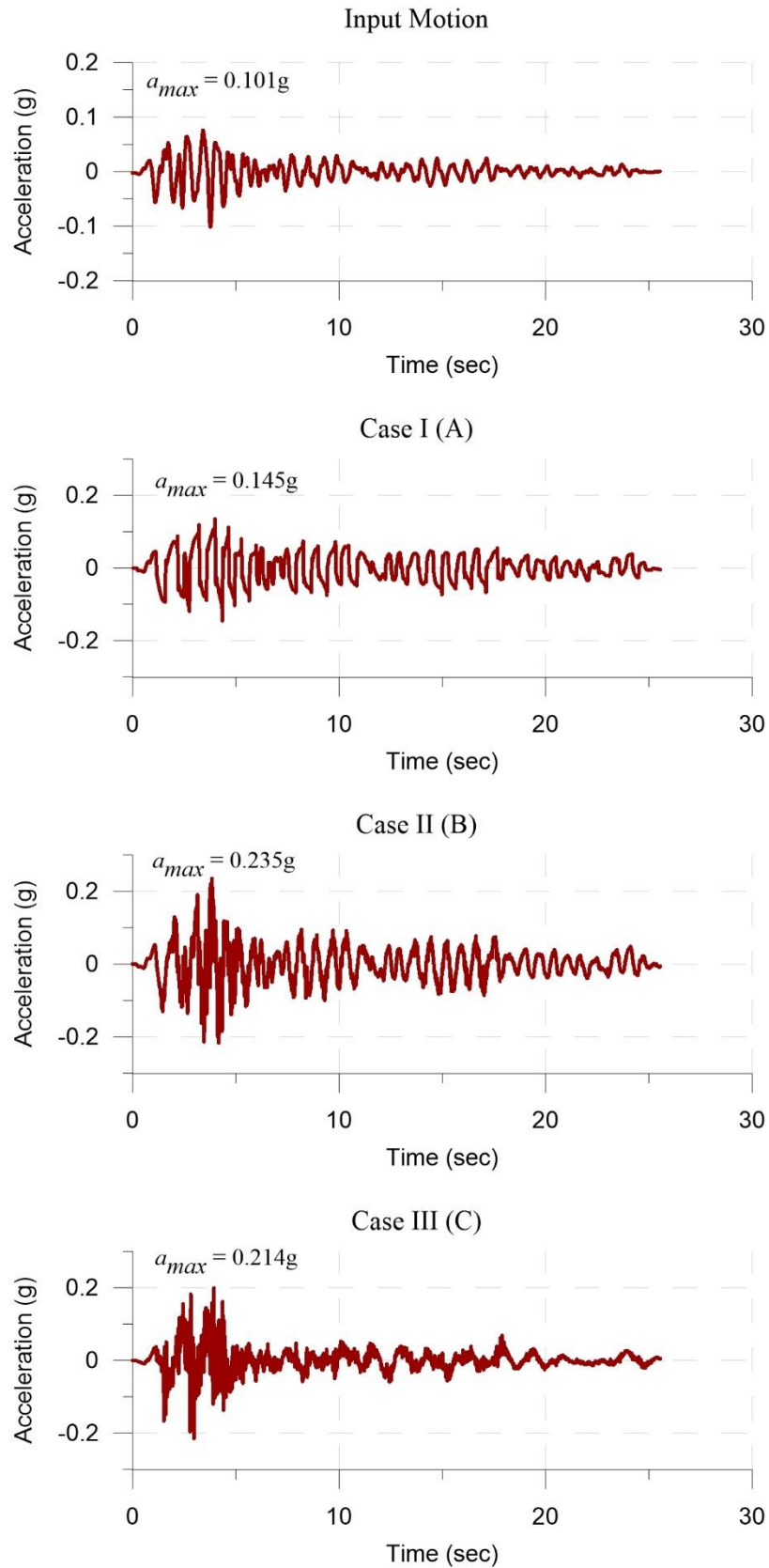


Figure 5.27 Time histories calculated at base level of SDOF system for different cases applying Kocaeli Earthquake Ereğli station record ($D = 1$ m; $T = 0.5$ sec)

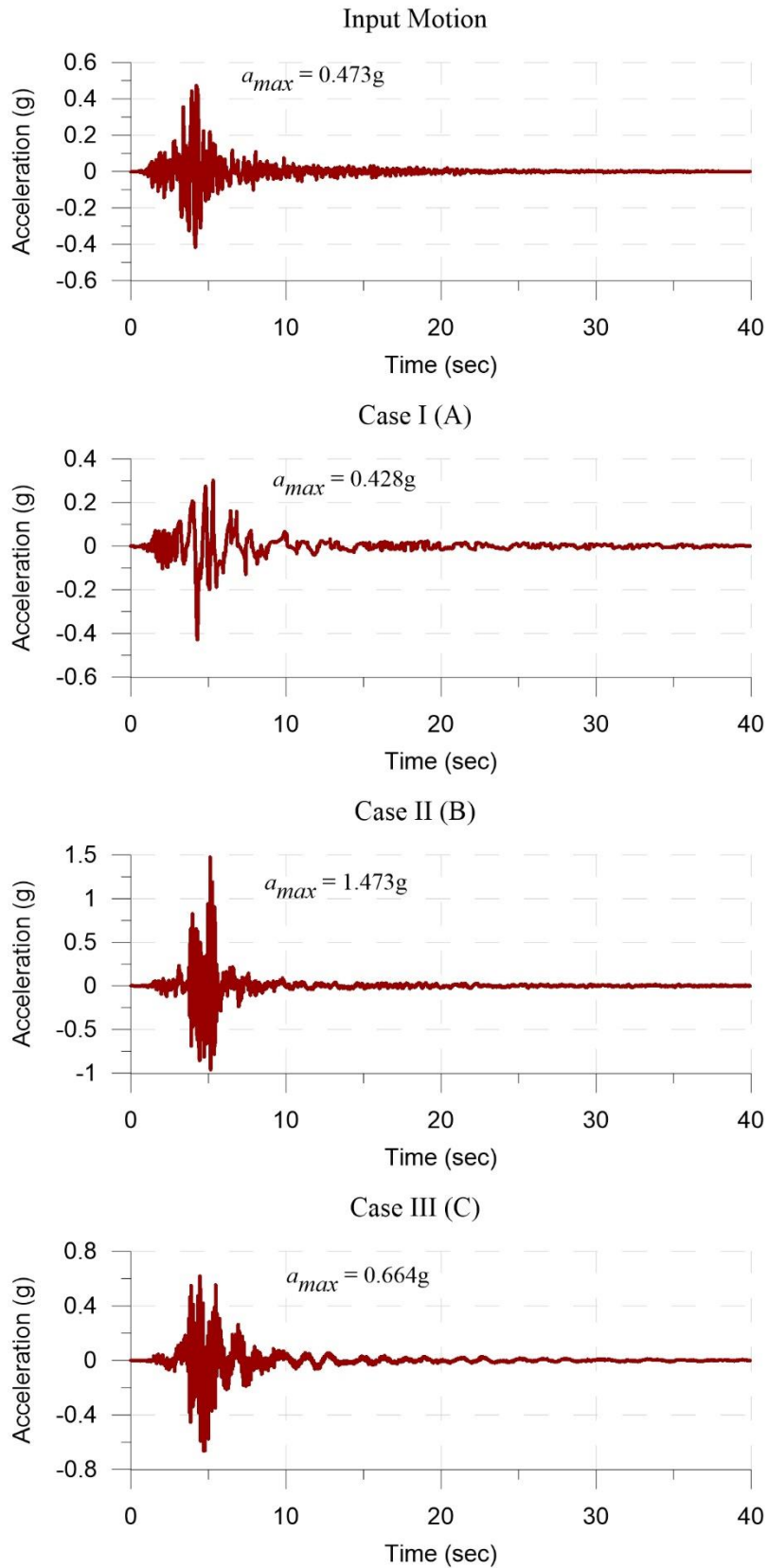


Figure 5.28 Time histories calculated at base level of SDOF system for different cases applying Loma Prieta Earthquake Gilroy #1 station record ($D = 1$ m; $T = 0.5$ sec)

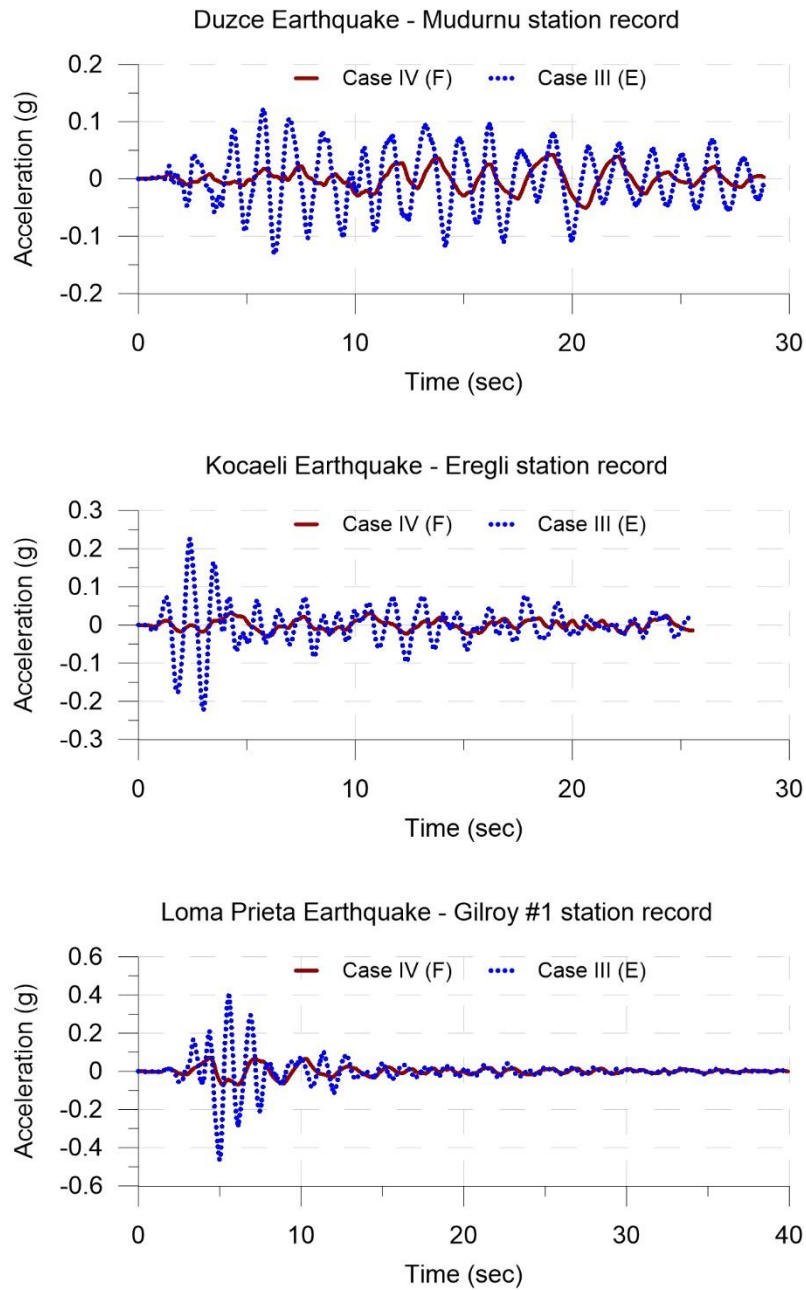


Figure 5.29 Acceleration time histories calculated at mass of SDOF system with and without pile ($D = 1.0$ m; $T = 0.5$ sec)

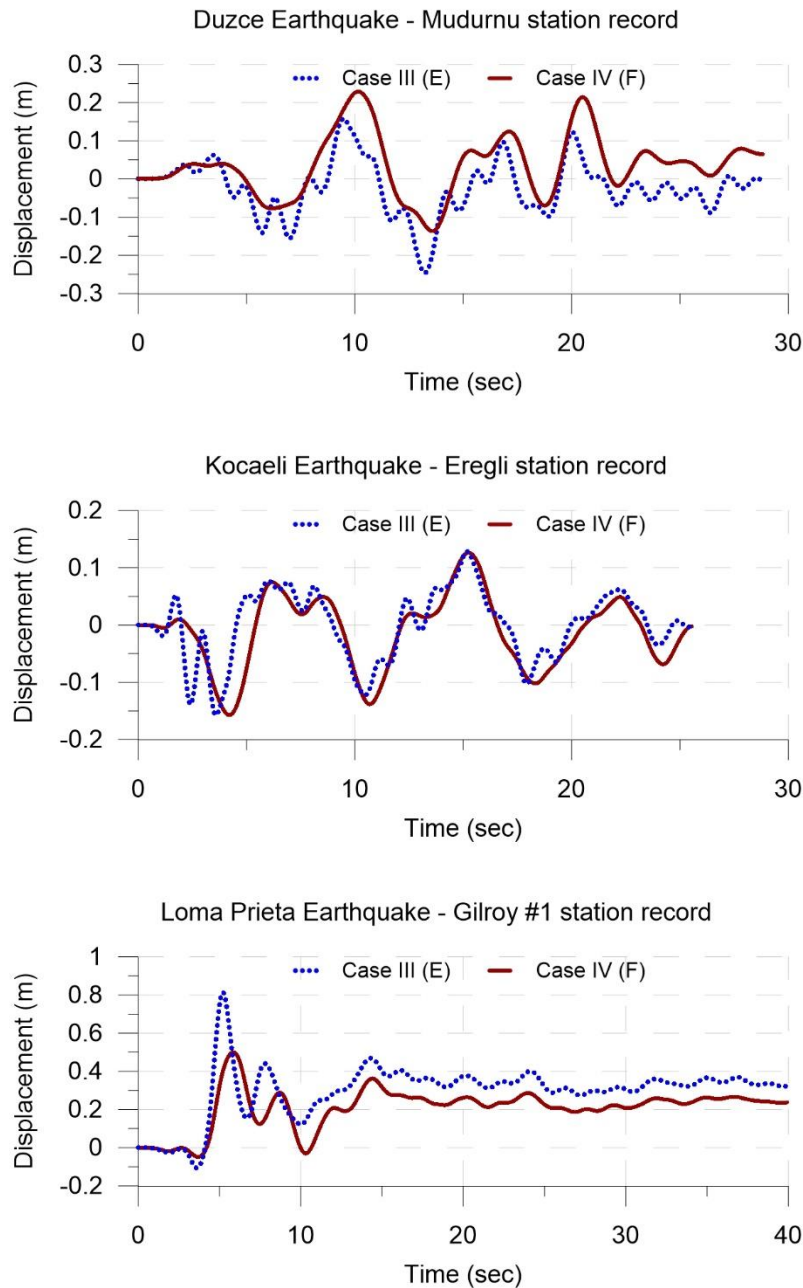


Figure 5.30 Displacement Time histories calculated at mass of SDOF system with and without pile ($D = 1.0$ m; $T = 0.5$ sec)

With respect to the motion used in calculations, elastic response spectra with damping of 5% for different cases under particular earthquake motions are presented in Figures 5.31 – 5.33. Larger peak spectral acceleration (PSA) arises in *Case II* and *Case V* in which free-head piles with only kinematic loading is considered. The vibration of superstructure and pile-head boundary condition (fixed-head) influence the system response. Linking pile heads by cap decreases the spectral acceleration; besides, taking

superstructure vibration (inertial effect) decreases spectral acceleration and changes period range of the system. Conversely, inertial interaction increases bending moment acting on piles seriously— actually, this reflects piled-structure response.

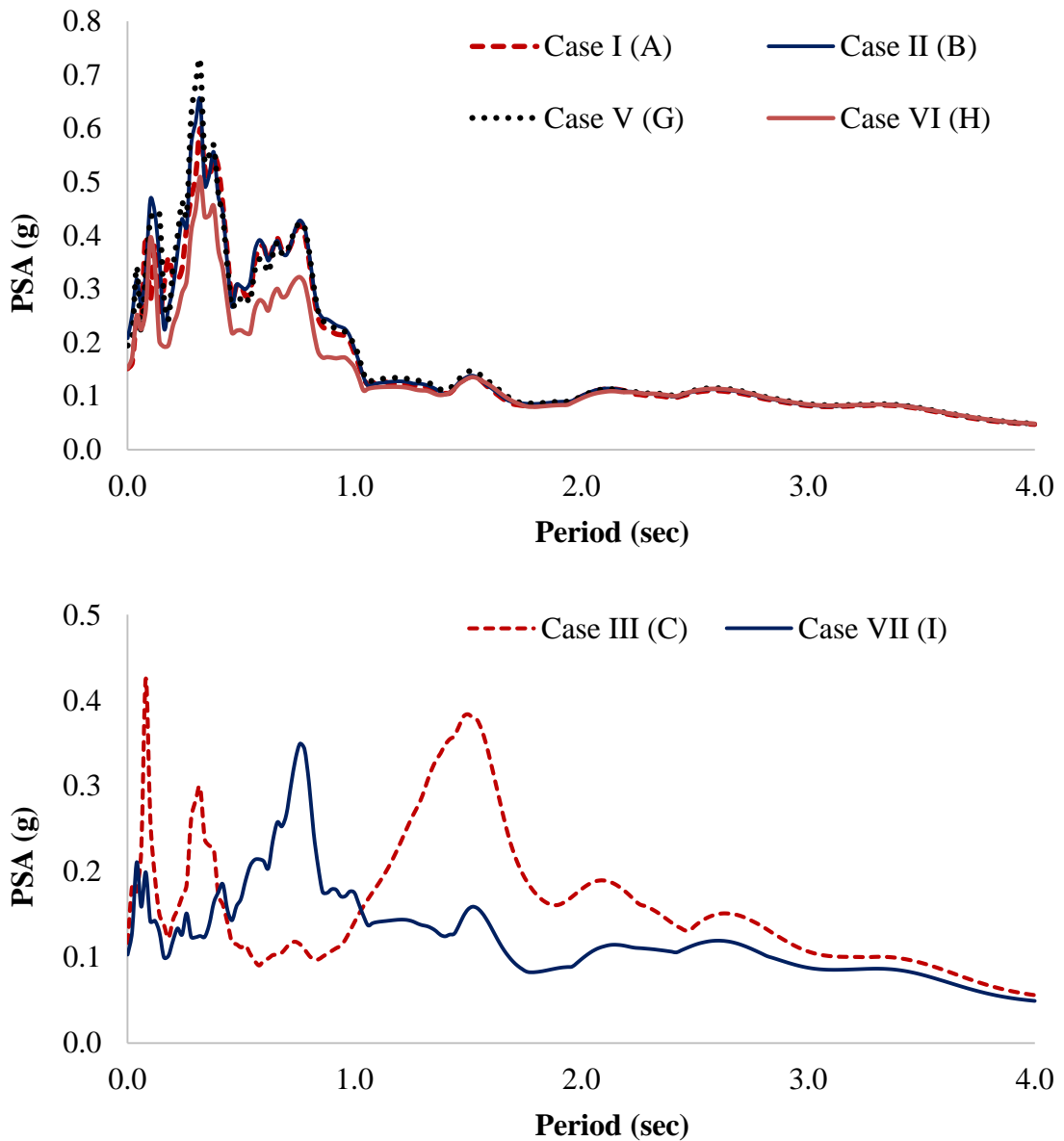


Figure 5.31 Response spectra for damping of 5 % for different cases applying Düzce motion ($D = 1$ m and $T = 0.5$ sec)

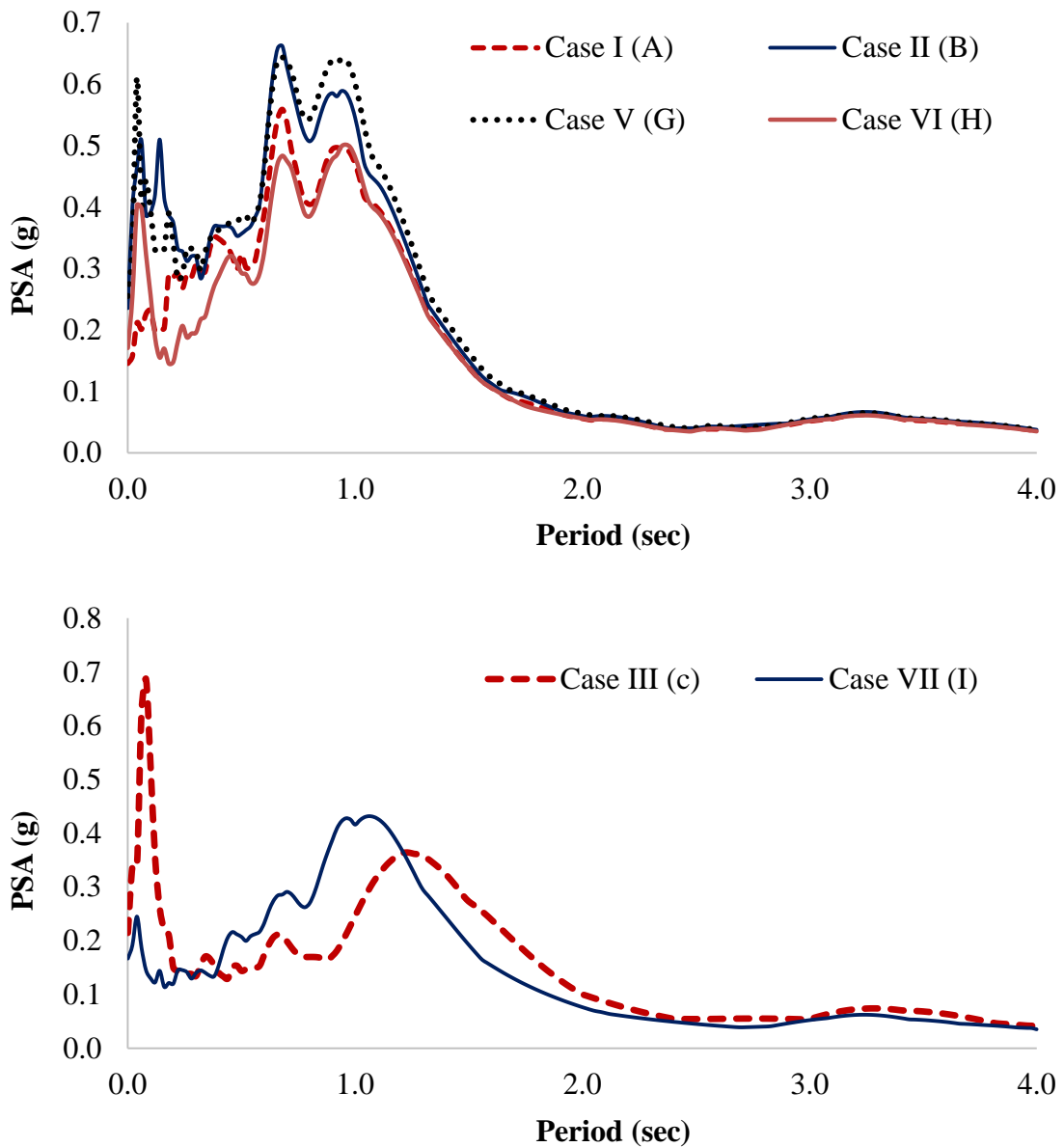


Figure 5.32 Response spectra for damping of 5 % for different cases applying Kocaeli motion ($D = 1$ m and $T = 0.5$ sec)

Seed et al. [137] plotted average acceleration elastic response spectra (Figure 5.34) for different site conditions. According to this, stiff site conditions have larger spectral acceleration in a narrow period range while soft site conditions have smaller spectral acceleration in a broad range. The embedded-piles make stiffer zone in soil domain influencing wave propagation. For this reason, higher spectral acceleration values appear in the piled zone.

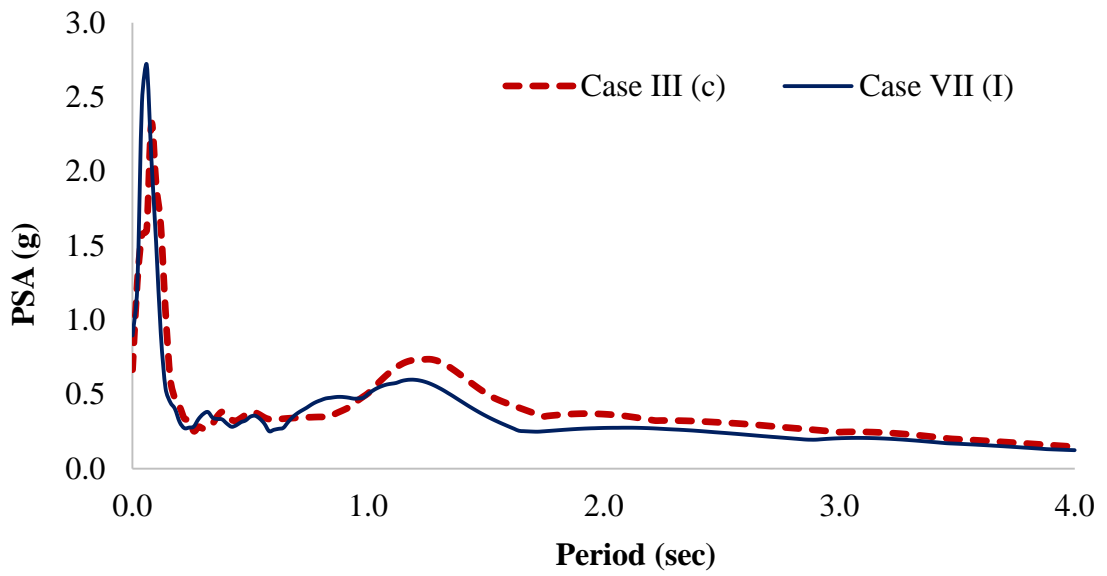
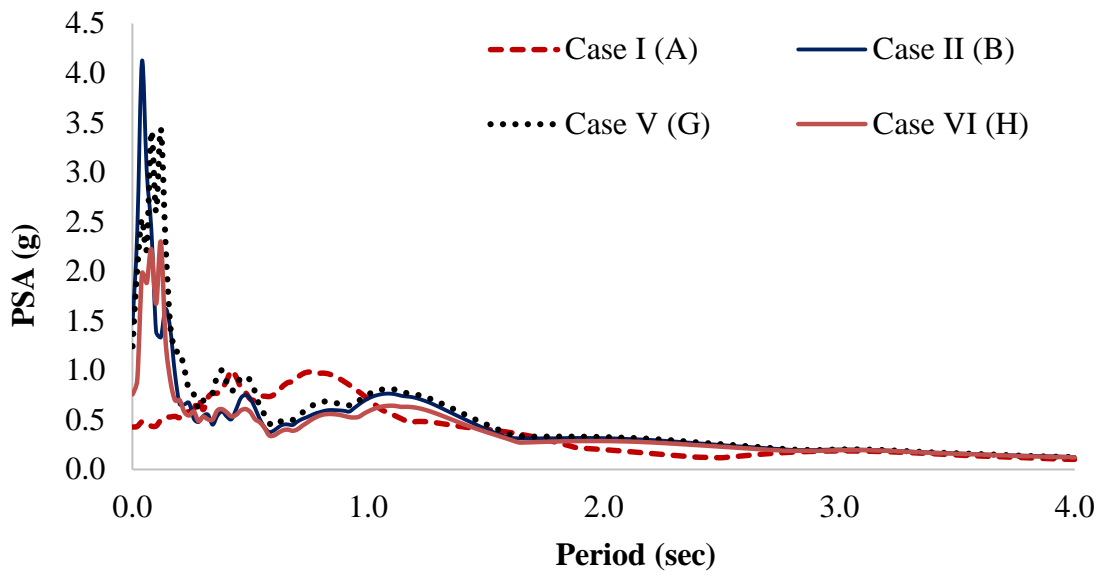


Figure 5.33 Response spectra for damping of 5 % for different cases applying Loma motion ($D = 1$ m and $T = 0.5$ sec)

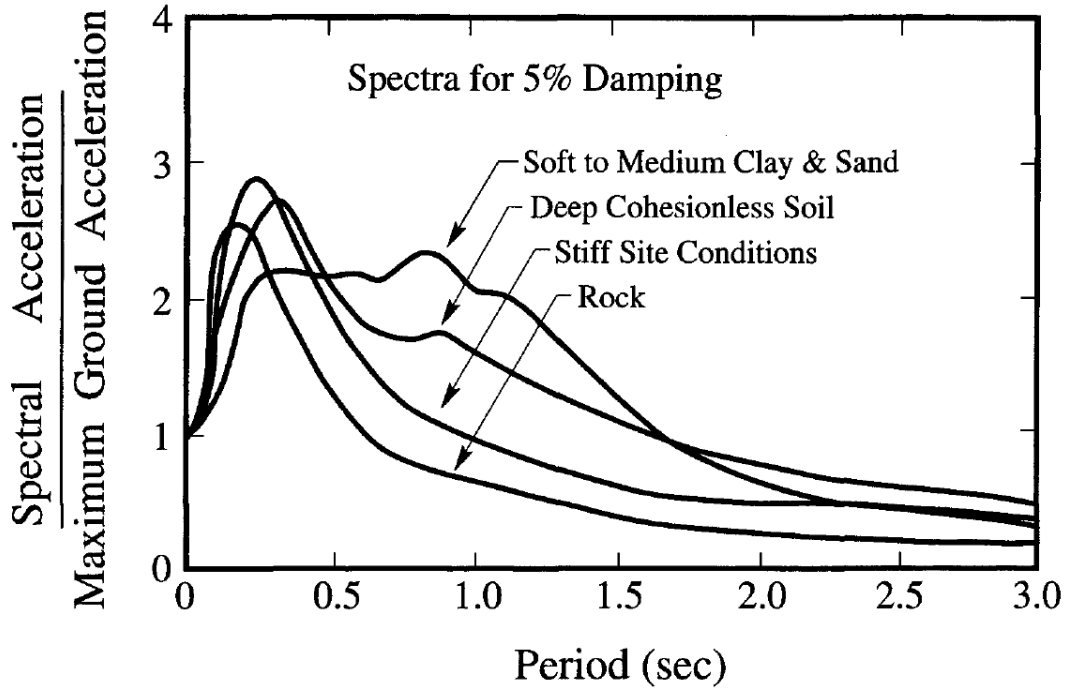


Figure 5.34 Average acceleration response spectra for different site conditions [137]

The effects of *SDOF* system period and pile diameter on soil – pile – structure interaction are also investigated considering *Case III* (single pile with structure). The engineering properties of motion are summarized in Table 5.8 for different cases (Figures 5.12 and 5.13) and earthquake motions. T_p is the predominant period at which the maximum spectral acceleration occurs; T_m represents the mean period and being estimated with the Equation (5.22) in which C_i are the Fourier amplitudes and f_i is the discrete Fourier transform frequencies between 0.25 and 20 Hz [138].

$$T_m = \frac{\sum C_i^2 / f_i}{\sum C_i^2} \quad (5.22)$$

Table 5.8 Summarization of results including the effects of pile diameter (slenderness) and structure period

Motion ID	Case (Point)	D (m)	T_{str} (sec)	a_{max} (g)	Amplification ($a_{max}/a_{max,input}$)	T_p (sec)	T_m (sec)
Düzce	Input motion	--	--	0.120	1.00	0.300	0.414
	Case I (A)	--	--	0.151	1.26	0.320	0.540
	Case II (B)	1	--	0.208	1.73	0.320	0.542
	Case III (C)	1	0.5	0.116	0.97	0.080	1.227
	Case III (C)	0.5	0.5	0.222	1.85	0.060	0.927
	Case III (C)	2	0.5	0.184	1.53	0.760	0.967
	Case III (C)	1	1	0.297	2.48	0.780	0.771
	Case III (C)	1	2	0.144	1.20	0.320	0.858
	Case V (G)	1	--	0.194	1.62	0.320	0.538
	Case VI (H)	1	0.5	0.152	1.27	0.320	0.648
	Case VII (I)	1	0.5	0.103	0.86	0.760	1.040
Kocaeli	Input motion	--	--	0.101	1.00	0.640	0.688
	Case I (A)	--	--	0.145	1.44	0.680	0.752
	Case II (B)	1	--	0.235	2.33	0.680	0.742
	Case III (C)	1	0.5	0.214	2.12	0.080	0.923
	Case III (C)	0.5	0.5	0.176	1.74	0.060	0.813
	Case III (C)	2	0.5	0.426	4.22	0.120	0.899
	Case III (C)	1	1	0.515	5.10	0.940	0.769
	Case III (C)	1	2	0.177	1.75	0.100	0.940
	Case V (G)	1	--	0.255	2.52	0.680	0.780
	Case VI (H)	1	0.5	0.170	1.68	0.960	0.841
	Case VII (I)	1	0.5	0.144	1.43	1.080	1.030
Loma Prieta	Input motion	--	--	0.473	1.00	0.380	0.392
	Case I (A)	--	--	0.428	0.90	0.420	0.909
	Case II (B)	1	--	1.473	3.11	0.040	0.511
	Case III (C)	1	0.5	0.664	1.40	0.080	0.752
	Case III (C)	0.5	0.5	1.359	2.87	0.020	0.876
	Case III (C)	2	0.5	0.667	1.41	0.120	0.766
	Case III (C)	1	1	1.676	3.54	0.060	0.388
	Case III (C)	1	2	0.867	1.83	0.080	0.355
	Case V (G)	1	--	1.242	2.63	0.120	0.423
	Case VI (H)	1	0.5	0.756	1.60	0.120	0.622
	Case VII (I)	1	0.5	0.895	1.89	0.060	0.590

In Table 5.8, *Case III* with the pile diameter of 1 m and the structure period of 1 sec is the most critical condition, in which the amplification has maximum value, for all earthquake motion. The system (complete soil-pile-structure) period and the motion period may coincide in that condition. Considering all the results, consequently, the

motion characteristics with embedded-pile and superstructure change seriously, and hence, the use of input motion in analysis (or design) directly might be erroneous.

In conclusion, an embedded structural element having more stiffness into ground forms a rigid zone. Wave propagation in such area is altered by refraction and reflection; and therefore, the free-field motion and near structure system motion show different features in frequency content, peak acceleration, peak displacement, predominant period, etc.

5.3 Concluding Remarks

In this chapter, complete soil – pile – structure interaction is investigated by FEM (using *Plaxis*). The findings are highlighted below:

- The inertial interaction due to superstructure vibration is more dominant on the pile response; however, the kinematic interaction should not be neglected since it increases the bending moment acting on pile.
- The pile is forced especially at the pile head during soil – pile – structure interaction while it is forced at a higher depth without a superstructure present (kinematic interaction).
- The presence of piles in the ground creates a stiffer area below the superstructure. This condition may increase forces acting on the superstructure, which can clearly be seen in the response spectra plotted with and without pile for different cases (Figures 5.31 – 5.33).

RESULTS AND DISCUSSION

The response of a pile-supported structures under seismic loading condition such as an earthquake is influenced by the interaction between the structure itself, the pile foundations, and the surrounding soil. Furthermore, the characteristics of input motion is influential in response.

During an earthquake, wave propagation in soil domain causes vibration (displacements) inducing soil deformations on the foundations (piles) and the supported structure – *kinematic interaction*. In turn, the vibrating superstructure reacts back with dynamic inertial loads to the pile foundations, which causes deformations within the surrounding soil – *inertial interaction*. The response of soil affects the motion of the structure and the response of the structure affects the soil motion. This phenomenon is called soil – structure interaction (SSI).

In design of pile-supported structures, SSI should be taken into account to analyze closer to reality. The most widely methods used to consider SSI: (i) the substructure method, in which inertial and kinematic interactions are evaluated separately, and then superposition theorem is applied for entire system; (ii) the direct method, where the overall seismic response of the whole soil-structure system is analyzed in single step.

In this study, pile-supported structures under dynamic loads are investigated by numerical models for different cases. Analyses are performed by two particular numerical tools (*OpenSees v.2.4.4* and *Plaxis 2D AE.02*). Detailed information regarding methodology is given in Chapter 3.

Chapter 4 focuses especially on kinematic interaction between soil and pile. To examine the kinematic interaction, parametric analyses are performed by established numerical model using *OpenSees v2.4.4* under dynamic loads (harmonic motion and real

earthquake records) considering soil behavior (linear or nonlinear), pile-soil stiffness ratio (E_p/E_s), and slenderness ratio defined as the pile length over pile diameter (L/D). The results are evaluated in terms of displacement and acceleration. Additionally, the phase angle (phase difference between force applied to the system and the current moving in soil domain in vertical and horizontal direction) effect is examined. A new kinematic interaction factor (ratio between pile and free-field motion) is recommended including phase angle variation.

In Chapter 5, complete soil-pile-structure model is discussed according to analysis results obtained by numerical model in *Plaxis 2D AE.02*. Sophisticated software features such as embedded-pile element and hypoplastic soil model are used. Kinematic interaction and inertial interaction are evaluated separately for different cases. Pile response and foundation input motion which is necessary for superstructure design are examined.

6.1 Conclusions

Some of the important findings of this study and recommendations are summarized in the following.

- An overall pattern of for the “*kinematic interaction*”, both in terms of displacement and acceleration, is presented for harmonic input motions (Figures 4.2 – 4.4). The effects of soil nonlinearity, the stiffness ratio between the pile and the soil, the pile slenderness ratio, and the dimensionless frequency are shown. The kinematic interaction factor for displacements (I_u) decreases or remains constant within the range of relevant frequencies ($a < 0.15$), whereas the kinematic interaction factor for accelerations (I_a) increases in general. The effect of soil plasticity can clearly be seen when comparing linear and elasto-plastic soil models, where the value of I_a decreases with frequency for linear soil while I_a increases for nonlinear soil. Under dynamic loading, the free-field acceleration considering plastic soil behavior is lower than that for linear elastic behavior in general because soil strain level has significant role on strength and damping of the soil.
- The three-layered soil profile with an intermediate soft layer introduced additional bending demands within the pile length in general -in comparison with the corresponding homogeneous soil- with more demand concentrations at

vicinity of the soft layer. On the other hand, the effects of pile head condition- i.e., fixed or free-on both the amplitude and the phase angle of the pile response- although significant at close proximity of the pile head- became negligible with depth. Moreover, it was shown that the kinematic interaction effect was more significant at input frequencies that are close to the fundamental natural frequency of the soil deposit. As input the frequency increased, these effects became more localized due to the increase of pile length with respect to the incoming shear wave wavelength.

- It was shown that the kinematically induced phase angle may cause significant changes in the steady state responses of the pile. For frequencies close to the natural frequency of the soil layer, these changes -although quite constant along the whole length of the pile- can significantly alter the pile response, especially for the studied pile embedded in the homogeneous soil deposit. As the frequency of the loading increases, kinematically induced phase angle variations become more oscillatory along the pile length for both homogeneous and layered soils, with patterns that are different from their corresponding free field phase angle profiles. This, in turn will change the free field motion profile, and may affect the response of not only pile but also the superstructure, after being combined with inertial interaction analysis.
- Response of pile foundation embedded in ground as single or an element of a pile group w/ or w/o superstructure under earthquake loading are evaluated by parametric studies considering different cases. In the condition no superstructure (*kinematic interaction*), the maximum bending moment appears at deep level ($\approx L_{pile}/2$) for free-head piles and its value is almost identical for single pile and pile in a group. If pile rotation is restrained by a pile cap in a group, the maximum moment occurs at pile head with approximate value. On the other hand, the maximum pile bending moment increases too much in case with superstructure (*inertial interaction*) and it occurs near surface. Consequently, *inertial interaction* (vibration of superstructure) is more dominant in pile response; however, kinematic interaction should not be neglected as it increases the bending moment.
- There is a misconception regarding piled-structure that the pile is always beneficial in response of the system. However, the presence of piles change the system response significantly and generally in damaging side. The input motion

used in analysis becomes a problem in seismic design since the pile, the superstructure, and the interaction between them affect the motion— the near structure motion and the free-field motion show different behavior. The rigid piles, with its vibration due to its mass, alter motion characteristics amplifying peak ground acceleration (indirectly spectral acceleration). Additionally, the superstructure vibration should be taken into consideration in input motion near piled-structure as it amplifies/de-amplifies the acceleration. As a result, the input motion including pile and superstructure vibration should be considered in analysis.

Some inferences could be made using results from transient analyses with earthquake records. However, they may not be valid for all situations; thus any generalization does not seem possible because there are a great numbers of parameters affecting the overall system behavior such as soil and pile properties, earthquake characteristics, and superstructure features.

6.2 Recommendations

The following suggestions are made for future work in this area.

- Engineering structures are located on or very close to earth's surface and surface waves (Rayleigh and Love) can be more damaging. Especially, waves are trapped (with reflection) between earth surface and bedrock in soft soil layer on semi-infinite bedrock. Kinematic interaction may be investigated in such cases in which surface waves are significant.
- In urban areas, existing (pile-supported) structures (many of these tall buildings) may be placed close to each other. Wave propagation close to surface in such areas can show more different behavior. Building interactions and other near pile groups are also included in the soil-pile-structure problem.
- The performance-based design concepts are used in seismic design over the past 10-15 years. In the performance-based approach, structures and facilities may be analyzed and designed under anticipated seismic loading at two or more discrete hazard levels with an acceptable degree of accuracy. Kinematic interaction between soil and pile and complete *SPSI* may be analyzed by the performance-based approach.

REFERENCES

- [1] Kausel, E., (2010). “Early History of Soil–Structure Interaction”, *Soil Dynamics and Earthquake Engineering*, 30(9):822–832.
- [2] Kramer, S. L., (1996). *Geotechnical Earthquake Engineering*, Prentice-Hall USA.
- [3] Wolf, J. P., (1985). *Dynamic Soil-Structure Interaction*, Prentice-Hall USA.
- [4] Thomson, W., (1848). “On the Equations of Equilibrium of an Elastic Solid”, *Cambridge-Dublin Math. J.*, 3:87–89.
- [5] Stokes, G. G., (1849). “On the Dynamical Theory of Diffraction”, *Trans. Cambridge Philos. Soc.*, 9:1–62.
- [6] Boussinesq, V. J., (1878). “Equilibre D’élasticité D’un Sol Isotrope Sans Pesanteur, Supportant Diffèrent Poids”, *Comptes Rendus*, LXXXVI:1260–1263.
- [7] Boussinesq, V. J., (1878). “Sur La Dépression Que Produit, à La Surface D’un Horizontal Elastique Et Isotrope, Un Po Ids Qu’on Dépose, Et Sur La Répartition De ce Poids Entre Ses Divers Point D’appui”, *Comptes Rendus*, LXXXVII:402–405.
- [8] Boussinesq, V. J., (1878). “Sur La Manière Dont Se Distribue Entre Ses Points D’appui Le Poids D’un Corps Dur, Pose Sur Un Sol Poli, Horizontal Et Elastique: Identité De Ce Mode De Répartition, Pour Une Base De Sustentation Plane Et Horizontale, Avec Celui D’une Charge Electrique En”, *Comptes Rendus*, LXXXVII:519–522.
- [9] Lamb, H., (1904). “On the Propagation of Tremors over the Surface of an Elastic Solid”, *Philos. Trans. R. Soc. London*, 203:1–42.
- [10] Mindlin, R. D., (1936). “Force at a Point in the Interior of a Semi-Infinite Solid”, *Physics (College. Park. Md.)*, 7:195–202.
- [11] Reissnerr, E., (1936). “Stationare, Axisymetrische, Durch Eine Schüttelnde Masse Erregte Schwingung Eines Homogenen Elastischen Halbraum”, *Ingenieur-Archiv*, VII(6):381–396.
- [12] Sezawa, K. and Kanai, K., (1935). “Decay in the Seismic Vibrations of a Simple or Tall Structure by Dissipation of their Energy into the Ground”, *Bull. Earthq. Res. Inst.*, 13:681–696.
- [13] Sezawa, K. and Kanai, K., (1935). “Energy Dissipation in Seismic Vibrations of a Framed Structure”, *Bull. Earthq. Res. Inst.*, 13:698–714.

- [14] Sezawa, K. and Kanai, K., (1935). "Energy Dissipation in Seismic Vibrations of Actual Buildings", *Bull. Earthq. Res. Inst.*, 13:925–941.
- [15] Merrit, R. and Housner, G. W., (1954). "Effect of the Foundation Compliance on Earthquake Stresses in Multi-Story Buildings", *Bull. Seismol. Soc. Am.*, 44(4):551–569.
- [16] Housner, G. W., (1957). "Interaction of Building and Ground during an Earthquake", *Bull. Seismol. Soc. Am.*, 47(3):179–186.
- [17] Newmark, N. M., (1969). "Torsion of Symmetrical Buildings", *Fourth World Conference on Earthquake Engineering*, January 13-18 1969, Santiago.
- [18] Veletsos, A. S. and Wei, Y. T., (1971). "Lateral and Rocking Vibration of Footings", *J. Soil Mech. Found. Div.*, 97:1227–1248.
- [19] Luco, J. E. and Westman, R. A., (1972). "Dynamic Response of Rigid Footing Bonded to Elastic Half-Space", *J. Appl. Mech.*, 39(2):527–534.
- [20] Kausel, E., (1976). "Soil-Structure Interaction, Soil Dynamics for Earthquake Design", *International Centre for Computer-aided Design*, Santa Margherita, Italy.
- [21] Seed, H. B., Whitman, R. V., and Lysmer, J., (1977). "Soil-Structure Interaction Effects in the Design of Nuclear Power Plants", *Structural and Geotechnical Mechanics*, Chapter 13, Prentice Hall.
- [22] Parmelee, R. A., Penzien, J., Scheffey, C. F., Seed, H. B., and Thiers, G. R., (1964). *Seismic Effects on Structures Supported on Piles Extending Through Deep Sensitive Clays*, *Inst. Eng. Res., Rep. SESM64-2*, Uni. Of California, Berkeley, USA.
- [23] Tajimi, H., (1966). *Earthquake Response of Foundation Structures*, Report of Faculty Science and Engineering, Nihon University, Japan.
- [24] Penzien, J., (1970). "Soil - Pile Foundation Interaction", *Earthquake Engineering*, Ed. Wiegel, R. L., Prentice Hall:349–381.
- [25] Novak, M., (1974). "Dynamic Stiffness and Damping of Piles", *Can. Geotech. J.*, 11(4): 574–598.
- [26] Novak, M., (1991). "Piles Under Dynamic Loads", *Second International Conference on Recent Advances in Geotechnical Earthquake Engineering and Soil Dynamics*, March 11-15 1991, St. Louis.
- [27] Blaney, G. W., Kausel, E., and Roesset, J. M., (1976). "Dynamic Stiffness of Piles", *Second International Conference on Numerical Methods in Geomechanics*, June 1976, Blacksburg.
- [28] Wolf, J. P. and von Arx, G. A., (1978). "Impedance Functions of a Group of Vertical Piles", *ASCE Specialty Conference on Earthquake Engineering and Soil Dynamics*, June 19-21 1978, Pasadena.
- [29] Kuhlemeyer, R. L., (1979). *Static and Dynamic Laterally Loaded Piles*, Research Report No. CE76-9, Dept. of Civil Engineering, University of Calgary.

- [30] Banerjee, P. K., (1978). "Analysis of Axially and Laterally Loaded Pile Groups", *Developments in Soil Mechanics*, Ed. Scott, C. R., Applied Science Publication.
- [31] Banerjee, P. K. and Sen, R., (1987). "Dynamic Behavior of Axially and Laterally Loaded Piles and Pile Group", *Dynamic behavior of foundations and buried structures*, Elsevier.
- [32] Matlock, H., Foo, H. C., and Bryant, L. M., (1978). "Simulation of Lateral Pile Behavior under Earthquake Motion", *ASCE Specialty Conference on Earthquake Engineering and Soil Dynamics*, June 19-21 1978, Pasadena.
- [33] Matlock, H. and Foo, H. C., (1980). "Axial Analysis of Piles Using a Hysteretic Degrading Soil Model", *Conference on Numerical Methods in Offshore Piling*, Institution of Civil Engineers, London.
- [34] Trochanis, A. M., Bielak, J., and Christian, P., (1988). *A Three-Dimensional Nonlinear Study of Piles Leading to the Development of a Simplified Model*, Research Report R-88-176, Carnegie Institute of Technology, PA, USA.
- [35] Dobry, R. and Gazetas, G., (1988). "Simple Method for Dynamic Stiffness and Damping of Floating Pile Groups", *Géotechnique*, 38(4):557–574.
- [36] Fan, B. K., Gazetas, G., Kaynia, A., Kausel, E., and Ahmad, S., (1991). "Kinematic Seismic Response of Single Piles and Pile Groups", *J. Geotech. Eng.*, 117(12):1860–1879.
- [37] Scott, R., Tsai, C., Steussy, D., and Ting, J., (1977). "Full - Scale Dynamic Lateral Pile Tests", *6th World Conference on Earthquake Engineering*, January 10-14 1977, New Delhi.
- [38] Finn, W. L. and Gohl, E., (1987). "Centrifuge Model Studies of Piles under Simulated Earthquake Lateral Loading", *Dynamic Response of Pile Foundations – Experiment, Analysis, and Observation*, Geotechnical Special Publication No.11, ASCE.
- [39] Kubo, K., (1969). "Vibration Test of a Structure Supported by Pile Foundation", *4th World Conference on Earthquake Engineering*, January 13-18 1969, Santiago.
- [40] Kagawa, T. and Kraft, L., (1980). "Seismic p-y Responses of Flexible Piles", *Journal Geotech. Eng.*, 106(8):899–918.
- [41] Mylonakis, G., (1995). *Contributions to Static and Seismic Analysis of Piles and Pile-Supported Bridge Piers*, PhD Thesis, State University of New York at Buffalo.
- [42] Gazetas, G. and Mylonakis, G., (1998). "Seismic Soil -Structure Interaction: New Evidence and Emerging Issues", *Geotechnical Earthquake Engineering and Soil Dynamics III, A Specialty Conference*, August 3-6 1998, Seattle.
- [43] El Naggar, M. H. and Novak, M., (1995). "Nonlinear Lateral Interaction in Pile Dynamics", *Soil Dyn. Earthq. Eng.*, 14(2):141–157.
- [44] El Naggar, M. H. and Novak, M., (1996). "Nonlinear Analysis for Dynamic Lateral Pile Response", *Soil Dyn. Earthq. Eng.*, 15(4):233–244.

- [45] Boulanger, R. W., Curras, C. J., Kutter, B. L., Wilson, D. W., and Abghari, A. (1999). "Seismic Soil-Pile-Structure Interaction Experiments and Analyses", *J. Geotech. Geoenvironmental Eng.*, 125(9):750–759.
- [46] Tokimatsu, K., Suzuki, H., and Sato, M., (2005). "Effects of Inertial and Kinematic Interaction on Seismic Behavior of Pile with Embedded Foundation", *Soil Dyn. Earthq. Eng.*, 25:753–762.
- [47] Anoyatis, G., Di Laora, R., Mandolini, A., and Mylonakis, G., (2013). "Kinematic Response of Single Piles for Different Boundary Conditions: Analytical Solutions and Normalization Schemes", *Soil Dyn. Earthq. Eng.*, 44:183–195.
- [48] Chidichimo, A., Cairo, R., Dente, G., Taylor, C., and Mylonakis, G., (2014). "1-g Experimental Investigation of Bi-layer Soil Response and Kinematic Pile Bending", *Soil Dyn. Earthq. Eng.*, 67:219–232.
- [49] Dezi, F., Carbonari, S., and Leoni, G., (2010). "Kinematic Bending Moments in Pile Foundations", *Soil Dyn. Earthq. Eng.*, 30(3):119–132.
- [50] Maheshwari, B. K. and Sarkar, R., (2011). "Seismic Behavior of Soil-Pile-Structure Interaction in Liquefiable Soils: Parametric Study", *Int. J. Geomech.*, 11(4):335–347.
- [51] Di Laora, R., Mylonakis, G., and Mandolini, A., (2013). "Pile-Head Kinematic Bending in Layered Soil", *Earthq. Eng. Struct. Dyn.*, 42:319–337.
- [52] Kaynia, A. M. and Mahzooni, S., (1996). "Forces in Pile Foundations under Seismic Loading", *J. Eng. Mech.*, 122(1):46–53.
- [53] Gazetas, G., (1984). "Seismic Response of End-Bearing Single Piles", *Int. J. Soil Dyn. Earthq. Eng.*, 3(2):82–93.
- [54] Madabhushi, G., Knappett, J., and Haigh, S., (2010). *Design of Pile Foundations in Liquefiable Soils*, Imperial College Press.
- [55] Mizuno, H., (1987). "Pile Damage during Earthquake in Japan (1923 – 1983)", *Dynamic Response of Pile Foundations – Experiment, Analysis, and Observation*, Geotechnical Special Publication No. 11, ASCE.
- [56] Ross, G., Seed, H., and Migliacio, R., (1973). "Performance of Highway Bridge Foundations", *The Great Alaska Earthquake of 1964*, National Academy of Sciences.
- [57] Matsui, T. and Oda, K., (1996). "Foundation Damage of Structures", *Soils Fond. Spec. Issue Geotechnical Asp. January 17 1995 Hyokogen Nambu Earthquake*, *JSSMFE*, 36(1): 189–200.
- [58] Tokimatsu, K., Mizuno, H., and Kakurai, M., (1996). "Building Damage Associated with Geotechnical Problems", *Soils Fond. Spec. Issue Geotechnical Asp. January 17 1995 Hyokogen Nambu Earthquake*, *JSSMFE*, 36(1):219–234.
- [59] Esashi, Y. and Yoshida, Y., (1980). "Convenient Aseismic Design of Pile Foundation", *7th World Conference on Earthquake Engineering*, September 8-13 1980, İstanbul.

- [60] Makris, N., Badoni, D., Delis, E., and Gazetas, G., (1994). “Prediction of Observed Bridge Response with Soil-Pile-Structure Interaction”, *J. Struct. Eng.*, 120(10):2992–3011.
- [61] Nikolaou, S., Mylonakis, G., Gazetas, G., and Tazoh, T., (2001). “Kinematic Pile Bending during Earthquakes: Analysis and Field Measurements”, *Geotechnique*, 51(5):425–440.
- [62] Meymand, P. J., (1998). *Shaking Table Scale Model Tests of Nonlinear Soil-Pile-Superstructure Interaction in Soft Clay*, PhD Thesis, University of California, Berkeley.
- [63] Novak, M., Nogami, T., and Aboul-Ella, F., (1978). “Dynamic Reactions for Plane Strain Case”, *J. Eng. Mech. Div.*, 104: 953–959.
- [64] Makris, N. and Gazetas, G., (1992). “Dynamic Pile-Soil-Pile Interaction. Part II: Lateral and Seismic Response”, *Earthq. Eng. Struct. Dyn.*, 21:145–162.
- [65] Kavvadas, M. and Gazetas, G., (1993). “Kinematic Seismic Response and Bending of Free-Head Piles in Layered Soil”, *Geotechnique*, 43(2):207–222.
- [66] Mylonakis, G., (2001). “Simplified Model for Seismic Pile Bending at Soil Layer Interfaces”, *Soils Found.*, 41(4):47–58.
- [67] Lysmer, J. and Kuhlemeyer, R. L., (1969). “Finite Dynamic Model for Infinite Media”, *J. Eng. Mech. Div.*, 95:859–877.
- [68] Kausel, E., Waas, G., and Roesset, M., (1975), “Dynamic Analysis of Footings on Layered Media”, *J. Eng. Mech. Div.*, 101(5):679–693.
- [69] Bielak, J., Loukakis, K., Hisada, Y., and Yoshimura, C., (2003). “Domain Reduction Method for Three-Dimensional Earthquake Modeling in Localized Regions , Part I : Theory”, *Bull. Seismol. Soc. Am.*, 93(2):817–824.
- [70] Lu, J., Elgamal, A., Yan, L., Law, K. H., and Conte, J. P., (2011). “Large-Scale Numerical Modeling in Geotechnical Earthquake Engineering”, *Int. J. Geomech.*, 11(6):490–503.
- [71] Butterfield, R. and Banerjee, P. K., (1971). “The Elastic Analysis of Compressible Piles and Pile Groups”, *Geotechnique*, 21(1):43–60.
- [72] Kaynia, A. M., (1982). *Dynamic Stiffness and Seismic Response of Pile Groups*, PhD Thesis, Massachusetts Institute of Technology.
- [73] Sen, R., Davies, T. G., and Banerjee, P. K., (1985). “Dynamic Analysis of Piles and Pile Groups Embedded in Homogeneous Soils”, *Earthq. Eng. Struct. Dyn.*, 13:53–65.
- [74] Ahmad, S. (1986). *Linear and Nonlinear Dynamic Analysis by Boundary Element Method*, PhD Thesis, University of New York at Buffalo.
- [75] Padron, L. A., Aznarez, J. J., and Maeso, O., (2007). “BEM – FEM Coupling Model for the Dynamic Analysis of Piles and Pile Groups”, *Eng. Anal. Bound. Elem.*, 31:473–484.
- [76] Mylonakis, G., Nikolaou, A., and Gazetas, G., (1997). “Soil-Pile-Bridge Seismic Interaction: Kinematic and Inertial Effects. Part I: Soft Soil”, *Earthq. Eng. Struct. Dyn.*, 26:337–359.

- [77] Margason, E., (1975). “Pile Bending during Earthquakes”, Lecture given as part of ASCE/UC-Berkeley sponsored Seminar on Design Construction and Performance of Deep Foundations.
- [78] Flores-Berrones, R. and Whitman, R. V., (1982). “Seismic Response of End-Bearing Piles”, *J. Geotech. Eng. Div.*, 108(4):554–569.
- [79] Padrón, L. A., Mylonakis, G., and Beskos, D. E., (2012). “Simple Superposition Approach for Dynamic Analysis of Piled Embedded Footings”, *Int. J. Numer. Anal. Methods Geomech.*, 36:1523–1534.
- [80] McKenna, F., Fenves, G. L., and Scott, M. H., (2000). Open System for Earthquake Engineering Simulation (OpenSees), Pacific Earthquake Engineering Research Center.
- [81] Zhang, Y., Conte, J. P., Yang, Z., Elgamal, A., Bielak, J., and Acero, G., (2008). “Two-Dimensional Nonlinear Earthquake Response Analysis of a Bridge-Foundation-Ground System”, *Earthq. Spectra*, 24(2):343–386.
- [82] Aygün, B., Dueñas-osorio, L., Padgett, J. E., and Desroches, R., (2011). “Efficient Longitudinal Seismic Fragility Assessment of a Multispan Continuous Steel Bridge on Liquefiable Soils”, *J. Bridg. Eng.*, 16:93–107.
- [83] Khosravifar, A., (2012). Analysis and Design for Inelastic Structural Response of Extended Pile Shaft Foundations in Laterally Spreading Ground during Earthquakes, PhD Thesis, University of California Davis.
- [84] Chiamonte, M. M., (2011). An Analysis of Conventional and Improved Marginal Wharves, MSc Thesis, University of Washington.
- [85] Zienkiewicz, O. C., Bicanic, N., and Shen, F. Q., (1989). “Earthquake input definition and the transmitting boundary conditions, *Advances in Computational Nonlinear Mechanics*”, *Adv. Comput. Nonlinear Mech.*, 300:109–138.
- [86] McGann C. and Arduino, P., Effective Stress Site Response Analysis of a Layered Soil Column, OpenSees Example, <http://opensees.berkeley.edu/wiki/index.php/examples>. July 25 2014.
- [87] Padrón, L. A., Aznarez, J.J., and Maeso, O., (2008). “Dynamic Analysis of Piled Foundations in Stratified Soils by a BEM – FEM model”, *Soil Dyn. Earthq. Eng.*, 28:333–346.
- [88] Yang, Z., Lu, J., and Elgamal, A., (2008). OpenSees Soil Models and Solid-Fluid Fully Coupled Elements User’s Manual, University of California, San Diego.
- [89] McGann, C. G., Arduino, P., and Mackenzie-Helnwein, P., (2012). “Stabilized Single-Point 4-node Quadrilateral Element for Dynamic Analysis of Fluid Saturated Porous Media”, *Acta Geotech.*, 7(4):297–311.
- [90] Potyondy, J. G. (1961). “Skin Friction between Various Soils and Construction Materials”, *Géotechnique*, 11:339–353.
- [91] Tiwari, B., Ajmera, B., and Kaya, G., (2010). Shear Strength Reduction at Soil Structure Interface, *GeoFlorida 2010: Advances in Analysis, Modeling & Design*, GSP 199, ASCE.

- [92] Jalali, M. M., Golmaei, S. H., Jalali, M. R., Alistair, B., Ahmadi, M. K. Z., and Moradi, R., (2012). “Using Finite Element method for Pile-Soil Interface (through PLAXIS and ANSYS)”, *J. Civ. Eng. Constr. Technol.*, 3:256–272.
- [93] Potts, D. M. and Zdravkovic, L., (1999). *Finite Element Analysis in Geotechnical Engineering: Theory*, Thomas Telford.
- [94] Trochanis, A. M., Bielak, J., and Christiano, P., (1991). “Three-Dimensional Nonlinear Study of Piles”, *J. Geotech. Eng.*, 117(3):429–447.
- [95] Jeremic, B., Jie, G., Preisig, M., and Tafazzoli, N., (2009). “Time Domain Simulation of Soil – Foundation – Structure Interaction in Non-uniform Soils”, *Earthq. Eng. Struct. Dyn.*, 38:699–718.
- [96] Joyner, W. B. and Chen, A. T. F., (1975). “Calculation of Nonlinear Ground Response in Earthquakes”, *Bulletin of Seismological Society of America*, 65(5):1315–1336.
- [97] Liu, M. and Corman, D. G., (1995). “Formulation of Rayleigh damping and its extensions”, *Computers & Structures*, 57(2):277–285.
- [98] Rayleigh, J. M., (1945). *The Theory of Sound*. Dover Publications.
- [99] Rathje, E. M. and Bray, J. D., (2001). “One- and Two-Dimensional Seismic Analysis of Solid-Waste Landfills”, *Can. Geotech. J.*, 38(4):850–862.
- [100] Kwok, A. O., Stewart, J. P., Hashash, Y. M. A., Matasovic, N., Pyke, R., Wang, Z., and Yang, Z., (2007). “Use of Exact Solutions of Wave Propagation Problems to Guide Implementation of Nonlinear Seismic Ground Response Analysis Procedures”, *J. Eng. Mech. Div.*, 133(11):1385–1398.
- [101] Eurocode 8, (2013). *Design of Structures for Earthquake Resistance —Part 1: General Rules, Seismic Actions and Rules for Buildings*, CEN, Brussels.
- [102] Brinkgreve, R. B. J., Engin, E., and Swolfs, W. M., (2014). *Plaxis 2D Reference Manual*, Plaxis bv.
- [103] Brinkgreve, R. B. J., Engin, E., and Swolfs, W. M., (2014). *Material Models Manual*, Plaxis bv.
- [104] Mašín, D., (2010). *PLAXIS Implementation of Hypoplasticity*, Plaxis bv.
- [105] Özyaydın, K., (2014). Interview by Author, İstanbul.
- [106] Schnabel, P. B., Lysmer, J., and Seed, H. B., (1972). *Shake: A Computer Program for Earthquake Response Analyses of Horizontally Layered Sites*, Tech. Rep. UCB/EERC-72.
- [107] Hashash, Y. M. A., (2012). *DeepSoil v5.1: User Manual and Tutorial*, University of Illinois at Urbana-Champaign.
- [108] Mayne, P. W., Christopher, B. R., and Dejong, J., (2001). *Manual on Subsurface Investigations*, FHWA NHI-01-031.
- [109] Vucetic, M. and Dobry, R. (1991). “Effect of Soil Plasticity on Cyclic Response”, *J. Geotech. Eng.*, 117(1):89–107.
- [110] Yoshida, N., Kobayashi, S., Suetomi, I., and Miura, K., (2002). “Equivalent Linear Method Considering Frequency Dependent Characteristics of Stiffness and Damping”, *Soil Dyn. Earthq. Eng.*, 22:205–222.

- [111] TDY, (2007). Specification for Structures to be Built in Disaster Areas, Turkey Ministry of Environment and Urban Planning, Ankara.
- [112] De Sanctis, L., Maiorano, R. M. S., and Aversa, S., (2010). "A Method for Assessing Kinematic Bending Moments at the Pile Head", *Earthq. Eng. Struct. Dyn.*, 39:1133–1154.
- [113] Makris, N. and Gazetas, G., (1993). "Displacement Phase Differences in a Harmonically Oscillating Pile", *Géotechnique*, 43(1):135–150.
- [114] Kirkit, M., Seylabi, E. E., Jeong, C., and Taciroğlu, E., (2014). "Kinematic Interaction Factor for a Single Pile Embedded in Homogeneous Soil," ICESA 2014 International Civil Engineering & Architecture Symposium for Academicians, May 17-20 2014, Antalya.
- [115] Carbonari, S., Dezi, F., and Leoni, G., (2012). "Nonlinear Seismic Behaviour of Wall-Frame Dual Systems Accounting for Soil – Structure Interaction", *Earthq. Eng. Struct. Dyn.*, 41:1651–1672.
- [116] NEHRP, (2012). Soil-Structure Interaction for Building Structures, National Institute of Standards and Technology, USA.
- [117] Herle, I., (2008). "On Basic Features of Constitutive Models for Geomaterials", *J. Theor. Appl. Mech.*, 38(1):61–80.
- [118] Goldscheider, M., (1975). "Dilatanzverhalten von Sand bei geknickten Verformungswegen," *Mech. Res. Commun.*, 2:143–148.
- [119] Kolymbas, D., (1978). Ein Nichtlineares Viskoplastisches Stoffgesetz für Böden, Veröffentlichungen des Institutes für Bodenmechanik und Felsmechanik.
- [120] Kolymbas, D., (1991). "An Outline of Hypoplasticity", *Arch. Appl. Mech.*, 61:143–151.
- [121] Davis, R. O., and Selvadurai, A. P. S., (2002). *Plasticity and Geomechanics*, Cambridge University Press.
- [122] Niemunis, A. and Krieg, S., (1996). "Viscous Behaviour of Soil under Oedometric Conditions", *Can. Geotech. J.*, 33:159–168.
- [123] Herle, I. and Kolymbas, D., (2004), "Hypoplasticity for Soils with Low Friction Angles", *Comput. Geotech.*, 31(5):365–373.
- [124] Mašin, D., (2005). "A Hypoplastic Constitutive Model for Clays", *Int. J. Numer. Anal. Methods Geomech.*, 29(4):311–336.
- [125] Lanier, J., Caillerie, D., Chambon, R., Viggiani, G., Bésuelle, P., and Desrues, J., (2004). "A General Formulation of Hypoplasticity", *Int. J. Numer. Anal. Methods Geomech.*, 28(15):1461–1478.
- [126] Weifner, T. and Kolymbas, D., (2007). "A Hypoplastic Model for Clay and Sand", *Acta Geotech.*, 2(2):103–112.
- [127] Fuentes, W., Triantafyllidis, T., and Lizcano, A., (2012). "Hypoplastic Model for Sands with Loading Surface", *Acta Geotech.*, 7(3):177–192.
- [128] Mašin, D., (2014). "Clay Hypoplasticity Model Including Stiffness Anisotropy", *Géotechnique*, 64(3):232–238.

- [129] Gasparre, A., (2005). Advanced Laboratory Characterisation of London Clay, PhD Thesis, Imperial College London.
- [130] Brinkgreve, R. B. J., Kappert, M. H., and Bonnier, P. G., (2007). “Hysteretic Damping in a Small-Strain Stiffness Model”, Numerical Models in Geomechanics - NUMOG X, April 25-27 2007, Rhodes.
- [131] Sadek, M. and Shahrour, I., (2004), “A Three Dimensional Embedded Beam Element for Reinforced Geomaterials”, Int. J. Numer. Anal. Methods Geomech., 28(9):931–946.
- [132] Brinkgreve, R. B. J., Engin, E., and Swolfs, W. M., (2014). PLAXIS Scientific Manual, Plaxis bv.
- [133] Sluis, J., (2012). Validation of Embedded Pile Row in Plaxis 2D, MSc Thesis, University of Technology.
- [134] Das, B., (2011). Principles of Foundation Engineering, Cengage Learning.
- [135] Mylonakis, G. and Gazetas, G., (2000). “Seismic Soil-Structure Interaction: Beneficial or Detrimental?”, J. Earthq. Eng., 4(3):277–301.
- [136] Jeremić, B., Kunnath, S., and Xiong, F., (2004). “Influence of Soil-Foundation-Structure Interaction on Seismic Response of the I-880 Viaduct”, Eng. Struct., 26(3):391–402.
- [137] Seed, H. B., Ugas, C., and Lysmer, J., (1976). “Site Dependent Spectra for Earthquake-Resistant Design”, Bull. Seismol. Soc. Am., 66:221–244.
- [138] Rathje, E. M., Abrahamson, N. A., and Bray, J. D., (1998). “Simplified Frequency Content Estimates of Earthquake Ground Motions”, J. Geotech. Geoenvironmental Eng., 124(2):150–159.

OPENSEES SCRIPT FOR SOIL – PILE INTERACTION

A small model (Figure A.1) and its “*tcl*” (which is a programming language named “*tool command language*” used by *OpenSees*) script regarding geometry, boundary conditions, and analysis steps are presented in the following. Researchers may create their own model with large geometry utilizing this small model.

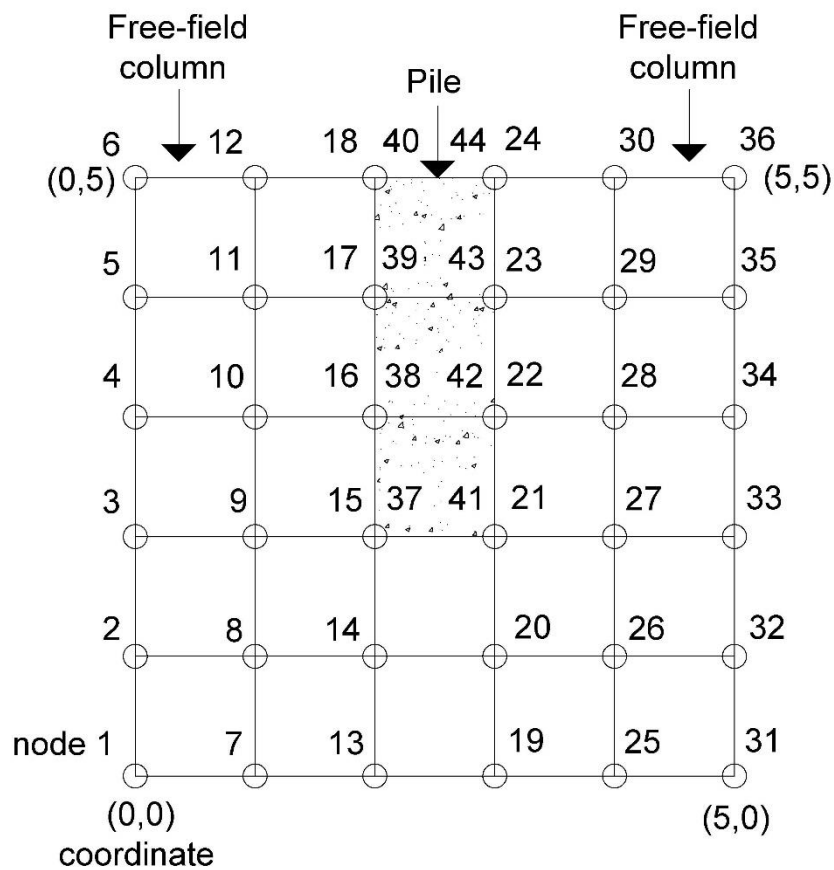


Figure A.1 Small model to demonstrate analysis performed by OpenSees

Tcl Script

```
#-----  
# Step 1: Creating geometry  
#-----  
  
wipe  
  
# Soil nodes are created in 2 dimensions, with 2 translational dof  
  
model BasicBuilder -ndm 2 -ndf 2  
  
# node number Coordinate X Coordinate Y  
# soil nodes  
node 1 0.00 0.00  
node 2 0.00 1.00  
node 3 0.00 2.00  
node 4 0.00 3.00  
node 5 0.00 4.00  
node 6 0.00 5.00  
node 7 1.00 0.00  
node 8 1.00 1.00  
node 9 1.00 2.00  
node 10 1.00 3.00  
node 11 1.00 4.00  
node 12 1.00 5.00  
node 13 2.00 0.00  
node 14 2.00 1.00  
node 15 2.00 2.00  
node 16 2.00 3.00  
node 17 2.00 4.00  
node 18 2.00 5.00  
node 19 3.00 0.00  
node 20 3.00 1.00  
node 21 3.00 2.00  
node 22 3.00 3.00  
node 23 3.00 4.00  
node 24 3.00 5.00  
node 25 4.00 0.00  
node 26 4.00 1.00  
node 27 4.00 2.00  
node 28 4.00 3.00  
node 29 4.00 4.00  
node 30 4.00 5.00  
node 31 5.00 0.00  
node 32 5.00 1.00  
node 33 5.00 2.00  
node 34 5.00 3.00  
node 35 5.00 4.00  
node 36 5.00 5.00  
  
# pile nodes  
node 37 2.00 2.00  
node 38 2.00 3.00  
node 39 2.00 4.00  
node 40 2.00 5.00  
node 41 2.00 2.00  
node 42 2.00 3.00  
node 43 2.00 4.00  
node 44 2.00 5.00  
  
# dashpot nodes  
node 101 0.00 0.00  
node 102 0.00 0.00
```

```

#-----
# Step 2: Defining material, motion, and analysis parameters
#-----

# Soil Parameters
set rho 1.7; # soil mass density (Mg/m^3)
set Vs 120.0; # soil shear wave velocity (m/s)
set G [expr $rho*$Vs*$Vs]; # soil shear modulus (kPa)
set nu 0.4; # poisson's ratio of soil
set E [expr 2*$G*(1+$nu)]; # soil elastic modulus (kPa)
set bulk [expr $E/(3*(1-2*$nu))]; # soil bulk modulus (kPa)
set cohesion 40.0; # soil cohesion (kPa)
set gammaPeak 0.1; # peak shear strain
set phi 0.0; # soil friction angle
set refPress 100.0; # reference pressure
set pressCoeff 0.0; # pressure dependency coefficient

# Pile Parameters
set pileE 28000000.0; # pile elastic modulus (kPa)
set pileNu 0.15; # poisson's ratio of pile
set pileDen 2.5; # pile mass density (Mg/m^3)

# Dashpot Material
set rockDen 2.5; # rock mass density (Mg/m^3)
set rockVs 760; # rock shear wave velocity (m/s)
set baseArea 203; # calculated by hand
set mC [expr $rockDen*$rockVs*$baseArea]
set dashpotCoeff [expr $rockDen*$rockVs]

# Base area = 2*100*1 + 3*1 = 203 m^2 (Extended free-field 100 m)

# Input Motion
set lBloadTag 1
set VelFile HarmonicMotion.out; #time history is loaded from separate file
set numSteps 500; #number of steps in motion record
set dt 0.01; #time step in motion record
set sizeEleX 1.0

# Define constant scaling factor for applied velocity
set cFactor [expr $baseArea*$dashpotCoeff]

# Rayleigh Damping Parameters
set pi 3.141592654
set damp 0.05; # damping ratio
set omega1 [expr 2*$pi*1]; # lower frequency
set omega2 [expr 2*$pi*5]; # upper frequency
set a0 [expr 2*$damp*$omega1*$omega2/($omega1 + $omega2)]; # damping coefficients
set a1 [expr 2*$damp/($omega1 + $omega2)]
puts "Damping Coefficients: a_0 = $a0; a_1 = $a1"

# Newmark Parameters
set gamma 0.5
set beta 0.25

#-----
# Step 3: Materials and Elements
#-----

# Soil Material
nDMaterial PressureInDependMultiYield 1 2 $rho $G $bulk $cohesion $gammaPeak \
    $phi $refPress $pressCoeff 25

# Pile Material
nDMaterial ElasticIsotropic 2 $pileE $pileNu $pileDen

```

Dashpot Material

uniaxialMaterial Viscous 3 \$mC 1

Interface Material between soil and pile

uniaxialMaterial Elastic 4 [expr 0.8*\$E];

set wgtX 0.0
set wgtY [expr -9.81*\$rho]
set wgtPX 0.0
set wgtPY [expr -9.81*\$pileDen]
set thick 1.0
set thickf 100

Soil Elements

element SSPquad 1 1 7 8 2 1 "PlaneStrain" \$thickf 0.0 \
0.0 \$wgtX \$wgtY
element SSPquad 2 2 8 9 3 1 "PlaneStrain" \$thickf 0.0 \
0.0 \$wgtX \$wgtY
element SSPquad 3 3 9 10 4 1 "PlaneStrain" \$thickf 0.0 \
0.0 \$wgtX \$wgtY
element SSPquad 4 4 10 11 5 1 "PlaneStrain" \$thickf 0.0 \
0.0 \$wgtX \$wgtY
element SSPquad 5 5 11 12 6 1 "PlaneStrain" \$thickf 0.0 \
0.0 \$wgtX \$wgtY
element SSPquad 6 7 13 14 8 1 "PlaneStrain" \$thick 0.0 \
0.0 \$wgtX \$wgtY
element SSPquad 7 8 14 15 9 1 "PlaneStrain" \$thick 0.0 \
0.0 \$wgtX \$wgtY
element SSPquad 8 9 15 16 10 1 "PlaneStrain" \$thick 0.0 \
0.0 \$wgtX \$wgtY
element SSPquad 9 10 16 17 11 1 "PlaneStrain" \$thick 0.0 \
0.0 \$wgtX \$wgtY
element SSPquad 10 11 17 18 12 1 "PlaneStrain" \$thick 0.0 \
0.0 \$wgtX \$wgtY
element SSPquad 11 13 19 20 14 1 "PlaneStrain" \$thick 0.0 \
0.0 \$wgtX \$wgtY
element SSPquad 12 14 20 21 15 1 "PlaneStrain" \$thick 0.0 \
0.0 \$wgtX \$wgtY
element SSPquad 13 19 25 26 20 1 "PlaneStrain" \$thick 0.0 \
0.0 \$wgtX \$wgtY
element SSPquad 14 20 26 27 21 1 "PlaneStrain" \$thick 0.0 \
0.0 \$wgtX \$wgtY
element SSPquad 15 21 27 28 22 1 "PlaneStrain" \$thick 0.0 \
0.0 \$wgtX \$wgtY
element SSPquad 16 22 28 29 23 1 "PlaneStrain" \$thick 0.0 \
0.0 \$wgtX \$wgtY
element SSPquad 17 23 29 30 24 1 "PlaneStrain" \$thick 0.0 \
0.0 \$wgtX \$wgtY
element SSPquad 18 25 31 32 26 1 "PlaneStrain" \$thickf 0.0 \
0.0 \$wgtX \$wgtY
element SSPquad 19 26 32 33 27 1 "PlaneStrain" \$thickf 0.0 \
0.0 \$wgtX \$wgtY
element SSPquad 20 27 33 34 28 1 "PlaneStrain" \$thickf 0.0 \
0.0 \$wgtX \$wgtY
element SSPquad 21 28 34 35 29 1 "PlaneStrain" \$thickf 0.0 \
0.0 \$wgtX \$wgtY
element SSPquad 22 29 35 36 30 1 "PlaneStrain" \$thickf 0.0 \
0.0 \$wgtX \$wgtY

Pile Elements

element SSPquad 23 37 41 42 38 2 "PlaneStrain" \$thick 0.0 \
0.0 \$wgtPX \$wgtPY
element SSPquad 24 38 42 43 39 2 "PlaneStrain" \$thick 0.0 \
0.0 \$wgtPX \$wgtPY

```

element      SSPquad 25      39      43      44      40      2      "PlaneStrain"      $thick      0.0 \
              0.0      $wgtPX  $wgtPY

```

```
# Dashpot Element
```

```
element zeroLength 100 101 102 -mat 3 -dir 1
```

```
# Interface Elements
```

```

element      zeroLength      51      15      37      -mat      3      3      -dir      1      2
element      zeroLength      52      16      38      -mat      3      3      -dir      1      2
element      zeroLength      53      17      39      -mat      3      3      -dir      1      2
element      zeroLength      54      18      40      -mat      3      3      -dir      1      2
element      zeroLength      55      41      21      -mat      3      3      -dir      1      2
element      zeroLength      56      42      22      -mat      3      3      -dir      1      2
element      zeroLength      57      43      23      -mat      3      3      -dir      1      2
element      zeroLength      58      44      24      -mat      3      3      -dir      1      2

```

```
#-----
```

```
# Step 4: Boundary Conditions
```

```
#-----
```

```
# Base boundary (horizontal: free — vertical: fixed)
```

```

fix          1          0          1
fix          7          0          1
fix          13         0          1
fix          19         0          1
fix          25         0          1
fix          31         0          1

```

```
# Dashpot boundary
```

```

fix          101         1          1
fix          102         0          1

```

```
# Base dashpot
```

```

equalDOF     1          102         1
equalDOF     1          7           1
equalDOF     1          13          1
equalDOF     1          19          1
equalDOF     1          25          1
equalDOF     1          31          1

```

```
# Free-field soil columns
```

```

equalDOF     2          8           1      2
equalDOF     3          9           1      2
equalDOF     4          10          1      2
equalDOF     5          11          1      2
equalDOF     6          12          1      2

```

```
#-----
```

```
# Step 5: Analysis Commands and Recorders
```

```
#-----
```

```
# update material to consider elastic behavior (0: linear elastic, 1: non-linear)
```

```
updateMaterialStage -material 1 -stage 0
```

```
# Gravity Analysis
```

```

constraints Transformation
test      NormDisplncr 1e-2 40 1
algorithm Newton
numberer  RCM
system    ProfileSPD
integrator Newmark $gamma $beta
analysis  VariableTransient
analyze   10 5.0e2
puts     "Finished with elastic gravity analysis..."

```

```
# update material to consider elastoplastic behavior (0: linear elastic, 1: non-linear)
```

```

updateMaterialStage -material 1 -stage 1

# plastic gravity loading
analyze 40 5.0e2

puts "Finished with plastic gravity analysis..."

#Define Dynamic Recorder and Perform Analysis

recorder Node -file Freefieldacc.out -time -dT $dt -node 1 2 3 \
         4 5 6 -dof 1 accel

recorder Node -file Pileacc.out -time -dT $dt -node 13 14 15 16 \
         17 18 -dof 1 accel

recorder Node -file Freefielddisp.out -time -dT $dt -node 1 2 3 \
         4 5 6 -dof 1 disp

recorder Node -file Piledisp.out -time -dT $dt -node 13 14 15 16 \
         17 18 -dof 1 disp

# rezero time
setTime 0.0
wipeAnalysis

# timeseries object for force history
set mSeries "Path -dt $dt -filePath $VelFile -factor $cFactor"

# loading object
pattern Plain 10 $mSeries {
  load 1 1.0 0.0
}

rayleigh $a0 $a1 0.0 0.0

# Determine Stable Analysis Time Step
set duration [expr $dt*$nSteps]; # duration of ground motion (s)
set kTrial [expr $sizeEleX/(pow($Vs,0.5))]; # trial analysis time step
# Define time step and number of steps for analysis
if { $dt <= $kTrial } {
  set nSteps $nSteps
  set dT $dt
} else {
  set nSteps [expr floor($duration/$kTrial)+1]
  set dT [expr $duration/$nSteps]
}
puts "number of steps in analysis: $nSteps"
puts "analysis time step: $dT"

# Analysis objects
constraints Transformation
test NormDispIncr 5e-3 30 1
algorithm Newton
numberer RCM
system ProfileSPD
integrator Newmark $gamma $beta
analysis VariableTransient

# Analyze
set startT [clock seconds]
analyze $nSteps $dT
set endT [clock seconds]
puts "Execution time: [expr $endT-$startT] seconds."

```

PILE BENDING AND DISPLACEMENT FOR DIFFERENT
PILE GROUP CASES

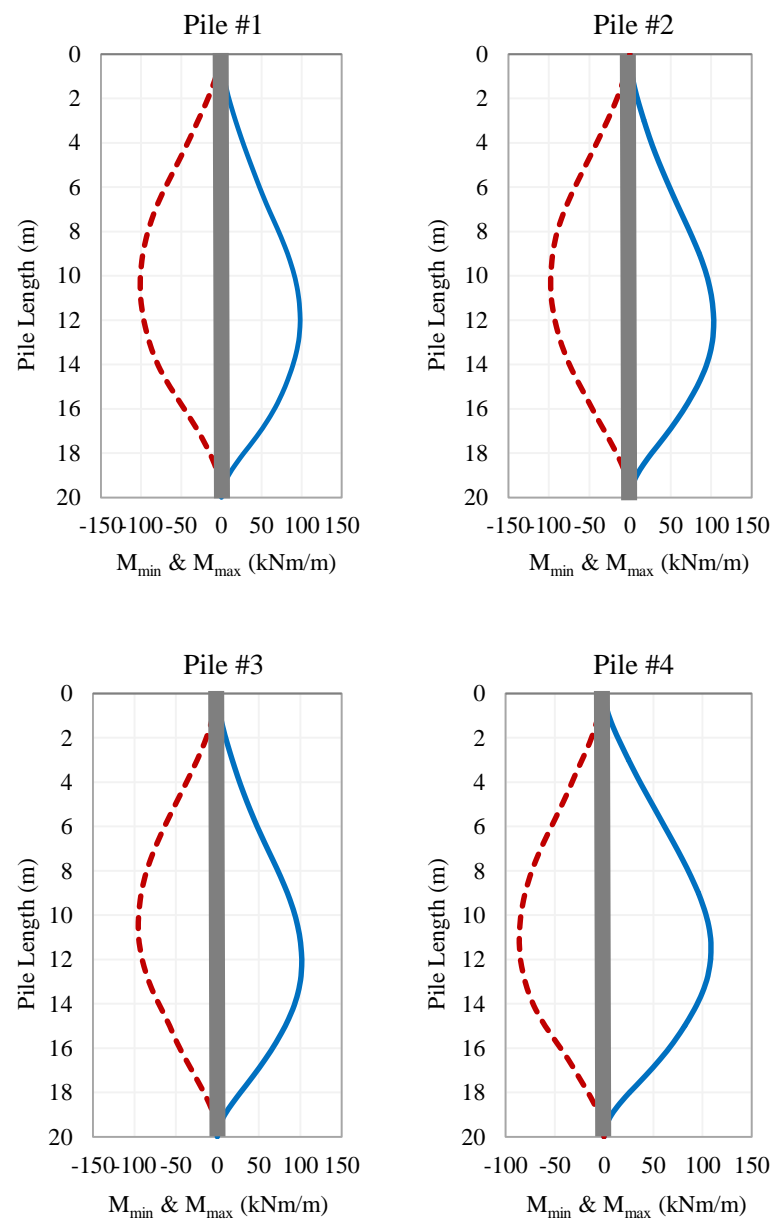


Figure B.1 M_{min} & M_{max} calculated by applying Kocaeli earthquake motion for Case V

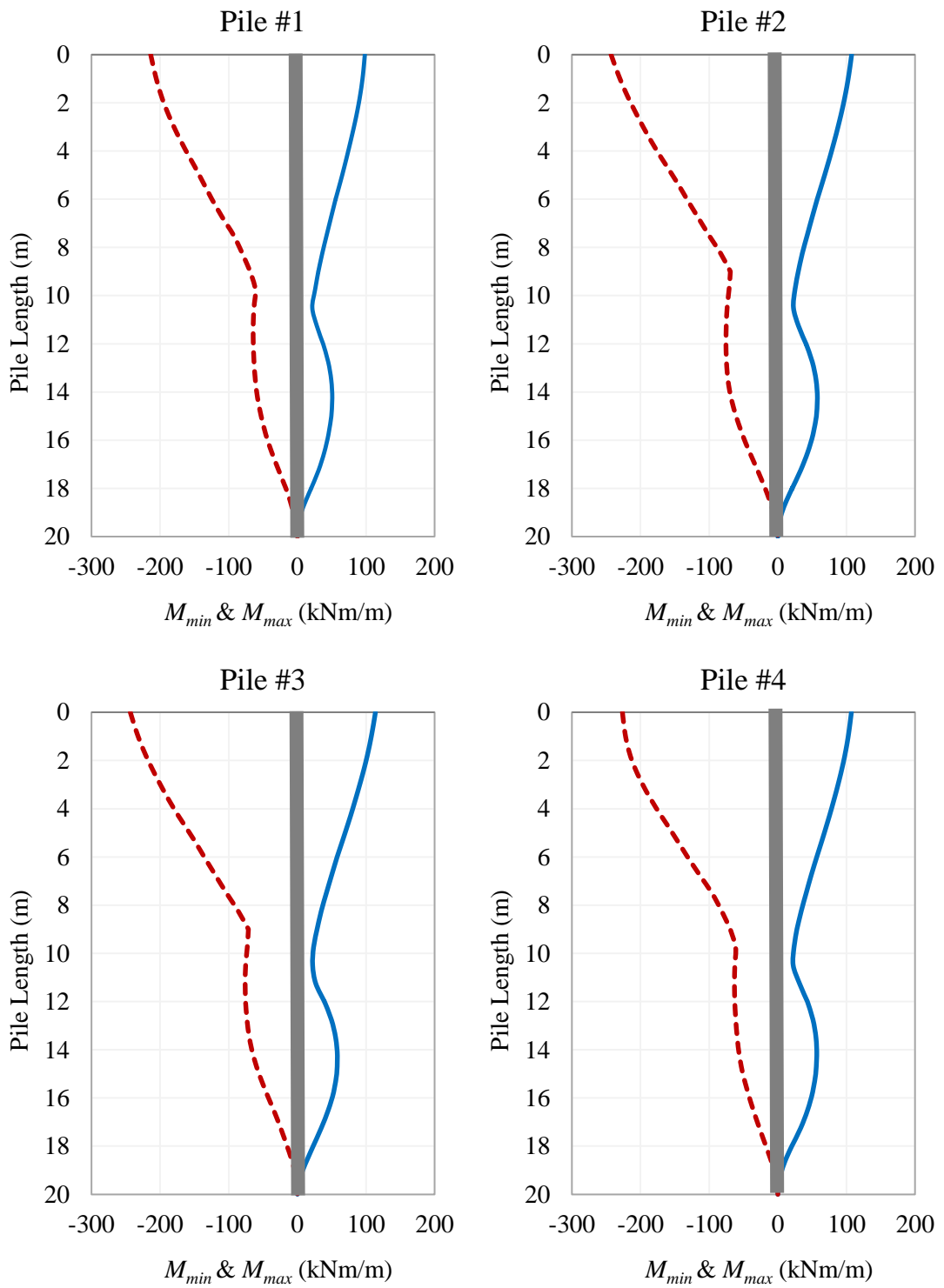


Figure B.2 M_{min} & M_{max} calculated by applying Kocaeli earthquake motion for Case VI

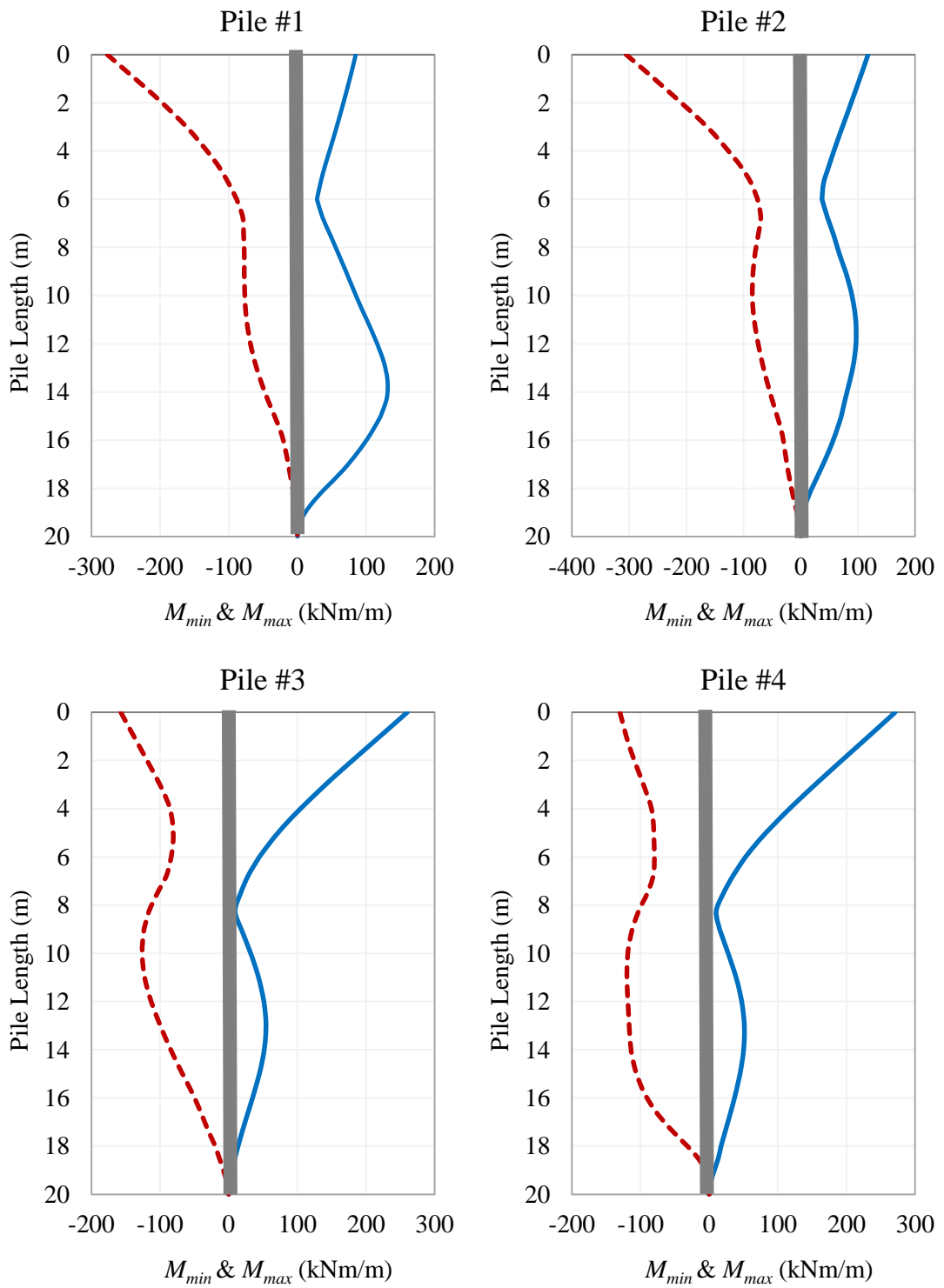


Figure B.3 M_{min} & M_{max} calculated by applying Kocaeli earthquake motion for *Case VII*

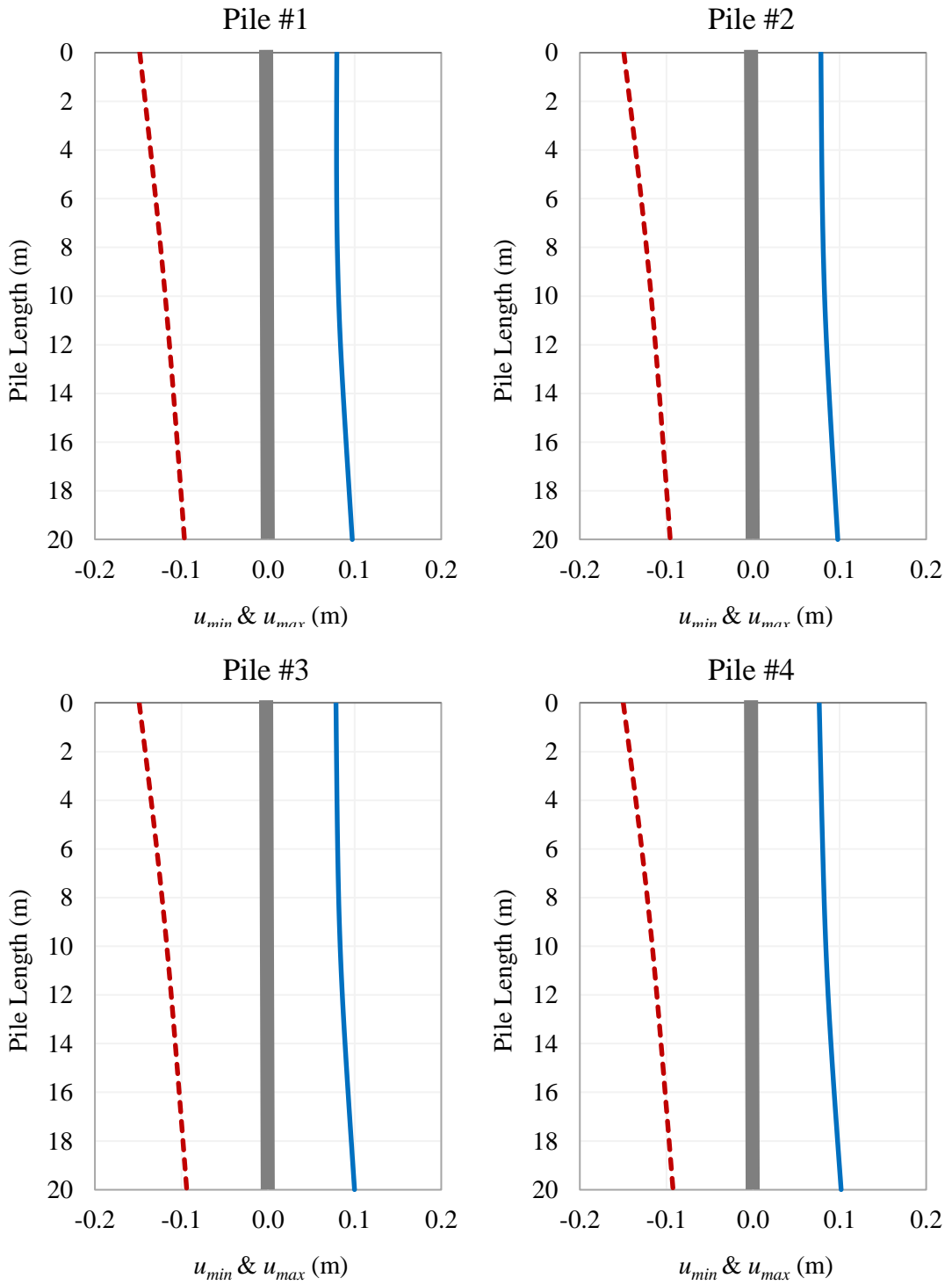


Figure B.4 u_{min} & u_{max} calculated by applying Kocaeli earthquake motion for *Case V*

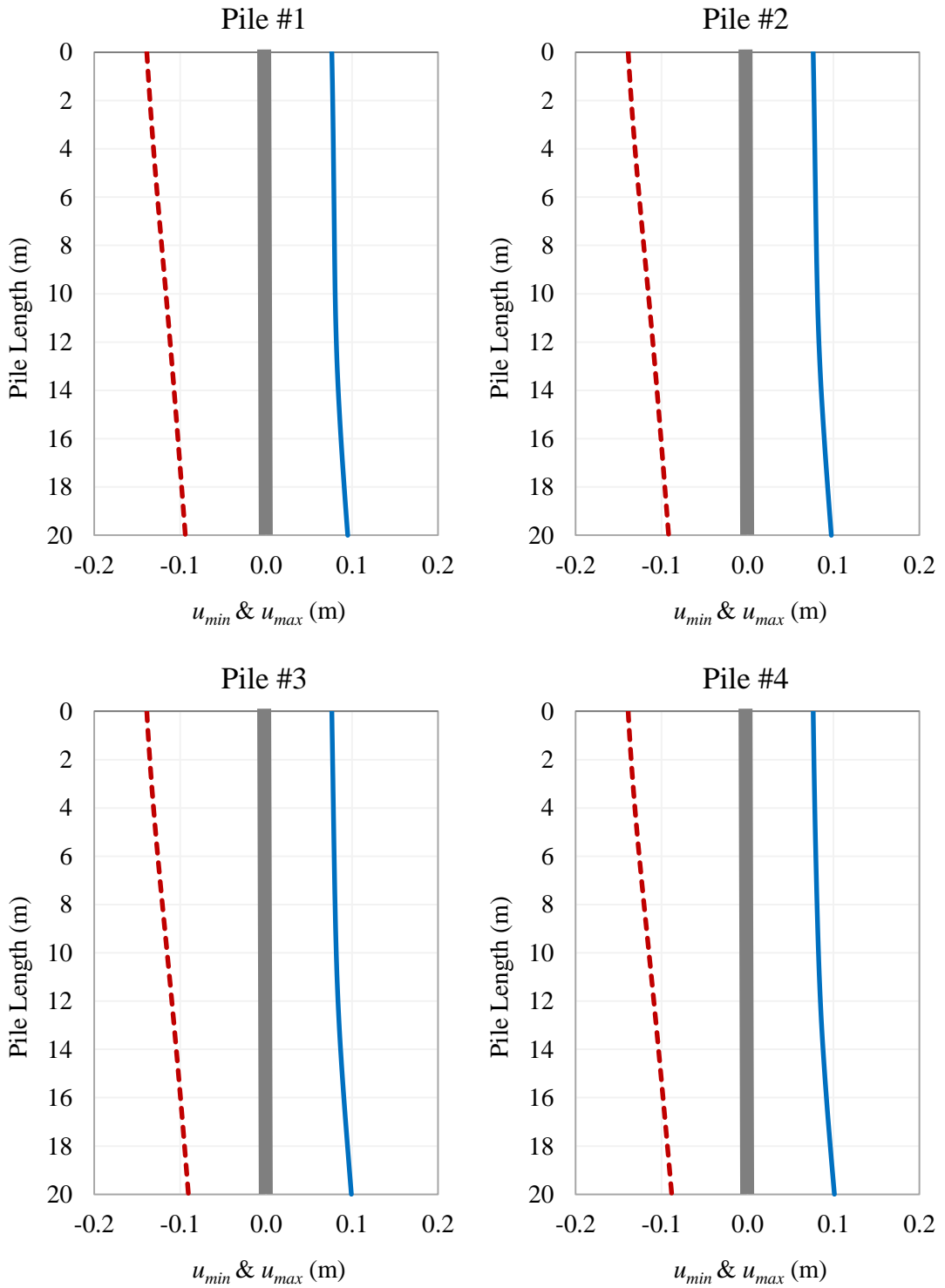


Figure B.5 u_{min} & u_{max} calculated by applying Kocaeli earthquake motion for *Case VI*

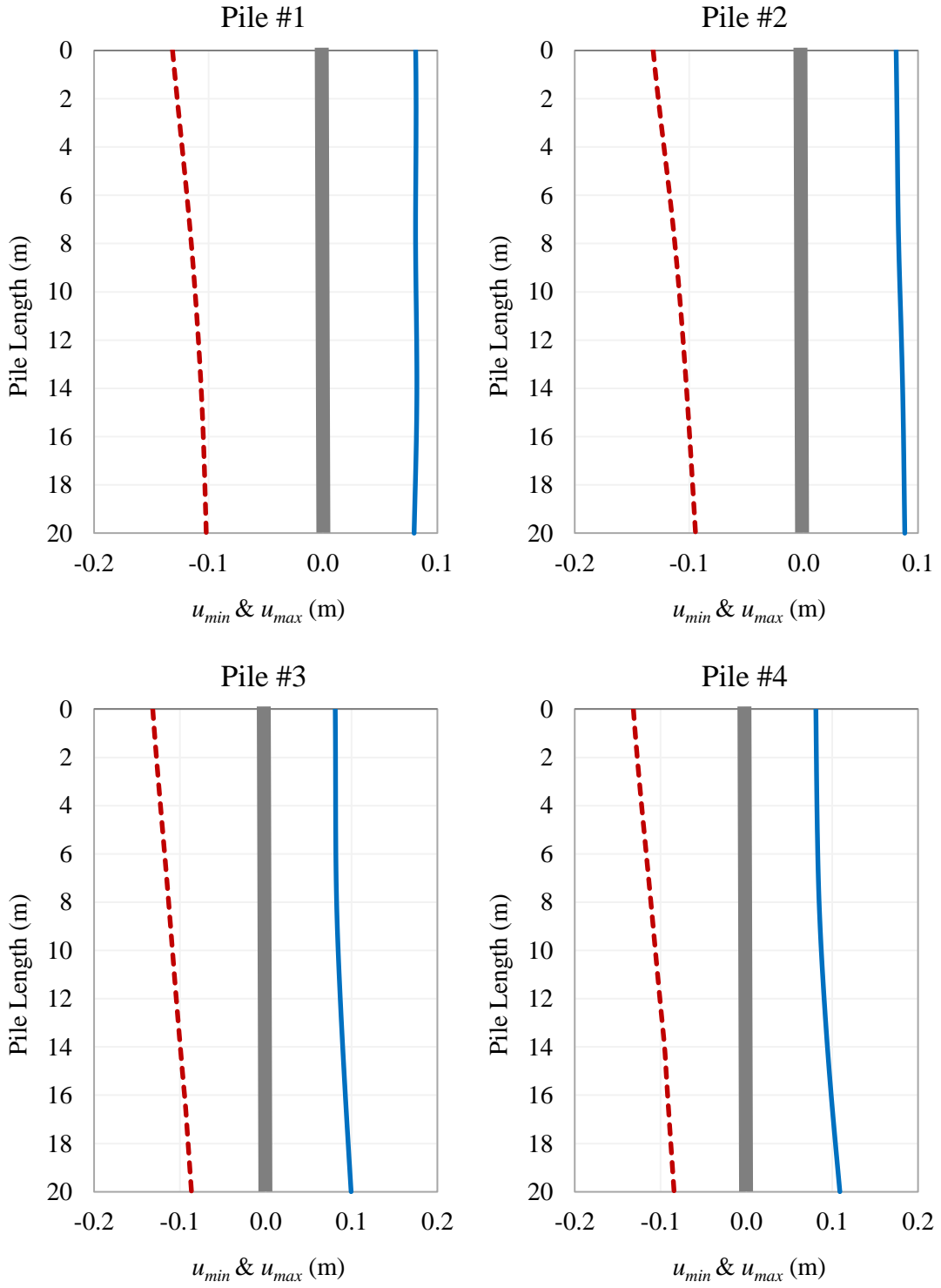


Figure B.6 u_{min} & u_{max} calculated by applying Kocaeli earthquake motion for Case VII

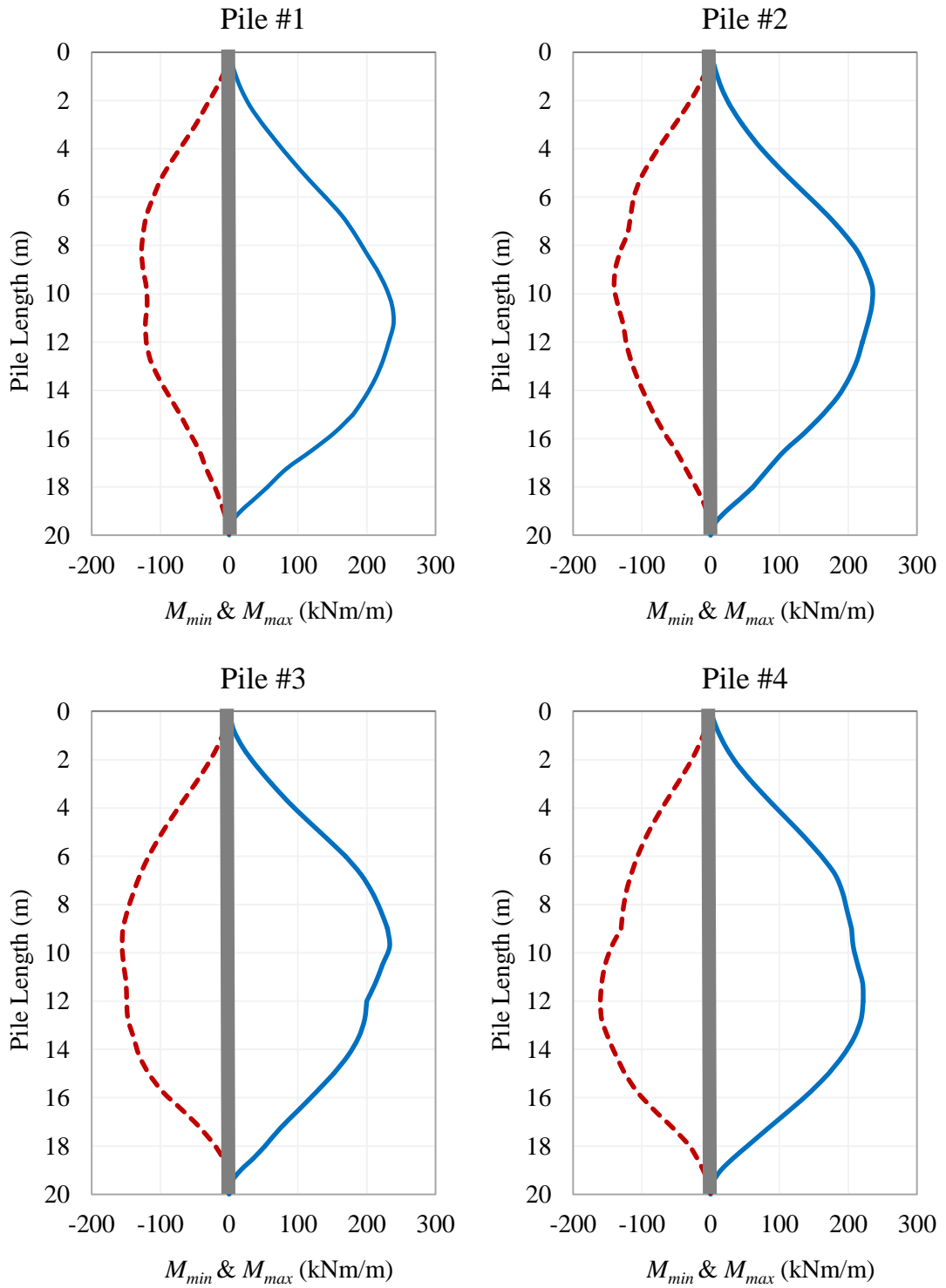


Figure B.7 M_{min} & M_{max} calculated by applying Loma Prieta earthquake motion for Case V

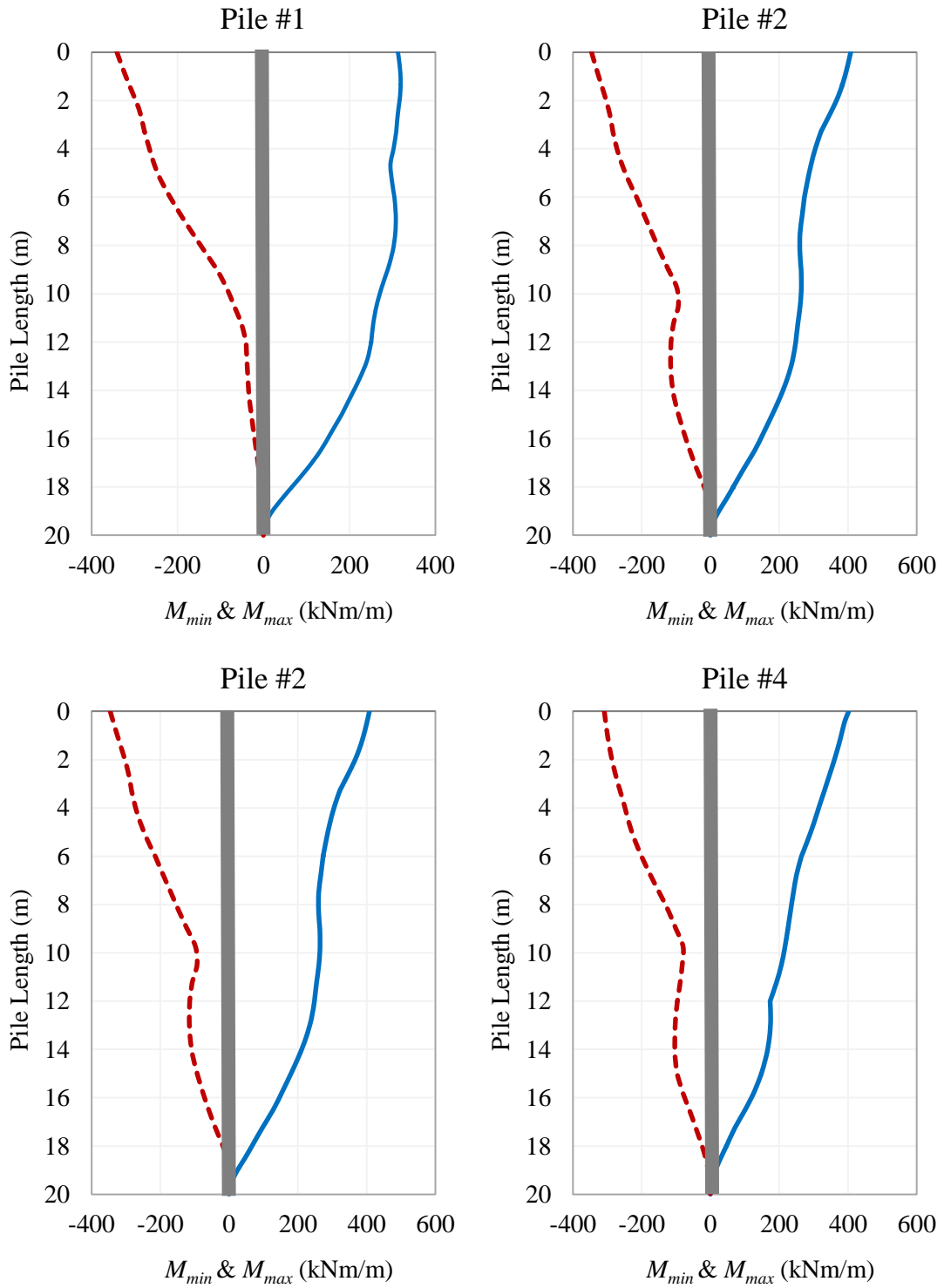


Figure B.8 M_{min} & M_{max} calculated by applying Loma Prieta earthquake motion for Case VI

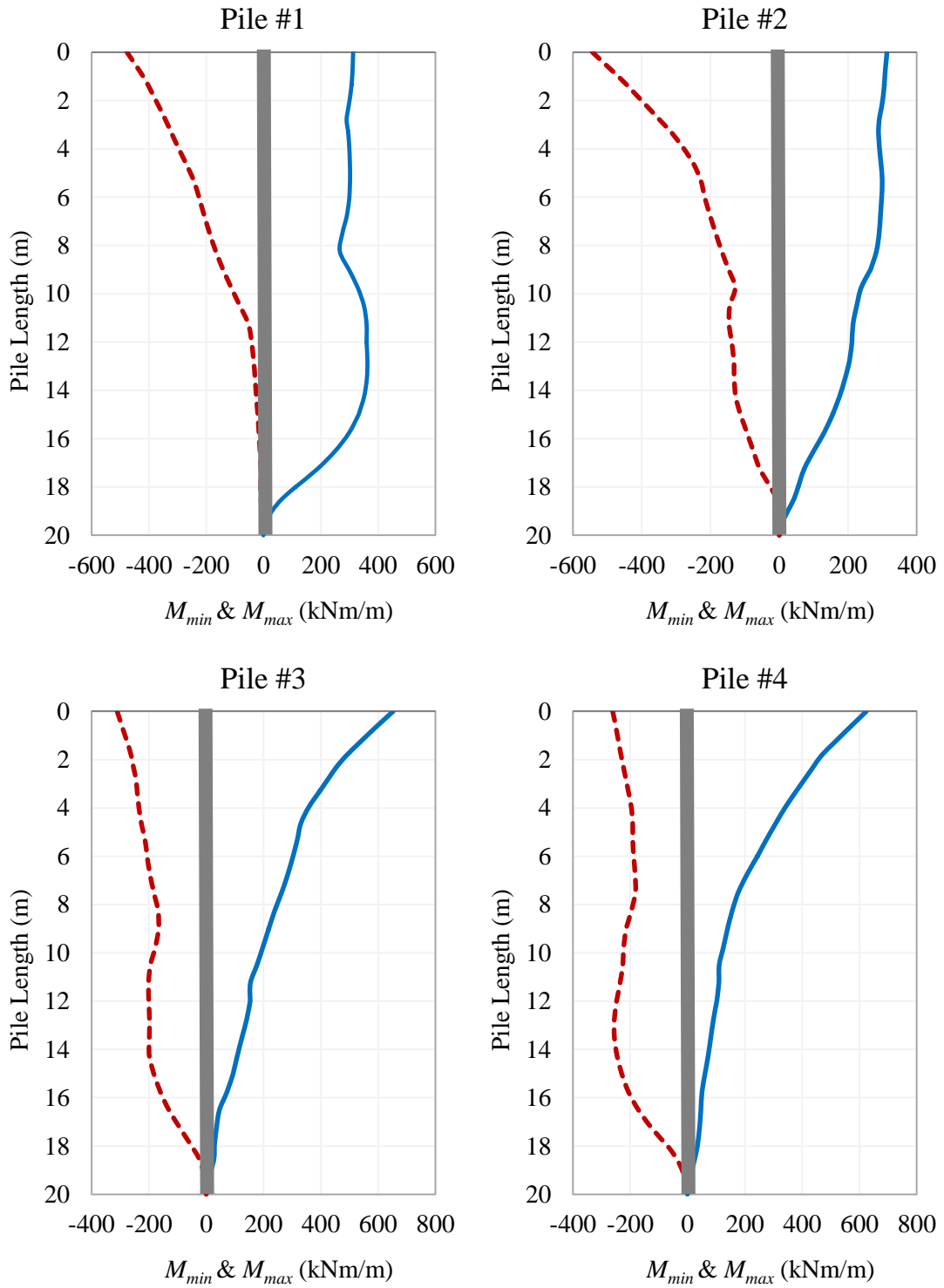


Figure B.9 M_{min} & M_{max} calculated by applying Loma Prieta earthquake motion for Case VII

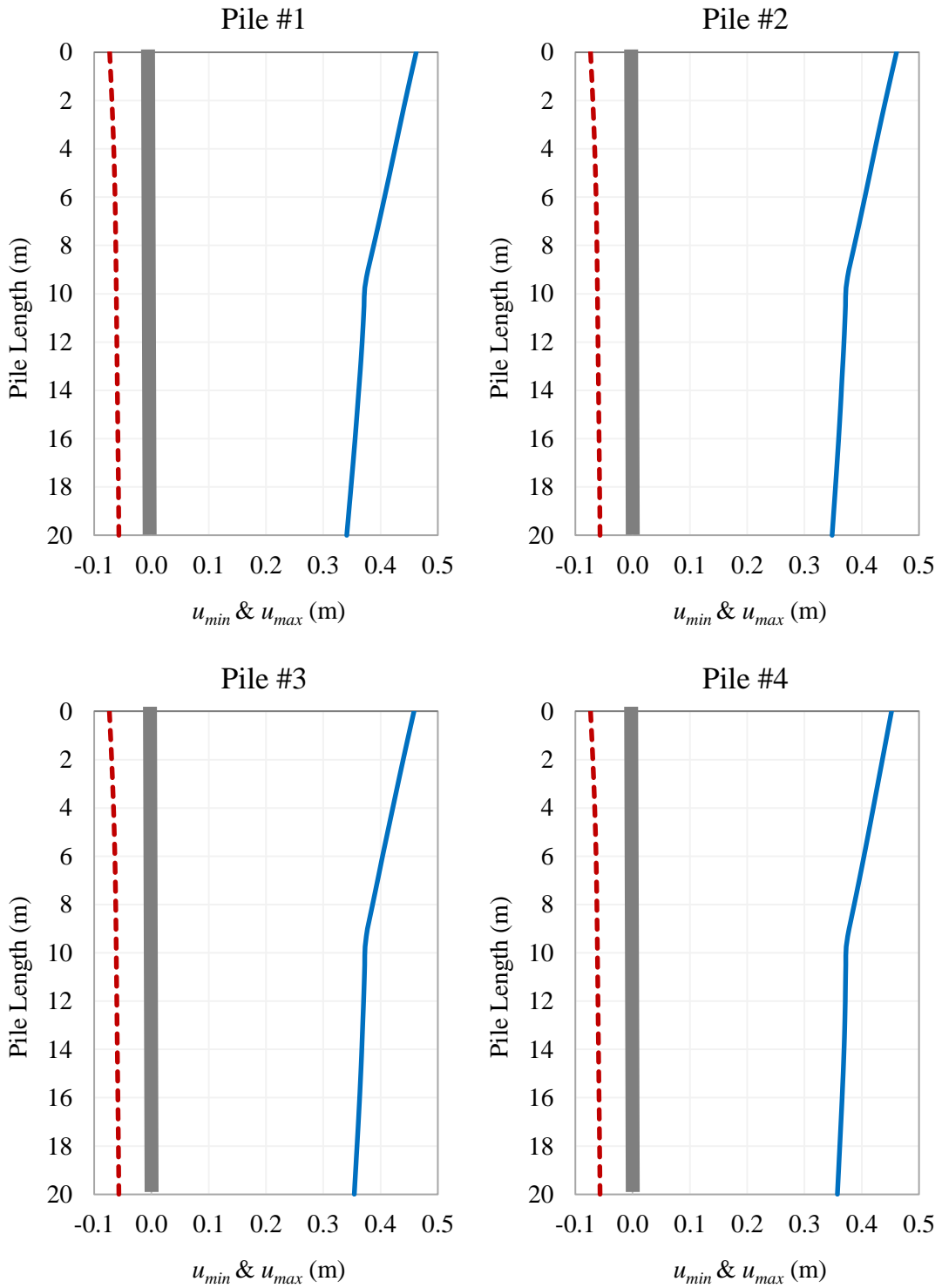


Figure B.10 u_{min} & u_{max} calculated by applying Loma Prieta earthquake motion for Case V

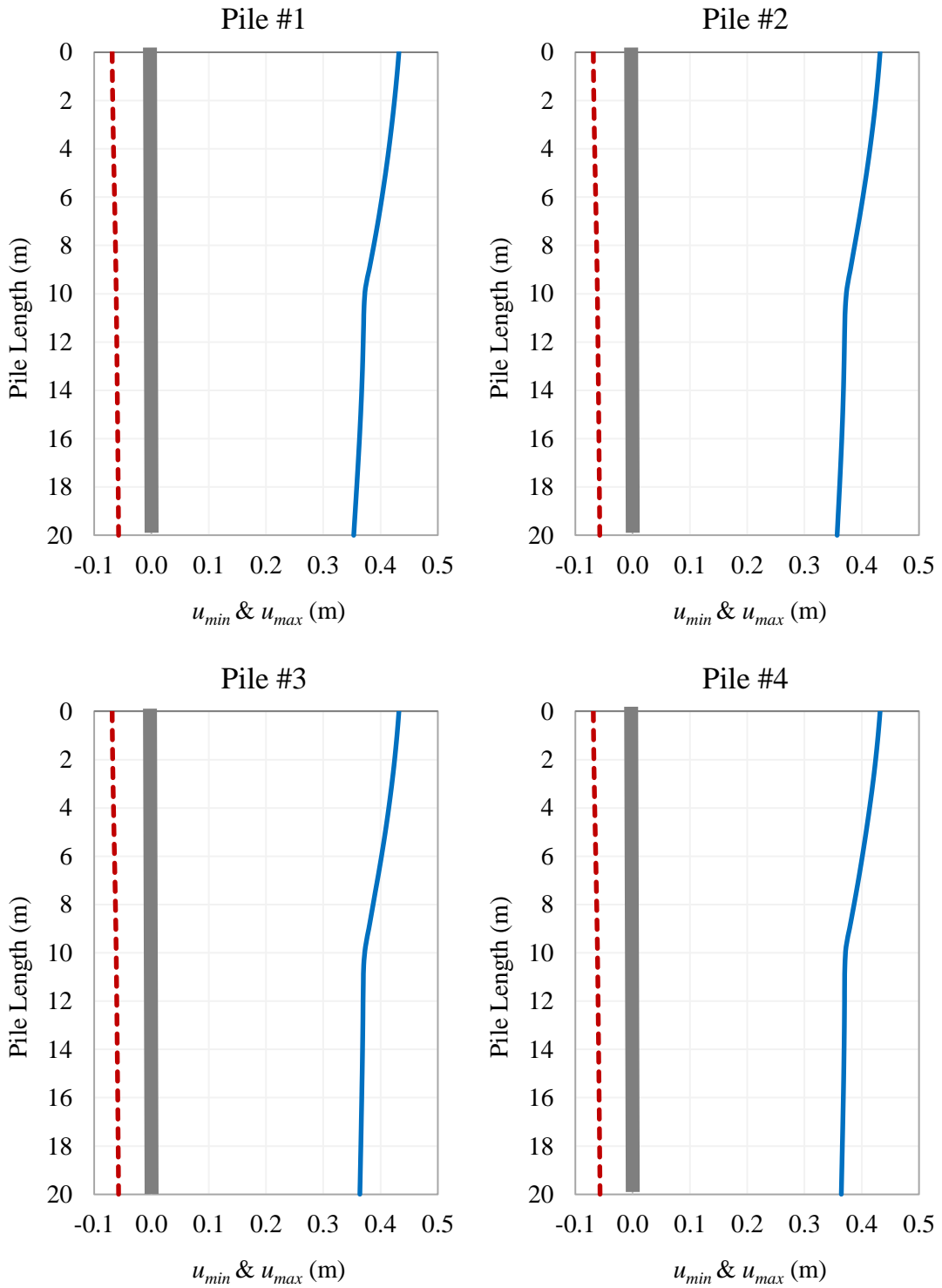


Figure B.11 u_{min} & u_{max} calculated by applying Loma Prieta earthquake motion for Case VI

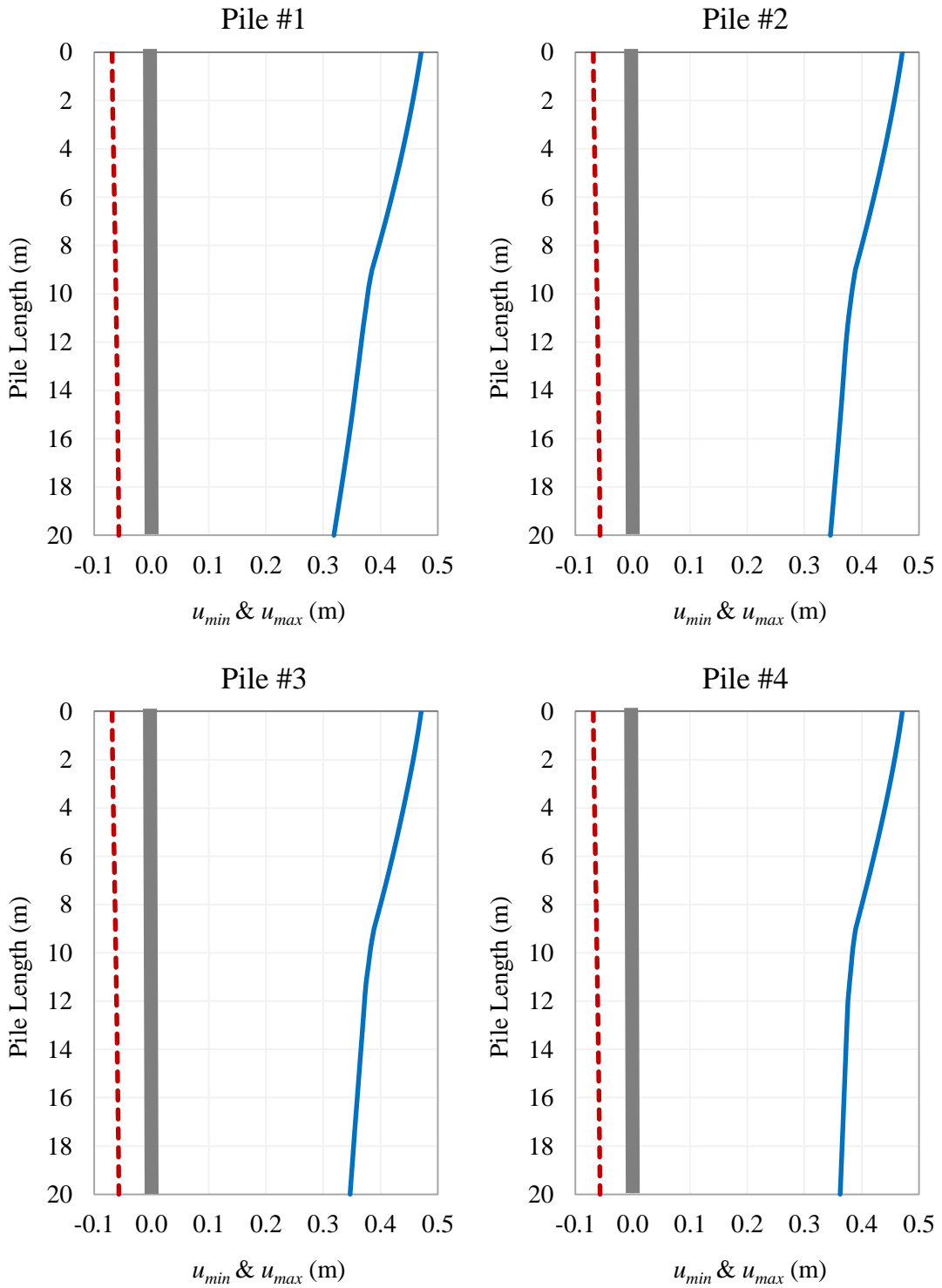


Figure B.12 u_{min} & u_{max} calculated by applying Loma Prieta earthquake motion for Case VII

CURRICULUM VITAE

PERSONAL INFORMATION

Name Surname : Mustafa KİRKİT
Date of birth and place : December 4, 1985 / Kayseri
Foreign Languages : English
E-mail : mustafakirkit@gmail.com

EDUCATION

Degree	Department	University	Date of Graduation
Master	Civil Engineering Geotechnical	Yıldız Technical University	2009
Undergraduate	Civil Engineering	Selçuk University	2007
High School	Develi Anatolian High School		2003

WORK EXPERIENCE

Year	Corporation/Institute	Enrollment
2010	Yıldız Technical University	Research Assistant

PUBLICATIONS**Papers**

- 1- Akgüner, C. and Kirkit, M., (2012). “Axial Bearing Capacity of Socketed Single Cast-in-Place Piles”, *Soils and Foundations*, 52(1):59-68.
- 2- Akgüner, C. and Kirkit, M., (2011). “Kayaya Soketli Kazıkların Yükleme Deneyi ve Ampirik Yöntemlerle Belirlenen Kapasitelerinin Karşılaştırılması”, *Teknik Dergi*, 22(4):5713-5723.

Conference Papers

- 1- Kirkit, M., Seylabi, E. E., Jeong, C., and Taciroğlu, E., (2014). “Kinematic Interaction Factor for a Single Pile Embedded in Homogeneous Soil”, *International Civil Engineering & Architecture Symposium for Academicians*, May 17-20 2014, Antalya.
- 2- Kirkit, M., Akgüner, C., Berilgen, M., and Taciroğlu, E., (2014). “Tabakalı Zeminlerde Kazık - Zemin Etkileşimi”, *Zemin Mekaniği ve Temel Mühendisliği 15. Ulusal Kongresi*, October 16-17 2014, Ankara.
- 3- Kirkit, M., Berilgen, M., Akgüner, C., and Taciroğlu, E., (2014). “Kazıklı Temellerde Tabaka Kalınlığının Zemin - Yapı Etkileşimine Etkisi”, *Zemin Mekaniği ve Temel Mühendisliği 2. Özel Konulu Sempozyumu*, April 24-25 2014, Antalya.
- 4- Kirkit, M., Taciroğlu, E., Berilgen, M., and Akgüner, C., (2013). “Effect of Single Pile on Site Response”, *11th International Conference on Vibration Problems*, September 9-12 2013, Lisbon.
- 5- Kirkit, M., Demir, S., Akgüner, C., and Kılıç, H., (2012). “Soketli Bir Fore Kazığın Sayısal ve Ampirik Analizi”, *Zemin Mekaniği ve Temel Mühendisliği 14. Ulusal Kongresi*. October 4-5 2012, Isparta.
- 6- Dadaloğlu, S., Akgüner, C., and Kirkit, M. (2011)., “Derin Kazılarda Nümerik Yöntemlerin Karşılaştırılması - Bir Vaka Analizi”, *Prof. İsmet Ordemir'i Anma Toplantısı ve 6. ODTÜ Geoteknik Mühendisliği Sempozyumu*, November 23 2011, Ankara.
- 7- Kirkit, M., Kılıç, H., and Akgüner, C., (2010). “Numerical Analyses of Axial Load Capacity of Rock Socketed Piles in Turkey”, *Proceedings of the Seventh European Conference on Numerical Methods in Geotechnical Engineering*, June 2-4 2010, Trondheim.

- 8- Kirkit, M., Siyahi, B., and Akgüner, C., (2010). “Kohezyonlu Zeminlerin Davranış Analizinde Doğrusal ve Eşdeğer Doğrusal Yaklaşımlarının Karşılaştırılması”, Zemin Mekaniği ve Temel Mühendisliği 13. Ulusal Kongresi, September 30 – October 1 2010, İstanbul.
- 9- Kirkit, M., Akgüner, C., Kılıç, H., and Serbest, E., (2010). “Kazık Yükleme Deneyleri Veri Tabanı Programı”, Zemin Mekaniği ve Temel Mühendisliği 13. Ulusal Kongresi, September 30 – October 1 2010, İstanbul.
- 10- Kirkit, M., Akgüner, C., and Karadayılar, T., (2009). “Kayaya Soketli Fore Bir Kazığın Taşıma Gücü”, Prof. İsmet Ordemir'i Anma Toplantısı ve 5. ODTÜ Geoteknik Mühendisliği Sempozyumu, November 23 2009, Ankara.

AWARDS

2214 – Foreign Research Program for Doctoral Student from TUBITAK (The Scientific and Technological Research Council of Turkey)

2211 – Scholarship for Doctoral Student from TUBITAK (The Scientific and Technological Research Council of Turkey)

2210 – Scholarship for Master Student from TUBITAK (The Scientific and Technological Research Council of Turkey)